Leibniz-Institut für Arbeitsforschung an der TU Dortmund

Dissertation

The critical role of oxalate in the liver-kidney axis and its effect on glucose metabolism

Zur Erlangung des akademischen Grades des Doktors der Naturwissenschaften (Dr. rer. nat.) an der Fakultät für Chemie und chemische Biologie der Technischen Universität Dortmund

Vorgelegt von

Philipp Gabrys, M.Sc.

Dortmund 2024

1. Gutachter: Prof. Dr. med. Jan G. Hengstler (TU Dortmund)

2. Gutachter: Prof. Dr. rer. nat. Christoph van Thriel (RU Bochum)

Datum der Einreichung: 23.08.2024

Datum der Disputation: 14.10.2024

Content

Summary vi

Zusammenfassung viii

Abbreviations xi

1 Introduction 16

1.1 Glucose metabolism 16

1.1.1 Hepatic gluconeogenesis 17

1.1.2 Renal gluconeogenesis 20

1.2 Dysregulated glucose metabolism in Non-Alcoholic Fatty Liver Disease (NAFLD) 23

1.2.1 Prevalence, diagnosis and risk factors 24

1.2.2 NAFLD and the metabolic syndrome 25

1.2.3 NAFLD and T2DM 26

1.2.4 Extrahepatic consequences of NAFLD 28

1.2 4.1 Cardiovascular implications 28

1.2.4.2 Chronic kidney disease, kidney stones and hyperoxaluria 28

1.2.4.3 A molecular linkage between NAFLD and hyperoxaluria: Agxt promotor hypermethylation in steatosis 31

1.3 The role of Agxt in hyperoxaluria 33

1.3.1 Hepatic formation of oxalate 33

1.3.1 Alanine: glyoxylate aminotransferase 35

1.3.1.1 Subcellular distribution 35

1.3.1.2 Transcriptional regulation and activity of Agxt 36

1.4 The role of Agxt in gluconeogenesis 36

1.4.1 Serine: pyruvate aminotransferase activity 36

1.4.2 Evidence for a contribution of Agxt in amino-acid driven gluconeogenesis ... 37

1.4.3 Inhibition of gluconeogenesis by oxalate 37

1.5 Aim of this work 38

2 Material and methods 41

2.1 Material 41

2.1.1 Technical equipment 41

2.1.2 Consumables 43

2.1.3 Chemicals and Dyes 44

2.1.4 Commercial buffers and reagents 46

2.1.5 Prepared buffers and reagents 46

2.1.6 Cell culture constituents ... 50
2.1.7 Animals ... 51
2.1.8 Antibodies ... 51
2.1.8.1 Primary antibodies ... 51
2.1.8.2 Secondary antibodies ... 51
2.1.9 TaqMan gene expression assays ... 52
2.1.10 Adeno-associated viral vectors ... 52
2.2 Methods ... 53
2.2.1 *in vivo* ... 53
2.2.1.1 Housing of mice ... 53
2.2.1.2 Collection of organs, tissue and blood from mice ... 53
2.2.1.3 24h urine collection ... 54
2.2.1.4 Histology staining of embedded tissue ... 54
2.2.1.4.1 Fixation and paraffin embedding ... 54
2.2.1.4.2 Hematoxylin and eosin Y staining ... 55
2.2.1.4.3 Periodic acid Schiff (PAS) staining ... 55
2.2.2 *in vitro* ... 56
2.2.2.1 Isolation of primary hepatocytes ... 56
2.2.2.1.1 Murine hepatocytes ... 56
2.2.2.1.2 Human hepatocytes ... 57
2.2.2.2 Cultivation of primary hepatocytes ... 57
2.2.2.2.1 Hepatic glucose production assay ... 58
2.2.3 Gene expression analysis ... 59
2.2.3.1 RNA isolation ... 59
2.2.3.2 Synthesis of cDNA ... 60
2.2.3.3 Quantitative real time polymerase chain reaction (qPCR) ... 60
2.2.4 Protein analysis ... 62
2.2.4.1 Protein extraction from different specimen ... 62
2.2.4.2 Quantification of protein ... 62
2.2.4.3 Western Blot ... 63
2.2.4.3.1 SDS-Polyacrylamide gel electrophoresis (SDS-PAGE) ... 63
2.2.4.3.2 Protein transfer on PVDF membrane ... 64
2.2.4.3.3 Protein detection ... 65
2.2.5 Colorimetric assays ... 66

2.2.5.1 Quantification of glucose 66
2.2.6 Enzyme-linked immunosorbent assay (ELISA) 66
2.2.6.1 Insulin quantification 66
2.2.6.2 Glucagon quantification 67
2.2.7 Amino acid quantification in plasma and tissue 67
2.2.8 Oxalate quantification in urine, plasma, supernatant and tissue 68
2.2.9 Quantification of creatinine in urine 69
2.2.10 Cell Titer Blue® viability assay 69
2.2.11 Gene transfer using an adeno-associated viral transfer expressing Agxt . 70
2.2.12 Statistical analysis 70
3 Results 71
3.1 Establishment of an *in vitro* hepatic glucose production (HGP) assay in hepatocytes 71
3.1.1 Primary mouse hepatocytes are capable to produce glucose from various glucogenic precursors 71
3.1.2 Expression of glucogenic genes in response to different substrates 74
3.1.3 Pck1 protein induction after exposure to pyruvate/lactate and various amino acids – not via glycerol 76
3.2 The role of oxalate as inhibitor of gluconeogenesis 78
3.2.1 Oxalate accumulates intracellularly in primary mouse hepatocytes 79
3.2.2 Oxalate inhibits glucose production from pyruvate/lactate and alanine 80
3.2.3 Glycerol-driven gluconeogenesis is not influenced by oxalate exposure in primary mouse hepatocytes 81
3.2.4 Primary human hepatocytes are more sensitive to increased concentrations of oxalate compared to mouse hepatocytes 82
3.2.5 Production of glucose from pyruvate/lactate and amino acids is influenced by oxalate in primary human hepatocytes 83
3.2.6 Primary human hepatocytes are not influenced by oxalate when glucose is produced from glycerol 84
3.3 Inhibition of gluconeogenesis from hydroxyproline-derived oxalate 85
3.3.1 Determination of a non-toxic effect concentration of hydroxyproline 85
3.3.2 Intra- and extracellular quantification of hydroxyproline-derived intermediates 86
3.3.3 Agxt-deficient hepatocytes display elevated intracellular levels of oxalate 89
3.3.4 Gluconeogenesis from pyruvate/lactate and amino acids is significantly reduced in Agxt-deficient hepatocytes exposed to hydroxyproline 90

3.3.5 Glycerol-driven gluconeogenesis is not influenced by hydroxyproline catabolism nor Agxt-deficiency 92
3.4 Identifying mouse models high in systemic oxalate levels 93
3.4.1 Agxt Knockout (AgxtKO) mice represent a mouse model for Primary hyperoxaluria type 1 (PH1) 93
3.4.2 Rescuing Agxt using AAV-mediated transfer prevents hyperoxaluric phenotype in AgxtKO mice 94
3.4.3 Steatotic mice display downregulated Agxt gene and protein expression 95
3.4.4 Agxt downregulation in liver steatosis leads to increased oxalate production from dietary hydroxyproline and is rescued by AAV-mediated Agxt transfer 95
3.5 Characterization of glucose homeostasis in the AgxtKO mice 97
3.5.1 Fasting glucose levels do not differ in Agxt-deficient mice 97
3.5.2 Plasma amino acids levels show different pattern in wt and AgxtKO mice 100
3.5.3 Gene expression of glyoxylate pathway-genes in liver and kidney show no differences between wt and AgxtKO mice 103
3.5.4 Expression of genes involved in gluconeogenesis in liver and kidney 105
3.5.4.1 Hepatic gene and protein expression of gluconeogenesis-related genes do not significantly differ between wt and AgxtKO mice 106
3.5.4.2 Renal gluconeogenesis is affected by oxalate 108
3.5.5 Starvation induces NAD^+-signaling pathways 111
3.6 Expression of Agxt in correlation with its role in gluconeogenesis 112
3.6.1 Response of Agxt to glucagon in control mice *in vivo* 112
3.6.1.1 Glucagon leads to an increase of blood glucose levels 113
3.6.1.2 Glucagon injection results in persistent elevated glucagon and acute rise of insulin levels in plasma 114
3.6.1.3 Agxt mRNA is induced by glucagon injection in mice 114
3.6.1.4 Protein induction of Agxt via glucagon stimulation is an glucose-independent effect 115
3.6.2 Agxt expression is driven by substrate exposure in gluconeogenesis at an early and late time point 116
4 Discussion 119
4.1. Pyruvate/lactate is a physiological substrate for gluconeogenesis 120
4.2 The effect of oxalate on gluconeogenesis in primary mouse hepatocytes 123
4.3 Consumption of NAD^+ by glyoxylate detoxification may influence gluconeogenesis 126
4.4 No influence of oxalate on glucose levels in hyperoxaluric mice *in vivo* 127
4.5 Glucagon-induced Agxt protein expression is independent of glucose kinetics 130

4.6 A link between Agxt and muscle proteolysis 132
6 Appendix 135
6.1 Bibliography 135
6.2 List of tables 149
6.3 List of figures 150
6.4 Publications 155
6.5 Eidesstaatliche Erklärung (Affidavit) 156
6.6 Acknowledgements 158

Summary

Glucose metabolism is a highly regulated and conserved pathway, which is orchestrated by several factors like hormones, nutritional state, enzymes and substrate availability. The organs, which are responsible to maintain normal blood glucose levels are the liver and to a lesser extent the kidney. Under prolonged fasting, the body makes use of the *de novo* production of glucose from non-carbohydrate substrates – mainly lactate, glycerol and amino acids. This process is called gluconeogenesis.

In the non-alcoholic fatty liver disease (NAFLD) hepatic gluconeogenesis is frequently elevated which results in hyperglycemia and manifests the progression to type 2 diabetes mellitus. NAFLD is a chronic liver disease that does not only affect the liver but also causes extrahepatic complications. In our previous study, a steatosis-associated downregulation of the alanine-glyoxylate aminotransferase (Agxt) was observed in mouse models and patients with NAFLD, and this was accompanied by increased urinary oxalate levels. The physiological function of Agxt is to detoxify glyoxylate to prevent the formation of the harmful waste product oxalate. Therefore, decreased Agxt expression in the fatty liver could represent a mechanism that explains a higher risk of hyperoxaluria in patients with NAFLD.

In addition to the well-established role of Agxt in preventing oxalate production, evidence for a role of Agxt in amino acid-driven gluconeogenesis exists, which has to date not been completely understood. At the same time, oxalate has been reported to inhibit pyruvate carboxylase, a key enzyme of the gluconeogenesis pathway. Altogether, this leads to the hypothesis, that Agxt may support gluconeogenesis by restricting oxalate generation.

To investigate this hypothesis, the inhibitory effect of oxalate on gluconeogenesis was first studied *in vitro*. An *in vitro* hepatic glucose production assay with various glucogenic substrates recapitulating gluconeogenesis was set up and characterized. The exposure of oxalate and the oxalate precursor hydroxyproline to human and murine hepatocytes in this assay revealed an inhibitory effect of oxalate on the glucose production from pyruvate, lactate and alanine, but not from glycerol. The findings demonstrated a direct influence of oxalate on glucose synthesis from precursors that require pyruvate carboxylase to enter the gluconeogenesis pathway.

To translate the *in vitro* findings to an *in vivo* model, glucose homeostasis was studied in AgxtKO mice, which display high plasma and urinary oxalate levels. The results revealed no

changes in the plasma glucose levels, but, intriguingly, a decreased body weight loss after an overnight starvation. In plasma, levels of the glucogenic amino acid glutamine were decreased after fasting in Agxt-deficient compared to wildtype mice. Glucose metabolism-associated gene expression analysis in the liver showed no difference between AgxtKO and wt mice, whereas in the kidney, gene expression changes were observed, suggesting upregulation of compensatory pathways to overcome oxalate inhibition, such as glycerol-driven gluconeogenesis. The results demonstrated that renal gluconeogenesis is more affected by oxalate in the kidney of hyperoxaluric AgxtKO mice, and when hepatic Agxt deficiency appears it affects muscle protein breakdown and glutamine release.

Since Agxt is inducible by the hormone glucagon, the time course of Agxt expression in response to glucagon was investigated. The stimulation with glucagon led to an upregulation of *Agxt* mRNA followed by a more pronounced protein expression of Agxt compared to untreated controls. The upregulation of Agxt was not an immediate response towards glucagon, occurring 6h and 24h post stimulation. In a subsequent approach, *in vitro* data displayed a direct stimulation of *Agxt* mRNA by common glucogenic precursors like pyruvate, lactate, alanine and glutamine but not by glycerol. This indicates a role of Agxt in gluconeogenesis, since other key enzymes of gluconeogenesis were also upregulated.

All in all, the results suggest a small contribution of Agxt in glucose homeostasis *via* regulation of oxalate generation within hepatocytes. In the absence of Agxt, mice can maintain glycemia. However, the levels of oxalate generated in the liver appear to affect the kidney, as judged by the observed gene expression changes. We propose that in kidney, gluconeogenesis from glycerol and other compensatory pathways will be predominant when Agxt is downregulated and oxalate levels become high enough to inhibit gluconeogenesis via pyruvate carboxylase. Conversely, upregulation of Agxt – e.g. by glucagon or pyruvate availability - will prevent oxalate generation and allow pyruvate-driven gluconeogenesis. The hypothesis that levels of oxalate may determine substrate utilization for glucose production in glucose-producing organs like liver and kidney in health and disease should be further explored using 13C metabolic flux analysis. Finally, further experiments are also needed to understand the influence of hepatic Agxt on muscle protein breakdown.

Zusammenfassung

Der Glukosestoffwechsel ist ein hochregulierter und konservierter Stoffwechselweg, der von mehreren Faktoren wie Hormonen, Ernährungszustand, Enzymen und Substratverfügbarkeit beeinflusst wird. Die Organe, die für die Glukose-Homöostatse verantwortlich sind, sind die Leber und, in geringerem Maße, die Niere. Bei längerem Fasten greift der Körper auf die *de-novo*-Produktion von Glukose aus nicht-kohlenhydrathaltigen Substraten – hauptsächlich Laktat, Glycerin und Aminosäuren – zurück. Dieser Prozess wird als Glukoneogenese bezeichnet.

Bei der nicht-alkoholischen Fettlebererkrankung (NAFLD) ist die hepatische Glukoneogenese in den häufigsten Fällen erhöht, was zu Hyperglykämie führt und das Fortschreiten zu Typ-2-Diabetes mellitus begünstigt. NAFLD ist eine chronische Lebererkrankung, die nicht nur die Leber betrifft, sondern auch extrahepatische Komplikationen verursacht. In unserer vorherigen Studie wurde eine steatose-assoziierte Herunterregulierung der Alanin-Glyoxylat-Aminotransferase (Agxt) in Mausmodellen und Patienten mit NAFLD beobachtet, begleitet von erhöhten Oxalatwerten im Urin. Die physiologische Funktion von Agxt besteht darin, Glyoxylat zu entgiften, um die Bildung des toxischen Abfallprodukts Oxalat zu verhindern. Daher könnte die verringerte Agxt-Expression in der Fettleber einen Mechanismus darstellen, der ein höheres Risiko für Hyperoxalurie bei Patienten mit NAFLD begünstigt.

Neben der bekannten Rolle von Agxt gibt es Hinweise auf eine Rolle von Agxt bei der aminosäurebasierten Glukoneogenese, die bisher nicht vollständig verstanden wurde. Gleichzeitig wird beschrieben, dass Oxalat die Pyruvat-Carboxylase hemmt, ein Schlüsselenzym des Glukoneogenese. Aus diesen Befunden lässt sich folgende Hypothese ableiten, die besagt, dass Agxt die Glukoneogenese unterstützt, indem es die Oxalatproduktion einschränkt.

Um diese Hypothese zu untersuchen, wurde die hemmende Wirkung von Oxalat auf die Glukoneogenese zunächst *in vitro* untersucht. Ein *in vitro*-Glukoseproduktionsassay , der die Glukoneogenese nachahmt, wurde mit verschiedenen glukogenen Substraten erfolgreich etabliert. Die Exposition von menschlichen und murinen Hepatozyten gegenüber Oxalat und dem Oxalatvorläufer Hydroxyprolin in diesem Assay zeigte eine hemmende Wirkung von Oxalat auf die Glukoseproduktion aus Pyruvat, Laktat und Alanin, jedoch nicht aus Glycerin. Die Ergebnisse zeigten einen direkten Einfluss von Oxalat auf die Glukosesynthese aus

Vorläuferstoffen, die Pyruvat-Carboxylase benötigen, um die Glukoneogenese zu ermöglichen.

Um die *in vitro*-Ergebnisse in ein *in vivo*-Modell zu übertragen, wurde der Glukosestoffwechsel bei AgxtKO-Mäusen untersucht. Diese Mäuse sind durch hohe Plasma- und Urinoxalatspiegel gekennzeichnet. Die Ergebnisse zeigten keine Veränderungen des Blutzuckerspiegels, aber einen verringerten Gewichtsverlust nach nächtlichem Fasten. Im Plasma waren die Spiegel der glukogenen Aminosäure Glutamin nach dem Fasten bei Agxt-defizienten Mäusen im Vergleich zu Wildtyp-Mäusen reduziert. Die Analyse der Glukosestoffwechsel-assoziierten Genexpression in der Leber zeigte keinen Unterschied zwischen AgxtKO- und Wildtyp-Mäusen, während Genexpressionsveränderungen in der Niere beobachtet wurden, die auf eine Hochregulation von Kompensationswegen zur Überwindung der Oxalatinhibition hindeuten, vorallem durch die Glycerin-getriebene Glukoneogenese. Die Ergebnisse zeigten, dass die renale Glukoneogenese in den Nieren von hyperoxalurischen AgxtKO-Mäusen stärker von Oxalat beeinflusst wird, und dass ein hepatischer Agxt-Mangel den Muskelproteinabbau und die Glutaminfreisetzung beeinflusst.

Da Agxt durch das Hormon Glukagon induzierbar ist, wurde im Zeitverlauf die Agxt-Expression auf Protein- und mRNA-Ebene als Reaktion auf Glukagon untersucht. Die Stimulation mit Glukagon führte zu einer Hochregulierung der *Agxt*-mRNA, gefolgt von einer stärkeren Proteinexpression von Agxt im Vergleich zu unbehandelten Kontrollen. Die Hochregulation von Agxt war keine unmittelbare Reaktion auf Glukagon und trat erst 6 Stunden und 24 Stunden nach der Stimulation auf. In einem nachfolgenden Ansatz zeigten *in vitro*-Daten eine direkte Stimulation von Agxt-mRNA durch gängige glukogene Vorläufer wie Pyruvat/Laktat, Alanin und Glutamin, jedoch nicht durch Glycerin. Dies weist auf eine Rolle von Agxt in der Glukoneogenese hin, da auch andere Schlüsselenzyme der Glukoneogenese hochreguliert wurden.

Die Ergebnisse deuten auf einen kleinen Beitrag von Agxt zur Glukosehomöostase hin, indem es die Oxalatproduktion in Hepatozyten reguliert. In Abwesenheit von Agxt können Mäuse die Glykämie aufrechterhalten. Allerdings scheinen die in der Leber erzeugten Oxalatwerte die Niere zu beeinflussen, wie die beobachteten Genexpressionsveränderungen zeigen. Daraus resultiert, dass in der Niere die Glukoneogenese aus Glycerin und anderen Kompensationswegen vorherrschend ist, wenn Agxt herunterreguliert wird und die

Oxalatspiegel hoch genug sind, um die Glukoneogenese über Pyruvat-Carboxylase zu hemmen. Umgekehrt verhindert die Hochregulation von Agxt – z.B. durch Glukagon oder Pyruvatverfügbarkeit – die Oxalatbildung und ermöglicht die Pyruvat-getriebene Glukoneogenese. Die Hypothese, dass Oxalatspiegel die Substratnutzung für die Glukoseproduktion in glukoseproduzierenden Organen wie Leber und Niere in Gesundheit und Krankheit bestimmen könnten, sollte weiter mit Hilfe der 13C-Metabolitenflussanalyse untersucht werden. Schließlich sind weitere Experimente erforderlich, um den Einfluss von hepatischem Agxt auf den Muskelproteinabbau zu verstehen.

Abbreviations

%	Percent
Adj	Adjusted
Agxt	Alanine-glyoxylate aminotransferase
APS	Ammonium persulfate
BCA	Bicinchoninic acid
BisTris	Bis-(2-hdroxy-ethyl)-amino-tris(hdroxymethyl)-methane
BMI	Body Mass Index
BSA	Bovine Serum Albumine
°C	Degree Celsius
$CaCl_2$	Calcium chloride
cAMP	Cyclic adenosine monophosphate
cDNA	Complementary DNA
CKD	Chronic kidney disease
CpG	5‘-cytosine-phosphate-guanine-3‘
CRE	cAMP response element
CREB/pCREB	cAMP response element binding protein/ phosphorylated cAMP response element binding protein
CRTC2	CREB regulated co-activator 2
CVD	Cardiovascular disease
C_t	Cycle threshold
D	days
DAPI	4‘,6-diamidino-2-phenylindole
DEPC	Diethyl pyrocarbonate

DMEM	Dulbecco's modified Eagles' ,edoi,
DNA/RNA	Deoxyribonuleic acid/ Ribonucleic acid
DNMT	DNA methyltransferase
DPPIV	Dipeptidyl peptidase 4
DTT	Dithiothreitol
EDTA	Ethylenediaminetetraacetic acid
EGTA	Ethylene glycol-bis (β-aminoethylether)-N,N,N,N'-tetra acetic acid
Eif2a	Eucaryotic translation inititation factor 2a
e.g.	for example
et al.	And others
ESKD	End stage kidney disease
FM	Glucose-free media
g/mg/µg	gram/milligram/microgram
G6Pase	Glucose-6-phosphatase
GAPDH	Glyceraldehyde 3-phosphate dehydrogenase
GCGR	G-protein coupled glucagon receptor
GPB	Glucose production buffer
GRHPR	Glyoxylate reductase/hydroxypyruvate reductase
h	hours
HAO1	4-hydroxy-2-ocoglutarate aldolase 1
HRP	Horseradish peroxidase
HEPES	4-(2-hydroxyethyl)-1-piperazineethanesulfonic acid
HOGA1	4-Hydroxy-2-oxoglutarate aldolase
HE	Haematoxylin and Eosin Y

Hyp	Hydroxyproline
i.E.	that is
IfADo	Leibniz-Institut für Arbeitsforschung an der TU Dortmund
IFNγ	Interferon gamma
IHC	Immunhistochemistry
Il-6/Il-10	Interleukin 6/ Interleukin 10
IR	Insulin resistance
JNK	c-Jun N-terminal kinase
KH_2PO_4	Potassium dihydrogen phosphate
L/mL/µL	liter/ milliliter/ microliter
LC-MS/MS	liquid chromatography-mass spectrometry/ mass spectrometry
LDH/LDHA	Lactate dehydrogenase A
LPS	Lipopolysaccharide
KO	Knock-out
MAFLD	Metabolic-associated fatty liver disease
M/mM/µM/nM	Molar/millimolar/micromolar/nanomolar
$MgSO_4$	Magnesium sulfate
MTS	Mitochondria target sequence
N	number of biological replicates
Na_2HPO_4	Sodium hydrogen phosphate
NaCl	Sodium chloride
NAFL	Non-alcoholic fatty liver
NAFLD	Non-alcoholic fatty liver disease
NASH	Non-alcoholic steatohepatitis

NCD/WD/HFD	Normal chow diet/Western Diet/ High-fat diet
NF-κB	Nuclear factor kappa-light-chain-enhancer of activated B cells
NF-Y	Nuclear transcription factor Y
nm	nanometer
NP-40	Nonidet P-40 substitute
o/n	overnight
PAGE	Polyacrylamide gel electrophoresis
PBS	Phosphate-buffered saline
PFA	Paraformaldehyde
PH (1, 2, 3)	Primary hyperoxaluria (type 1,2,3)
PHH	primary human heptatocytes
PKA	Protein kinase A
PKCα	Protein kinase Cα
PMH	Primary mouse hepatocytes
PRODH2	Proline dehydrogenase 2
PVDF	Polyvinylidene fluoride
qRT-PCR	Quantitative real-time polymerase chain reaction
RFU	Relative fluorescence unit
Rpm	Rounds per minute
ROS	Reactive oxygen species
RPBS	Reduced representation bisulfite sequencing
RT	Room temperature
SDS	Sodium dodecyl sulphate
siRNA	Small interfering RNA

SREBP-1c	Sterol regulatory element-binding protein-1c
STZ	Streptozotocin
T2DM	Type 2 diabetes mellitus
TBS-T	Tris-buffered saline
TEMED	Tetramethylethylenediamine
Tris	Tris(hydroxymethyl)aminoethane
UBS	Ubiqutin C
UPR	Unfolded protein response
Vs	versus
v/v; w/v	volume per volume; weight per volume
xg	standard gravity

1 Introduction

1.1 Glucose metabolism

Glucose homeostasis refers to the maintenance of blood glucose levels within a tight range and is a highly regulated process in every living organism. To maintain a balanced glucose homeostasis, several factors play a role, ranging from the uptake and intestinal absorption of carbohydrates in the first place and the distribution of glucose by the liver and the kidney to peripheral organs to maintain energy balance in the second place (Anyamaneeratch et al., 2015; Pilkis and Claus, 1991). On the organ level, the liver takes over most of the part for the maintenance since it controls its distribution between blood stream and hepatocytes by controlling uptake and storage of glucose via glycolysis and glycogenesis under feeding conditions and production of glucose via glycogenolysis and gluconeogenesis under fasting conditions (Nordlie et al., 1999). Besides the storage of glucose in glycogen, excessive glucose can also be used by other metabolic pathways like lipogenesis and stored in white adipose tissue (Towle et al., 1997).

Among the hormones that control glucose homeostasis, the anabolic hormone insulin that is secreted from the β-cells of the pancreas stimulates the uptake of glucose from the bloodstream to the liver under feeding conditions after binding to the insulin receptor (Campbell and Newgard, 2021). Constantly high levels of glucose in the bloodstream (hyperglycemia) can cause severe problems including kidney damage, cardiovascular disease and diabetes (Giri et al., 2018). Under physiological conditions, the secretion of insulin activates key enzymes like glycogen synthase (GS) for glycogenesis and phosphofructokinase, pyruvate kinase for glycolysis in the liver. This activation is mostly mediated by the well-characterized PI3K/Akt pathway induced by insulin (De Meyts, 2004). Further, lipogenic enzymes - fatty acid synthase and acetyl CoA carboxylase - are activated to induce lipogenesis (Hatting et al., 2018; Oh et al., 2013). Insulin does not only regulate glucose uptake and metabolism in the liver, it also regulates the uptake in peripheral organs which also express insulin receptor on their cell membrane, for instance the skeletal muscle and the brain, which require large amounts of glucose to maintain their functionality (Mergenthaler et al., 2013; Merz and Thurmond, 2020). Moreover, insulin prevents glycogenolysis and gluconeogenesis (De Meyts, 2004), therefore antagonizing the effects of glucagon, which will be explained next.

The orchestration of euglycemia under fasting conditions in an organism is mediated mostly by the hormone glucagon that is secreted from α-cells of the pancreas (MacDonald and Rorsman, 2023). When glucagon is secreted, it reaches the hepatic glucagon receptor via the systemic circulation. Here, it binds to the G-protein coupled receptor and induces a conformational change of the glucagon-receptor complex (Engelking, 2015; Janah et al., 2019). This leads to the activation of Gsα protein. The activated protein consequently promotes the adenylate cyclase (AC) to produce the messenger protein cyclic adenine monophosphate (cAMP). After this, cAMP activates the cAMP-dependent protein kinase A (PKA), which can phosphorylate multiple target proteins involved in glycogenolysis and transcription factors that upregulate gluconeogenic enzymes (Janah et al., 2019)(see Fig. 1).

Under short-term fasting periods, the organism makes use of the available glycogen storages in order to maintain glucose homeostasis (Rui, 2014). Whereas after long-term fasting periods, the organism makes use of the *de novo* synthesis of glucose from any non-carbohydrate substance (Petersen et al., 2017). This process is termed gluconeogenesis. It occurs mainly in liver and kidney, hepatocytes and proximal tubular cells respectively. In the next chapters, the focus will be on the hepatic and renal gluconeogenesis.

1.1.1 Hepatic gluconeogenesis

The precursors mostly used to produce glucose de novo in the liver are lactate, glycerol and alanine. They make up to 90% of the newly synthesized glucose (Petersen et al., 2017; Rui, 2014). They can either be synthesized in the liver or brought to the liver from extrahepatic tissue, e.g., muscle or white adipose tissue.

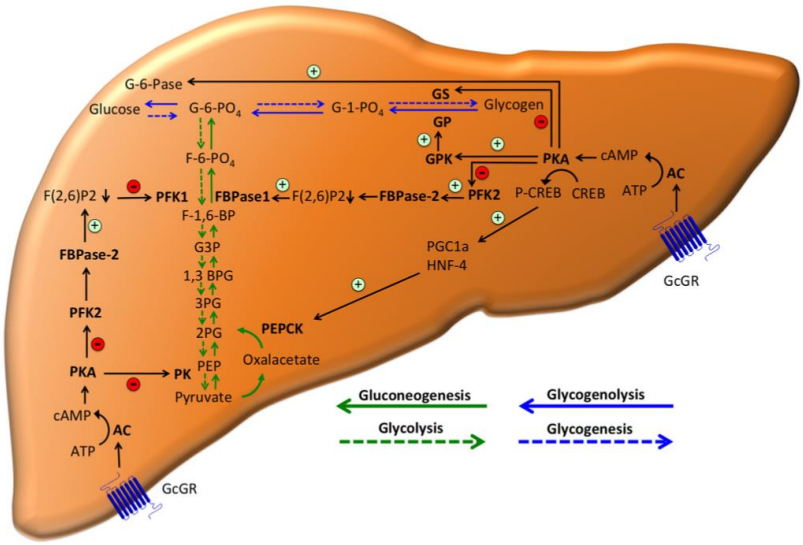

Figure 1: Metabolic pathways in the generation of glucose under fasting (glycogenolysis, gluconeogenesis) and *ad libitum* conditions (glycogenesis, glycolysis) (adapted from Müller et al., 2017b).

Gluconeogenesis is stimulated by glucagon. The actions of glucagon are mainly mediated by the cAMP-PKA pathway. PKA can translocate to the nucleus where it phosphorylates the cAMP response element binding protein (CREB). The phosphorylated CREB then binds to its CRE sequence facilitating the gene and protein expression of key enzymes in gluconeogenesis and other CRE-containing genes (MacDonald and Rorsman, 2023). Key enzymes involved in gluconeogenesis are glucose-6-phosphatase (G6pc), fructose-1,6-bisphosphatase (Fbp1), pyruvate carboxylase (Pc) and phosphoenolpyruvate carboxykinase (Pck1). Their activity and transcriptional expression are regulated via several different mechanism, e.g. hormonal stimulation via glucagon (Pck1, Pc and G6pc) or by changes in allosteric regulators (Fbp1). The glucogenic genes of Pc, Pck1, and G6pc are all immediately activated by the CREB transcription factor which contains a CRE sequence in the promotor region (Thiel et al., 2005; Thonpho et al., 2010; Xing and Quinn, 1993). The glucogenic pathway is the reversal of glycolysis except for four steps, which are circumvented by different enzymes. The rate-limiting enzyme in this pathway is Pck1 catalyzing the conversion of oxaloacetate to phosphoenolpyruvate. The reaction requires GTP to mediate it in an energetically-efficient way. In most organisms, Pck1 is found in the cytosol of the cells (Zimmer and Magnuson, 1990). Studies in a global Pck1-knock-out (KO) have revealed that mice are not viable postnatal and die within the first three days (She et al., 2000). In contrast, liver-specific Pck1-KO mice are viable but they cannot produce glucose from lactate and amino acids by gluconeogenesis. This resulted in high levels of TCA cycle intermediates in hepatocytes and in a steatotic liver via enhanced flux of such intermediates towards lipogenesis. Nevertheless, these mice were able to maintain

euglycemia by the production of glucose derived from glycerol after a 24h fasting period (Burgess et al., 2004). The second important enzyme is the Fbp1, which dephosphorylates fructose-1,6-bisphospate to fructose-6-phosphate and represents the antagonist of phosphofructokinase in glycolysis. The deficiency of Fbp1 results in hypoglycemia, while the overexpression of this gene results in hyperglycemia and an impaired insulin secretion (Kebede et al., 2008; Moey et al., 2018). The last enzyme before glucose is generated under fasting conditions is G6pc. This enzyme removes a phosphate group from glucose-6-phosphate to produce glucose (Foster et al., 1997). This glucose can enter the blood stream and reach the respective tissue. Ultimately, this causes the rise in the blood stream. A hepatocyte-specific KO of G6pc led to hypoglycemia, hyperlipidemia, lactic acidosis, glycogen accumulation and hepatic steatosis. Genetic mutations in the *G6PC* gene are highly associated with glycogen storage disease (GSD)(Chou et al., 2010). As stated before, glucose can also be produced from triglyceride-derived glycerol. Glycerol kinase (Gyk) is the enzyme that phosphorylates glycerol to glycerol-3-phosphate and ultimately results in the formation of dihydroxyacetone phosphate, which can be incorporated in the glucogenic pathway. Compared to the two enzymes before, this reaction is not a direct reversal of the glycolytic pathway (Rui, 2014).

The initial step to induce lactate/pyruvate and amino acid-driven gluconeogenesis is facilitated by Pc. Pc converts pyruvate to oxaloacetate, and therefore it does not only play a role in gluconeogenesis, but also in anaplerosis, replenishing TCA cycle intermediates (Jitrapakdee and Wallace, 1999). Pc is the only enzyme that is not expressed in the cytosol of the cells, it is exclusively found in mitochondria (Gray et al., 2014). The reaction requires ATP and bicarbonate as substrates and is allosterically activated by higher levels Acetyl-CoA in the mitochondria (Valle, 2017). One would wonder why pyruvate is not directly converted to phosphoenolpyruvate in gluconeogenesis. This is a highly inefficient reaction and therefore oxaloacetate is formed as an intermediate substrate (Prochownik and Wang, 2021). Subsequently, oxaloacetate needs to be further metabolized to malate, which then can be shuttled out of mitochondria and into the cytosol where it is oxidized back to oxaloacetate via malate dehydrogenase. This oxaloacetate is metabolized via Pck1 for glucogenic purposes (Hanson and Owen, 2013). Additional studies suggest that mitochondrial Pck2 can directly phosphorylate oxaloacetate to produce phosphoenolpyruvate without being shuttled to the cytosol before (Méndez-Lucas et al., 2013). A deletion of Pc in a liver-specific KO led to an

impaired hepatic anaplerosis, suppressed gluconeogenesis and a compensatory ketogenesis and renal gluconeogenesis, which did not alter euglycemia after fasting (Cappel et al., 2019). Loss of PC also hinders food-derived hyperglycemia and insulin resistance. Though it did not affect glucose homeostasis directly, Pc is essential for biosynthesis and oxidation that is related to the TCA cycle (Cappel et al., 2019).

Apart from the enzymatic modulation of gluconeogenesis and the substrate availability to produce glucose, other regulators influence the process of gluconeogenesis, such as the metabolic state and the circadian clock (Lamia et al., 2011). Even growth hormone and nuclear receptors, e.g., glucocorticoids influence gluconeogenesis (Mueller et al., 2012). Of note, several different studies have reported that the hepatic gluconeogenesis is also highly regulated by the cellular redox state in the hepatocytes. For example, the pyruvate/lactate driven gluconeogenesis in the liver requires high levels of NAD^+ to maintain Ldha functioning. When NADH/NAD^+ ratio is high, it was observed that glucose production derived from pyruvate/lactate was inhibited (Madiraju et al., 2014; Meng et al., 2022). Additionally, cytokines and gastrointestinal hormones like GLP-1 have been well established to influence hepatic glucose production by the secretion of insulin (Rui, 2014). Further, the endoplasmic reticulum can also modulate hepatic gluconeogenesis in both directions, negatively or positively, depending on the downstream signaling pathway. The ER-bound protein CREBH is one example as its levels are higher in fasting state and trigger the dephosphorylation of CREB-regulated transcription coactivator-1 to induce gene expression of glucogenic enzymes (Rui, 2014).

In some diseases that are affecting the glucose metabolism, e.g. in the fatty liver or in type 2 diabetes mellitus, hepatic gluconeogenesis is perturbed. This phenotype is characterized by an increased hepatic gluconeogenesis and elevated glucagon levels, which will be explained in a later chapter (Barroso et al., 2024).

1.1.2 Renal gluconeogenesis

Historically, the liver was seen as the organ controlling euglycemia and being responsible for the production of glucose under fasting conditions. In 1937, first evidence emerged that also the kidney can produce glucose from pyruvate and lactate (Elliott and Greig, 1937). It took almost four decades along with the development of the isotopic tracing method until it was confirmed that the kidney is a major organ for gluconeogenesis. Gluconeogenesis takes place

only in the proximal tubules, where all the required enzymes for the pathway are expressed (Guder and Schmidt, 1974; Vandewalle et al., 1981). In contrast to this, key enzymes for the consumption of glucose (glycolysis) are highly abundant in the distal part of the nephron, displaying a distinct pattern of anabolic and catabolic processes (Guder and Ross, 1984; Legouis et al., 2020). In 1995, scientists were able to discriminate between renal uptake and release of glucose using isotopic methods. In a human study, after a 14-16 h overnight fast, glucose levels in the blood were stable in the post absorptive phase, indicating that systemic glucose uptake and release were equivalent. In this study, the kidney was shown to contribute to about 30% of the systemic glucose rate. Additional studies revealed a renal contribution of 20 % to systemic gluconeogenesis, which is comparable to the previous study. Assuming that glycogenolysis and gluconeogenesis share a 50:50 ratio after an overnight fasting and that the renal glucose is only synthesized via gluconeogenesis (as glycogen storages are rarely found in the kidney), this enhances the contribution of renal gluconeogenesis to maintain glucose homeostasis *in vivo* (Chandramouli et al., 1997; Petersen et al., 1996). This becomes even more important after prolonged fasting, when hepatic glycogen stores are depleted, and 90% of glucose production rely completely on gluconeogenesis. At this condition, gluconeogenesis derived from kidney attributes almost 50% of the systemic glucose production in human (Owen et al., 1969). This indicates a critical role for the kidney in glucose homeostasis under fasting conditions.

As previously stated, hepatic gluconeogenesis can be driven from various substrates like lactate, alanine and glycerol, the latter derived from triacylglyceride. This is very similar in the kidney; the main substrates utilized to produce glucose are lactate, glutamine and glycerol accounting for 50%, 20% and 10% respectively (Meyer et al., 2002). Thus, the main difference is that the amino acid preferentially used by the renal gluconeogenesis are glutamine and to a lesser extent alanine.

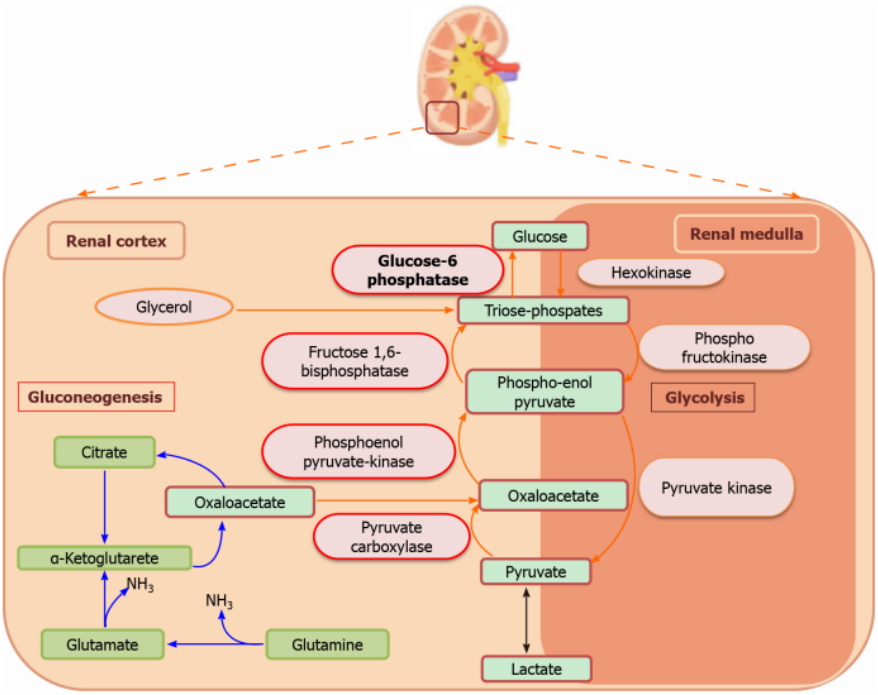

Figure 2: Schematic illustration of the *de novo* production of glucose in the kidney. Glucogenic enzymes are restricted to the cortical space of the kidney, whereas glycolytic enzymes are exclusively expressed in the medullar space of the kidney (adapted from Sharma and Tiwari, 2021)

In another study, Björkman *et al.* reported that the kidney can also produce glucose from fructose in humans after a 60 h fasting period using a fructose tracing method (Björkman and Felig, 1982). Lactate is however the most common substrate for renal gluconeogenesis. Interestingly, the kidney is lactate utilizer and lactate producer at the same time with differences between medulla and cortex. The distal nephron of the kidney (medulla) relies mainly on glycolysis, producing ATP and elevated levels of lactate (see Fig. 2). The cortex instead relies on oxidative phosphorylation for ATP production (Klein et al., 1981). The produced lactate from the glycolysis in the distal nephron can also be used for cortical gluconeogenesis, indicating a corticomedullary lactate cycle loop (Bartlett et al., 1984). In consequence, this leads to the assumption that renal re-uptake of lactate is not related to oxygen consumption rather it is used for immediate gluconeogenesis (Brand et al., 1974).

The onset of renal gluconeogenesis is triggered by hormonal stimuli. Hormones attributed to induce renal gluconeogenesis are stress hormones like hydrocortisone, epinephrine and glucagon. In dogs, these stress hormones accounted for 22% of the overall glucose production with the kidney being more sensitive to the hormonal stimulus than the liver (McGuinness et al., 1993). Further studies revealed that the hormonal secretion increased the net glucose balance via the upregulation and higher activity of common glucogenic enzymese Pck1 and Pc

(Iynedjian and Hanson, 1977; Meisner et al., 1985). After an infusion of epinephrine in humans in the post-absorbative phase, glucose net balance was increased 2-fold accounting for 40 % of the systemic glucose homeostasis. On the contrary, insulin represents the suppressor of renal gluconeogenesis and is even more sensitive compared to its suppression in the liver (Cersosimo et al., 2000).

Besides this finding, evidence exist that substrate availability of lactate, glycerol and glutamine and substrate concentrations determine efficiency and regulation of renal gluconeogenesis (Meyer et al., 2002). Apart from this, glucose itself is a regulator of renal gluconeogenesis. In a glucose-rich environment, reabsorption of glucose increases the ratio of oxidized and reduced nicotine adenine dinucleotide (NAD^+/NADH) leading to a downregulation of Pck1 and inhibition of gluconeogenesis (Sasaki et al., 2017). This mechanism is thus meant to prevent hyperglycemia. The opposite effect which induces renal gluconeogenesis is facilitated by acidosis in the proximal tubular cells by elevated levels of lactate. This leads to the upregulation of *Pck1* mRNA and its activity (Curthoys and Moe, 2014). Acidosis describes a disease in which the plasma acidity is elevated - which means that the plasma pH levels are lower than the physiological range of 7.35-7.45 - mainly due to elevated hydrogen ion concentrations that arise from elevated lactate levels in the renal microenvironment (Soleimani and Rastegar, 2016). To summarize, renal gluconeogenesis seems to be regulated either by hormones or by the acidic environment that the kidney is exposed to.

Since gluconeogenesis is malfunctioning in diabetes due to insulin resistance, the explicit role of renal gluconeogenesis in this term has been poorly investigated. In an *in vivo* model of diabetes, renal gluconeogenesis was elevated and comparable to hepatic gluconeogenesis by an increased activity of G6pc and Pck1 in fasting conditions (Eid et al., 2006; Sharma and Tiwari, 2021). In addition, increased renal gluconeogenesis is attributed to increased level of fasting glucose in type 2 diabetes mellitus (T2DM) (Chang and Schneider, 1970). Furthermore, several human studies also reported an elevated glucose release by the kidney in the fasting state in T2DM patients (Meyer et al., 1998). It seems very likely that insulin resistance is the key driver of impaired renal gluconeogenesis in T2DM.

1.2 Dysregulated glucose metabolism in Non-Alcoholic Fatty Liver Disease (NAFLD)

Non-alcoholic fatty liver disease (NAFLD) is the most common cause of liver disease on a global scale especially in Western countries. Its term encompasses a whole spectrum of disease

stages from fatty liver (NAFL) to the advanced form of steatosis, steatohepatitis (NASH) (Benedict and Zhang, 2017). In NAFLD, the liver is affected by the accumulation of lipids within liver tissue, which represents a hallmark for the diagnosis of a fatty liver. Throughout energy imbalance, when energy intake exceeds energy expenditure and the body is no longer able to store excessive energy in the adipose tissue in form of triacylglycerol, the organism adapts and stores lipids in organs normally not designated to store it. Here, the liver is one central organ to store lipids. The term which describes this phenomenon is “ectopic fat accumulation” (Bugianesi et al., 2010; Byrne, 2013). It is estimated that NAFLD will represent the most frequent indication for liver transplantation until 2030 (Gadiparthi et al., 2020). During the last decades, it has been shown that the clinical burden becomes more and more challenging for the healthcare system (Pouwels et al., 2022) due to the pathological progression of NAFLD to more severe liver disease and the associated morbidity and mortality from cirrhosis, liver failure and hepatocellular carcinoma (Byrne and Targher, 2015). However, NAFLD is not only a liver-related disease. Other extrahepatic consequences and metabolic disorders result from the progression of NAFLD, with cardiovascular disease (CVD), chronic kidney disease (CKD) and T2DM being the most crucial ones (Deprince et al., 2020; Targher et al., 2021b). These premises point out why NAFLD is also described as a multi-organ disease.

1.2.1 Prevalence, diagnosis and risk factors

Current population-based estimation revealed a NAFLD prevalence of 40% among men and 15-20% among women. For poorly known reason, cases are more frequent in men compared to women (Browning et al., 2004). Demographically, cases of NAFLD vary parallel to obesity cases indicating a relationship between those two parameters. Further, it is evident that also ethnicity plays a role for the development of NAFLD showing that Hispanic populations are the most susceptible group to develop NAFLD followed by white and African Americans (Browning et al., 2004).

An initial radiological diagnosis of NAFLD is confirmed when ≥5% of accumulation of lipid droplets is present in absence of drug abuse or alcohol (Masuoka and Chalasani, 2013). Nowadays, the most reliable method to confirm the diagnosis of NALFD is the liver biopsy (Brunt et al., 2015).

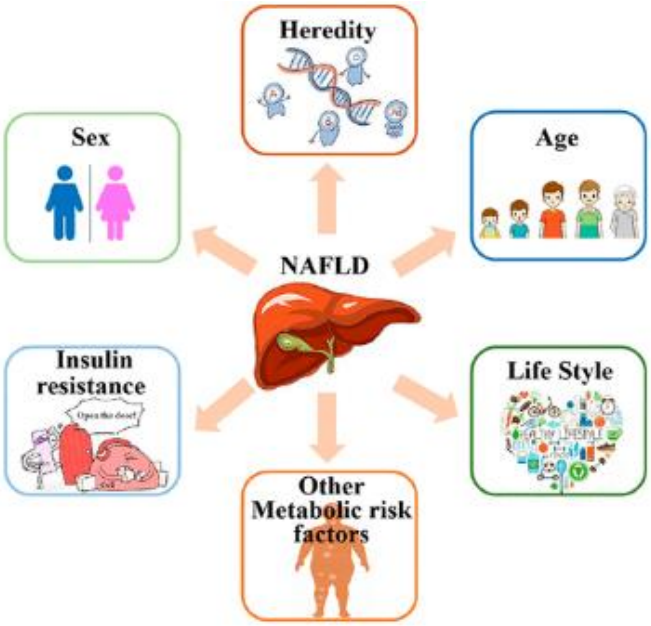

Figure 3: Illustration of the possible origins contributing to the progression and manifestation of NAFLD (adapted from Xu et al., 2023)

Since liver biopsy represents an invasive method and requires a surgery, it is not regarded as a screening method for regular practice. Therefore, additional non-invasive methods like imaging techniques (Magnetic resonance imaging, ultrasonography) are applied (Lee et al., 2013). Unfortunately, these methods are less sensitive compared to liver biopsy and therefore the latter remains the gold standard for investigating NAFLD.

The predisposition to suffer from a fatty liver can vary tremendously. It begins with the accumulation of lipids promoting the progression of NAFLD. Several other risk factors have been characterized in detail in the last couple of decades e.g., age ≥50 years, nutritional status, sedentary lifestyle, obesity, T2DM, insulin resistance and genetic disorders like papatin-like phospholipase domain-containing 3(PNPLA3) I148M polymorphism (Huang et al., 2021; Xu et al., 2023; Younossi et al., 2018). This genetic disorder results in lower plasma triacylglycerol and impaired lipolysis. Consequently excessive hepatic fat accumulation and inflammation occurs (Romeo et al., 2008). By now, the pathological mechanisms by which the progression of NAFLD is promoted is still not well understood.

1.2.2 NAFLD and the metabolic syndrome

A term that is highly associated with NALFD is the metabolic syndrome. The metabolic syndrome is not a disease itself; it is a predisposition which increases the susceptibility for cardiovascular disease, kidney disease and T2DM. Origins of the metabolic syndrome are either cause or consequence of insulin resistance in obese patients. Clinicians refer to the

metabolic syndrome when three of the following criteria are fulfilled: (1) elevated fasting glucose levels, (2) hypertriglyceridemia, (3) low high-density lipoprotein cholesterol, (4) increased waist circumference and (5) hypertension (Yki-Järvinen, 2014). The probability to be diagnosed with the metabolic syndrome is higher in obese patients, but there are also exceptions occurring. Many criteria of the metabolic syndrome can also be found in the progression of NAFLD, e.g., T2DM and hypertriglyceridemia so that a connection of the two seemed logic (Francque et al., 2021). Scientists stated that NAFLD is an independent disease not related to the metabolic syndrome; rather it goes along with the metabolic syndrome and is not exclusively concurrent. Others refer to NAFLD as the hepatic manifestation of the metabolic syndrome, but this is controversially discussed (Gastaldelli, 2017; Medina-Santillán et al., 2013). Recent activity has been made that the term NAFLD is inappropriately used, because it implies what it is *not* (non-alcoholic). As a result, it is currently stated as metabolic dysfunction-associated fatty liver disease (MASLD) which emphasizes on the metabolic disorder as a key event in the progression of a fatty liver (Chan et al., 2023; Eslam et al., 2020).

1.2.3 NAFLD and T2DM

Up to date, T2DM is affecting around 450 million people worldwide (Tanase et al., 2020). For three decades, the prevalence of this disease has continuously been increasing due to high-fat diet, sedentarism and obesity (Cloete, 2022; Fletcher et al., 2002). The clinical measure for the manifestation of T2DM is abnormally elevated fasting glucose levels, which is also often the case in patients suffering from NAFLD. Understanding the mechanisms underlying the development of T2DM in NAFLD is issue of worldwide research. It is believed that the ectopic fat accumulation in the liver of NAFLD patients is accompanied by the secretion of hepatokines inducing chronic inflammation, increased gluconeogenesis and lipogenesis, decreased glycogen synthesis and an impaired insulin signaling, which results in the manifestation of T2DM (Samuel et al., 2004; Zhang et al., 2020). Insulin resistance seems to be the key driver for the severity in both diseases, T2DM and NAFLD. Nevertheless, it is still elusive whether insulin resistance is the cause or the consequence in both disease progression (Brar and Tsukamoto, 2019). Diabetic individuals have a three times higher probability to die from a chronic liver disease, which is in most cases attributable to NAFLD (Campbell et al., 2012). Studies, aimed at understanding the relationship between T2DM and NAFLD, and considering biochemical and anthropogenic properties like serum alanine aminotransferase (AAT), gamma-glutamyl transferase (GGT), fatty liver indices or imaging techniques, have shown that

NAFLD effectively increases the risk of incidence of T2DM (Byrne and Targher, 2015). This susceptibility highly correlates also with the severity of NAFLD. However, there are exceptions where patients diagnosed with NALFD do not become obese or develop T2DM and vice versa. Regardless of this complex relationship between NAFLD and T2DM, hepatic insulin resistance results in hyperglycemia because pathways involved in glucose production by the liver, mostly gluconeogenesis, cannot be shut down by insulin and are abnormally increased.

In addition to insulin resistance, the hormone glucagon, which is the counterpart of insulin, is attributed to be a driver in the progression of NAFLD. Studies in different forms of diabetes, type 1 and type 2, displayed high levels of glucagon in the plasma (Unger and Orci, 1975). These patients suffer from excessive hepatic glucose production resulting in a hyperglycemic phenotype (Müller et al., 2017b). This highly correlates with obese patients displaying elevated levels of glucagon in the plasma. In mice, studies with glucagon receptor KO mice show improved glucose levels which was overturned when glucagon receptor was re-expressed in these mice displaying hyperglycemic, diabetic phenotype (Gelling et al., 2003; Lee et al., 2011).

Historically and even nowadays, Metformin has been the *state of the art* drug used to treat patients suffering from T2DM (Gnesin et al., 2020). However, it is not completely understood how Metformin modifies hepatic glucose metabolism in those patients. Among the various targets of Metformin, new evidence showed that the gut is a crucial facilitator. On a physiological level, it reduces hepatic glucose production by AMPK-dependent and independent pathways and by inhibition of mitochondrial respiration (LaMoia and Shulman, 2021; Rena et al., 2017). Current pharmacological approaches ameliorating T2DM and obesity focus on the generation of glucagon/Glucagon-like peptide 1 (GLP-1) agonists/antagonists preventing the excessive production of hepatic glucose and, hence, reduce body weight (Capozzi et al., 2022; Holst, 2019; Janah et al., 2019). However, inhibition of the glucagon receptor by antagonists showed poor clinical outcome and was not longer followed up on (Bergman et al., 2017; Pearson et al., 2016). A very recent drug that was approved by the FDA was the GLP-1 agonist semaglutide for treatment of T2DM and adipositas (Chao et al., 2023; Singh et al., 2022). The binding of semaglutide to the GLP1-receptor leads to the glucose-dependent secretion of insulin from the α-cells of the pancreas and the inhibition of glucagon from the β-cells from the pancreas (Nauck et al., 2021).

Due to the fact that elevated gluconeogenesis is a common hallmark of NAFLD and T2DM, targeting this pathway achieve lower blood glucose levels could be a promising approach (Barroso et al., 2024). Since, as previously stated, gluconeogenesis can be fueled by several substrates, including lactate, amino acids and glycerol, the questions arises whether limiting substrate availability can be used as a therapeutical approach (Barroso et al., 2024). For this reason it is important to understand the regulation of the gluconeogenesis flux under physiological conditions and in diseased states.

1.2.4 Extrahepatic consequences of NAFLD

1.2 4.1 Cardiovascular implications

NAFLD and CVD are both endpoints of the manifestation of the metabolic syndrome (Targher et al., 2021a). In how far one of the two diseases contribute to the progression of the other one is difficult to estimate. The mechanism that links both diseases together are very complex and involve several different pathways. What is known is that impaired glucose metabolism and hepatic insulin resistance are major hallmarks in NAFLD and crucial for the pathogenesis of CVD in NAFLD patients (Kasper et al., 2021). Targher *et al.* reported that NAFLD patients have a 64% higher risk to develop fatal or non-fatal cardiovascular events compared to patients without NAFLD (Targher et al., 2016). These include arterial hypertension, coronary artery disease and cardiac arrhythmias (Adams et al., 2017; Ryoo et al., 2014). Along with this finding, meta-analysis showed that mortality of CVD highly correlates with the severity of NAFLD (Mahfood Haddad et al., 2017). However, Wu *et al.* published no correlation between an increased mortality between NAFLD and CVD compared to healthy controls (Wu et al., 2016). This difference in outcomes between the two studies might be explained by the heterogeneity of the cohort along with co-morbidities (obesity, diabetes) and the different recruitment and diagnostic criteria of the study. Current evidence implies NAFLD to be a driving force of the development of cardiovascular CVD and cardiovascular events.

1.2.4.2 Chronic kidney disease, kidney stones and hyperoxaluria

Besides NAFLD, CKD represents an enormous health burden especially in western countries where it affects almost 25% of adults ≥65 years of age (McCullough et al., 2012). Evidence-based data shows that NAFLD is a risk- and causative factor in the development of CKD (Loomba and Sanyal, 2013). Clinically, a patient is diagnosed with CKD when the glomerular filtration rate (GFR) is decreased and/or the elevated levels of proteinuria are present (Targher et al., 2014). Other risk factors like obesity, hypertension and dyslipidemia, are very similar to

NAFLD and often associated, which makes it difficult to predict independent causative relationship. Two meta-analyses tried to decipher a potential correlation of NAFLD and CKD. Musso *et al.* reported that NAFLD independently correlates to incident and prevalent CKD compared to healthy controls. Here the correlation of NAFLD and CKD increased with the severity of NAFLD (Musso et al., 2014). This was confirmed by a very recent meta-analysis by Mantovani *et al.* involving 13 longitudinal studies accounting for over a million participants. In this study, a significant association between NAFLD and incident CKD was confirmed over a median follow-up of up to 10 years (Mantovani et al., 2022).

A subtype of CKD is the renal formation of kidney stones, which is termed renal kidney disease and can ultimately result in urolithiasis. This has become of high interest in the field of NAFLD research, as there seems to be a putative link between NAFLD and urolithiasis. Noteworthy, kidney stone formation is also highly associated with traits of the metabolic syndrome. Akarken *et al.* reported a strong correlation of obesity and kidney stone formation (Akarken et al., 2015). Furthermore, evidence exist showing hypertension and dyslipidemia to be also positively associated with the formation of kidney stones and nephrolithiasis (Ding et al., 2019; Shavit et al., 2015). Regarding NAFLD, a total of 7 longitudinal study exist investigating the correlation between NAFLD and the formation of kidney stones via different imaging techniques (Qin et al., 2018). Badillo *et al.* stated a 33% prevalence between NAFLD and urolithiasis. Importantly, when checking only steatotic patients, they observed urolithiasis in almost 75% of subjects indicating a causal relationship between these two pathologies (Lubinus Badillo et al., 2020). Another study from Einollahi *et al.* confirmed the previously described observation reporting a prevalence of 30% of NAFLD and kidney stone formation using ultra sonographic techniques (Einollahi et al., 2013). To date, different factors of the metabolic syndrome seem to boost the progression of NAFLD and the formation of kidney stones. However, how they interact mechanistically is still not well understood.

Most of the stones formed in kidney and the urinary tract are attributed to calcium oxalate precipitates. Oxalate was discussed to promote the bridge between the metabolic syndrome and CKD (Eisner et al., 2010; Kohjimoto et al., 2013). In an additional study, Walker and Brzica noticed elevated urinary levels of oxalate (termed as hyperoxaluria) as indicators in the progression of CKD (Brzica et al., 2013; Waikar et al., 2019). This is also true in the context of T2DM. In multiple studies, it was observed that T2DM patients have elevated urinary oxalate levels compared to healthy controls. Thereby, glyoxylate was found to be potential marker for

the diagnosis of T2DM in a retrospective study (Lieske et al., 2006; Meydan et al., 2003). Anyhow, the hepatic contribution of oxalate in the progression NAFLD was not elucidated.

Hyperoxaluria is a disease, which is characterized by a urinary oversaturation of calcium oxalate. This can ultimately lead to the formation of calcium crystals, contributing to urolithiasis and deposits in the kidney parenchyma. The origins for hyperoxaluria can be different: (1) inherited disorder of the glyoxylate pathway (*primary hyperoxaluria*) leading to a hepatic overproduction of oxalate, which we will focus on in the next few pages, or (2) by an increased intestinal absorption of oxalate (secondary hyperoxaluria) (Demoulin et al., 2022). In the US, the prevalence of the formation of kidney oxalate stones amounts to 10.1% reaching up to 17% for males older than 60 years. In a younger American cohort, the prevalence is increasing continuously to almost 8% (Chen et al., 2020). Different mechanisms are considered for the formation of oxalate crystals; however, the urinary oxalate concentration is one hallmark for the progression. Oxalate originates from the hepatic production or from the absorption from bowel by food (Demoulin et al., 2022).

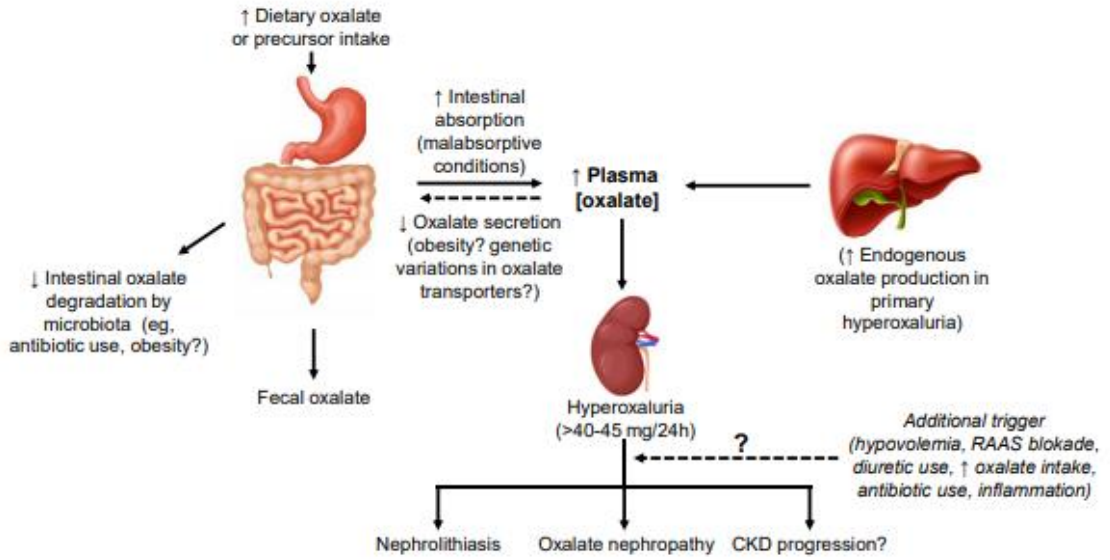

Figure 4: Dietary uptake of oxalate or precursors of oxalate can result in less intestinal oxalate degradation by microbiota. Additionally, higher intestinal malabsorption of oxalate results in less-efficient oxalate secretion resulting in elevated plasma oxalate levels. In primary hyperoxaluria, the liver produces more endogenous oxalate due to malfunctioning of respective enzymes leading to chronic kidney disease (adapted from Demoulin et al., 2022).

Food-derived products rich in oxalate are vegetables, nuts and fruits. Endogenously produced oxalate is generated as a harmful end product of the glyoxylate pathway (Cochat and Rumsby, 2013). The daily dietary intake of oxalate is 80 – 130 mg of which only approx. 15% is passively

absorbed in the gut while the rest is eliminated via the stool or urine (Ermer et al., 2016). However, there is evidence that oxalate is actively absorbed and secreted by the gut via the anion exchangers of the solute-linked carrier 26 (Slc26) family (Whittamore and Hatch, 2017). The three variants Slc26a1, Slc26a3and Slc26a6 are expressed in basolateral and apical membrane of the intestine and mediate uptake and secretion of oxalate (Ermer et al., 2016). These transporters are not only expressed in the intestine. In tubular cells of the kidney, Slc26a6 actively transports oxalate into the urinary filtrate on the apical membrane. In contrast, Slc26a1 is expressed at the basolateral membrane and reduces the urinary excretion (Bergsland et al., 2011; Bhasin et al., 2015). The excretion level of oxalate in the urine ranges from 30 – 44 mg/day. Nephrologists speak of hyperoxaluria when the oxalate levels in the urine is >45 mg/day, which predisposes the patient to develop an oversaturation of salts in the urine resulting in a precipitation of calcium oxalate crystals (Evan, 2010). By now, plasma oxalate has no purpose in mammalian blood circulation and is rapidly excreted via glomerular filtration and tubular secretion. In disease state situation like end-stage CKD, in which the kidney is not working properly anymore, plasma oxalate levels are elevated (Pfau et al., 2020). The consequences of high levels of plasma oxalate are very broad ranging from oxalosis, atherosclerosis in the cardiac system and, hence, sudden cardiac death (Liu et al., 2021).

1.2.4.3 A molecular linkage between NAFLD and hyperoxaluria: Agxt promotor hypermethylation in steatosis

Despite the strong association between NAFLD and risk of kidney stone formation, the molecular mechanism explaining this association are largely unknown. A study conducted in our group at IfADo in collaboration with the DEEP consortium (Gianmoena et al., 2021) revealed a mechanism that could explain why patients suffering from NAFLD are at higher risk of hyperoxaluria. The study showed that genes involved in the detoxification of glyoxylate are altered in the steatotic liver, resulting in insufficient detoxification of glyoxylate and thus excessive formation of oxalate. In particular, the authors reported a hypermethylation in the promotor region of the alanine-glyoxylate aminotransferase (Agxt) as reason for this malfunction (Gianmoena, 2017).

The study was initiated with the goal of understanding the role of epigenetic modifications in the progression of NAFLD. To identify transcriptomic and epigenetic fingerprints in NAFLD in human and mice, publicly available genome-wide data sets of patients suffering from NASH, cirrhosis and liver carcinoma were obtained and compared to those of mice models mimicking

NAFLD, e.g. leptin deficient obese/obese (ob/ob) mice model. In a subsequent step, mRNA expression via RNA-Seq as well as DNA methylation (by RRBS) were investigated in ob/+ (control) and ob/ob (steatotic) liver tissue and hepatocytes. Further, chromatin accessibility was also analyzed by DNase I-seq. To draw conclusions on the received data, differently methylated regions (DMRs) and differently open region (DORs) were put in context to the gene expression patterns of ob/ob and ob/+. From this data, 649 differently expressed genes (DEGs) were related to DMRs or DORs. Of the 649 DEGs in mice and the 62 DEGs from human data sets, 12 were found to be deregulated in NAFLD in both, human as well as in mice (Gianmoena et al., 2021). Among the 12 deregulated genes, Agxt was one of the downregulated genes in the steatotic liver of human and mice, and also accompanied with hypermethylation of its promoter and less chromatin accessibility (Gianmoena, 2017), two epigenetic alterations that are usually associated with decreased transcription. In addition, it was shown that the downregulation of Agxt was accompanied by elevated urinary excretion and lower levels of hepatic glycine in the ob/ob steatotic mouse model. Thus, this observation indicated a physiological role for Agxt in preventing hyperoxaluria in NAFLD. *In vitro*, steatotic hepatocytes derived from ob/ob mice were also more susceptible to produce oxalate when exposed to the precursor hydroxyproline in comparison to ob/+-control hepatocytes (Gianmoena et al., 2021). Further, the epigenetic analysis in human hepatoctyes from NAFLD donors also revealed a hypermethylation in the promotor region of AGXT as a possible cause for its downregulation. This would imply a steatosis-associated downregulation and silencing of Agxt, which was further confirmed in a second mouse model of NAFLD, feeding mice with a high caloric Western-diet . However, downregulation but not hypermethylation of Agxt was reported in an inducible *in vitro* model of steatosis generated by feeding hepatocytes with oleic acid. This leads to the assumption that other factors or regulatory mechanisms, and not necessarily promoter hypermethylation, are causally involved in the downregulation of Agxt in the context of NAFLD, or, alternatively, that the contribution of epigenetic mechanisms is only observed *in vivo* and not in vitro (Gianmoena, 2017).

Despite this uncertainty, this study was the first one to reveal that a downregulation of Agxt occurs in the fatty liver and that this may provide and explanation for the higher risk of hyperoxaluria in NAFLD patients.

1.3 The role of Agxt in hyperoxaluria

1.3.1 Hepatic formation of oxalate

Erythrocytes and mostly the liver are responsible for the endogenous production of oxalate (Baker et al., 2004; Holmes et al., 2001). The liver produces glyoxylate, which is the direct precursor of oxalate, and also mediates the detoxification of glyoxylate. This pathway is termed the glyoxylate pathway. Oxalate is a harmful waste product of the glyoxylate pathway that is generated when glyoxylate detoxification is insufficient or when overproduction exceeds its detoxification. As described in the chapter before, two types of hyperoxaluria exist, primary and secondary hyperoxaluria. Three pathogenic variants of the genes AGXT (alanine: glyoxylate-aminotransferase; Serine: pyruvate aminotransferase), GRHR (glyoxylate reductase–hydroxypyruvate reductase) and HOGA1 (4-hydroxy-2-oxoglutarate aldolase) are responsible for the primary hyperoxaluria type 1,2 and 3 (Cochat and Rumsby, 2013). In PH1 and PH2, the impaired conversion of glyoxylate to glycine or glycolate respectively leads to an increased conversion of glyoxylate to oxalate. In PH3, the situation is more complex. PH3 is characterized by a mutation in the HOGA1 gene encoding for a mitochondrial aldolase that facilitates the breakdown 4-hydroxy-2-oxoglutarate downstream of the hydroxyproline catabolism (Belostotsky et al., 2010; Kemper et al., 1997). If this protein is malfunctioning, glyoxylate is formed by other cytosolic aldolases causing elevated levels of oxalate.

All three primary hyperoxalurias lead to hepatic overproduction of oxalate and subsequent hyperoxaluria, oxalemia and eventually accumulation of oxalate in other organs. Comparing all three variants, primary hyperoxaluria 1 is the most common and severe form of hyperoxaluria causing kidney failure within the first three decades (Hoppe, 2012).

The current therapy options for people suffering from various types of hyperoxaluria remains a liver transplantation or a simultaneous liver/kidney transplantation (Devresse et al., 2020). But there has been successful market access approved by FDA with *Lumasiran*, which is a RNA interference (RNAi)-therapy showing additional treatment options for hyperoxaluria. The mode of action of Lumasiran is based on to shut down the enzyme encoded by the gene HAO1 (Hydroxyacid oxidase 1) to diminish glyoxylate synthesis and oxalate generation (Garrelfs et al., 2021).

One of the best-known sources of glyoxylate is the catabolism of hydroxyproline in the mitochondria of hepatocytes (see Fig. 3). Hydroxyproline is derived from collagen-rich food,

e.g. meat and gelatin, or from the endogenous breakdown of collagen, which is not reused any longer (Phang, 2022; Salido et al., 2012). The daily turnover of hydroxyproline is up to 400 mg and results in a maximum of 240 mg glyoxylate available for metabolism per day (Knight et al., 2006). Due to the toxic property of glyoxylate, it is important to metabolize it to a less harmful product. In liver mitochondria, GRHPR catalizes the conversion of glyoxylate to glycolate (see Fig. 5). In mice, in addition to Grhpr, also Agxt in the present in the mitochondria and catalyzes the transamination of glyoxylate to glycine. In the peroxisomes, the hydroxyacid oxidase 1 (Hao1/GO) converts glycolate to glyoxylate, which is subsequently detoxyfied by peroxisomal AGXT/Agxt to glycine (see Fig. 5). It is believed that any excess of glyoxylate can shuttle into the cytosol where it is metabolized to oxalate by lactate dehydrogenase (LDH) (Salido et al., 2012) (see Fig. 5). This reaction should be prevented at any cost, because high levels of oxalate are unfavorable for the organ and organism. The key enzymes Agxt and Grhpr are therefore essential to prevent excessive conversion of glyoxylate to oxalate. To what extent each of these key enzymes contributes, is difficult to predict because glyoxylate pathway intermediates can shuttle within the different organelles of hepatocytes due to their anionic structure, making it difficult to establish a general pathway (Rokka et al., 2009).

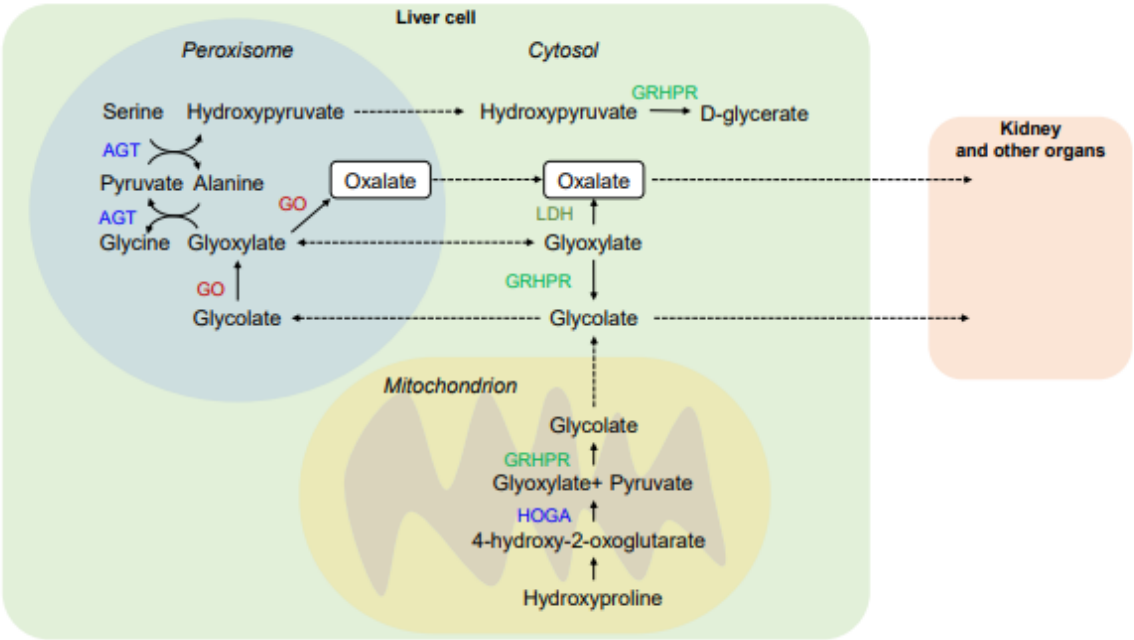

Figure 5: Schematic illustration of the glyoxylate metabolism in the hepatocytes and its genetic deficiencies in PH. PH1 and PH2 indicated by a downregulation of AGXT (blue) and GRHPR (light green),which results in accumulation of glyoxylate, which is further metabolized by LDH to oxalate. PH3 is the consequence of malfunctioning of HOGA (blue)(adapted from Demoulin et al., 2022).

Unlike in mice, human AGXT expression is limited to the peroxisome (Cellini et al., 2007). In the next chapter, the focus will be on the role of Agxt.

1.3.1 Alanine: glyoxylate aminotransferase

1.3.1.1 Subcellular distribution

Foremost, Agxt was characterized in 1978 in the rat liver (Noguchi and Takada, 1978). Agxt is a pyridoxal 5'-phosphate-dependent enzyme having a molecular weight of approx. 43.6 kDa (Cochat and Rumsby, 2013). Its protein catalyzes the transamination of alanine to detoxify glyoxylate, which results in the two products glycine and pyruvate (see Fig. 6). The fate of those two products will not be further addressed.

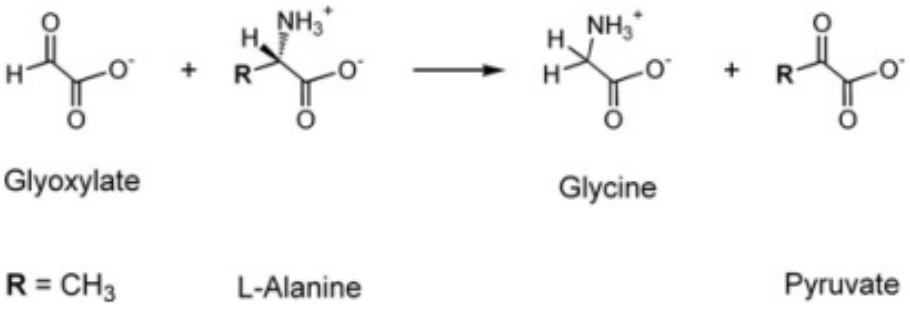

Figure 6: Illustration of the detoxifying reaction mediated by Agxt. L-alanine is deaminated and glyoxylate represents the amino group acceptor producing glycine. As a result of the deamination of L-Alanine, pyruvate is produced (adapted from Donini et al., 2009).

The localization of Agxt in the organelles differs in animals depending on their nutritional habits. In herbivores, where glycolate represents a precursor of glyoxylate and is highly abundant in the diet, Agxt is present in the peroxisome. In contrast, in carnivores, Agxt expression is restricted to mitochondria because of excessive production of glyoxylate derived from hydroxyproline in this organelle. In omnivores, Agxt is expressed in both compartments, peroxisomal and mitochondrial (Birdsey et al., 2004; Danpure, 1997).

By now, more than 190 mutations of the Agxt gene have been identified, the majority of which affect its enzymatic activity. In addition, some mutations lead to mistargeting of AGXT, resulting in transport of AGXT to the mitochondria instead of the peroxisome, with the most prominent one, G170R, accounting for up to 30% of mutant alleles (Hopp et al., 2015). Targeting of AGXT to the peroxisome is facilitated by the peroxisomal targeting sequence type 1 (PTS1) which binds to PTS1 receptor Pexp5 and shuttles into the peroxisome. A minor allele of AGXT present in the human population encodes an N-terminal mitochondrial targeting

sequence (MTS). However, this MTS motif is rather ineffective and results in import of only up to 5% Agxt protein to the mitochondria (Purdue et al., 1990). In addition, AGXT is known to form dimers and dimerization could influence peroxisomal trafficking. In 2021, a study reported that mistrafficking is related to a lack in protein dimerization (Dindo et al., 2021).

In comparison to this, subcellular localization of mouse Agxt is determined by the expression of two different Agxt transcripts, one with and one without MTS. This explains the expression of Agxt in both compartments, peroxisome and mitochondria in mice (Li et al., 1999). Regarding the homology of genes between the two species, human and mice, the identity is very similar for gene expression as well as protein, 75 % and 76 % respectively.

A second less prominent reaction facilitated by Agxt is the conversion of serine to hydroxypruvate, which is considered to play a role in the gluconeogenesis and will be addressed in a later chapter (Donini et al., 2009; Noguchi and Takada, 1978).

1.3.1.2 Transcriptional regulation and activity of Agxt

In 1969, Roswell initially reported a potential role for Agxt in gluconeogenesis, when rat Agxt was induced by the hormonal stimulus of glucagon (Rowsell et al., 1969). The stimulation was mediated by the PKA/cAMP/CREB pathway and was confirmed by an independent stimulus experiment in rats using glucagon and cAMP (Uchida et al., 1994). It is known that the rat Agxt gene contains a cAMP responsive element (CRE) sequence as well as a glucocorticoid responsive element (GRE) sequence, which is also conserved in the mouse Agxt gene (Oda et al., 1990). Moreover, the glucagon and cAMP treatments showed that the enzymatic activity of Agxt was also elevated (Li et al., 1999). Of note, even though Agxt is expressed in peroxisome and mitochondria in mice, mRNA induction was only observed for the mitochondrial transcript (Ferrara et al., 2008). There is additional evidence that also insulin can induce *Agxt* mRNA upregulation in mice and rat (Miyajima et al., 1989). However, its physiological function has not been further elucidated.

1.4 The role of Agxt in gluconeogenesis

1.4.1 Serine: pyruvate aminotransferase activity

As already mentioned, Agxt catalyzes two different reaction. The first reaction, which Agxt is primarily known for, is the detoxification of glyoxylate to form glycine and pyruvate. The second reaction is the serine:pyruvate transamination (Agxt/Spt), high levels of which are found in carnivores. With L-serine being one of the main glucogenic amino acids in several

vertebrates, it represents a reaction that is not considered at the forefront of gluconeogenesis, but should be considered when amino-acid driven gluconeogenesis is taking place (Youngson et al., 1982). Spt converts L-serine and pyruvate to hydroxypyruvate and L-alanine (Noguchi and Takada, 1978). The newly formed hydroxypruvate can be used in subsequent reactions to form glucose via D-glycerate (see Fig. 7). However, the relevance of this reaction in gluconeogenesis has not been further elucidated by now.

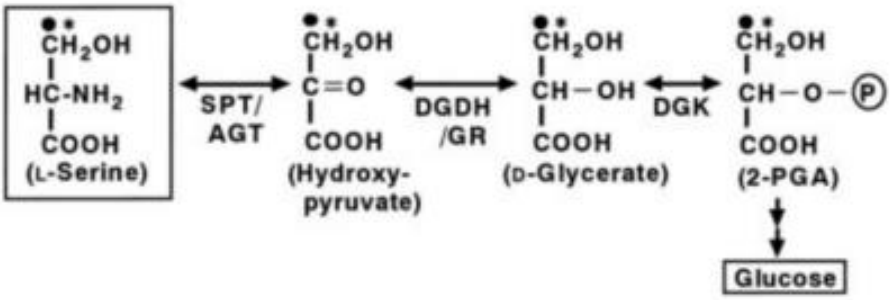

Figure 7*:* A possible involvement of Agxt in gluconeogenesis (adapted from Xue et al., 1999).

1.4.2 Evidence for a contribution of Agxt in amino-acid driven gluconeogenesis

Recently, Just *et al*. showed a new mechanism by which liver kinase b1 (Lkb1) suppresses amino acid-driven gluconeogenesis. Lkb1 resembles a serine/threonine kinase which phosphorylates and activates AMPK. AMPK itself is a metabolic sensor, which orchestrates many different metabolic pathway. Among those pathways is the glucose metabolism that is taking place mainly in the liver (Steinberg and Hardie, 2023). The authors showed that in a liver-specific KO of Lkb1 the amino acid-driven gluconeogenesis was enhanced at the expense of the muscle tissue, which ultimately led to cachexia and sarcopenia in those mice. Accompanying this effect, Agxt was upregulated, showing that Agxt was one of the downstream targets of Lkb1 and that it acts as an effector of Lkb1 suppression (Just et al., 2020). This justifies investigating a possible role for Agxt in gluconeogenesis. Together with the previous findings, which reported that Agxt facilitates the conversion of L-serine, which is a common one-carbon unit utilized for the generation of glucose via hydroxypruvate (Xue et al., 1999), it seems highly relevant to understand in how far Agxt leads to changes in amino-acid driven gluconeogenesis (see Fig. 7).

1.4.3 Inhibition of gluconeogenesis by oxalate

Agxts´ main function is to detoxify glyoxylate to prevent the formation of the toxic waste product oxalate . Interestingly, in addition to its poor solubility and its tendency to precipitate

as calcium oxalate, oxalate appears to exert additional effects by its ability to inhibit several metabolic enzymes that use pyruvate as a substrate, including pyruvate kinase and pyruvate carboxylase (Reed and Morgan, 1974; Yount and Harris, 1980). As previously mentioned, pyruvate carboxylase is important for both gluconeogenesis and the TCA cycle. Little is known about the consequences oxalate has on gluconeogenesis. In 1980, Yount *et al.* investigated the effect of oxalate on gluconeogenesis. They showed that oxalate inhibits gluconeogenesis from pyruvate/lactate and amino acids except for glutamine and dihydroxyacetone, which is an intermediate in the glycerol-derived gluconeogenesis. Mechanistically, they proposed that this effect is due to the inhibition of pyruvate carboxylase (Yount and Harris, 1980). In line with this, Buc *et al.* also reported an inhibitory effect of oxalate on the tricarboxylic acid cycle via Pc inhibition indirectly affecting gluconeogenesis (Buc et al., 1983). Similar results are obtained from a study in which perfused rat liver was co-administrated with oxalate and glucogenic precursors. Oxalate affected glucose production from pyruvate/lactate and amino acids, inhibited glycolysis and triggered glycogenolysis. Glycerol and glycerol-derived precursors were not affected in glucose production (Tonon et al., 1998).

All these findings suggest that a high concentration of oxalate within the hepatocytes may compromise the flux of pyruvate/lactate and selected amino acids towards gluconeogenesis. Therefore, Agxt, as an enzyme that prevents excessive formation of oxalate, should indirectly support gluconeogenesis. This concept is the main focus of this thesis.

1.5 Aim of this work

Increased gluconeogenesis results in fasting hyperglycemia and is a common hallmark of NAFLD and T2DM. Therefore, targeting this pathway to lower blood glucose levels could be a promising approach. Indeed, inhibitors of gluconeogenesis have been developed to treat T2DM. Since gluconeogenesis can be fueled by several substrates, including lactate, amino acids and glycerol, an open question is whether limiting substrate availability can be used as a therapeutical approach. For this reason it is important to understand the regulation of the gluconeogenesis flux under physiological conditions and in diseased states (Barroso et al., 2024). Which substrate is used at a given time and which factors determine substrate preference is still not understood.

Recent research has demonstrated the impact of an elevated activity of liver transaminases in T2DM by promoting gluconeogenesis from alanine, thereby leading to hyperglycemia and

muscle wasting (Okun et al., 2021). Among the liver transaminases, Agxt, is well known for its crucial role in the detoxification of glyoxylate and prevention of high oxalate production by the liver (Bacchetta and Lieske, 2022). However, despite some research indicating a possible role of Agxt in gluconeogenesis (Just et al., 2020; Li et al., 1999), the contribution of Agxt to glucose homeostasis remains elusive.

The harmful effects of oxalate in the body have been mostly attributed to its poor solubility and its ability to form calcium oxalate stones in the kidney. However, evidence is reported of a possible inhibitory role of oxalate on gluconeogenesis via pyruvate carboxylase. This suggests that Agxt could influence gluconeogenesis by regulating oxalate production in the liver. Increasing Agxt expression, and consequently avoiding oxalate production, should allow the gluconeogenesis flux via pyruvate carboxylase. Conversely, decreasing Agxt expression should lead to the opposite effect.

Hence, one of the goals in this thesis was to confirm the inhibitory properties of oxalate on the production of glucose and the substrate utilization for gluconeogenesis. To this aim, an *in vitro* hepatic glucose production assay (HGP) should be established which should recapitulate gluconeogenesis from different gluconeogenic substrates, and that could subsequently be used to assess in detail the influence of oxalate in this process in a concentration-dependent manner.

In addition to studying the possible inhibitory effects of oxalate on gluconeogenesis *in vitro*, a further major goal of this work was to identify whether such effects are also observed *in vivo* and whether they would translate to systemic complications in glucose homeostasis. A mouse model suitable for this analysis would be a hyperoxaluric mice model, such as AgxtKO mice, characterized by its high oxalate production, which is shown by high oxalate concentration in plasma and in the urine. Here, Agxt deficiency would be indirectly causing an effect on gluconeogenesis pathways *via* oxalate. To investigate this, the AgxtKO mice should be studied in fasting conditions, in which the gluconeogenesis pathway is essential for the maintenance of blood glucose, and several different parameters, e.g. blood glucose, gene expression in the liver and in the kidney, amino acid profile should be recorded. The questions that should be answered in this mouse model are, whether hepatic or renal amino acid utilization for gluconeogenesis is affected by the high oxalate burden in this mouse model and whether this results in a phenotypical alteration or can be compensated. One potential scenario could be

that overall glucose homeostasis itself is not affected, but that the hyperoxaluric AgxtKO mice might compensate by adapting its substrate utilization, e.g. increased glycerol, and organ contribution to maintain glucose levels (see Fig. 8).

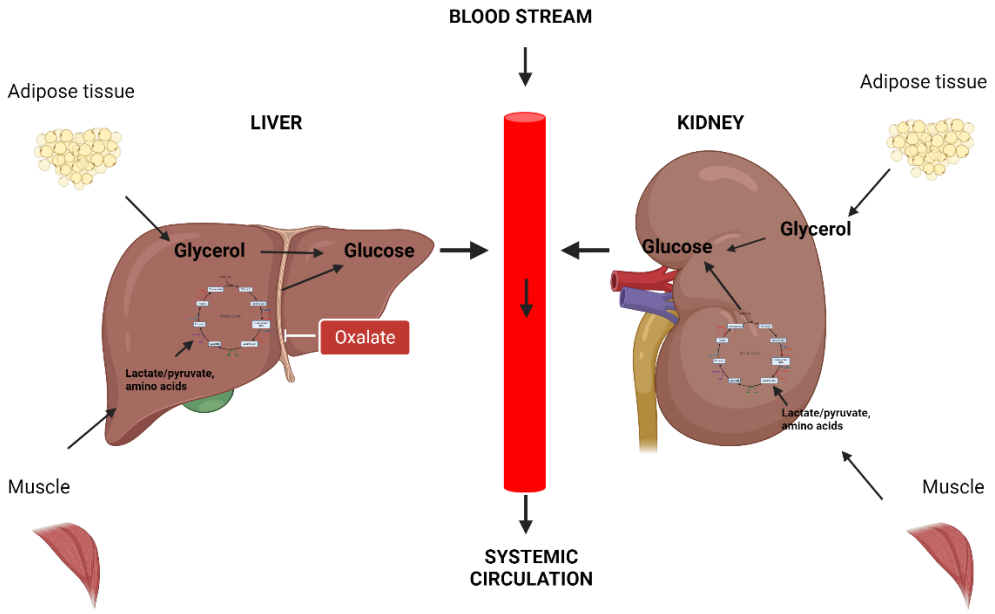

Figure 8: The current hypothesis claims that due to elevated levels of oxalate in the liver inhibition of key enzyme in TCA cycle takes place, which leads to a compromisation of glucose production under fasting conditions in hyperoxaluric mice. This figure was created with BioRender.com

Finally, the significance of the glucagon-stimulated upregulation of Agxt in gluconeogenesis should be investigated. There is evidence that glucagon induces Agxt via the PKA/cAMP/CREB pathway, but its influence on glucose production is still unclear. Therefore, a third goal of this thesis was to investigate the expresssion of Agxt *in vivo* in response to glucagon as well as in vitro in response to glucogenic substrates to draw possible conclusion about its contribution to glucose homeostasis.

Previous work at IfADo had shown that Agxt is downregulated in human NAFLD and also in mouse models of NAFLD (ob/ob and Western diet-induced), which was accompanied by increased oxalate production when challenged with a the precursor hydroxyproline (Gianmoena et al., 2017). However, a causal role for Agxt in this process was not formally proofed. Therefore, one further goal of this work was to demonstrate the role of Agxt in oxalate production in a mouse model of NAFLD (ob/ob) by rescue experiments using adeno-associated viral transfer. These experiments, which will be described in this thesis, resulted in the publication of the final study (Gianmoena et al., 2021).

2 Material and methods

2.1 Material

2.1.1 Technical equipment

Table 1: Equipment

Equipment	**Company**
Autoclave Systec VX-150	Systex
Autosampler Sil-20AC cr	Shimadzu
Balance	EW, Kern
Bunsen Brenner	IBS Fireboy Plus, Integra Biosciences
Blot Imager Vilber Fusion Fx7	Vilber Lourmat
Centrifuge with cooling function	Biofuge Fresco, Heraeus
Centrifuge with cooling function 5424R	Eppendorf
Centrifuge MiniSpin plus	Eppendorf
CO_2 ncubator C150R Hinge	Binder
Electrophoresis unit Mini-Protean®	BioRad
Electrophoresis unit SE260	Höfer
EVOQ™ Elite Triple Quadrupole	Bruker
Fume hood	Waldner
LC system LC-20AD XR	Shimadzu
LC column: PL Hi-Plex-H (100x4mm)	Agilent
Magnetic stirrer IKAMAG RCT	Ikamag
Microscope BX41	Olympus
Microscope eclipse TsS100	Nikon
Microscope Primo Vert	Zeiss, Software Zen from Zeiss
Microwave oven	Bosch
MiSeq	Illumina
Modular tissue embedding center	Thermo Fisher Scientific
Nanodrop ND-1000	Thermo Fisher Scientific
pH meter	Schott
Pipettes (2 µL, 10 µL, 20 µL, 100 µL, 200 µL; 500 µL, 1000 µL, 5000 µL	Eppendorf

Pipet boy	Inetgra
Plate reader infinite M200 Pro	Tecan
Power pack HC	BioRad
Power pack P25T	Biometra
Precision balance EW150-3M	Kern
Precision balance ME235P	Sartorius
qPCR system ABI7500	Applied Biosystem
QTRAP 5500 LC-MS/MS system	Sciex
Rocking platform	VWR
Shaker KS260	IKA
Slide drying oven TDO SAHARA	Medite
Sliding microtome HM450	Microm
Sonicator sonoplus mono	Bandelin
Spin tissue Processor STP120	Thermo Fisher Scientific
Sterile hood	Hereaus
Thermo cycler T gradient	Biometra
Thermomixer	Eppendorf
Thermo shaker PHMT Grant-bio	Keison
Thermo shaker	Peqlab
Transfer chamber fast blot B44	Biometra
Transfer chamber Trans-Blot SD	BioRad
Vacuum pump	Vacuubrand
Vortex-Genie2	Bender & Hobein
Water purification	Maxima Ultra-Pure Water, ELGA
Water purification system	Milli-Q® Integral 15 System, Merck
Waterbath	GFL 1083, Gesellschaft für Labortechnik
Waterbath	Precision GP28 Thermo Scientific

2.1.2 Consumables

Table 2: Consumables

Consumable	**Company**
Cell scraper	Sarsted
Cover slips	VWR
Embedding cassettes	Carl Roth
Glass inserts, 200L	VWR
Glass vials (1,5 mL – 4 mL)	VWR
Metabolic cages for single mouse	Tecniplast
MicroAmp® Optical Adhesive Film	Thermo Fisher Scientific
MicroAMP® Optical 96-Well Reaction plate	Thermo Fisher Scientific
Microscope slide Superfrost Plus	Thermo Fisher Scientific
Minsart® syringe filter (0.45µM)	Sartorius
Needle (22, 24, 26G)	BD Bioscience
NuPAGE®4- 12% Bis-Tris	Thermo Fisher Scientific
Pestle and Microtube	VWR
Pipette tips (filtered/non-filtered)	Eppendorf
PVDF Membrane	Perkin Elmer
PCR SInglCAP 8er-Softstrips 0.2mL	Biozym Scientific
RNase-free Microfuge Tubes 1.5mL	Thermo Fisher Scientific
Reaction tubes (0.5 mL-50mL)	Sarstedt
Serological pipets (5 mL, 10 mL, 25 mL, 50 mL)	Sarstedt
Syringe 1 mL	BD bioscience
Tissue culture plates (6-,12-,24-,96-well format)	Sarsted
95-well plates black	Greiner Bio
96-well plates transparent	Greiner, Sarstedt
Whatman paper 3mm	VWR
Thick Blot Filter paper, Precut	BioRad

2.1.3 Chemicals and Dyes

Table 3: Chemicals and dyes

Chemicals/Dyes	**Company**
Acetic acid	Carl Roth
Acrylamide (30% (v/v))	PAN Biotech
Alanine	Sigma Aldrich
Amino acid solution	PAN Biotech
Ammonium persulfate	Sigma Aldrich
Bovine serum albumin (BSA)	Carl Roth
Bovine serum albumin, fatty acid free	Sigma Aldrich
Bromophenol blue	Carl Roth
Calcium chloride	Carl Roth
Chloroform	Carl Roth
Citric acid monohydrate	Carl Roth
Collagenase from Clostridium histolyticum	Sigma Aldrich
p-Coumaric acid	Sigma Aldrich
Creatinine hydrochloride	Sigma Aldrich
Dimethylsulfoxide (DMSO)	Sigma Aldrich
Dithiothreitol (DTT)	Sigma Aldrich
Triethylene glycol diamine tetra acetic acid (EGTA)	Carl Roth
Entellan®	Merck
Eosin Y disodium salt	Sigma Aldrich
Ethanol, absolute	Carl Roth
Ethylene diamine tetra acetic acid (EDTA)	Carl Roth
Fetal Calf Serum (FCS), Sera Plus	PAN Biotech
FluorPreserve reagent	Calbiochem
Glucagon	Cayman Chemicals
Glucose	Carl Roth
L-Glutamine	Sigma Aldrich
Glycerol	Sigma Aldrich

Glycine	Carl Roth
HEPES	Carl Roth
Hydrochloric acid, 32%	Carl Roth
Hydrogen peroxide, 30%	Merck
L-Hydroxyproline	ApplChem
L-lactic acid	Sigma Aldrich
Luminol	Sigma Aldrich
Magnesium chloride	Carl Roth
Magnesium sulphate	Sigma Aldrich
Methanol, HPLC grade	Carl Roth
Nonidet P-40 substitute (NP-40)	Roche
Paraffin Histoway Surgipath paraplast	Leica
Paraformaldehyde 4% (PFA)	Carl Roth
Picric acid	Sigma Aldrich
Potassium chloride	Carl Roth
Potassium dydrogen phosphate	Carl Roth
2-Propanol	Carl Roth
Rotihistol	Carl Roth
SDS pellets	Carl Roth
Sodium chloride	Carl Roth
Sodium deoxycholate	Carl Roth
Sodium glycolate	Carl Roth
Sodium hydrogen phosphate	Carl Roth
Sodium hydroxide pellets	Carl Roth
Sodium pyruvate	Sigma Aldrich
Tetramethylethylenediamine (TEMED)	Carl Roth
Tris	Carl Roth
Tris-HCl	Carl Roth
TritonX-100	Sigma Aldrich
Tween20	Sigma Aldrich
Tween80	Sigma Aldrich

Xylol	VWR

2.1.4 Commercial buffers and reagents

Table 4: Commercial buffer and reagents

Buffer/reagent	Company
Anode-/Cathode-bufffer concentrate A & K	Carl Roth
Diethylpyrocarbonate treated (DEPC) water	Thermo Fisher scientific
Duotrol® urine level 1 + 2	Biomed Labordiagnostik GmbH
Ketamine 100 mg/mL	Ratipharm
Mayer's Haemalaun solution	Merck
NuPAGE® MES SDS Running Buffer (20x)	Thermo Fisher Scientific
Phosphate Inhibitor Cocktail II,III	Sigma Aldrich
Precision Plus Protein Dual color standards	BioRad
Protease-Inhibitor cocktail	Sigma Aldrich
QIAzol Lysis-Reagent	Qiagen
Rompun 2%	Bayer Health Care
TaqMan Universal PCR Master Mix	Thermo Fisher Scientific

2.1.5 Prepared buffers and reagents

Table 5: Prepared buffered and reagents

Buffer	Substances	Concentration
Anode buffer	Buffer concentrate A Methanol Ultrapure water	10% 20% 70%
APS solution	Ammonium persulfate in ultrapure water	10% (w/v)
Blocking solution	BSA in TBS-T	5% (w/v)
Cathode Buffer	Buffer concentrate K Methanol Ultrapure water	10% 20% 70%

Chemiluminescent solution	Luminol p-Coumaric acid in 0.1 M Tris	2.5 mM 0.2 mM
Glucose Production Buffer	DMEM HEPES Sodium pyruvate Lactic acid	 10 mM 2 mM 20 mM
Loading buffer	Bromophenol blue DTT Glycerol SDS Tris-HCl	0.05% (w/v) 0.25 M 50% (w/v) 5% (w/v) 0.225 M
PBS (10x)	KCl KH_2PO_4 Na_2HPO_4 NaCl in ultrapure water	27 mM 18 mM 100 mM 1.37 M
RIPA Buffer	Tris-HCl NaCl NP-40 Sodium deoxycholate SDS	50 mM (pH 7.5) 150 mM 1% 0.5% 0.5%
Running Buffer (10x)	Glycine SDS Tris in ultrapure water, pH 8.3	1.92 M 1% 0.25 M
SDS Solution	SDS in ultrapure water	10% (w/v)
Separation buffer	Tris in ultrapure water, pH 8.8	3 M
Stacking buffer	Tris in ultrapure water, pH 6.8	0.47M

Stripping buffer	Glycine SDS Tween20 In ultrapure water, pH 2.2	0.2 M 0.1% (w/v) 1% (v/v)
TBS (10x)	NaCl Tris in ultrapure water, pH 7.4	1.5 M 0.5 M
TBS-T	10x TBS Tween20	10% (v/v) 1% (v/v)

Table 6: Buffers for histological stainings

Buffer	**Substance**	**Concentration**
Citrate buffer	Citrate 1xH_2O in ultrapure water, pH 6	0.01 M
Haematoxylin	Mayer's Haemalaun in ultrapure water	20% (v/v)

Table 7: Perfusion buffers

Buffer	**Substance**	**Concentration**
Collagenase Buffer	Amino acid solution $CaCl_2$ solution (19g/L $CaCl_2$*2 H_2O) Collagenase Type 1 Glucose solution (9g/L) Glutamine (7g/mL) Hepes (60g/L, pH 8.5) KH Buffer	30 mL 10 mL 100 mg 155 mL 2.5 mL 25 mL 25 mL
EGTA Buffer	Amino acid solution EGTA solution (47.5g/L) Glucose solution (9g/L)	60 mL 1.6 mL 248 mL

	Glutamine (7g/L) Hepes (60g/L) KH buffer	4 mL 30 mL 30 mL
KH Buffer	KCl KH_2PO_4 NaCl In 1L ultrapure water, pH 7.4	1.75 g 1.6 g 60 g
Suspension Buffer	Albumin Fraction V Amino acid solution $CaCl_2$ solution (19g/L $CaCl_2$*2 H_2O) Glucose solution (9g/L) Glutamine (7g/L) HEPES KH buffer $MgSO_4$ solution (24.6g/L $MgSO_4$* 7 H_2O)	400 mg 30 mL 1.6 mL 124 mL 2 mL 20 mL 20 mL 0.8 mL

Table 8: Commercial assay and kits

Kits	**Company**
BCA Protein assay	Thermo Fisher Scientific
CellTiter-Blue® assay	Promega
DAB Peroxidase substrate kit	Vector laboratories
Glucagon assay	Mercodia
High-Capacitiy cDNA Reverse Transcription Kit	Thermo Fisher Scientific
Insulin assay	Mercodia
Vectastain Elite ABC Kit (rabbit)	Vector laboratories

2.1.6 Cell culture constituents

Table 9: Medium and supplements

Cells	Medium	Company
Primary human and mouse hepatocytes	William's E Medium + Dexamethasone (100nM) + Gentamycine (10µg/mL) + Insulin (ITS) (2ng/mL) + Penicilin/Streptomycin (100 U/mL) + Stable L-Glutamine (2mM) For attaching of cells: + 10% Sera plus	PAN Biotech Sigma Aldrich PAN Biotech Sigma Aldrich PAN Biotech PAN Biotech PAN Biotech
Primary human and mouse hepatocytes	Glucose-free DMEM Medium + Penicilin/Streptomycin (100U/mL)	PAN Biotech

Table 10: Additional supplements for cell culture

Supplement	Company
Acetic acid glacial	Carl Roth
Casyton	Roche
Collagen rat tail lypholised	Roche
Dexamethasone	Sigma Aldrich
DMEM (10x, 1 g/L glucose)	Pan Biotech
DMSO	Sigma Aldrich
OptiMEM	Life technologies
10x PBS	See table 2.5
Trypan blue	Sigma Aldrich
Trypsin 0.05% EDTA	Pan Biotech

2.1.7 Animals

Table 11: Mice

Mouse	Gender	Age at experiment	Provider
$Agxt^{-/-}$	male/female	8-12 weeks	Eduardo Salido
Lep^{ob}/Lep^{ob} and $Lep^{ob/+}$	male	8-12 weeks	Janvier labs
C57BL6/J	male/female	8-12 weeks	Janvier labs

Table 12: Mice feeding

Reagents	Company
Pellet standard diet R/M-10-mm	Ssniff, Soest, Germany
Powder standard diet R/M-H	Ssniff, Soest, Germany
R/M-H 10-mm pellet with 1% hydroxyprolin	Ssniff, Soest, Germany

2.1.8 Antibodies

2.1.8.1 Primary antibodies

Table 13: Primary antibodies for Western blotting and Immunhistochemistry

Antibody	Host	Cat-No./ Company
anti Agxt	Rabbit	HPA035370, Sigma Aldrich
Anti-G6pc	Rabbit	22169-1-AP, Proteintech
anti Gyk	Rabbit	MA5-36209, Thermo Fisher
anti Pck1	Rabbit	ab70358, Abcam
Anti β-aktin	Mouse	A5316, Sigma Aldrich

2.1.8.2 Secondary antibodies

Table 14: Secondary antibodies for Western Blotting

Antibody	Host	Cat-No./ Company
anti-mouse HRP-linked	Horse	7076, Cell Signaling
anti-rabbit HRP-linked	Goat	7074, Cell Signaling

2.1.9 TaqMan gene expression assays

Table 15: Taqman gene expression assay for qRT-PCR (Life technologies)

Target gene	Mouse	Supplier
Agxt	Mm00507980	Life technologies, Darmstadt
Eif2a	Mm01289723	Life technologies, Darmstadt
Fbp1	Mm00490181	Life technologies, Darmstadt
Gapdh	4352932E	Life technologies, Darmstadt
G6pc	Mm00839363	Life technologies, Darmstadt
Got1	Mm01195792	Life technologies, Darmstadt
Gpd1	Mm00515846	Life technologies, Darmstadt
Gpt1	Mm00805379	Life technologies, Darmstadt
Grhpr	Mm00519119	Life technologies, Darmstadt
Gyk	Mm00433896	Life technologies, Darmstadt
Hao1	Mm00439249	Life technologies, Darmstadt
Hoga1	Mm00470609	Life technologies, Darmstadt
Ldha	Mm01612132	Life technologies, Darmstadt
Nampt	Mm00451938	Life technologies, Darmstadt
Pck1	Mm01247058	Life technologies, Darmstadt
Prodh2	Mm00457662	Life technologies, Darmstadt

2.1.10 Adeno-associated viral vectors

Table 16: Adeno-associated viral vectors used for gene transfer in mice

Name	Description	Vector ID/Supplier
pAAV[Exp]-CMV > EGFP	-	VB150925-10026, VectorBuilder
pAAV-TBG-mAgxt	Liver-specific expression of Agxt under control of the hepatic thyroxine-binding globulin (TBG) promoter	VB200115-1168mpa, VectorBuilder

2.2 Methods

2.2.1 *in vivo*

2.2.1.1 Housing of mice

Mice arrived at an age of 8 weeks from the respective supplier and were kept for one week to acclimatize without performing any experiment with them. They had free access to water and food *ad libitum* and were held under a 12h light/dark cycle. Experiments were approved and performed according to the guidelines of the local animal welfare authority, which means that the Principles of Laboratory Care and recommendations of the Society of Laboratory Animal Science (Gesellschaft für Versuchstierkunde, GV-SOLAS, Germany, 2022) were guaranteed.

2.2.1.2 Collection of organs, tissue and blood from mice

When *in vivo* collection was performed, different organs e.g., liver, kidney or pancreas were collected for further subsequent analysis. Therefore, the animals were anesthetized with an intraperitoneal injection of Rompun® and Ketamine. When the mice were fully narcotized by checking defined reflex, they were placed in a dorsal position and the abdominal cavity was opened by using a surgical scissor longitudinally. In some experiments, the mice were killed by cervical dislocation when no anesthesia was necessary. The liver was extracted surgically and weighed. The left lobe was cut into two pieces: the left piece was used for cryosectioning, and the other was put in histological cassettes and placed in 4% PFA. The rest of the remaining liver was placed in a clamp and afterwards crushed by using mortar and the powder was transferred to a 5mL tube. The clamp was placed in liquid nitrogen to prevent the sticking of the organ to the clamp. For the kidneys, the procedure was basically similar. The left kidney was cut in two halves longitudinally. One piece was used for the histological analysis and the other for cryo-sectioning. The second kidney was crushed in the same way as described for the liver.

Blood was collected from two different places. When sacrificing mice, either by cervical dislocation or anesthesia, blood was also collected by taking it from the heart chambers using a syringe when the abdominal cavity was opened or by stitching the facial vein via 24G needle. These two different approaches were used when larger amounts of blood were needed for analysis. Depending on the specimen of the blood – plasma or serum – the samples were differently prepared. For serum, the blood was placed at room temperature for 30min and afterwards spun down at 4000rpm for 10min. Later, the serum (supernatant) was transferred

to a new tube and kept at -80°C. For plasma, the blood was chelated by using respective volume of EDTA to prevent coagulation of the blood. In the next step, blood was centrifuged at 12000rpm for 10 minutes. After that, the supernatant was transferred into a new tube and stored at -80°C.

2.2.1.3 24h urine collection

To analyze and measure the urinary oxalate levels of mice, mice were placed in metabolic cages to collect 24h urine for up to three consecutive days. Those mice had free access to water and food throughout the experiment. The urine was collected in a tube, which contained 35 µL of 6 M HCl to acidify the urine preventing the conversion of ascorbic acid to oxalic acid. Otherwise, this could lead to misinterpretation of the data. The collected urine was centrifuged down at room temperature for 10 min at 179xg to remove food residues from the urine. The supernatant was aliquoted in various tubes and stored at -80°C for further analysis.

2.2.1.4 Histology staining of embedded tissue

2.2.1.4.1 Fixation and paraffin embedding

After collecting tissue in histological cassettes, the cassettes were placed in 4% paraformaldehyde (PFA) at 4°C for fixation the next two days. Afterwards, the PFA solution was removed and replaced by 1x PBS. Cassettes were left in 1x PBS until further processing. Next, STP120 processor (Thermo Fisher Scientific) performed fixation procedure. During this process, the tissue is dehydrated by an ethanol gradient, followed by xylene and finally infiltrated by paraffine to increase the stiffness of the tissue for sectioning. A detailed procedure is depicted in the next table.

Table 17: Fixation protocol for histological stainings

Step	Reagent	Time (min)
1	70% ethanol	30
2	70% ethanol	60
3	90% ethanol	30
4	90% ethanol	30
5	99% ethanol	30
6	99% ethanol	35

7	99% ethanol	60
8	Xylol	30
9	Xylol	35
10	Xylol	60
11	Paraffin histowax	80
12	Paraffin histoway	105

After finishing the program, the tissue was embedded in paraffine using the Microm HM450 automated embedding device. If not otherwise stated, 4µm-thick formalin-fixed organ tissue was sectioned and used for common staining as well for immunohistochemical staining. The tissue sections were mounted on glass slides and placed in an oven at 60°C for 20 minutes. Prior usage, slides were stored at 4°C.

2.2.1.4.2 Hematoxylin and eosin Y staining

In the first step, tissue sections were deparaffinized in Roti®-Histol four times for 5 minutes before being placed in an ethanol gradient reaching from 100% to 70% ending up in ultrapure water (5 minutes in each solution). Next, the slides were incubated in freshly prepared Hematoxylin for 5 minutes. After that, the tissue was blued under running tap water for another 10 minutes. Then, the sections were stained for three minutes with 1% filtered eosin Y and immediately rinsed with ultrapure water. Afterwards, the sections were rehydrated in an ascending ethanol gradient (70%, 90%, 95%, 2x 100%, 5s each). This was followed by exposing the sections to Roti®-Histol two times for 5 minutes. Lastly, the sections were covered with a glass slide using Entellan®.

2.2.1.4.3 Periodic acid Schiff (PAS) staining

For the histological detection of glycogen, a common technique is the PAS staining. Same as for the H&E staining, the slides were deparaffinized and hydrated to water in an ethanol gradient reaching from 100% to 70% terminating in ultrapure water (5 minutes in each solution). Next, the sections were oxidized in 0.5% periodic acid solution for 5 minutes. After that, the sections were rinsed in distilled water for a few seconds. In order to start the color reaction, the sections were kept in Schiff reagent for 15 minutes which led to a light pink color change. Afterwards, the sections were washed in lukewarm tap water for 5 minutes leading to an immediate dark pink color change. To visualize the cell nuclei of each cell, the sections

were counterstained via Mayer's hematoxylin for one minute. After that, tap water was used for washing of the sections for 5 minutes. Finally, the sections were dehydrated, and cover slipped by using Entellan®. The glycogen staining results in a purple colorization of glycogen and a blue staining for the cell nuclei.

2.2.2 *in vitro*

2.2.2.1 Isolation of primary hepatocytes

2.2.2.1.1 Murine hepatocytes

For the isolation of murine hepatocytes an adapted two-step perfusion method was used by which the liver was dissected from the animal and the modified into a suspension of viable hepatocytes (Seglen, 1976). In the first step, the mice were anesthetized by using a cocktail of Rompun® (25-40 mg/kg) and Ketamine (50-80 mg/kg). The anesthesia was checked by testing different reflex of the mice. Procedure was continued after the animal showed no signs of reflex anymore. Then, the animal was placed in a dorsal position and the abdominal cavity was opened using a surgical scissor longitudinally. In the next step, organs which hamper the view on the vena cava were removed very carefully. Having direct access to the vena cava, a blunted needle was inserted in the incised vena cava. The needle was stuck to a flexible tube which was connected to a flowing pump and ended in a bottle where different buffers could be filled in. When inserted with the needle, the liver is perfused firstly with pre-warmed EGTA buffer at a flow rate of 15 mL/min for 10-15min. This is meant to remove blood and Ca^{2+}-dependent adhesion factors. To cleave the extracellular matrix and cell-cell connections, in the next step the EGTA buffer was replaced by Collagenase buffer(37°C). Flow rate and perfusion duration were kept constant as in the step before. This step was stopped when the liver seemed to become slimy and soft. Subsequently, the liver was excised carefully and removed by using forceps and then placing the liver in a petri dish. Under the laminar air flow system, the petri dish was filled with suspension buffer. In the following, the liver capsule was broken up and the hepatocytes were gently bruised into the suspension buffer. The cell suspension was then filtered through a 100µm cell strainer and transferred into a new 50mL tube. Next, the suspension was centrifuged for 5min at 50xg at 4°C to remove non-parenchymal cells (NPC) from hepatocytes. The NPC-containing supernatant was discarded and the pellet which contained hepatocytes was resuspended in 10mL suspension buffer. The isolated hepatocytes were placed on ice and a small fraction of cells was diluted with suspension buffer and trypan blue (1:2) in order to determine the cell number by using a Neubauer counting chamber.

2.2.2.1.2 Human hepatocytes

Cryopreserved primary human hepatocytes (PHHs) were purchased from Lonza or BioIVT. In addition to this a non-commercial collaborator by the group of Dr. Georg Damm was able to provide us with freshly isolated human hepatocytes from patients who suffered from a first to second degree liver tumor. The patients gave their agreement on sharing the hepatocytes for research purposes according to the ethical guidelines of the University of Leipzig. The isolation of the PHHs was performed by using a two-step isolation protocol described above with minor deviations (Lee et al., 2013). The hepatocytes were then transferred to the institute and on the next day they were suspended in William's E medium and cell number was determined by using trypan blue. Cells were cultivated in sandwich-on-top culture system as described in the next chapter.

2.2.2.2 Cultivation of primary hepatocytes

Hepatocytes were incubated under sterile conditions at 37°C and 5% CO_2 with aqueous saturated vapor. Two different methods for cultivating the cells were applied here in this thesis: The first one was the monolayer, which is described by a thin layer of collagen only on the bottom of a well. The second method was a Sandwich-On-Top (SOT) system, which is described by a thin layer on the bottom of the well and a thick layer on top of the plated cells. For the two different layers of collagen, 10mg of rat-tail collagen was dissolved in either 9mL or 40mL 0.2% acetic acid, which resulted in a concentration of 250 µg/mL and 1.1 mg/mL respectively. The process of dissolving took place at 4°C overnight. The next day, cell culture plates were flushed with thin layer collagen solution and left to dry for several hours under the laminar airflow hood or stored in the incubator. After that, the plates were washed with William's E medium without any additives to adjust the pH of the monolayer. Afterwards, Williams's E medium with additives + 10% sera plus and the respective numbers of cells were added into each well (see. table 18). To guarantee homogenous distribution primary hepatocytes the plates were gently shaken in every direction. Then the plates were incubated for 3h at 37°C for attaching to the monolayer. After 3h, the plated were washed for three times with pre-warmed Williams' E medium to get rid of dead and unattached hepatocytes. The second layer collagen was further modified by adding 1 mL of 10x DMEM to the 9mL collagen for a concentration of 1 mg/mL collagen which was indicated by a yellowish color.

Table 18: Overview of different plating systems for in vitro experiments

Plate	**Cell number**	**1mg/mL collagen**	**Williams' E + additives/ Glucose-free DMEM**
6 well plate	$0.85*10^6$ cells/well	350 µL	2 mL
12-well plate	$0.4*10^6$ cells/plate	200 µL	1 mL
24-well plate	$0.2*10^6$ cells/plate	100 µL	0.5 mL

Subsequently, the pH value of the solution needed to be adjusted by adding 1 M NaOH solution carefully, which turned the yellowish color into a purple/pink. Next, the adequate volume of second collagen layer was added to the well and the plates were put back into the incubator for 45min for polymerization of the second layer. When experiments were performed in monolayer system, the steps for preparation of the second layer were skipped. Finally, Williams' E medium + additives was added to the wells.

2.2.2.2.1 Hepatic glucose production assay

To mimic the glucogenic conditions *in vitro*, we established a hepatic glucose production assay. The general procedure is also illustrated in the figure below. After the 3h attachment of hepatocytes, cells were washed three times with glucose-free DMEM and then the cells were exposed to glucose-free DMEM medium without any additives except antibiotics for 3h hours. This step is meant to exclude any glucose leftovers from glycogen storages of the hepatocytes. After this incubation, hepatocytes were treated with glucogenic precursor like pyruvate/lactate, glycerol or amino acids.

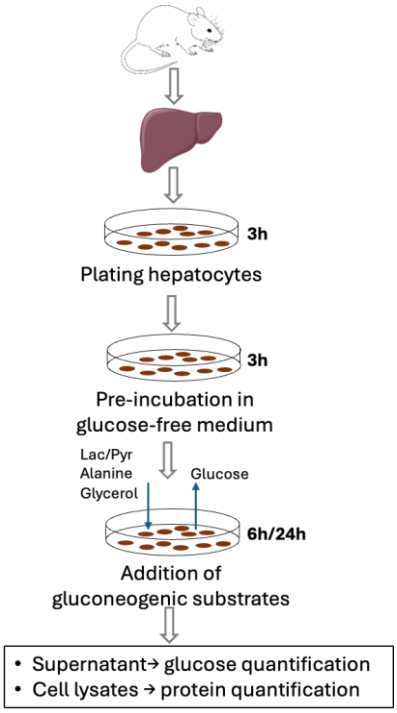

Figure 9: Brief description of the hepatic glucose production (HGP) assay

Depending on the setup and the duration of the experiment (6h/ 24h), cells were collected for protein or gene expression analysis. Additionally, the supernatant was also collected to quantify the glucose that was produced from the precursors.

2.2.3 Gene expression analysis

2.2.3.1 RNA isolation

RNA from tissue or cells was isolated by using the QIAzol reagent (Qiagen) for phenol-chloroform extraction. QIAzol reagent consists of guanidinium thiocyanate and phenol, which causes the lysis of cell membranes and inhibits RNases to prevent degradation (Chomczynski and Sacchi, 1987). For tissue, 1mL of the reagent was added independent of the weight of snap-frozen tissue being isolated. It was further homogenized by using a pestle before continuing. In the next step, samples were sonicated (50% power for 30s, 5s pulse – s break) while placed on ice. Cells, that were cultivated in a 6-, 12- or 24-well plates, were placed on ice and the media was aspirated and then 1 mL, 500 µL, 250 µL was added, respectively. Detaching of the cells from the well was mediated by using cell scraper. The cells lysates were then transferred to a 2 mL tube and sonicated on ice in the same way as described before. Next, 200 µL of chloroform was added to each tube and the tubes were shaken for 10 to 15 seconds. Subsequently, tubes were kept at room temperature and incubated to improve phase separation. In the next step, samples were centrifuged for 15 minutes at 12000 rpm

and 4°C, which resulted in a visible two-phase separation. The aqueous supernatant, which contains the isolated RNA, was carefully transferred in a new tube containing 500 µL of 2-propanol for precipitation of RNA. Again, the samples were centrifuged for 15 minutes at 12000rpm. Afterwards, the supernatant was discarded, and the pellet displayed the isolated RNA. Following this, the RNA was washed and purified by several steps using 100%-, 80%-, and 75%-pure ethanol. Between the washing steps, the RNA was centrifuged by adding 850 µL of the respective ethanol solution. After the last washing step, the supernatant was discarded carefully by pipetting and the RNA pellet was kept at room temperature allowing to air-dry. Finally, the RNA was dissolved in 15-100 µL DEPC-treated water, and its concentration was determined photometrically via the NanoDrop2000 (Thermo Fisher Scientific). Isolated RNA was stored at -80°C.

2.2.3.2 Synthesis of cDNA

Prior a real-time polymerase chain reaction (rt-PCR), the isolated RNA needed to be transcribed to cDNA. This was mediated by reverse transcription using the cDNA reverse transcription kit (Applied Biosystems) in order to receive a single-stranded cDNA fragment. For the reverse transcription, 0.5-2 µg of RNA were mixed with appropriate volumes of 10x RT-Buffer, 10x random primer, 25x DNTP mic, reverse transcriptase and DEPC water. The total volume of a single reaction was 20 µL. The program for the cDNA transcription is displayed in the table below showing the chosen conditions for the thermo cycler (Tgradient, Biometra). After finishing the program, the cDNA was diluted to a concentration of 10ng/µL with DEPC water and stored at -20°C.

Table 19: Program for reverse transcription of RNA to cDNA

Step	**Temperature (°C)**	**Time (min)**
Incubation	25	10
Reverse transcription	37	120
Inactivation	85	5
Hold-stage	4	∞

2.2.3.3 Quantitative real time polymerase chain reaction (qPCR)

qPCR is a quantitative, sensitive technique to detect changes in the gene expression of a target gene (Higuchi et al., 1993). The principle of this method relies on the binding of so-called

TaqMan probes that hybridize to the DNA template strand between the primers and are conjugated with a fluorescent reporter on the 5'- end and a quencher on the 3'end. Consequently, a fluorescence resonance energy transfer (FRET) between the quencher and the reporter suppresses the fluorescent signal. To detect a fluorescent signal, the applied DNA polymerase has a 5'-3' exonuclease activity which results in a separation of the TaqMan probe from the template cleaving into single nucleotides (Holland et al., 1991). Consequently, reporter and quencher are split apart and a fluorescent signal, which is proportionally to the amplified DNA concentration, can be detected and quantified. The fluorescence signal provided is displayed as a function of time and called the C_t- value. This C_t describes the necessary number of cycles which are needed to reach a defined threshold and reaches the exponential phase so that a signal can be detected. Every gene expression analysis was performed with a 7500 Real-Time PCR System (Applied Biosystems). In total, 25ng of cDNA were mixed with 2x universal master-mix and 20x specific TaqMan probe and filled up with DEPC water to a volume of 20 µL. Samples were measured in technical duplicates and water was used as a negative control. The standard operation procedure is listed in table XX.

Table 20: Program for PCR amplification

Step	Temperature (°C)	Time (min)	Cycles/Repetitions
(1) Activation of DNA Polymyerase	50	2	1
(2) DNA denaturation	95	10	1
(3) Annealing and Elongation	95/ 60	1.25	40

For the calculation of gene expression levels the $2^{-\Delta\Delta Ct}$method was applied which is a relative quantification approach that relies on the levels of a gene of interest (GOI) and of a housekeeping gene (HKG) in an unknown sample. (Livak and Schmittgen, 2001). The housekeeping gene is meant to be stable even under conditions where cells or tissue is stressed, consequently they serve as endogenous control and give information on the quality of the sample. In this thesis, different housekeeping genes were used as endogenous controls, e.g., Eif2a, Gapdh and UBC. The expression of the gene of interest was subtracted from the

housekeeping gene ($\Delta C_t = C_{tGOI} - C_{tHKG}$). In the following step, the ΔC_t of the control sample was subtracted from the values of the test sample ($\Delta\Delta C_t = \Delta C_{t1} - \Delta C_{t2}$) resulting from the intervention. In case of a higher value compared to control, the intervention induced an upregulation of the respective gene and vice versa.

2.2.4 Protein analysis

2.2.4.1 Protein extraction from different specimen

Protein was extracted from tissue like liver or kidney and from primary hepatocytes. For this, tissue and cells were lysed in RIPA buffer which contained protease inhibitor and phosphatase cocktail II and III, respectively 1:100 diluted. Depending on the source of the material e.g., liver tissue, 1mL of RIPA was added to snap-frozen tissue. If necessary, the mixture was homogenized by using a pestle, followed by a sonication step (50% power, 0.5s pulse, 0.2s break). After that, the homogenate was placed on ice for 20 minutes and then centrifuged for 10 minutes at 12000rpm at 4°C. The supernatant, which contained the protein, was transferred into a new tube.

For cells, the collection deviated from the one described before. The 6-, 12-, 24-well plates were placed on ice and the media was aspirated and after that 300 µL, 150 µL and 75 µL of RIPA was added, respectively. Extraction of the cells was performed by scraping out the cells from the well and transferring the lysate into tubes. Same as for the tissue, the cell lysates were sonicated and incubated on ice for 20 minutes. Next, the lysates were centrifuged for 10 minutes at 12000rpm at 4°C. The supernatant was then transferred into a new tube. Protein lysates were stored at -20°C or -80°C for long-term storage.

2.2.4.2 Quantification of protein

For the quantification of protein, the bicinchoninic acid (BCA) protein assay (Thermo Fisher Scientific) was used. The principle of this method relies on two different reactions. The first one is a modified biuret reaction, which outlines the conversion of Cu^{2+} to Cu^{+} by peptide bonds under alkaline conditions. In a second reaction, two molecules of BCA react with a Cu^{+}-ion forming a chelate complex with a purple color. The intensity of the colorization is measured at a wavelength of 562nm which is proportional to the protein concentration.(Walker, 2009).

In practical, 5µL of sample were mixed with 195 µL of BCA working reagent consisting of 49 parts of reagent A and one part of reagent B in a single well. For quantification of the protein

concentration, a calibration curve of bovine serum album (BSA) was prepared, ranging from 0 + 2000 µg/mL. Measurements were performed in duplicates. The prepared plate was incubated at 37°C for 30 minutes light protected. Plate reading was done in a plate reader (Infinite M200 Pro, Tecan). For tissue samples, a pre-dilution of 1:10 was conducted – for cell sample a dilution of 1.3 was necessary.

2.2.4.3 Western Blot

2.2.4.3.1 SDS-Polyacrylamide gel electrophoresis (SDS-PAGE)

SDS-Page is a commonly used technique to investigate protein expression in different cells and tissue. Put simply, it relies on the separation of protein in a protein mixture depending on the size and electrophilic mobility of the protein. This separation is mediated by applying an electric field. Sodium dodecyl sulfate (SDS), which is an anionic detergent, linearizes the protein and covers their charges negatively (Manns, 2011). In this thesis, the mobility of the protein depends on the size of the protein.

Freshly prepared gels were stacked in Mini-PROTEAN electrophoresis chamber (BioRad) as described in the manufacture's protocol. A recipe for two 1.5mm thick 10%-containing SDS separation gel is illustrated in the table below.

Table 21: Composition of separation buffer for Western blots

Chemicals/Reagents	**volume**
Ultrapure water	6.4 mL
Acrylamide solution (30% v/v)	5.28 mL
Separation buffer	4 mL
SDS (10% w/v)	160 µL
TEMED	6.4 µL
APS (10% w/v)	160 µL

The prepared solution was then transferred between the two glass plates and filled up to a defined height. To get rid of air bubbles on top of the gel, a thin layer of 2-propanol was added to avoid oxidation and evaporation. The gel was kept for 20 minutes to allow for polymerization. After polymerization. the 2-propanol was removed by inverting the gel and

the stacking gel was added on top of the separation gel and combs were added to form pockets. A list of the chemicals constituting for the stacking gel is displayed in the table below.

Table 22: Constitution of stacking buffer for Western blots

Chemicals/Reagents	**volume**
Ultrapure water	4.8 mL
Acrylamide solution (30% v/v)	1 mL
Stacking buffer	0.8 mL
SDS (10% w/v)	65 µL
TEMED	5 µL
APS (10% w/v)	100 µL

For the separation of protein, equal amounts of protein were mixed with 5x Loading buffer and denaturized at 95°C for 5min. The dithiothreitol (DTT) which is part of the loading buffer, reduced desulphated bonds of the protein and optimizes better protein separation during electrophoresis. The denaturized protein samples and a control ladder for protein sizes (4 µL) were added into each pocket and the electrophoresis was started. An initial current of 20mA/gel was applied and increased to 40mA/gel when all samples were on the same level. The electrophoresis was terminated when the sample almost reached the end of the gel.

2.2.4.3.2 Protein transfer on PVDF membrane

For the immobilization and detection of proteins by antibodies, the protein samples were transferred onto a PVDF membrane. The transfer was mediated by using the semidry transfer system by Biometra or BioRad. Every system consisted of an upper plate, displaying the anode, and a lower plate representing the cathode. Blotting papers were soaked in the anode or cathode buffer, respectively. The gel was removed from the cast and placed in the cathode buffer for equilibration. The PVDF membrane was shortly put in methanol for the activation of the membrane. The blotting papers soaked in anode buffer were placed on the anode plate of the transfer chamber and the activated PVDF membrane was put on top of it. In the following, the gel was added on top of the membrane. Finally, one in cathode buffer-soaked blotting paper completed the sandwich system. Subsequently, the chamber was closed with a cover and the run was performed at 234mA/blot for approx. 30 to 40 minutes. After the

transfer, the membrane was washed once with 1x TBS-T and then incubated with either 5% BSA or 5% milk - depending on the antibody – to block unspecific antibody binding.

2.2.4.3.3 Protein detection

Following the blocking step, the membrane was incubated with a specific primary antibody in 5% BSA or 5% milk in 1x TBS-T overnight at 4°C. The membrane was constantly shaken. Afterwards, the membrane was washed with 1x TBS-T for three times á 5 minutes prior the incubation with the secondary antibody which was labelled with a Horseradish Peroxidase (HRP). The secondary was incubated for one hour at room temperature (RT). Repeatedly, the membrane was washed with 1x TBS-T three times à 5 minutes. Further information regarding the incubation with the primary antibody is shown in the table below. The protein signal was detected by using chemiluminescence and hydrogen peroxide (5 mL ECL + 3 µL hydrogen peroxide). The chemiluminescent signal was provided by the catalyzation of luminol via oxidation. This oxidation was accompanied by a light emission at 428nm. This light emission was captured by Blot-Imager Vilber Fusion Fx7 (Vilber Lourmat). For the detection of a housekeeping protein, the membrane was incubated in stripping buffer for 30 minutes at room temperature. This was meant to detach the secondary antibody from the primary antibody. In the following, membrane was blocked again and incubated with primary and secondary antibody the way it was described for. Both, the signal of the protein of interest and the housekeeping gene were quantified densitometrically with the software ImageJ.

Table 23: Antibodies used for Western blots

1st antibody	**2nd antibody**	**Dilution**	**Incubation**
anti β-aktin	anti-mouse	1:5000/1:10000 in 5% BSA	30min RT / 1h RT
anti Agxt	anti-rabbit	1:1000/1:5000 in 5% BSA	o/n 4°C / 1h RT
Anti-G6pc	Anti-rabbit	1:100/1:1000 in 5% milk	o/n 4°C / 1h RT
anti Gyk	Anti-rabbit	1:1000/1:5000 in 5% BSA	o/n 4°C / 1h RT
anti Pck1	anti-mouse	1:1000/1:5000 in 5% milk	o/n 4°C / 1h RT

2.2.5 Colorimetric assays

2.2.5.1 Quantification of glucose

For the quantification of glucose in different specimen, e.g., cell supernatant or plasma, the Glucose Assay Kit (Sigma Aldrich) was used. In this kit, glucose is oxidized to generate a colorimetric product which is proportional to the amount of glucose present in the sample. There is the option to detect also a fluorescent signal, which is only applicable when small amounts of glucose are expected in the sample. In this thesis, only the colorimetric analysis was used. For cell supernatant, 2 µL of the sample was directly added to a well in a 96-well plate without diluting. For plasma, a dilution of 1:10 was determined as best suited. In the next step, the final volume of sample was brought up to 50 µL with Assay buffer. Afterwards, a master reaction mix was added to each well (50 µL). This master mix consisted of glucose assay buffer, glucose probe and glucose enzyme mix. The constituent of each reagent was applied according to manufacturer's protocol. The plate was then incubated for 30 minutes at 37°C under light protection. The absorbance was measured at a wavelength of 570nm with a plate reader (Infinite M200 Pro, Tecan). For quantification of the samples, a glucose standard curve was prepared according to manufactures protocol generating concentrations reaching from 0 up to 10 nmol/well. All samples were measured in duplicates.

2.2.6 Enzyme-linked immunosorbent assay (ELISA)

2.2.6.1 Insulin quantification

A very useful technique to quantify hormones (e.g., insulin and glucagon) is to use enzyme-linked immunosorbent assay as they display high sensitivity. The ELISA used here is a solid phase two-site enzyme immunoassay. It is based on the sandwich technique from which two monoclonal antibodies can bind to the antigen of interest at two different epitopes. During the incubation insulin can bind to the monoclonal anti insulin antibody that is attached to the bottom of the well plate and the peroxidase-conjugated anti insulin antibody. In a subsequent washing step, the unbound labelled antibody is removed. The bound conjugated antibody is detected by a reaction with 3,3', 5, 5'-tetramethylbenzidine (TMB). In a final step, the reaction is stopped by adding acid to give a colorimetric endpoint that is read-out photometrically.

For the reaction, 10µL of sample and standards were added to each well. Calibration standards were prepared as described in the manufacture's protocol. In the following, 100 µL of 1x enzyme conjugate was put into each well. Afterwards, the plate was placed on a plate shaker

for two hours at room temperature for distribution. After washing the plate 5 times, 200 µL of TMB substrate was added into each well and the plate was incubated for another 15 minutes. Finally, the reaction was stopped by adding 50 µL of stop solution. Then, the optical density was read at 450nm, and results were calculated.

2.2.6.2 Glucagon quantification

For the quantification of glucagon an ELISA was used. This ELISA was a solid phase two-site immunoassay. Its principle is based on the direct sandwich technique in which two monoclonal antibodies are directed against different antigenic determinants on the glucagon molecule. While incubating, glucagon in the test sample will react with peroxidase-labelled anti-glucagon antibodies (clone E6A11K) and with anti-glucagon antibodies (clone M5F9S) attached to the bottom of the well plate. After washing the plate, the conjugate is detected using 3,3', 5, 5'-TMB. The reaction was stopped by using acid to reach a colorimetric endpoint. Then, the colorimetric endpoint is read-out photometrically.

For the reaction, 10 µL of sample and standards were added to each well. Calibration standards were prepared as described in the manufacture's protocol. In the following, 50 µL of 1x enzyme conjugate was put into each well. Afterwards, the plate was placed on a plate shaker overnight at 2-8°C for equal distribution. The next day, the plate was washed 5 times and after that 200µL of TMB substrate was added into each well and the plate was incubated for 30 minutes. Finally, the reaction was stopped by adding 50 µL of stop solution. Then, the optical density was read at 450nm, and results were calculated.

2.2.7 Amino acid quantification in plasma and tissue

The analysis of amino acids and creatinine was accomplished as published elsewhere (Custodio et al., 2023). Therefore, mouse body fluids (5µL) were used for protein precipitation with 80% methanol containing stable-isotope labelled internal standards (MSK-CAA-1, Cambridge Isotope Laboratories; trans-4-Hydroxyprolin-d4, Toronto Research Chemicals; Creatinine-d3, Cayman Chemical; concentration 10 µmol/L). Proteins were pelleted by centrifugation at 21,000 xg. 1 µL of the supernatant was used for LC-MS/MS-analysis.

Cell and tissue samples were lysed in 300 µL 80% methanol containing 10 µmol/L of stable-isotope labelled internal standards (MSK-CAA-1, Cambridge Isotope Laboratories; trans-4-Hydroxyprolin-d4, Toronto Research Chemicals; Creatinine-d3, Cayman Chemical) using a

Bioruptor Pico (Diagenode) and proteins were pelleted by centrifugation at 21,000 xg. 1 µL of the supernatant was used for LC-MS/MS-analysis.

The analysis of amino acids was accomplished by LC-MS/MS using a Vanquish Horizon UHPLC coupled to a QExactive mass spectrometer(both ThermoFisher) equipped with a MN NucleoShell Bluebird RP18 (3 mm I.D. x 150 mm length, 90 Å, 2.7 µm particle size) using 400 µL/min flow rate and the following binary gradient (solvent A: 0.1% formic acid, 0.02% heptafluorobutyric acid; solvent B: 0.1% formic acid in acetonitrile): 2% B for 2.5 min, 2-50% B in 3.75 min, 50-90% B in 0.25 min, 90% B for 2.25 min, 90-2% in 0.25 min and re-equilibration at 2% B for 3 min. The QExactive mass spectrometer operated in positive mode acquiring alternatingly Full-MS and AIF spectra at a resolution of 140,000 and AGC 1x10^6; the m/z-range was 70-300 for Full-MS and 50-300 for AIF spectra.

Quantification was accomplished using Skyline Daily (v22.2.1.351) (Adams et al., 2020). Data were normalized to the respective stable-isotope-labelled standards. Calibration curves ranged from 1-100 µmol/L for amino acids and from 5-500 µmol/L for creatinine.

2.2.8 Oxalate quantification in urine, plasma, supernatant and tissue

The oxalate, glycolate and glyoxylate concentrations in urine samples (acidified), in plasma or in cell supernatants (in serum-free medium) were quantified by LC-MS/MS as previously described (Schriewer et al., 2017).

Urine samples were acidified and diluted appropriately; cell culture supernatants remained undiluted. Plasma samples were first subjected to precipitation with 100% methanol to remove plasma proteins while cell and tissue samples were lysed in 80% methanol. All samples were supplemented with uniformly 13C-labelled internal standards for oxalate and glycolate. Samples were dried down under nitrogen flow and reconstituted in 20 µL 0.1% formic acid. 5 µL of the sample were injected onto a Shimadzu UFLC system coupled to a QTrap4000 mass spectrometer (Sciex). Analytes were separated by ion exclusion chromatography using a Hi-Plex H column (100 x 4 mm; 8 µm particle size; Agilent) isocratically within 10 min at 60 °C with a flow rate of 0.2 mL/min of 0.1% formic acid with a post-column make-up flow of 0.1 mL/min acetonitrile. The mass spectrometer was operated in negative-ion multiple-reaction-monitoring (MRM)-mode using the transition given in Table Y with a dwell time of 150 ms per transition. Quantification was accomplished in the Analyst software using calibration curves from 2.5 – 200 µmol/L.

2.2.9 Quantification of creatinine in urine

Creatinine is a waste product that is excreted from the kidney into the urine. It is well-accepted that it is a suitable normalization marker independent of the urinary volume. Therefore, creatinine was used to normalize the urinary oxalate excretion of mice since mice do not always produce the same amount of urine per day. The creatinine levels were determined via the Jaffé reaction (Jaffe, 1886). Picric acid and creatinine form an orange mixture under alkanine conditions that was measured colorimetrically at a maximum wavelength of 492 nm. Technically, murine urine samples were diluted at a 1:20 ratio with ultrapure water and 50 µL of sample was pipetted in a 96-well plate. Additionally, 50 µL of two urine samples of known creatinine concentrations were analyzed to check for quality reasons. In the last step, 200 µL of the basic picric acid was added to each well and the plate was incubated light protected for 45min. Next, the absorbance was measured at a wavelength of 492 nm using a microplate reader.

2.2.10 Cell Titer Blue® viability assay

Cryopreserved human hepatocytes or primary mouse hepatocytes (approx. $0.5x10^5$ hepatocytes) were seeded in black 96-well plates. After the attachement of the hepatocytes, cells were treated with the compound of interest for which the toxicity should be evaluated. The test compound was dissolved in normal cultivation media without any sera. For the assay, only the 60 inner wells of the plate was used since edge effects might compromise the results. Each well of the 96-well plate requires 200 µL of medium with the appropriate compound concentrations. The cells were incubated with the test compound for 24h and after that a morphology check was performed to evaluate the viability. Thereafter, the cells were washed for three times with pre-warmed PBS. Then, Cell Titer Blue® reagent was added to the cells at a ratio of 1:10 in normal cultivation media (one fraction of reagent and 9 fractions of cultivation media). The added amount of volume of the Cell Titer Blue® mixture to the well was 100 µL. The assay itself measured the mitochondrial enzyme activity by reducing the dark blue indicator dye resazurin to the pink and highly fluorescent dye resorufin. This fluorescent signal was measured at a wavelength of 584nm. Vital cells exhibit a strong metabolic rate for resazurin so that the fluorescence intensity is increased. In contrast, non-viable cells showed a decreased metabolic rate for resazurin resulting in a low fluorescent intensity. In case of dead cells, the dark blue color of resazurin was not metabolized.

2.2.11 Gene transfer using an adeno-associated viral transfer expressing Agxt

For the gene transfer of Agxt in different mice models, the vector pAAV-TBG-mAgxt (vector ID: VB200115-1168mpa) was used. This vector was designed for the exclusive expression of Agxt in the liver under the control of the hepatic thyroxine-binding globulin (TBG) promotor and packaged into adeno-associated virus DJ (AAV-DJ) by Vector Builder. The transduction of the virus in the liver was performed by an i.v. administration of $4.5x10^{12}$ gene copies per mouse in PBS by using a 27G needle.

2.2.12 Statistical analysis

All experiments were performed in three different biological replicates if not stated differently. Statistical significance between groups or conditions was tested by applying a two-sided unpaired t-test. Significant differences were considered when the p-value was <0.05 and indicated by an asterisk and so on. All data is shown as mean ± SD. Calculations and graph presentation were performed by using GraphPad Prism 10.

3 Results

In previous studies, it has been shown that Agxt plays a significant role in the detoxification of glyoxylate *in vitro.* However, no mechanistic study was performed showing that Agxt in general and in the fatty plays a crucial role in the detoxification of glyoxylate causing an excessive production of oxalate. Little evidence exists that focuses on the role of oxalate on other organs and the systemic circulation apart from its devastating consequences in the kidney. It is reported that oxalate has an inhibitory function on pyruvate carboxylase, which is a key enzyme to facilitate glucose production from non-carbohydrate substrates under fasting. In the course of this chapter, a newly established *in vitro* hepatic glucose production assay will be introduced which covers the *de novo* production of glucose from various substrates. Next, this assay is used to demonstrate the inhibitory role of oxalate on glucose production *in vitro*. Moreover, the consequences of excessive systemic oxalate levels is addressed in a hyperoxaluric mouse model, which is the AgxtKO mice. Lastly, the hormonal and substrate-specific stimulation of Agxt is characterized *in vitro* and *in vivo*.

3.1 Establishment of an *in vitro* hepatic glucose production (HGP) assay in hepatocytes

To investigate the capability of primary mouse hepatocytes to produce glucose when the cells are exposed to different glucogenic substrates, and to later be able to test the influence of compounds on glucose production, a hepatic glucose production assay was set up. A detailed procedure of the assay is described in chapter 2.2.2.2.1. Here, a set of increasing concentrations of glucogenic substrates was given to the cells and glucose was quantified in the supernatant and normalized to the protein content. In addition, gene and protein expression analysis was performed. The results are described in the following chapter.

For exploring the hypothesis that oxalate may influence pyruvate-driven gluconeogenesis it was particularly important to previously demonstrate that primary mouse hepatocytes utilize pyruvate for glucose synthesis. This has been questioned in a recent study by Kalemba *et al.* which proposes a substrate preference for glycerol superior to that for pyruvate/lactate in hepatocytes *in vitro* and *in vivo* (Kalemba et al., 2019).

3.1.1 Primary mouse hepatocytes are capable to produce glucose from various glucogenic precursors

The hepatocytes were exposed to increasing concentrations of various glucogenic precursors, including pyruvate/lactate, glycerol, alanine and glutamine.Since the pyruvate/lactate ratio

under aerobic glycolysis in the plasma of human and mice is near to 10 and kept stable by the LDH catalyzing the reduction of pyruvate in lactate, we also considered this ratio in our hepatic glucose production (Looyens et al., 2021). The results showed that primary mouse hepatocytes can significantly produce glucose from different substrates in a concentration-dependent manner compared to the untreated media control, which contained no glucose since this would influence the endogenous production of glucose by hepatocytes (FM= glucose-free medium). The two most common glucogenic precursors, pyruvate/lactate and glycerol, which are either derived from the breakdown of muscle proteolysis or from adipose tissue via lipolysis, also result in the highest levels of produced glucose. After 6h, the highest concentration of pyruvate/lactate resulted in a significant increase in glucose when compared to untreated media control (see Fig. 10A). This was also true for glycerol; here the difference followed the same pattern (see Fig. 10B). Compared to this, glutamine and alanine, which are derived from the breakdown of muscle tissue in the organism in fasting conditions, are also capable of producing glucose but do not reach levels comparable to those of pyruvate/lactate and glycerol. Despite the lower capacity of producing glucose, the highest exposed concentrations of glutamine and alanine were also significantly higher compared to the media controls (see Fig. 10C, D).

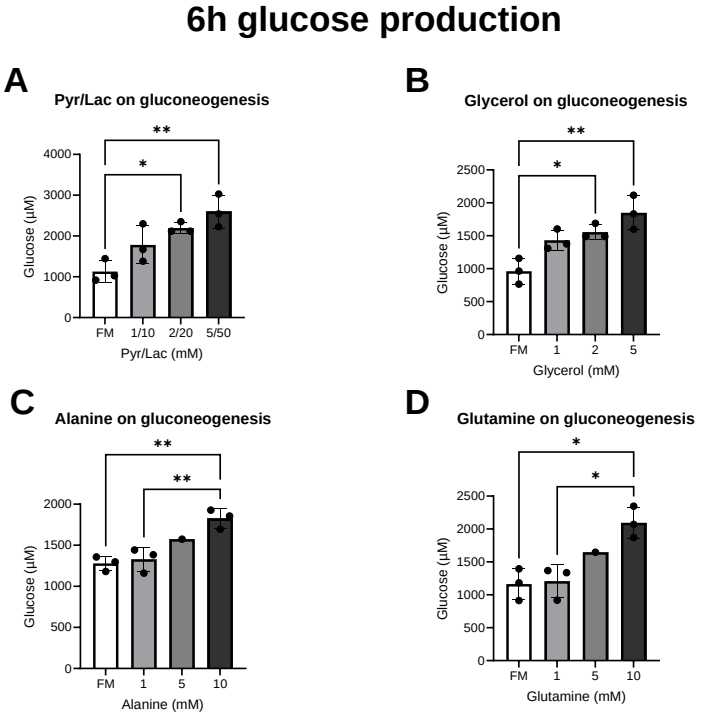

Figure 10: 6h exposure of glucogenic precursors in primary mouse hepatocytes; **(A)** glucose production from increasing concentration of pyruvate/lactate (n=3); **(B)** glucose production from increasing concentrations of

glycerol (n=3); **(C)** glucose production from increasing concentrations of alanine (n=1/3); **(D)** glucose production from increasing concentrations of glutamine (n=1/3). (All bar diagrams represent the mean ± SD. *p < 0.05; **p < 0.01; Student's t test, unpaired, two sided).

The capability of hepatocytes to produce glucose from precursors was higher when the exposure was prolonged for 24h. Here, like the previously described experiment, significant differences were observed for all concentration of pyruvate/lactate as well as for glycerol compared to full media control. The data analysis revealed that the highest concentration of pyruvate/lactate produced almost triple the amount of glucose when compared to the media control (see Fig. 11A). This holds true also for glycerol, where an increase of glucose production was already observed after the lowest concentration of 1 mM glycerol. This becomes significant when cells were exposed to 2mM or 5mM glycerol. For 5 mM glycerol, the increase in glucose production was very pronounced (see Fig. 11B). Regarding the production of glucose from the amino acids glutamine and alanine, the results showed that there is a concentration-dependent increase in glucose production from both precursors like the 6h time point. Here, the highest concentration of alanine resulted in a significant increase in glucose production compared to media control (see Fig. 11C). For glutamine, the highest concentration led to a significant increase in glucose production compared to the media control (see Fig. 11D).

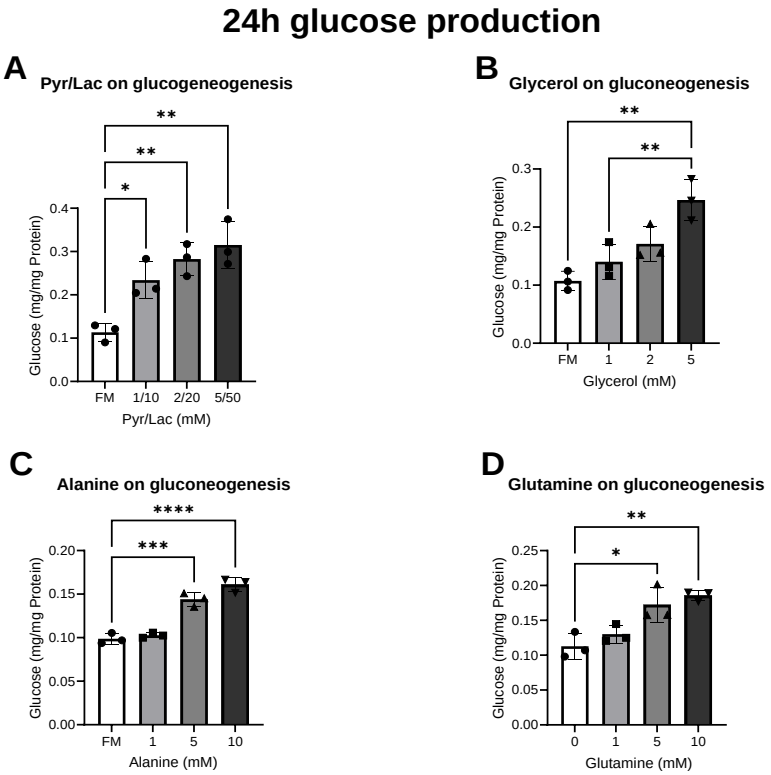

Figure 11*:* 24h exposure of glucogenic precursors in primary mouse hepatocytes; **(A)** glucose production from increasing concentration of pyruvate/lactate (n=3); **(B)** glucose production from increasing concentrations of glycerol (n=3); **(C)** glucose production from increasing concentrations of alanine (n=3); **(D)** glucose production from increasing concentrations of glutamine (n=3). (All bar diagrams represent the mean ± SD. *p < 0.05; **p < 0.01; ***p<0.001;****p<0.0001; Student's t test, unpaired, two sided)

3.1.2 Expression of glucogenic genes in response to different substrates

In addition to the capability to produce glucose from glucogenic precursors, also gene expression changes in response to the metabolites was analyzed. This had the purpose to investigate how transcription of key glucogenic enzymes changed and, if it translated into protein changes. The focus was on the glucogenic enzymes *Pck1* and *G6pc* when glucose was produced after 6h incubation. Kalemba *et al.* proposed that after the exposure to pyruvate/lactate the expression of *Pck1* and *G6pc* is not induced. However, in our experiment *Pck1* and *G6pc* were significantly induced in a concentration-dependent manner after exposure to pyruvate/lactate (see Fig. 12A). In contrast, when hepatocytes were exposed to glycerol, *Pck1* was not induced by glycerol (see Fig. 12B), whereas the stimulation of hepatocytes with glycerol led to a significant increase of *G6pc* after the treatment with 2 mM and 5 mM glycerol. This was expected to occur since the production of glucose from glycerol is highly dependent of *G6pc*, and *Pck1* is not required (see Fig. 12B). For the two-glucogenic precursors alanine and glutamine, limited data is available since only two concentrations – a low and high concentration – were tested. Concerning the exposure of glutamine to the

hepatocytes, significant induction of *Pck1* and *G6pc* was observed at the highest concentration compared to untreated control (see Fig. 12C). A similar trend was observed when the cells were exposed to alanine, showing significant upregulation of *Pck1* and *G6pc* compared to untreated control (see Fig. 12D).

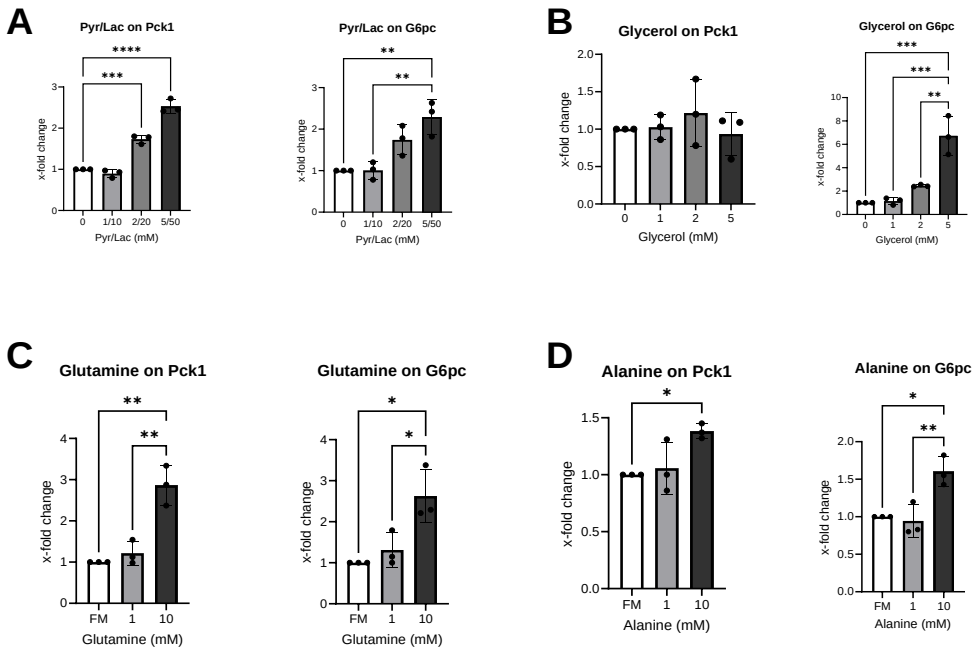

Figure 12: 6h mRNA expression analysis of **(A)** *Pck1* and *G6pc* after incubation with pyruvate/lactate (n=3); **(B)** *Pck1* and *G6pc* after incubation with glycerol (n=3); (**C)** *Pck1* and *G6pc* after incubation with glutamine (n=3); (**D)** *Pck1* and *G6pc* after incubation with alanine (n=3). (All bar diagrams represent the mean ± SD. *p < 0.05; **p < 0.01; ***p<0.001; ****p<0.0001, Student's t test, unpaired, two sided). Pck1= phosphoenolpyruvate carboxykinase, G6pc= glucose-6-phosphatase

To confirm the results from the 6h exposure experiment, the same experiment was set up and the hepatocytes were cultivated with the glucogenic precursors for 24h. As seen in a previous figure (see Fig. 11), the cells were able to produce glucose from various glucogenic precursors. When analyzing the transcriptional expression of glucogenic enzymes, one could see that *Pck1* and *G6pc* were highly induced after the exposure to pyruvate/lactate (see Fig 13A). The two lowest concentration of pyruvate/lactate exposure did show a trend, which was not significant after the statistical analysis. The gene expression changes for *Pck1* were highly significant at the highest concentration compared to untreated control (see Fig. 13A). The same pattern was observed for the gene expression changes of G6pc when hepatocytes were exposed to pyruvate/lactate. Here, the highest concentrations induced a significant increase in *G6pc* expression (see Fig 13A).

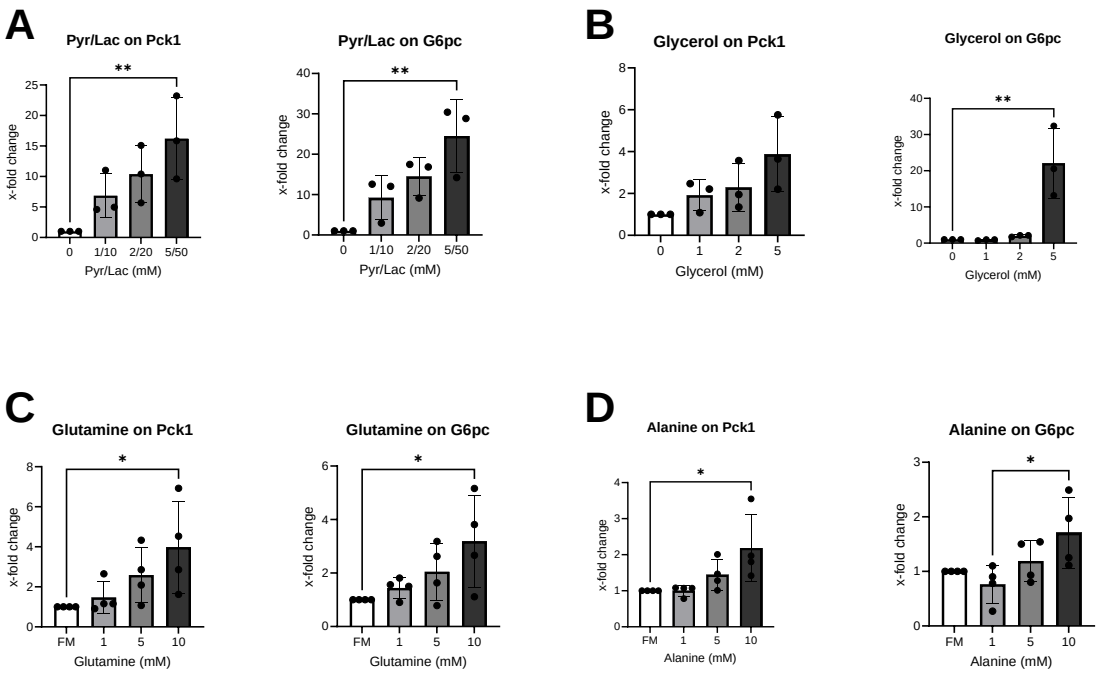

Figure 13*:* 24h mRNA expression analysis of **(A)** *Pck1* and *G6pc* after incubation with pyruvate/lactate (n=3); **(B)** *Pck1* and *G6pc* after incubation with glycerol (n=3); (**C)** *Pck1* and *G6pc* after incubation with glutamine (n=4); (**D)** *Pck1* and *G6pc* after incubation with alanine (n=4). (All bar diagrams represent the mean ± SD. *p < 0.05; **p < 0.01, Student's t test, unpaired, two sided). Pck1= phosphoenolpyruvate carboxykinase, G6pc= glucose-6-phosphatase

The exposure to glycerol led to a significant upregulation of *G6pc* only at the highest concentration (5 mM) compared to untreated control hepatocytes (see Fig 13B). In contrast to this, the expression patterns of glucogenic enzymes when they were exposed to amino acids glutamine and alanine were also significantly changed. Here, in line with the results from the 6h experiment, the expression levels significantly increased for the two genes. For *Pck1*, the exposure of the highest concentrations of glutamine and alanine led to a significant induction of *Pck1* (see Fig. 13C,D). The concentration-dependent exposure of alanine and glutamine exhibited an increase in the expression of *G6pc*, but only the highest concentration of glutamine significantly increased the expression of *G6pc* (see Fig. 13D).

3.1.3 Pck1 protein induction after exposure to pyruvate/lactate and various amino acids – not *via* glycerol

Based on the mRNA expression data from the 6h and 24h time point displaying induction of glucogenic enzymes like Pck1 and G6pc, the next step was to demonstrate whether this also led to induction of the protein expression. Therefore, immunoblots were prepared from the samples and densitometrically analyzed. The blots for pyruvate/lactate and glycerol are displayed in the next figure (see Fig. 14). In accordance with the results from the *Pck1* mRNA

after pyruvate/lactate exposure, the Pck1 protein expression increased in a concentration-dependent manner, which was also significantly higher after densitometric analysis compared to control hepatocytes (see Fig. 14A). Conversely, glycerol enhanced the downregulation of Pck1 on protein level in a concentration-dependent manner, which was also significant (see Fig. 14A). Comparing the protein expression data to the mRNA gene expression data for *Pck1* after glycerol exposure, it was not expected because the mRNA data did not reveal such a significant trend as it is shown here in figure 14.

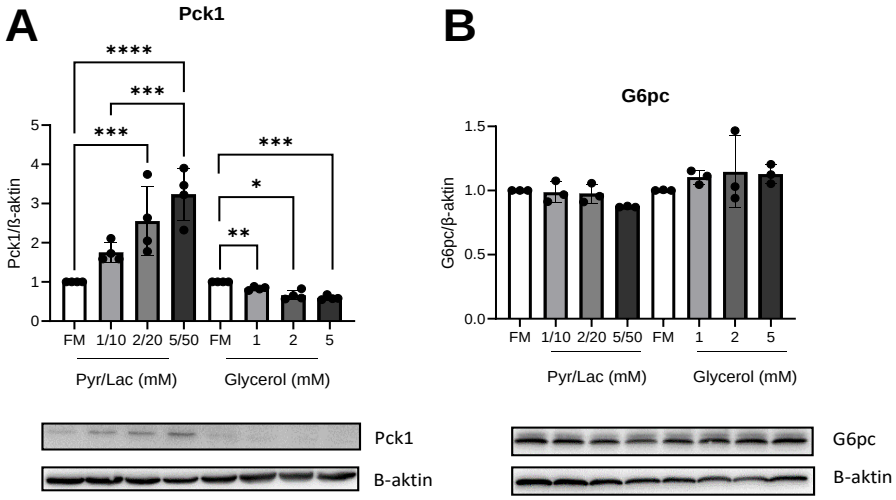

Figure 14: Western blot of **(A)** Pck1 after the exposure to pyruvate/lactate and glycerol (n=4); **(B**) G6pc after the incubation with pyruvate/lactate and glycerol (n=3). (All bar diagrams represent the mean ± SD. ***p < 0.001; ****p < 0.0001, Student's t test, unpaired, two sided). Pck1= phosphoenolpyruvate carboxykinase, G6pc= glucose-6-phosphatase

The same protein expression analysis was also performed for the treatment with the amino acids alanine and glutamine. Interestingly, a concentration-dependent increase in the expression of Pck1 protein was reported after the treatment with alanine as well as for glutamine (see Fig. 15). The protein expression for Pck1 after alanine exposure was more pronounced compared to the treatment with glutamine. The exposure of 10mM alanine led to a significant increase compared to the control. The exposure of 10 mM glutamine also significantly increased the expression of Pck1 (see Fig. 15A). Surprisingly, G6pc protein upregulation was also observable after the treatment with alanine and glutamine. However, due to large standard deviations no significant difference was achieved for alanine. For glutamine, though the results were not significantly different compared to FM, a trend for the induction was observed. To conclude, the results suggest that the exposure to

pyruvate/lactate and amino acids led to an induction of Pck1 protein. This was not entirely the case for G6pc.

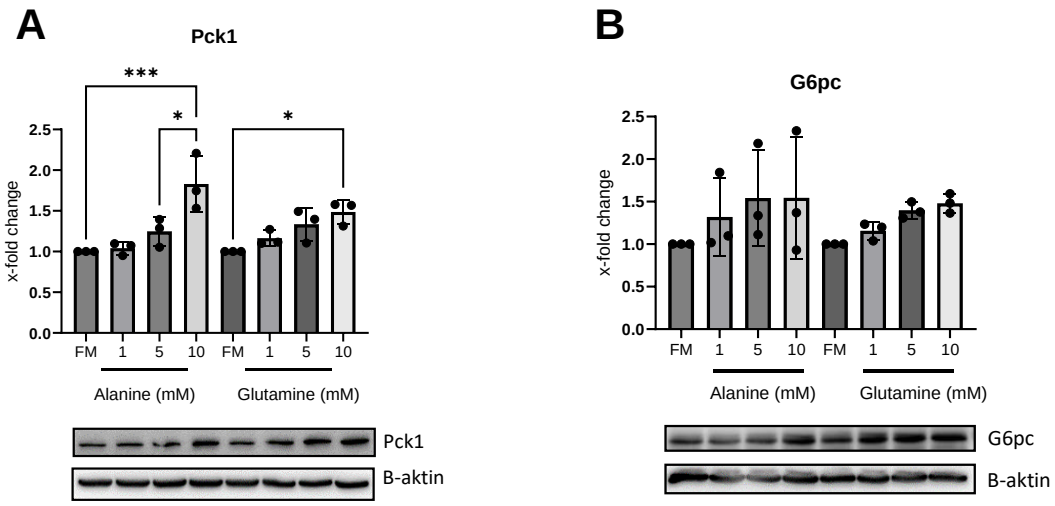

Figure 15*:* Western blot of **(A)** Pck1 after the exposure to alanine and glutamine (n=3); **(B**) G6pc after the incubation with alanine and glutamine (n=3). (All bar diagrams represent the mean ± SD. *p<0.05; ***p < 0.001, Student's t test, unpaired, two sided). Pck1= phosphoenolpyruvate carboxykinase, G6pc= glucose-6-phosphatase

To summarize the results so far, an *in vitro* hepatic glucose production assay was set up successfully and showed that primary mouse hepatocytes are able to use all substrates to produce glucose, which are known to contribute to gluconeogenesis *in vivo*. The assay revealed substrate-induced gene and protein expression changes *in vitro*, which might also be relevant for *in vivo* situations. Moreover, the results display discrepancies regarding the production of glucose from pyruvate/lactate. Kalemba *et al.* reported that exposure to pyruvate/lactate does not significantly lead to glucose production, compared to glycerol. This will be discussed in a later chapter.

3.2 The role of oxalate as inhibitor of gluconeogenesis

Since we could show that the *in vitro* hepatic glucose production (HGP) assay can be applied to study gluconeogenesis from all *in vivo*-relevant glucogenic substrates the next step was to apply this technique to study a possible influence of gluconeogenesis by oxalate. By now, only very little data exist that investigated a possible inhibition by oxalate on the gluconeogenesis via the two essential enzymes Pck1 and pyruvate carboxylase (Pc). Therefore, with the newly developed *in vitro* assay the question will be addressed to what extent oxalate influences the production of glucose from non-carbohydrate substrates. Prior to the HGP assay, a Cell titer Blue®-viability assay was performed to determine a concentration range of oxalate, in which

the cells were not affected in their viability. The results of the viability assay revealed an EC_{20} value of 2289.6 µM which is the concentration at which 20% of the cells died (see Fig. 16).

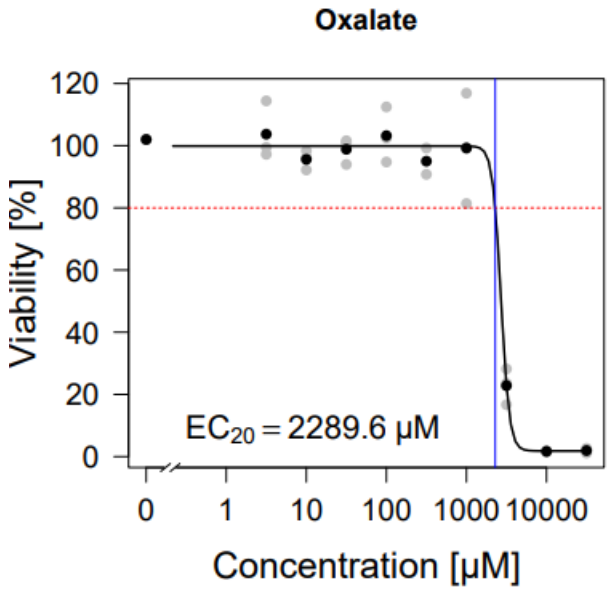

Figure 16: Concentration response curve of oxalate in primary mouse hepatocytes (grey dots represent the results of at least three biological replicates, black dots denote the concentration-wise mean. The vertical blue line indicate the EC20 (n=3)).

The estimated viability of the primary mouse hepatocytes was not affected by concentrations of up to 1 mM of oxalate. To gain more information about the accumulation of oxalate intracellularly, we monitored the intracellular levels of oxalate after the exposure to increasing concentrations of oxalate after a certain amount of time.

3.2.1 Oxalate accumulates intracellularly in primary mouse hepatocytes

To determine the levels of oxalate intracellularly, primary mouse hepatocytes were exposed to increasing concentrations of oxalate. The goal of this experiment was to understand if exposure to oxalate leads to intracellular oxalate accumulation (after entering the cells) in a time- and concentration-dependent manner and if there is a threshold of intracellular levels of oxalate that limits the uptake of oxalate. Untreated controls contained no oxalate in the cells within the first three hours of incubation. Surprisingly, after 18h and 24h the untreated control did accumulate intracellular oxalate. Regarding the lowest exposed concentration of 50 µM oxalate, a slight increase in the intracellular concentration was observed within the first three hours of the experiment (see Fig. 17). This pattern was followed by increasing oxalate concentrations. Oxalate concentration up to 300 µM resulted in very comparable intracellular levels of approximately 10 µM of oxalate. A dramatic increase in intracellular concentrations of oxalate was shown when cells were exposed to 1 mM and 3 mM. Here, the oxalate within

the cells reached concentrations of 30 µM to 50 µM compared to 15 µM of intracellular oxalate, when the cells were exposed to 300 µM of oxalate (see Fig. 17).

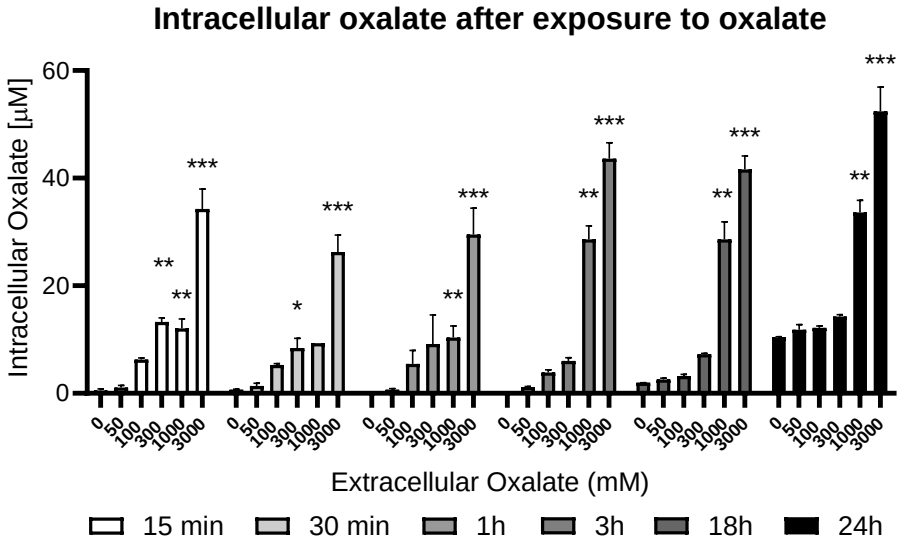

Figure 17: Quantification of intracellular oxalate in a time- and concentration-dependent manner (n=2/3). (All bar diagrams represent the mean ± SD.*p<0.05; **p<0.01; ***p < 0.001 compared to 0 µM oxalate; Student's t test, unpaired, two sided). Ala = alanine, Ox = oxalate

3.2.2 Oxalate inhibits glucose production from pyruvate/lactate and alanine

To study the influence of oxalate on gluconeogenesis, various substrates were tested, and the glucose was measured in the supernatant of the cells. Based on the results from the establishment of the newly introduced glucose production assay, the selected substrates and their concentrations were pyruvate/lactate (2/20 mM), glycerol (5 mM) and the amino acid alanine (10 mM). The cells were incubated for 24h hours. Interestingly, oxalate prevented the production of glucose from pyruvate/lactate in a concentration-dependent manner (see Fig. 18). The lowest concentration of 50 µM of oxalate did not lead to significant differences in the glucose production, but already showed a decrease in glucose production. Adding a concentration of 100 µM of oxalate to hepatocytes, the glucose production from pyruvate/lactate was lowered significantly compared to control hepatocytes (not exposed to oxalate (see Fig. 18A). The same is true for the exposure to 300 µM of oxalate, here the difference was even more pronounced compared to the 100 µM oxalate exposure and highly significant.

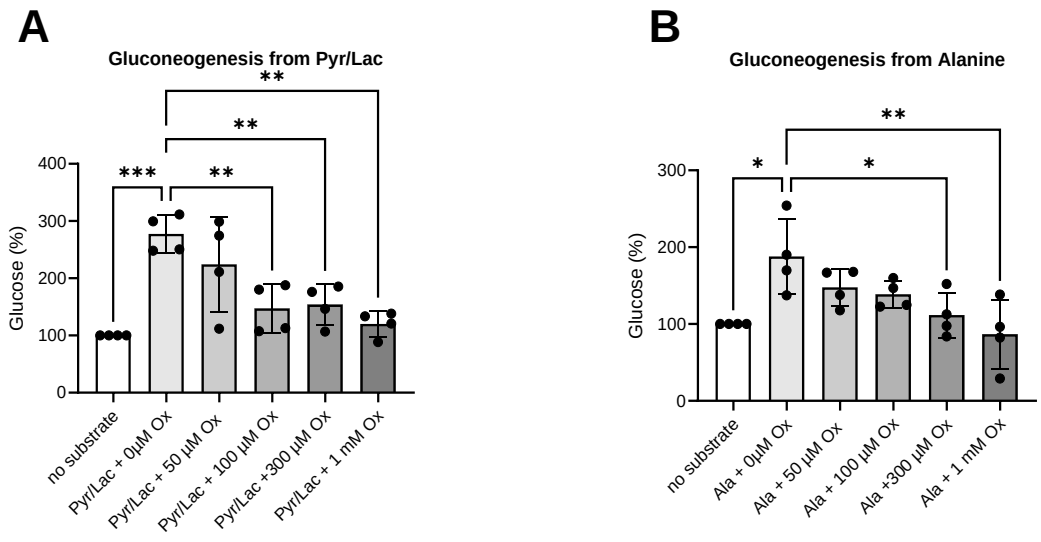

Figure 18: Glucose production in primary mouse hepatocytes from **(A)** pyruvate/lactate (2/20 mM) co-exposed with increasing concentrations of oxalate (n=4) **(B)** alanine (10 mM) co-exposed with increasing concentrations of oxalate (n=4) (All bar diagrams represent the mean ± SD.*p<0.05; **p<0.01; ***p < 0.001; Student's t test, unpaired, two sided). Ala = alanine, Ox = oxalate

A comparable result was obtained for the glucogenic precursor alanine. Basal production was less compared to the production of glucose from pyruvate/lactate. For the two lowest concentrations of oxalate, 50 µM and 100 µM, no significant decrease regarding the production of glucose was measurable; however, a trend for less production of glucose was obvious. Significance was reached with oxalate concentrations of 300 µM, which approximately corresponds to an intracellular concentration of 15 µM (Fig. 18B). The results indicate that oxalate impairs the pyruvate/lactate- and amino acid-driven gluconeogenesis in hepatocytes *in vitro*.

3.2.3 Glycerol-driven gluconeogenesis is not influenced by oxalate exposure in primary mouse hepatocytes

A very similar experiment was performed testing the influence of increasing concentrations of oxalate on glycerol-driven gluconeogenesis in primary mouse hepatocytes. Glycerol is like pyruvate/lactate and amino acids also an important glucogenic substrate for the *de novo* production of glucose, but it enters the glucogenic pathway at a different site and does not require Pc and Pck1. Interestingly, in contrast to the treatment with pyruvate/lactate and alanine, glucose production from glycerol was not perturbed by the co-exposure with oxalate (see Fig. 19). Even at the highest concentration of 1 mM oxalate, glucose production from glycerol was not diminished.

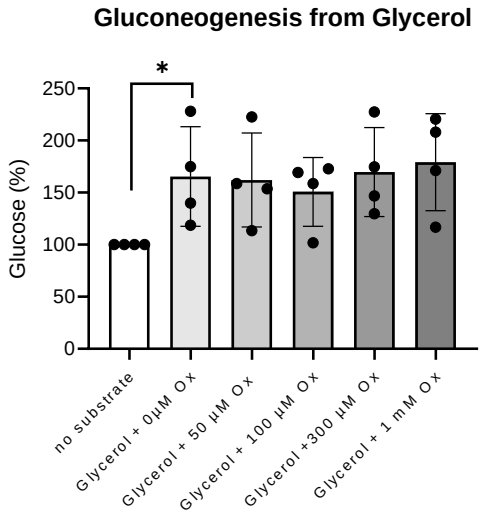

Figure 19: Glucose production in primary mouse hepatocytes from glycerol (5 mM) co-exposed with increasing concentrations of oxalate (n=4).

The results obtained showed that glycerol-driven gluconeogenesis is not affected by oxalate and are in line with the fact that glycerol bypasses the oxalate-inhibited step of Pc and Pck1. In the next chapter, the translational relevance of the inhibitory function of oxalate will be investigated in primary human hepatocytes.

3.2.4 Primary human hepatocytes are more sensitive to increased concentrations of oxalate compared to mouse hepatocytes

In a subsequent study, the effect of oxalate on the production of glucose *in vitro* was investigated with primary human hepatocytes. In the first place, a cell viability assay was performed to rule out different susceptibility regarding high concentration of oxalate.

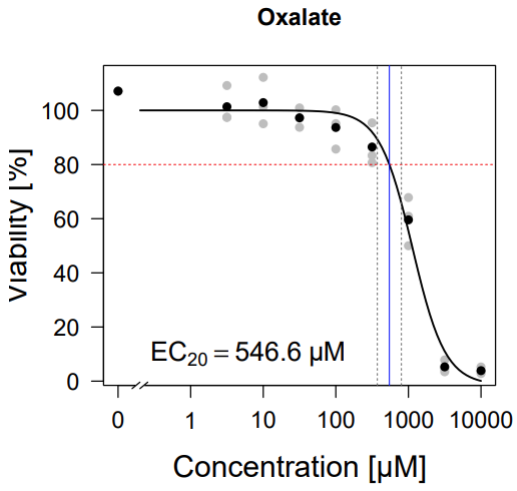

Figure 20*:* Concentration response curve of oxalate in human hepatocytes (grey dots represent the results of at least three biological replicates, black dots denote the concentration-wise mean. The vertical blue line indicate the EC20. The vertical dotted grey line indicate the confidence intervals (n=3)).

The results showed that human hepatocytes are more sensitive to higher oxalate concentrations compared to mouse hepatocytes. Here, the EC_{20}-value for oxalate was modelled to be at 546.6 µM (see Fig. 20). The difference for the EC_{20} value between mouse hepatocytes and human hepatocytes is almost 5-fold lower in primary human hepatocytes. This reveals that they are more sensitive compared to primary mouse hepatocytes (2289.6 µM vs. 546.6 µM). The non-toxic concentration range in which human hepatocytes were not affected by oxalate was between 0 and 300 µM. This concentration range was applied in the following experiments. The reason for the large difference in oxalate susceptibility might be explained by species differences.

3.2.5 Production of glucose from pyruvate/lactate and amino acids is influenced by oxalate in primary human hepatocytes

After the determination of the concentration range of oxalate for a subsequent glucose production assay, primary human hepatocytes were exposed to glucogenic precursor as seen in the previous experiments with primary mouse hepatocytes. The aim of this experiment was to investigate the translational relevance of the oxalate effect on gluconeogenesis - observed in mouse hepatocytes to the human situation. The basal production of glucose showed that human hepatocytes produce more glucose from pyruvate/lactate compared to alanine, which is in line with findings from mouse hepatocytes. Further, the results showed that oxalate inhibits the production of glucose from pyruvate/lactate in a concentration-dependent manner. A significant difference between untreated controls and oxalate-treated hepatocytes was observed at 100 µM oxalate, which was comparable to mouse primary hepatocytes (see Fig. 21A). This inhibitory effect was even stronger when 300 µM of oxalate were exposed to the hepatocytes. For alanine, the lowest concentration of oxalate did not result in a significant change in the glucose production. However, a significant inhibitory effect of oxalate was observable at a concentration of 100 µM (see Fig. 21B). This was also the case when the higher concentration of 300 µM oxalate was applied. The results indicate a similar physiology of oxalate inhibiting the glucose production from pyruvate/lactate and alanine.

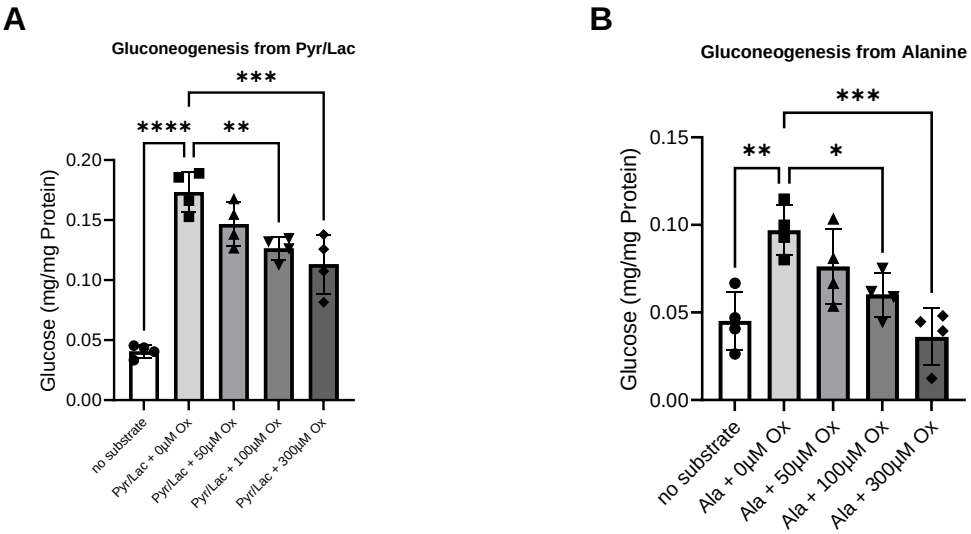

Figure 21: Glucose production in primary human hepatocytes from **(A)** pyruvate/lactate (2/20 mM) co-exposed with increasing concentrations of oxalate (n=4); **(B)** alanine (10 mM) co-exposed with increasing concentrations of oxalate (n=4). (All bar diagrams represent the mean ± SD.*p<0.05; **p<0.01; ***p < 0.001; Student's t test, unpaired, two sided). Ala = alanine, Ox = oxalate

3.2.6 Primary human hepatocytes are not influenced by oxalate when glucose is produced from glycerol

To investigate whether glycerol-driven gluconeogenesis is affected by the exposure of oxalate in human hepatocytes, a similar experiment was conducted. Increasing concentrations of oxalate were co-exposed together with glycerol. The results showed that the glycerol-driven gluconeogenesis was not affected by oxalate (see Fig. 22). The results matched the observation made in primary mouse hepatocytes.

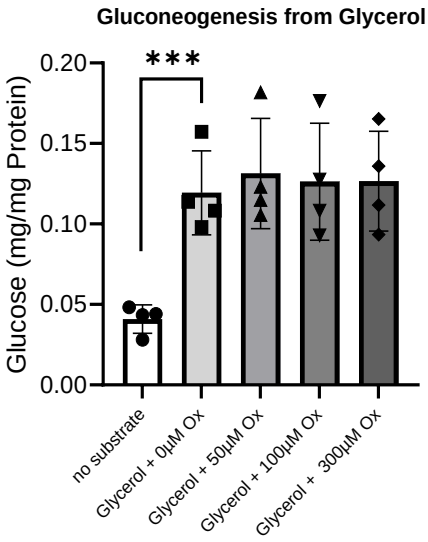

Figure 22: Glucose production in primary human hepatocytes from glycerol (5 mM) co-exposed with increasing concentrations of oxalate (n=4). Ox = oxalate

3.3 Inhibition of gluconeogenesis from hydroxyproline-derived oxalate

3.3.1 Determination of a non-toxic effect concentration of hydroxyproline

Having seen that extracellular oxalate itself can accumulate within hepatocytes, the next approach was to clarify whether this oxalate-associated inhibitory effect on gluconeogenesis can be reproduced when an immediate precursor of oxalate is given to the cells. Since hydroxyproline is one of the known precursors from which oxalate is produced in elevated amounts, we hypothesized that the exposure of hydroxyproline along with glucogenic substrates would also lead to a decrease in glucose production. A first step was to perform a viability assay in order to determine a non-toxic concentration range of hydroxyproline, which allows us to continue with the glucose production assay.

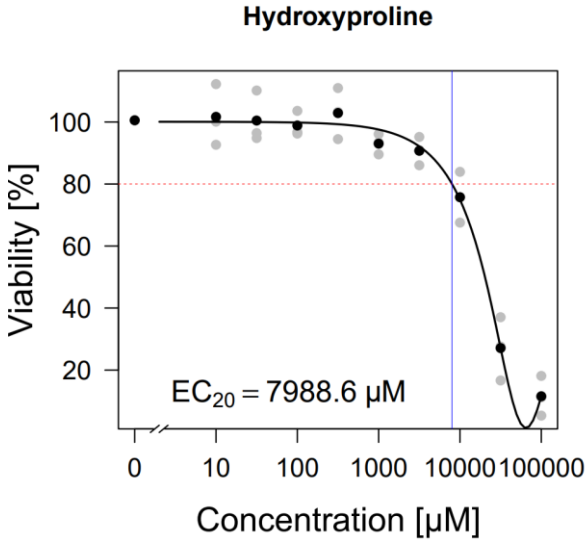

Figure 23: Concentration response curve of hydroxyproline in primary mouse hepatocytes (grey dots represent the results of at least three biological replicates, black dots denote the concentration-wise mean. The vertical blue line indicate the EC20 (n=3)).

The viability assay was performed with primary mouse hepatocytes in three biological replicates. The results from the viability assay and the modelling of the data revealed an EC_{20} value of 7988.6 µM, which means that the viability was decreased by 20 % at this particular concentration (see Fig. 23). With this information, we continued to evaluate and quantify the different intermediates of the glyoxylate pathway generated by hydroxyproline catabolism after addition of hydroxyproline in a time- and concentration-dependent manner up to 10 mM.

3.3.2 Intra- and extracellular quantification of hydroxyproline-derived intermediates

The three main metabolites generated from the catabolism of hydroxyproline that can be detected with the established LC/MS method are glyoxylate, glycolate and oxalate. Therefore, a time course experiment was set up and early and late time points were collected to quantify the intracellular and extracellular levels of these intermediates. The kinetics after the catabolism of hydroxyproline follow a very distinct pattern. Early after the exposure, the intracellular levels of glyoxylate increased significantly in a concentration-dependent manner indicating that hydroxyproline was immediately metabolized by hepatocytes (see Fig. 24). Over the time course of the experiment, the intracellular levels of glyoxylate decrease. The extracellular levels of glyoxylate did not follow a concentration-dependent manner (see Fig. 24). In the early time points, the glyoxylate levels are constant independent of the increasing concentrations of hydroxyproline exposure. The late time points display that a very small amount of glyoxylate is shuttled directly out of the cells, but this is also independent of the

treatment. To stress how small the amounts of glyoxylate extracellularly are, one can compare the values with the extracellular levels of glycolate, which are almost 100-fold higher than the glyoxylate levels. (see Fig 25).

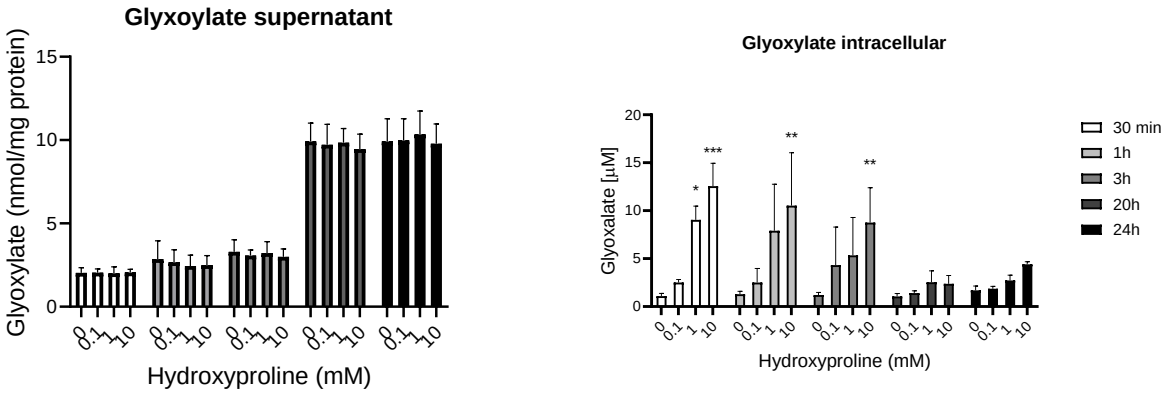

Figure 24: Supernatant and intracellular levels of glyoxylate from wt hepatocytes after exposure to increasing concentration of hydroxyproline (n=3). (All bar diagrams represent the mean ± SD.*p<0.05; **p<0.01; ***p < 0.01 compared to 0 mM Hyp; Student's t test, unpaired, two sided).

Overall, the glyoxylate data revealed that glyoxylate is not being exported out of the hepatocytes during the catabolism of hydroxyproline. Rather it is further metabolized to other intermediates of the glyoxylate pathway.

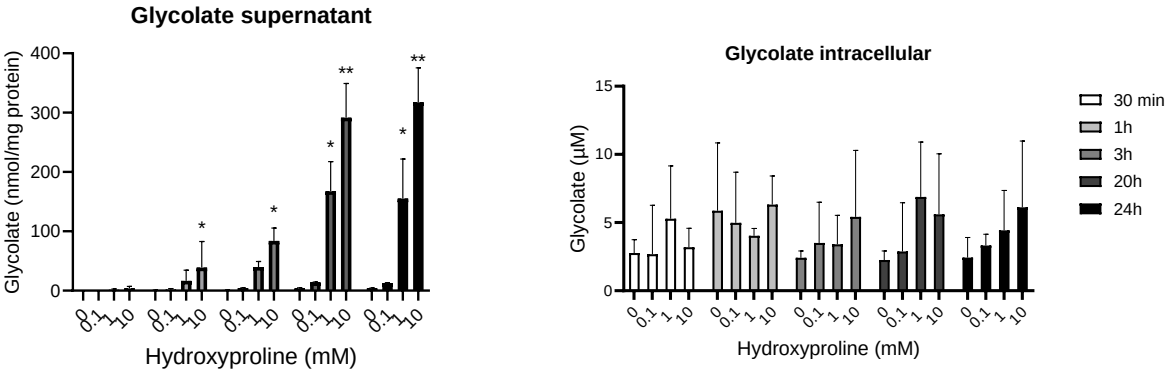

Figure 25: Supernatant and intracellular levels of glycolate from wt hepatocytes after exposure to increasing concentration of hydroxyproline (n=3). (All bar diagrams represent the mean ± SD.*p<0.05; **p<0.01 compared to 0 mM Hyp; Student's t test, unpaired, two sided).

Interestingly, glycolate and oxalate do not accumulate within the hepatocytes. The quantified levels for glycolate were in a narrow range of five to 10 µM independent of the concentration of hydroxyproline that the hepatocytes were exposed to and the duration of the experiment (see Fig. 25, 26). This was also the case for oxalate. Here, it was observed that the levels of

oxalate were also in a narrow range of 2 to 5 µM. No concentration- and time-dependent correlation was observed for intracellular oxalate..

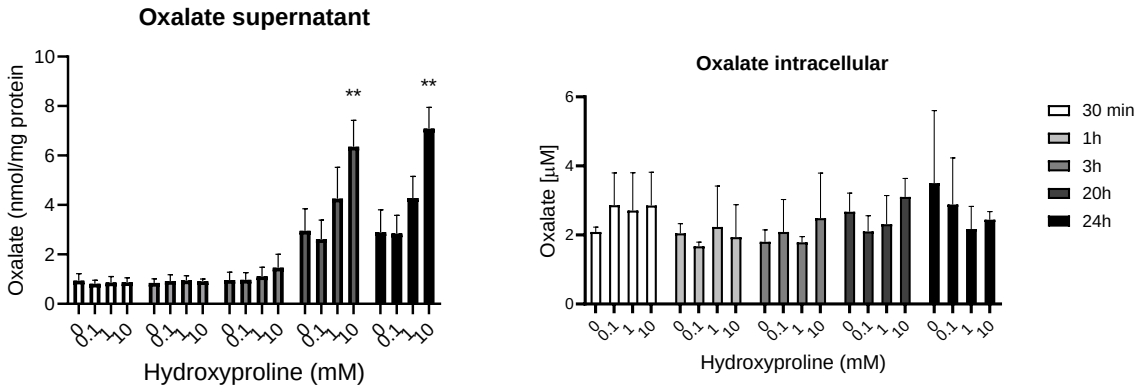

Figure 26: Supernatant and intracellular levels of oxalate from wt hepatocytes after exposure to increasing concentration of hydroxyproline (n=3). (All bar diagrams represent the mean ± SD.*p<0.05; **p<0.01; ****p < 0.001 compared to 0 mM Hyp; Student's t test, unpaired, two sided).

The results for the extracellular levels of glycolate were significantly higher compared to untreated controls after 24h (see Fig. 25).

The same pattern was observed for the extracellular quantification of oxalate. The highest concentration of hydroxyproline led to a significantly higher production of oxalate in comparison to untreated control after 24h of exposure (see Fig. 26). It was shown that the cells immediately export the metabolites in the supernatant, which also seems trivial since it is harmful for the cells to accumulate high levels of oxalate in the cells. The results fit in line with the results seen for the intracellular quantification, where only low levels of the intermediates were detected.

3.3.3 Agxt-deficient hepatocytes display elevated intracellular levels of oxalate

After the finding that oxalate does not accumulate within healthy primary mouse hepatocytes which are exposed to hydroxyproline, the next step was to evaluate whether this would happen in hepatocytes of a hyperoxaluric mouse model. Since Agxt-deficient mice - a primary hyperoxaluria 1 mouse model - were provided to us for previous experiments, we considered it as a suitable tool to investigate the oxalate-mediated inhibitory effect on gluconeogenesis. Therefore, Agxt-KO deficient hepatocytes and control hepatocytes were cultured and exposed to 10 mM hydroxyproline, after which the intracellular and extracellular concentration of glyoxylate, glycolate and oxalate were quantified. The results of the experiment (n=1) is illustrated in the figures below. The exposure of 10 mM hydroxyproline led to higher levels of oxalate in the supernatant of AgxtKO hepatocytes compared to wt hepatocytes after 20 and 24h of incubation (see Fig. 27). The intracellular levels of oxalate in AgxtKO hepatocytes showed also higher levels for oxalate at the early time points (0h – 1h) and have risen even higher at the later time points (20h – 24h) compared to wt hepatocytes. The intracellular pattern of glyoxylate was comparable between the two genotypes with the exception that the levels gradually increased in AgxtKO hepatocytes at late time points whereas the levels decreased in wt hepatocytes (see Fig. 27). The extracellular levels for glyoxylate and glycolate did not change between AgxtKO- and wt hepatocytes. The intracellular levels of glycolate were also slightly elevated in AgxtKO hepatocytes from 3h to 24h compared to wt hepatocytes (see Fig. 27).

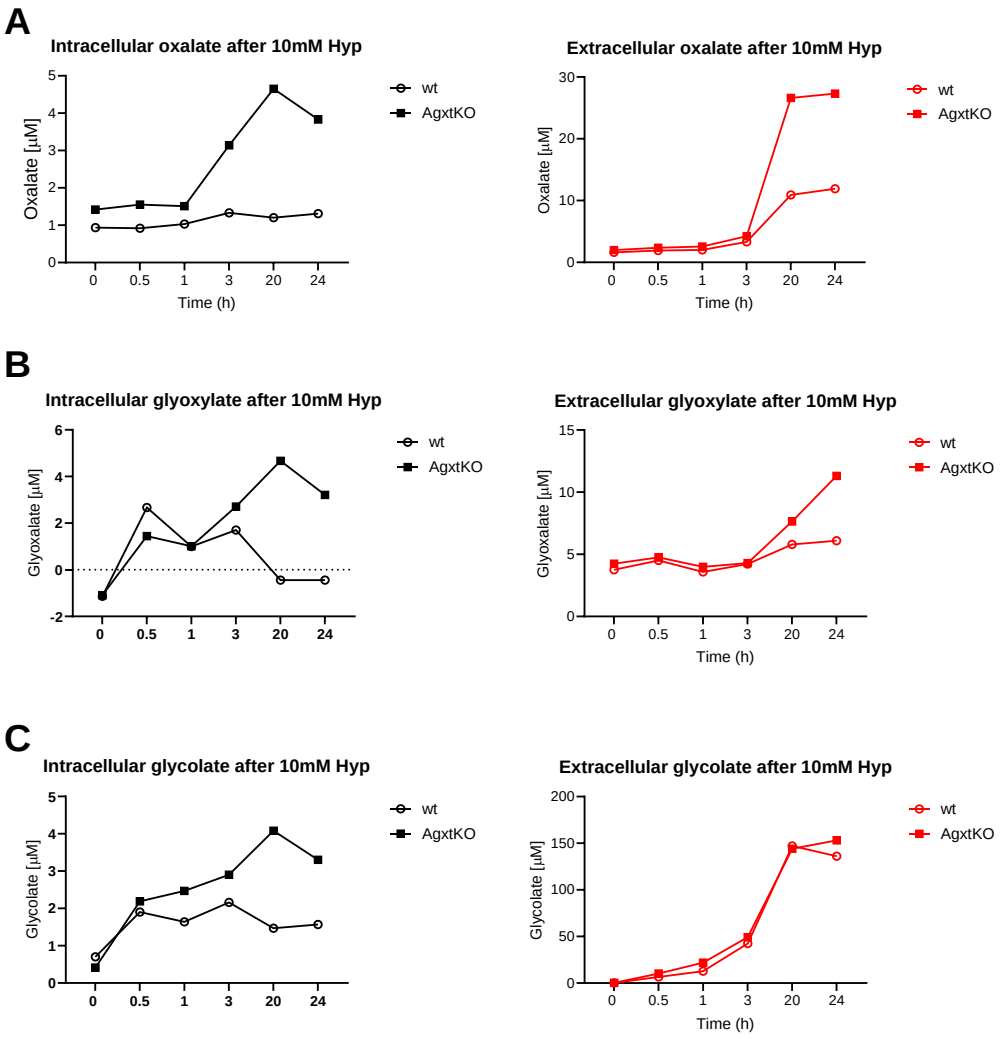

Figure 27: Intracellular and extracellular levels of **(A)** oxalate, **(B)** glyoxylate and **(C)** glycolate after the exposure to 10 mM Hydroxyproline in wt and AgxtKO hepatocytes (n=1). wt= wt, Hyp= hydroxyproline

3.3.4 Gluconeogenesis from pyruvate/lactate and amino acids is significantly reduced in Agxt-deficient hepatocytes exposed to hydroxyproline

To investigate the consequences of elevated endogenous production of oxalate on gluconeogenesis, Agxt-deficient and wt hepatocytes were exposed to glucogenic precursors along with hydroxyproline. The incubation period was 24h. Apart from the most common substrates used for gluconeogenesis, also serine was incorporated in this experiment. In addition to quantifying the glucose produced and released from the hepatocytes into the supernatant, also the oxalate produced from the catabolism of hydroxyproline was monitored. A schematic illustration of the experimental setup is shown in the figure below (see Fig. 28). After 24h, incubation with glucogenic precursor pyruvate/lactate (2/20 mM), alanine (10 mM) and glycerol (5 mM) together with hydroxyproline (10 mM) the hepatocytes

were harvested and the supernatant was collected. The supernatant was analyzed for the glucose produced from glucogenic precursor and the Hyp-derived oxalate levels.

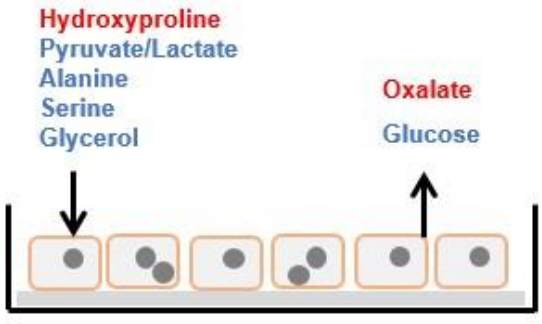

Figure 28: Experimental setup for the hepatic glucose production assay incubated with glucogenic precursor and hydroxyproline

As expected, an overall higher production of oxalate in Agxt-deficient hepatocytes compared to healthy controls was observed. The levels of oxalate in the supernatant of the cells were between 10 to 20 nmol/mg protein in control hepatocytes and about 30 to 40 nmol/mg protein in the Agxt-deficient hepatocytes, which is also known from previously performed experiments. A first finding of this experiment was that Agxt-deficient hepatocytes produced similar levels of glucose compared to wt controls in the absence of hydroxyproline (see Fig. 29A). This was independent of the treatment with either pyruvate/lactate or amino acids and can be interpreted as that Agxt itself is not directly involved in catabolizing any of the reactions required for gluconeogenesis of those substrates. For pyruvate/lactate, the hydroxyproline exposure significantly decreased the glucose production in both, wt and AgxtKO hepatocytes, but to a higher extent in AgxtKO hepatocytes (see Fig. 29A). A similar trend was observed for the amino acid alanine; although not significant, the exposure to hydroxyproline led to a reduction in the glucose production, which was more pronounced in Agxt hepatocytes compared to wt hepatocytes.

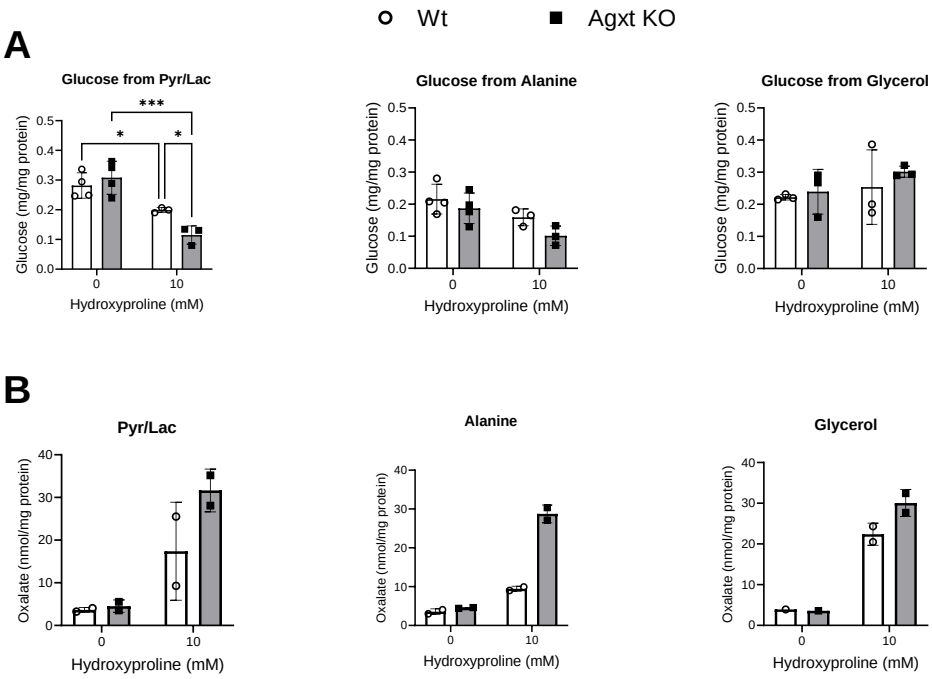

Figure 29: **(A)** Glucose production in primary mouse hepatocytes from pyruvate/lactate, alanine and glycerol when co-exposed with 10mM hydroxyproline (n=3/4); **(B)** Oxalate quantification in the supernatant of the same experiment from part (A) of this figure (n=1/2). (All bar diagrams represent the mean ± SD.*p<0.05; **p<0.01; ****p < 0.0001; Student's t test, unpaired, two sided). wt= wt

3.3.5 Glycerol-driven gluconeogenesis is not influenced by hydroxyproline catabolism nor Agxt-deficiency

Beside the *de novo* production of glucose from pyruvate/lactate and amino acids, also the influence of hydroxyproline-derived oxalate on glycerol-gluconeogenesis was investigated. Despite elevated levels of hydroxyproline-derived oxalate in wt and Agxt-deficient hepatocytes, glycerol-driven gluconeogenesis was not influenced (see Fig. 29A). There was also no difference between the genotypes showing that glycerol-derived glucose was not sensitive to the exposure of hydroxyproline in AgxtKO hepatocytes. The results obtained fit to those observed when primary cells were exposed directly to oxalate (see Fig. 11 and 12).

In summary, it could be shown that both exogenous oxalate itself and oxalate generated in the cell by the catabolism of its precursor hydroxyproline lowered gluconeogenesis from lactate/pyruvate and alanine *in vitro*. However, *in vitro* experiments always have limitations regarding their physiological relevance since cells cultivated in vitro do not represent a whole organism and only represent an isolated system. To explore the *in vivo* relevance of the *in vitro* findings, mouse models known to be associated with elevated oxalate levels should be explored.

3.4 Identifying mouse models high in systemic oxalate levels

3.4.1 Agxt Knockout (AgxtKO) mice represent a mouse model for Primary hyperoxaluria type 1 (PH1)

A well-established mouse model for PH1 that presents with hyperoxaluria and oxalemia are the previously introduced AgxtKO mice. In this thesis it was confirmed that these mice completely lack the Agxt protein (see Fig. 30A), resulting in an insufficient detoxification of the oxalate precursor glyoxylate and subsequently significantly elevated levels of oxalate in the plasma and in the urine (see Fig. 30B). Agxt is only expressed in the liver. Therefore hyperoxaluria in Agxt knockout mice is presumed to be due to hepatic oxalate production. Because the oxalate produced by the liver is secreted to the blood and eliminated *via* the kidney, the oxalate burden in both tissues - the liver, as the main "producer" and the kidney, as the main "disposer" - was quantified after tissue oxalate extraction. This was of particular interest because both organs are glucogenic, and therefore oxalate could influence gluconeogenesis, as already studied *in vitro*. Phenotypically, AgxtKO mice do not display any special conspicuity compared to healthy mice, as demonstrated by histological stainings of liver and kidney sections (see Fig. 30C). It was observed that AgxtKO mice show slightly elevated levels of oxalate accumulation in liver and kidney, which was significant in the latter one (see Fig. 30D).

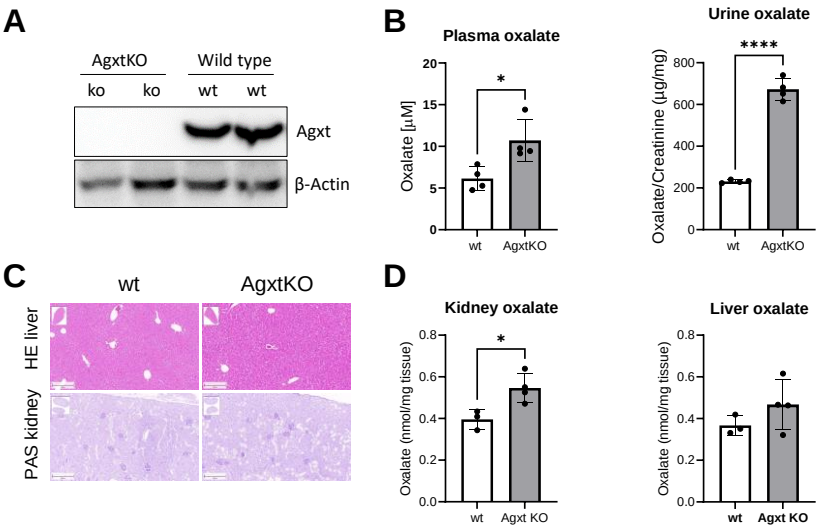

Figure 30: (A) Western Blot analysis of wt and AgxtKO mice; **(B)** Plasma and urine oxalate levels in wt and AgxtKO mice (n=4); **(C)** HE and PAS stainings of liver and kidney of wt and AgxtKO mice ; **(D)** Oxalate accumulation in kidney and liver tissue of wt and AgxtKO mice (n=4). (All bar diagrams represent the mean ± SD.*p<0.05; ****p < 0.0001; Student's t test, unpaired, two sided).HE= Haematoxylin/Eosin, PAS= Periodic acid Schiff, wt= wildtype

3.4.2 Rescuing Agxt using AAV-mediated transfer prevents hyperoxaluric phenotype in AgxtKO mice

To demonstrate that lack of Agxt in AgxtKO mice is responsible for the excessive formation of oxalate, a mechanistic study was performed rescuing the Agxt gene using an adeno-associated virus (AAV) carrying the Agxt cDNA under the control of a liver-specific promoter. This sub-chapter is part of the publication that was published in 2021 by Gianmoena *et al.* (Gianmoena et al., 2021). The experimental setup of the four-week study is illustrated in the figure below (see Fig. 31A). In this experiment, urine was collected before AAV-transfer was performed and on days 11, 21 and 28 post AAV-transfer. Mice were sacrificed on day 28 and plasma and organs were collected. The results show that the AAV-Agxt transfer has worked successfully. The recovery of Agxt protein expression was not only illustrated in the immunohistochemical staining by a brownish patchy distribution in the liver section (see Fig. 31B), but also in the Western blot (see Fig. 31C). Most importantly, after the AAV-transfer the elevated urine and plasma oxalate that are characteristic for AgxtKO mice were normalized to urinary levels comparable to wt mice carrying the Agxt gene (see Fig. 31D). This experiment underlined the relevant role of Agxt in the detoxification of glyoxylate.

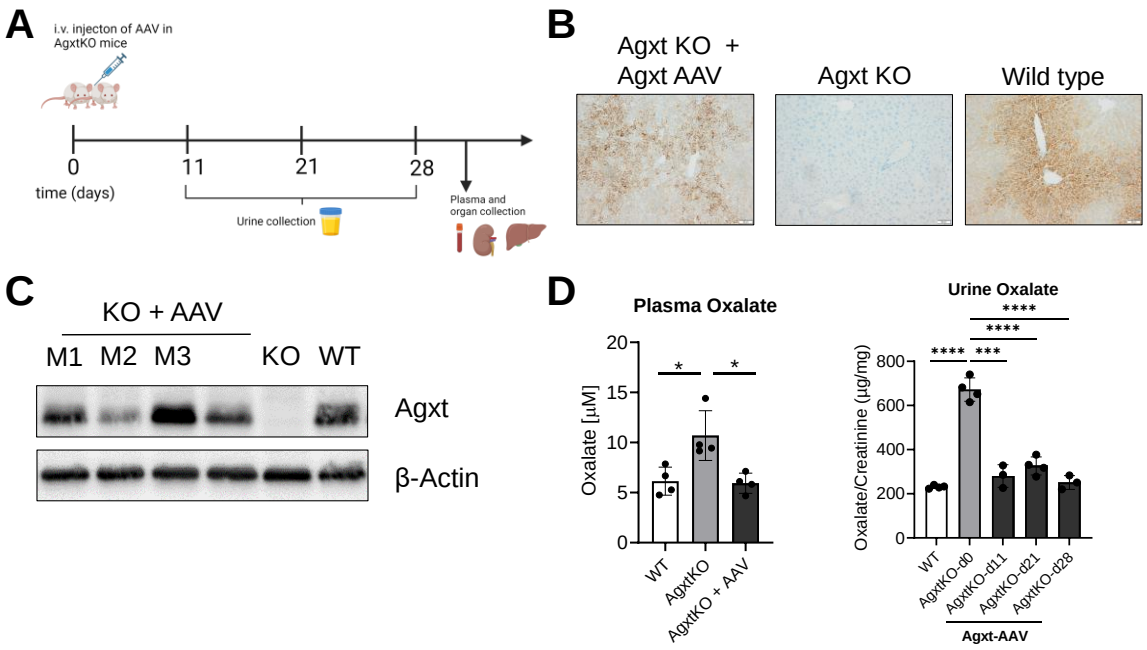

Figure 31: (A) Experimental outline of the AAV-experiment including urine collections on day 11 and 21 post AAV administration; **(B)** Immunohistochemical staining of Agxt in AgxtKO + AAV-Agxt, AgxtKO and wt mice; **(C)** Western Blot of AAV-transduced AgxtKO mice, AgxtKO mice and wt mice; **(D)** Plasma and urine oxalate levels of AgxtKO + AAV-Agxt, AgxtKO and wt mice (n=4). (All bar diagrams represent the mean ± SD.*p<0.05; ***p<0.001; ****p < 0.0001; Student's t test, unpaired, two sided).Figure (A) was created with BioRender.com. AAV= adeno-associated virus

3.4.3 Steatotic mice display downregulated Agxt gene and protein expression

It has been shown in a previous study, that Agxt protein expression is downregulated in steatotic ob/ob hepatocytes *in vitro* and *in vivo* due to a hypermethylation in the promotor region, which results in an insufficient detoxification of glyoxylate (Gianmoena et al., 2021). Ob/ob mice are characterized by overweight, increased liver/body weight ratio and a significant higher accumulation of triglycerides in the hepatocytes.

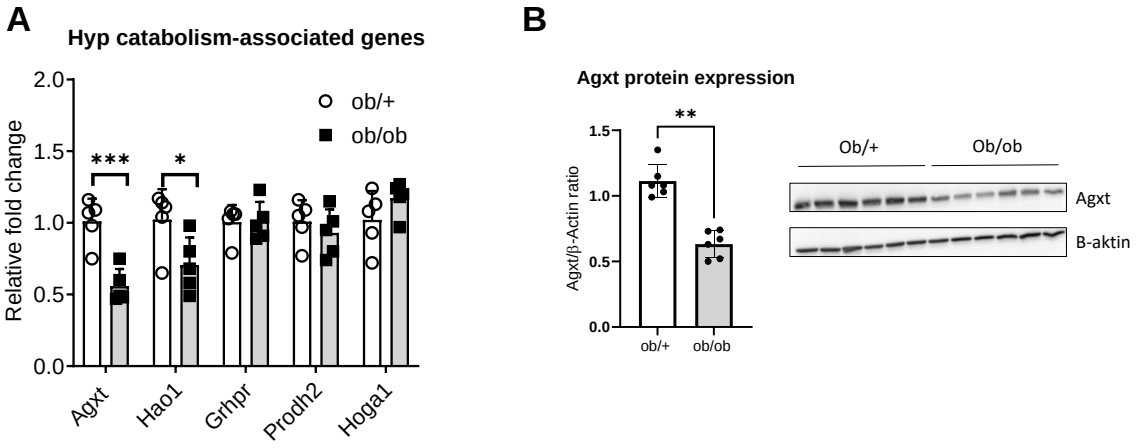

Figure 32: (A) mRNA expression analysis of various genes participating in the catabolism of hydroxyproline in ob/+ and ob/ob mice (n=5); **(B)** Quantification of Agxt protein expression and Western Blot of ob/+ and ob/ob mice (n=6). (All bar diagrams represent the mean ± SD.*p<0.05; **p<0.01; ***p<0.001; Student's t test, unpaired, two sided). Agxt= alanine-glyoxylate aminotransferase, Grhpr= glyoxylate and hydroxypyruvate reductase, Hao1= hydroxyacid oxidase1, Hoga1= 4-hydroxy-2-oxoglutarate aldolase1, Prodh2= proline dehydrogenase 2

Moreover, genes, which take part in the mitochondrial catabolism of hydroxyproline and detoxification of glyoxylate, did not show any significant changes in the liver of ob/ob mice. Only Hao1, which generates glyoxylate in the peroxisome, was downregulated (see Fig. 32A). To demonstrate a significant role of Agxt in the detoxification of glyoxylate to prevent a hyperoxaluric phenotype in steatosis the rescue study was performed with ob/ob mice *in vivo*. The experiment was similar to the experiment with AgxtKO mice (see Fig. 31) using an AAV-mediated transfer to show that gene therapy could be a feasible method to prevent severe accumulation of oxalate and urinary excretion.

3.4.4 Agxt downregulation in liver steatosis leads to increased oxalate production from dietary hydroxyproline and is rescued by AAV-mediated Agxt transfer

A mechanistic study using AAV gene transfer was performed in ob/ob and ob/+ mice receiving a dietary challenge of 1%Hyp or a NCD (Normal chow diet). Two weeks prior to the actual start of the experiment and beginning of the dietary feeding, ob/ob mice were either transfected with AAV carrying Agxt or with a control AAV carrying the reporter gene EGFP. After a resting

phase to allow expression of the transduced Agxt, AAV-transduced ob/ob mice and ob/+ mice were put on the allocated diet for two weeks (see Fig. 33A). On the last two days of the diet, urine was collected. Thereafter mice were sacrificed and plasma and organs were collected for various analysis (see Fig. 33A). The results showed that the gene transfer has worked successfully. Comparing the IHC staining in the liver of EGFP-AAV and Agxt-AAV-treated ob/ob mice, the intensity of the Agxt-AAV-transduced liver sections was stronger compared to the EGFP-AAV-transduced liver sections and became comparable to that of control ob/+ mice (see Fig. 33C). The same observation was made for the protein expression of Agxt using Western blots. Regarding the plasma oxalate levels and urinary oxalate excretion after 1% Hyp diet, ob/ob mice displayed higher levels of oxalate compared to ob/+ mice (see Fig. 31B). The viral transfer of Agxt in ob/ob mice led to a reduction of hepatic oxalate production and urinary excretion which was comparable to healthy ob/+ mice (see Fig. 31B). To sum this up, the results show that the steatotic liver of ob/ob mice produced elevated levels of oxalate representing a hyperoxaluric phenotype after dietary challenge that was prevented using an AAV-mediated gene transfer of Agxt.

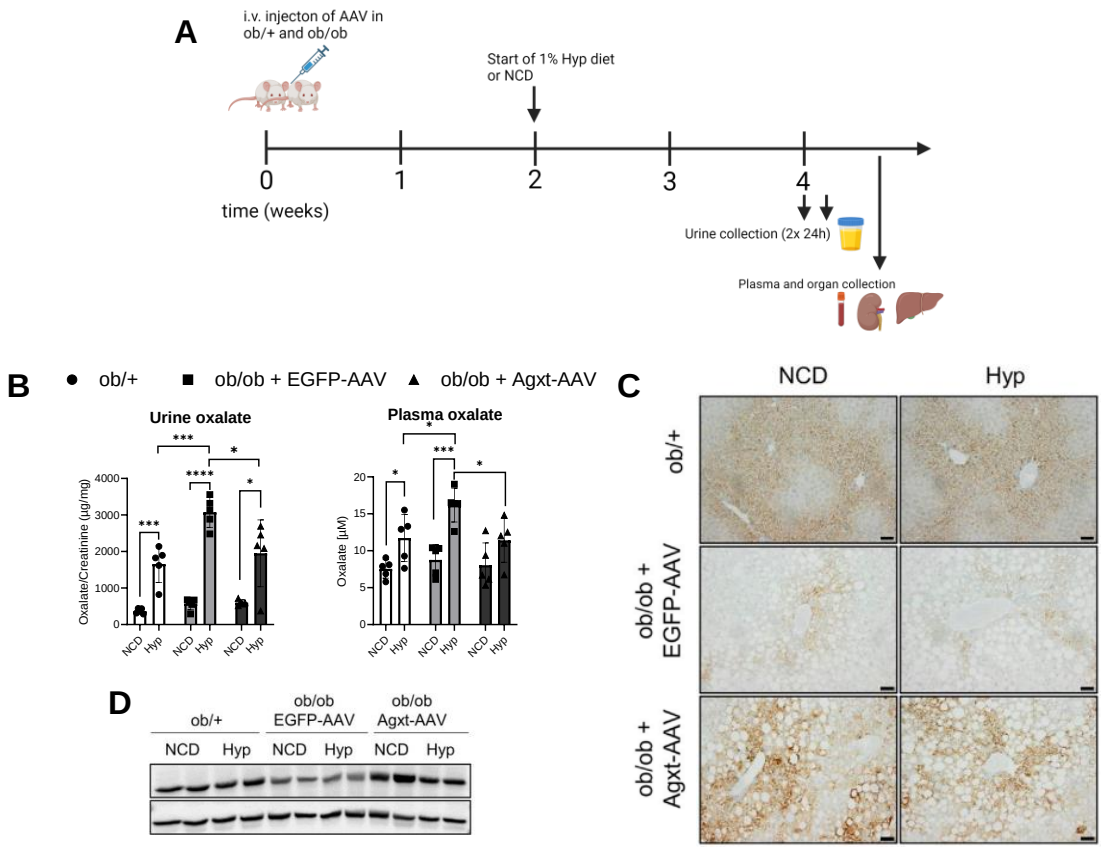

Figure 33: (A) Experimental outline of the AAV-experiment in ob/ob and control ob/+ mice; **(B)** Plasma and urine oxalate levels of AAV-Agxt-ob/ob mice, AAV-EGFP-obob mice and control ob/+ mice (n=5); **(C)**

Immunohistochemical staining of AAV-Agxt-ob/ob mice, AAV-EGFP-ob/ob mice and control ob/+ mice); **(D)** Western blot of AAV-Agxt-ob/ob mice, AAV-EGFP-ob/ob mice and control ob/+ mice . (All bar diagrams represent the mean ± SD.*p<0.05; **p<0.01; ***p<0.001; Student's t test, unpaired, two sided). Figure (A) was created with BioRender.com. AAV= adeno-associated virus, Agxt= alanine-glyoxylate aminotransferase, EGFP= enhanced green fluorescent protein, Hyp= hydroxyproline, NCD= normal chow diet

3.5 Characterization of glucose homeostasis in the AgxtKO mice

3.5.1 Fasting glucose levels do not differ in Agxt-deficient mice

In how far oxalate affects glucose homeostasis and gluconeogenesis was next investigated in the AgxtKO mouse model. As previously shown, lack of Agxt in these mice leads to elevated oxalate production by the liver, resulting in hyperoxaluria and oxalemia and increased deposition of oxalate in tissue, particularly in the kidney (see Fig. 30). A common approach to investigate glucose homeostasis and gluconeogenesis is to fast the mice overnight and measure the blood glucose levels. Fasting glucose levels of 80-100 mg/dl are normally shown in the plasma of healthy mice. Values above (hyperglycemia) or below (hypoglycemia) indicate perturbation in glucose homeostasis. AgxtKO and wt mice were fasted for about 16 hours starting in the afternoon until the next morning. Since mice are nocturnal animals, the fasting occurs during their active phase. As a control, mice of both genotypes were also collected in the *ad libitum* state.

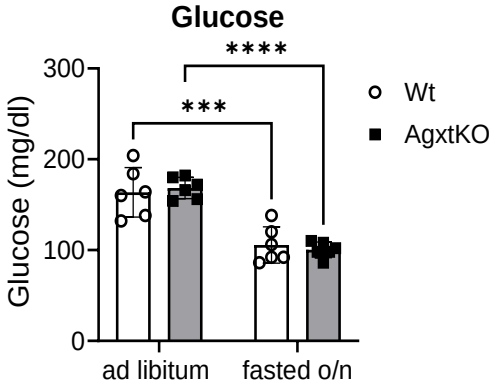

Figure 34: Blood glucose levels of wt and AgxtKO mice in the *ad libitum* and fasting state (n=6). (All bar diagrams represent the mean ± SD; ***p<0.001; ****p < 0.0001; Student's t test, unpaired, two sided)

The results showed that there was no difference in the blood glucose levels between wt and Agxt-deficient mice after an overnight fast (see Fig. 34). The *ad libitum* blood glucose levels were significantly higher compared to the fasted state, which was expected since they have free access to food. According to this result, AgxtKO mice are able to maintain the blood glucose levels after fasting despite their oxalate overproduction. This motivated the

investigation of possible compensatory mechanisms in the glucogenic organs, liver and kidney tissue.

One unexpected result was the difference in the body weight loss that resulted from an overnight fasting. AgxtKO mice generally lost less body weight compared to wt control mice although no difference in the fasting blood glucose levels was observed (see Fig. 35). Fasting-induced loss of body weight in mice is thought to reflect loss of muscle mass (Jensen et al., 2013). This suggests decreased muscle protein degradation in the muscle of AgxtKO, which may result in less release of amino acids for gluconeogenesis.

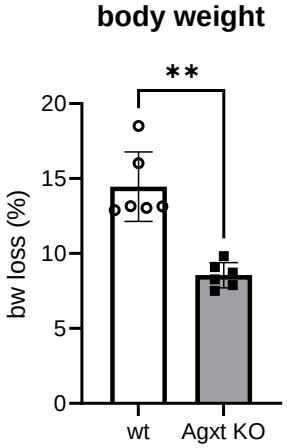

Figure 35: body weight loss of wt and AgxtKO mice after an overnight starvation (n=6). (All bar diagrams represent the mean ± SD; **p<0.01; Student's t test, unpaired, two sided). bw= body weight

Macroscopically, the phenotype of the AgxtKO mice did not differ from the wt controls. By now, the reasons for this robust observation remained unclear.

Subsequently, blood chemistry parameters were determined using the Piccolo Xpress Chemistry Analyzer. Blood urea nitrogen (BUN) stands for the nitrogen bound to urea in the plasma/serum and is an indirect measure for the protein catabolism. In the fasting state, the levels of BUN increased significantly in both, wt and AgxtKO mice, indicating that the fasting intervention results in an increased protein turnover. However, AgxtKO mice display significantly lower levels of urea compared to wt when fasted (see Fig. 36). This suggests that protein turnover is decreased in AgxtKO mice compared to wt mice. A second interesting finding was observed, when alkaline phosphatase (ALP) was analyzed. In fasted AgxtKO mice the levels of ALP were significantly lower compared to those of fasted wt mice, and also compared to the *ad libitum* state (see Fig. 36). ALP is thought to play a role in bone turnover

and one isoform of ALP is detected in patients suffering from CKD (Greenblatt et al., 2017; Nizet et al., 2020). However, little is known about the role of circulating ALP. Regarding the clinical parameters for albumin (ALB), total protein (TP) and aspartate-aminotransferase (AST) no significant difference was observed. For alanine-aminotransferase (ALT), a significant reduction in AgxtKO was detected after fasting of the mice compared to *ad libitum* state. However, since both ALT and AST lie within normal range values, this has no clinical significance.

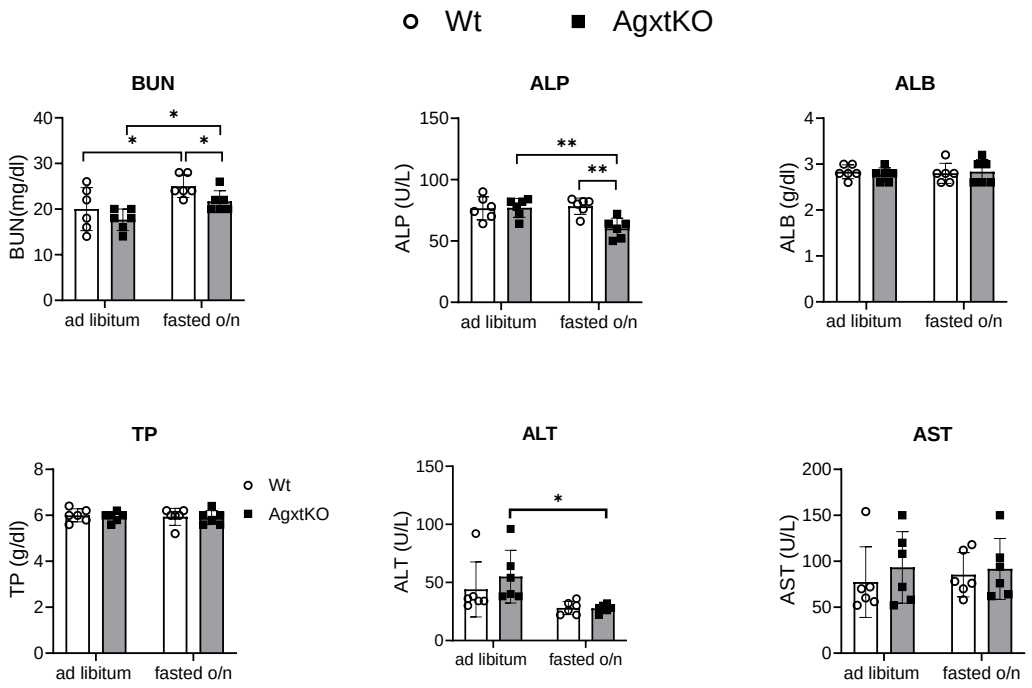

Figure 36: Clinical plasma parameters from wt and AgxtKO mice in the *ad libitum* and fasting state (n=6) (All bar diagrams represent the mean ± SD; *p<0.05; **p< 0.01; Student's t test, unpaired, two sided). BUN= blood urea nitrogen, ALP= alkaline phosphatase, ALB= albumin, TP= total protein, ALT= alanine aminotransferase, AST= aspartate aminotransferase

Based on these results possibly indicating minor but significant alterations on protein catabolism in AgxtKO mice after fasting, a next exploratory approach was to analyze the free amino acid levels in the plasma, liver and kidney tissue of the mice. Since gluconeogenesis can be driven by muscle-derived amino acids, the assessment of amino acids in the plasma and tissue of control and AgxtKO mice might be indicative for their utilization as glucogenic substrates, and might also correlate with the differences in the body weight loss after overnight fasting and the changes in BUN levels in AgxtKO mice.

3.5.2 Plasma amino acids levels show different pattern in wt and AgxtKO mice

To further characterize the adaptive response to the overnight fast, the next approach was to quantify the levels of amino acids in the plasma. This is of importance because amino acids derived from the breakdown of muscle tissue via proteolysis are released to the blood and can be taken up by the glucogenic organs for gluconeogenesis as an essential source to maintain blood glucose levels under fasting conditions. Here, we compared wt and AgxtKO mice in the *ad libitum* state and fasted overnight. In general, the most significant difference was noted in the response to fasting.

In general, when we compared amino acid levels in the *ad libitum* and fasting state of the mice, we observed for the amino acids glutamine and alanine decreased levels in both genotypes after fasting (compare Fig. 37A and B). These observations fit in line with observations made in rats (Holecek and Sispera, 2016). The only amino acid that was significantly elevated in AgxtKO compared to wt mice *ad libitum* was hydroxyproline *(*see Fig.37A*)*.

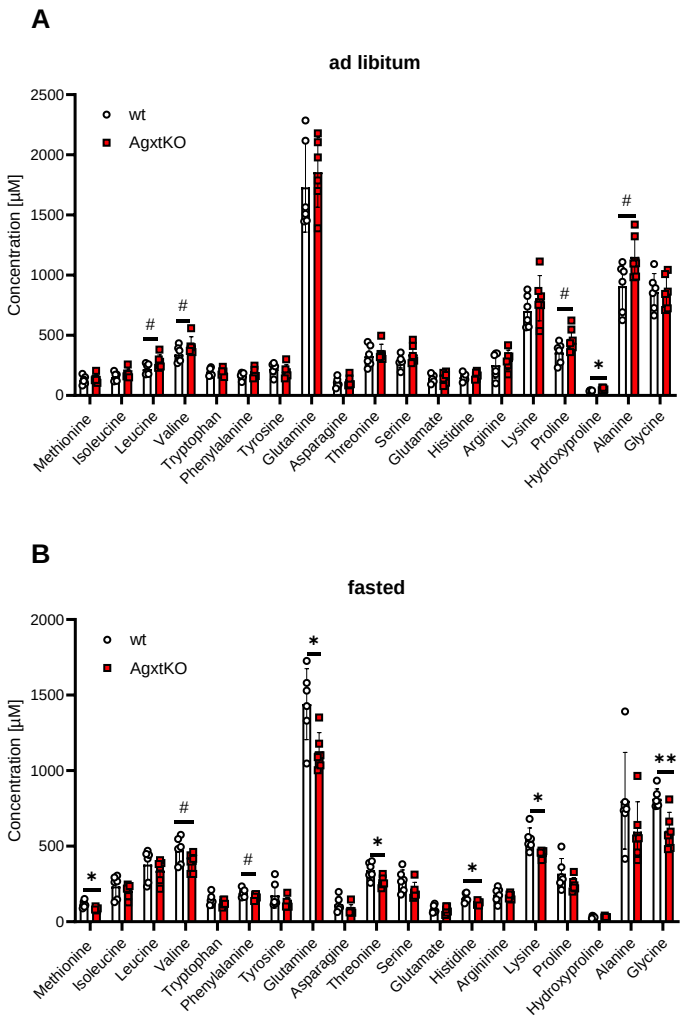

Figure 37: Plasma amino acid levels in wt and AgxtKO mice in the **(A)** *ad libitum* and **(B)** fasting state (n=6). (All bar diagrams represent the mean ± SD; *p<0.05; **p<0.01; #p>0.1; Student's t test, unpaired, two sided)

Although not significant, alanine, proline valine and leucine tended to be increased in the AgxtKO mice in the *ad libitum* state. The slightly elevated levels of alanine could be attributed to the lack of Agxt in hepatocytes, which use alanine to facilitate its intended reaction to detoxify gylxoxylate via transamination. Consequently, less alanine is used and this might result in increased levels of alanine in the plasma of AgxtKO mice. In the fasting conditions, amino acids methionine, glutamine, threonine, histidine, lysine and glycine were significantly decreased in the plasma of AgxtKO mice (see Fig. 37B).

Valine and phenylalanine showed a trend towards decreased levels in AgxtKO mice, but this was not significant. Decreased levels of glycine could be attributed to the missing Agxt protein which does not facilitate the conversion of alanine and glyoxylate to glycine and pyruvate. Hence, lower levels of glycine are present in the plasma. The lower levels of glutamine, one of the main glucogenic precursors derived from muscle protein breakdown after fasting may be

related to reduced protein degradation in muscle. Further, decreased levels of lysine, which is reported to be a marker of protein degradation, could represent a further evidence of this phenomenon (Houten et al., 2013).

Next, the free amino acid content of the liver tissue of the mice was quantified since the liver is the main organ responsible to produce glucose. In general, the data revealed no significant differences between wt and AgxtKO mice for most of the amino acids.

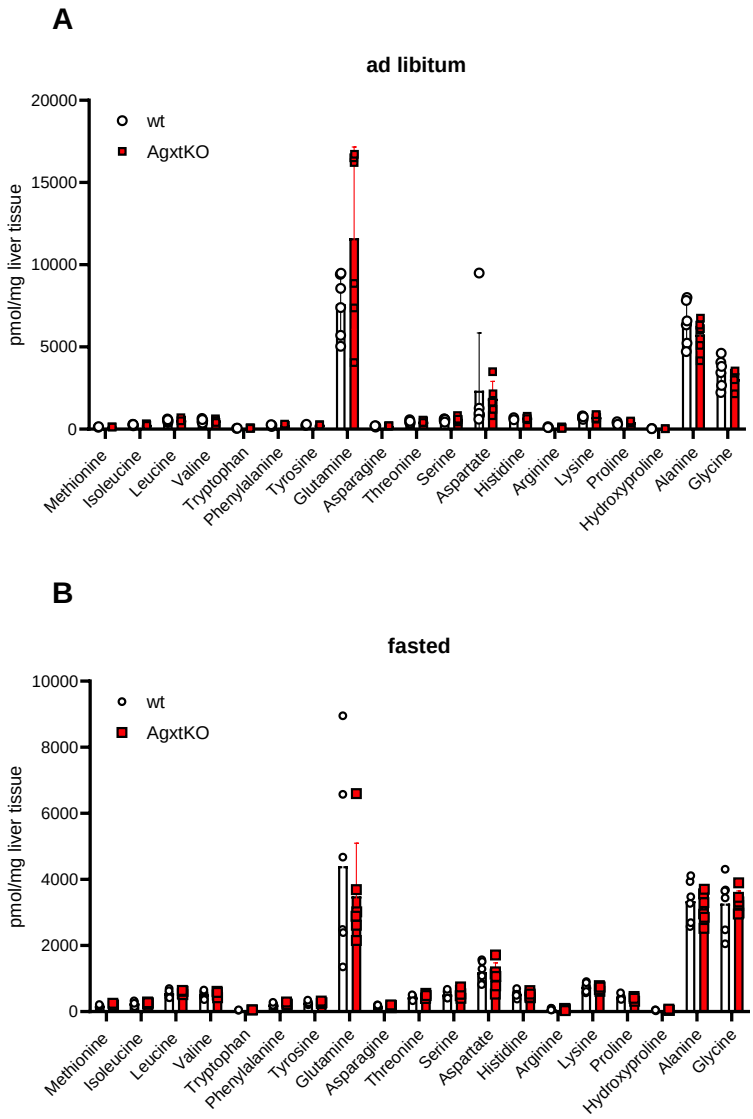

Figure 38: Liver tissue amino acid levels of wt and AgxtKO mice in the **(A)** *ad libitum* and **(B)** fasting state (n=6) (All bar diagrams represent the mean ± SD)

Since the kidney also contributes to gluconeogenesis under prolonged starvation, amino acids were quantified in kidney tissue as well. The results showed no significant difference in the amino acid levels between wt and AgxtKO mice when comparing the genotypes *ad libitum* or fasted; except for aspartate, which was significantly reduced in the AgxtKO mice (see Fig. 39B).

A reason for the reduction of aspartate could be that its conversion to oxaloacetate, which can enter the TCA cycle or fuel gluconeogenesis to produce glucose, is enhanced. Asparagine and phenylalanine only showed a trend towards reduction in AgxtKO mice.

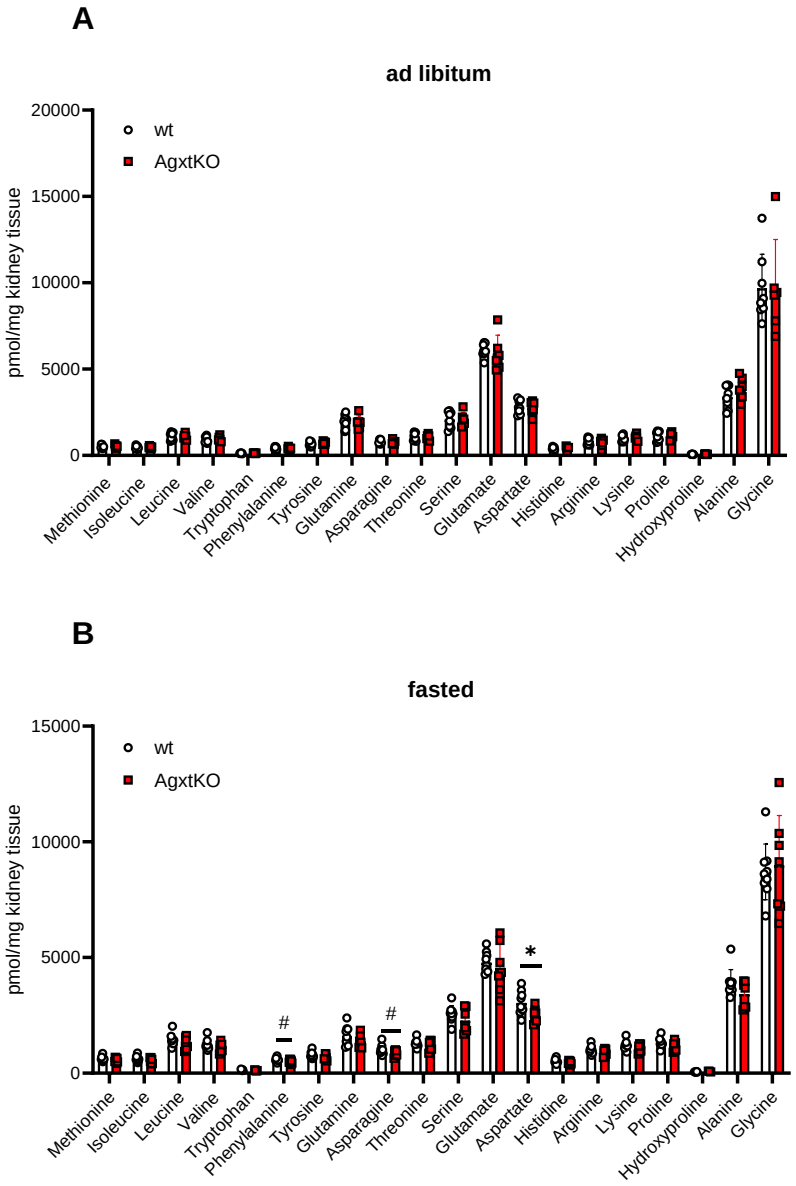

Figure 39: Kidney tissue amino acid levels in wt and AgxtKO mice in the **(A)** *ad libitum* and **(B)** fasting state (n=6) (All bar diagrams represent the mean ± SD; *p<0.05; Student's t test, unpaired, two sided)

3.5.3 Gene expression of glyoxylate pathway-genes in liver and kidney show no differences between wt and AgxtKO mice

The possibility that pathways generating oxalate are downregulated in AgxtKO mice was explored next. This could be a potential adaptive mechanism to limit oxalate production. Expression of genes involved in glyoxylate metabolism was studied by qPCR after isolation of mRNA from both the liver and the kidney of wt and AgxtKO in both *ad libitum* and fasted

states. In the liver, the gene expression of *Prodh2*, which facilitates the oxidation of L-proline to Δ1-pyrroline-5-carboxylate, did not differ between AgxtKO and wt mice independent of the treatment. This was also true for *Hoga1*, which catalyzes the final reaction of hydroxyproline catabolism releasing glyoxylate and pyruvate in the mitochondria. *Grhpr* mRNA was not changed between AgxtKO and wt mice independent of the treatment, which suggest that both are able to facilitate the reduction of glyoxylate to glycolate in the same way (see Fig. 40). For the gene *Hao1,* a significant fasting-induced downregulation was observed in both genotypes. Hao1 is essential for the oxidation of glycolate to glyoxylate in the peroxisome and can also catalyse the oxidation of glyoxylate to oxalate (Belostotsky and Frishberg, 2022). Thus, upon fasting, peroxisomal production of oxalate could indeed be reduced as an adaptive mechanism to prevent excessive oxalate generation. The opposite trend was observed for *Ldha*, mRNA levels of Ldha were significantly upregulated after an overnight starvation in both genotypes (see Fig. 40). This could mean either that Ldh facilitates the oxidation of glyoxylate to oxalate at higher rates in fasting state or it is related to its function in gluconeogenesis converting lactate to pyruvate to form glucose (Chourpiliadis and Mohiuddin, 2024).

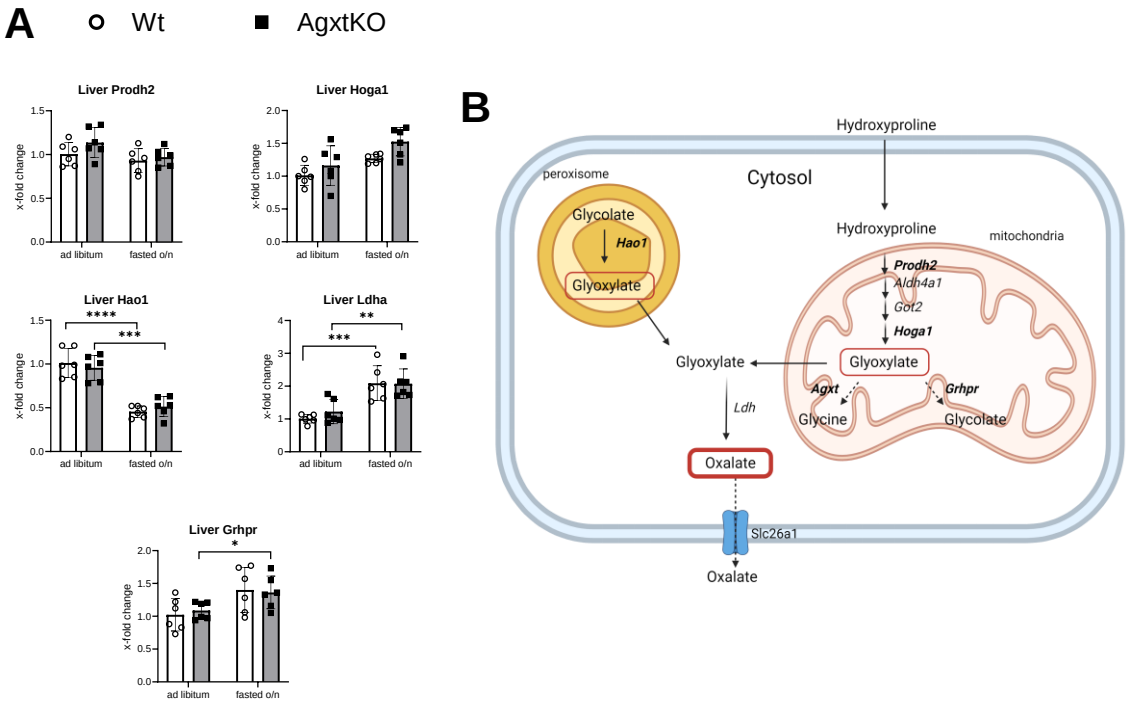

Figure 40: (A) mRNA expression of essential hydroxyproline catabolism gene of wt and AgxtKO mice in the liver after either *ad libitum* or starvation (n=6). **(B)** Illustration of hydroxyproline catabolism and its essential enzymes (All bar diagrams represent the mean ± SD; *p<0.05; *p<0.01; ***p<0.001, ****p<0.0001; Student's t test, unpaired, two sided). This figure was created with BioRender.com. Grhpr= glyoxylate and hydroxypyruvate reductase, Hao1= Hydroxyacid oxidase1, Hoga1= Hydroxy-oxoglutarate aldolase, Ldha= Lactate dehydrogenase, Prodh2= Proline dehydrogenase

In the kidney of *ad libitum* mice, the results showed no significant changes in the gene expression between the two genotypes (see Fig. 41). Interestingly in the fasting state, *Hoga1* mRNA levels in AgxtKO mice were significantly higher compared to wt mice, indicating higher glyoxylate production in the kidney of AgxtKO mice. In addition, the expression of *Ldha* was significantly downregulated in wt but not in AgxtKO mice upon fasting.

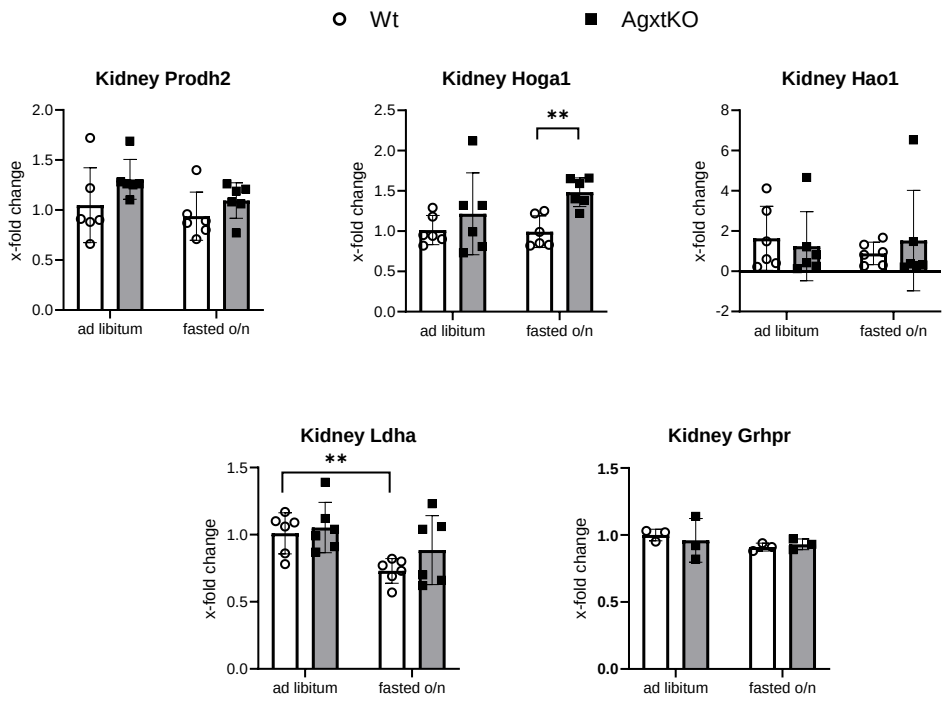

Figure 41: mRNA expression of essential hydroxyproline catabolism gene of wt and AgxtKO mice in the kidney after either *ad libitum* or starvation (n=6; for Grhpr: n=3).(All bar diagrams represent the mean ± SD;**p<0.01; Student's t test, unpaired, two sided). Grhpr= glyoxylate and hydroxypyruvate reductase, Hao1= Hydroxyacid oxidase1, Hoga1= Hydroxy-oxoglutarate aldolase, Ldha= Lactate dehydrogenase, Prodh2= Proline dehydrogenase

To summarize the results that are shown in this chapter, the results of the gene expression do not reveal major differences in the glyoxylate pathways at the mRNA level between wt and AgxtKO mice apart from the missing Agxt expression in AgxtKO mice. It can be concluded that the resulting elevated levels of oxalate observed in AgxtKO mice are solely attributed to the lack of Agxt gene/protein and that this does not lead to a negative regulation of oxalate producing pathways.

3.5.4 Expression of genes involved in gluconeogenesis in liver and kidney

In a next step, it was investigated whether gene expression changes in the liver or in the kidney for glucogenic genes occur, which could give insight into their contribution to maintain

glycemia, particularly in the overnight fasted AgxtKO mice. This is the topic in the next two sub-chapters.

3.5.4.1 Hepatic gene and protein expression of gluconeogenesis-related genes do not significantly differ between wt and AgxtKO mice

The genes encoding enzymes that catalyze the three key reactions of the gluconeogenesis pathway are *G6pc*, the terminal enzyme converting glucose-6-phosphate to glucose, *Pck1*, mediating the conversion oxaloacetate to phosphoenolpyruvate, and fructose-1-bisphosphatase (*Fbp1*), which dephosphorylates fructose-1, 6-bisphosphate to fructose-1-phosphate. The pathway associated with the glycerol-derived gluconeogenesis includes two additional key genes *Gyk* and *Gpd1*, which phosphorylate glycerol and facilitate the conversion of glycerol-3-phosphate to dihydroxyacetone phosphate (DHAP), respectively. Both genes are essential driving the glycerol-derived glucose production with *Gyk* mediating the onset of glycerol utilization in gluconeogenesis (Engelking, 2015). To characterize the amino acid-driven gluconeogenesis in these mice, the expression of the glutamine oxaloacetic transaminase 1 (Got1) and glutamate pyruvate transaminase (Gpt1) was also analyzed to investigate possible changes between the genotypes and the treatments. Got1 is thought to play a role especially in the amino acid metabolism catalyzing the transamination of L-aspartate to produce oxaloacetate (Song et al., 2022). Gpt1 catalzyes the reversible transamination of alanine and oxo-glutarate to form pyruvate and glutamate (Guo et al., 2020).

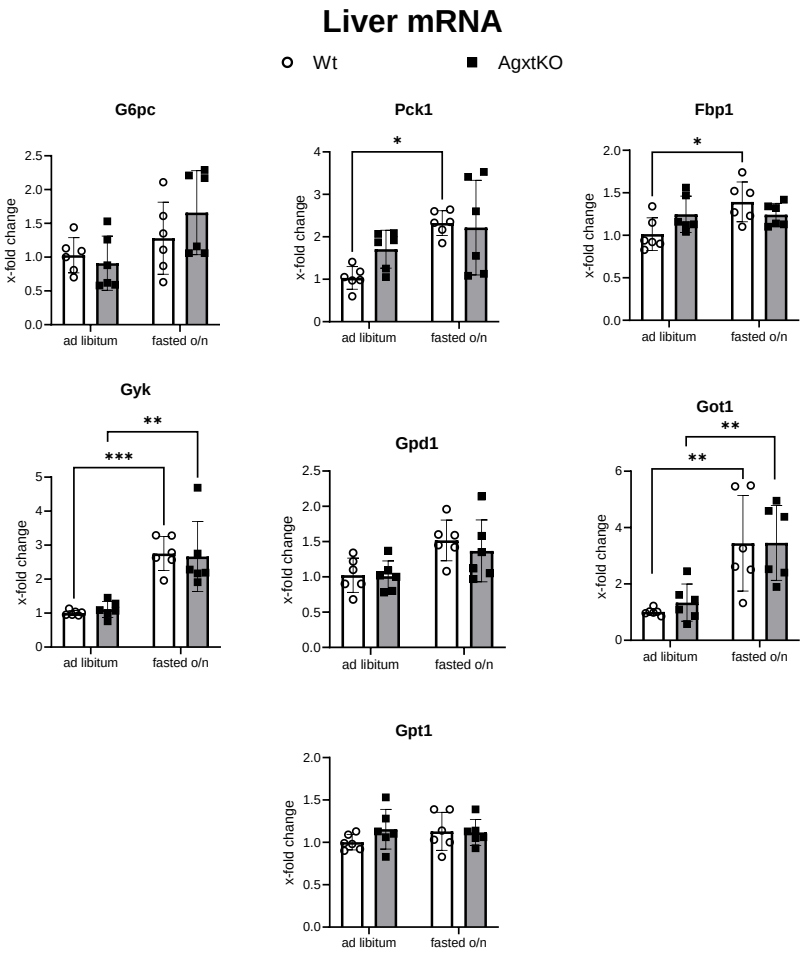

Figure 42: Liver mRNA expression of various glucose-associated genes of wt and AgxtKO mice in *ad libitum* and fasting state (n=6). (All bar diagrams represent the mean ± SD; *p<0.05; **p< 0.01; ***p<0.001; Student's t test, unpaired, two sided). G6pc= glucose-6-phosphatase, Pck1= phosphoenolpyruvate carboxykinase, Fbp1= fructose-1, 6-bisphosphatase, Gyk= glycerol kinase, Gpd1= glycerol-3-phosphate dehydrogenase, Gpt1= Glutamic pyruvic transaminase 1, Got1= glutamic-oxaloacetic transaminase 1

The results from *G6pc* mRNA in the liver of wt and AgxtKO mice did not display a difference between the two genotypes when kept *ad libitum*. Fasting of the mice showed a slight trend of induction for *G6pc* for both genotypes, which did not show significance compared to the *ad libitum* state. The second key enzyme for gluconeogenesis, *Pck1*, showed a fasting-triggered induction in wt mice. In the AgxtKO liver, *Pck1* was already upregulated in the *ad libitum* state in comparison to the wt mice (see Fig. 42). However, the starvation did not lead to a significant upregulation of *Pck1* as it was seen for the wt mice. The results for *Fbp1* in wt mice were comparable to *Pck1* showing that the fasting of the mice led to a significant upregulation of *Fbp1*. This was not the case for AgxtKO mice independent of the treatment. Here, the expression was the same. Regarding the expression of genes associated with the glycerol-driven gluconeogenesis, *Gyk* gene expression was comparable in the *ad libitum* state between

wt and AgxtKO mice (see Fig. 42). Fasting led to a significant upregulation in the gene expression for both genotypes compared to their *ad libitum*-littermates. No difference was seen between wt and AgxtKO mice after fasting. *Gpd1* gene expression was also significantly induced after starvation in wt mice when compared to the *fed* state (see Fig. 40). The trend was similar in AgxtKO mice; however, the results were not significant. Regarding the gene expression changes that are associated with amino acid metabolism, *Got1* mRNA expression was significantly upregulated after fasting in wt and AgxtKO mice, but no difference was observed between the genotypes (see Fig. 42).The second gene associated with amino acid metabolism Gpt1 did not show any difference between wt and AgxtKO independent of the feeding status. Since mRNA expression changes sometimes do not match protein expression, the goal was to assess if the result is translatable to the protein. Here, the focus was on the protein expression of Pck1 and Gyk. Like the results from the mRNA expression, the protein expression for Pck1 was elevated in comparison to the *ad libitum* mice for both genotypes. Regarding the protein expression of Gyk, no difference was observed between the fasting and the *ad libitum* state regardless of the genotype of the mice (see Fig. 43).

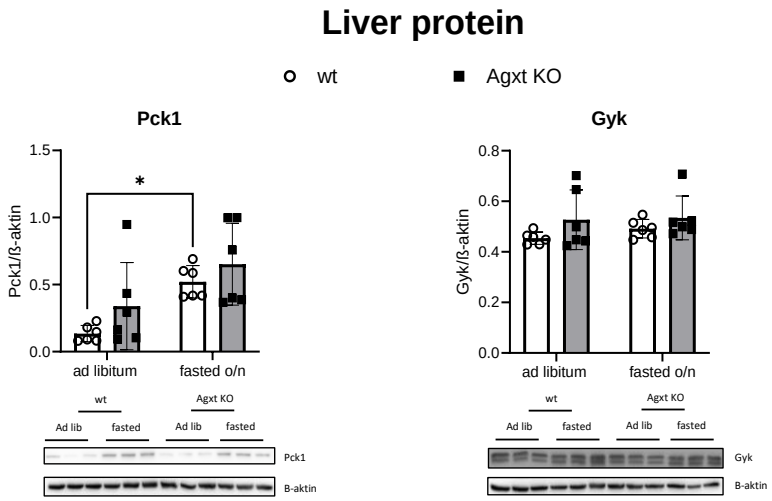

Figure 43: Liver protein expression of common glucogenic genes Pck1 and Gyk in wt and AgxtKO mice in *ad libitum* and fasting state (n=6). (All bar diagrams represent the mean ± SD; *p<0.05; Student's t test, unpaired, two sided). Pck1= phosphoenolpyruvate carboxykinase, Gyk= glycerol kinase

3.5.4.2 Renal gluconeogenesis is affected by oxalate

The analysis of the gene expression in the liver for glucogenic markers revealed no significant differences in gene expression of glucogenic genes between the two genotypes implicating that the hepatic gluconeogenesis is not impaired in AgxtKO livers. As described in the literature, the kidney can also contribute to the *de novo* production of glucose after prolonged

fasting (Legouis et al., 2022). Therefore, the aim was to investigate for possible effects in the gene expression patterns of glucogenic genes in the kidney.

Interestingly, the gene expression for *G6pc* displayed a significant higher expression for AgxtKO compared to wt mice after fasting (see Fig. 44).

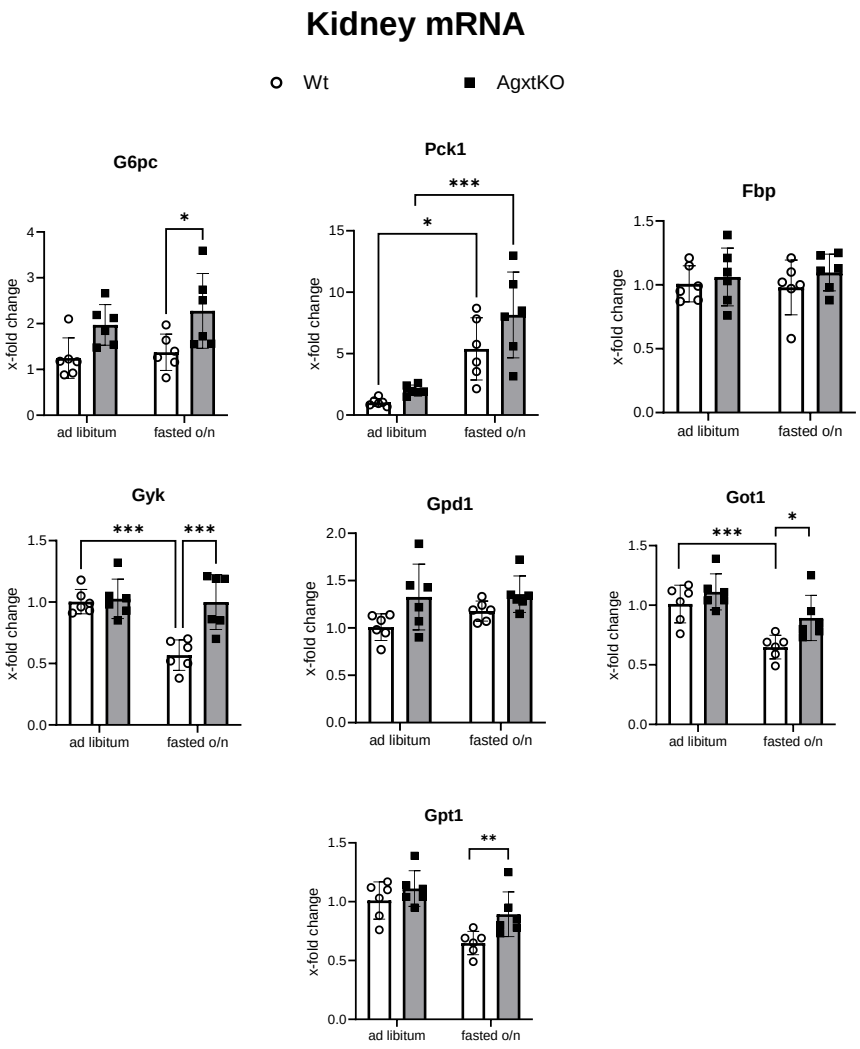

Figure 44: Kidney mRNA expression of various glucose-associated genes of wt and AgxtKO mice in *ad libitum* and fasting state (n=6). (All bar diagrams represent the mean ± SD; *p<0.05; ***p<0.001; Student's t test, unpaired, two sided). G6pc= glucose-6-phosphatase, Pck1= phosphoenolpyruvate carboxykinase, Fbp= fructose-1,6-bisphosphatase, Gyk= glycerol kinase, Gpd1= glycerol-3-phosphate dehydrogenase, Gpt1= Glutamic pyruvic aminotransfase 1, Got1= glutamic-oxaloacetic transaminase 1

Moreover, *Pck1* gene expression was significantly induced in both genotypes when mice were fasted. In the *ad libitum* state, *Pck1* expression was also significantly elevated in AgxtKO mice compared to wt mice (see Fig. 44). *Fbp1* did not show any difference independent of the treatment and genotype. For *Gyk*, the gene expression was significantly elevated for AgxtKO mice compared to control when fasted. Interestingly, fasting led to a downregulation of *Gyk*

in the kidneys of wt but not in the AgxtKO mice (see Fig. 44). The second gene *Gpd1*, that is associated with glycerol-driven gluconeogenesis, did not show significantly elevated gene expression in AgxtKO mice compared to wt mice in the fasting state (see Fig. 44). Genes that are associated with amino acid metabolism like *Got1* showed that there was a significantly large decrease after fasting of the wt mice, which was not the case for the AgxtKO mice. Additionally, after fasting *Got1* mRNA expression in AgxtKO mice was significantly higher compared to wt mice (see Fig. 44). Similar to the results of Got1, Gpt1 was also reduced after starvation in both mice. Focusing on the gene expression after fasting of the mice, *Gpt1* was significantly higher in the AgxtKO mice compared to wt mice. This finding was in line with the other aminotransferase Got1. To summarize, the data showed that it is the kidney which is showing more gene expression changes in the AgxtKO mice upregulating glycerol and amino-acid associated genes.

Additionally, the protein expression of selected genes was also investigated in this setup. Pck1 protein was induced in the kidney of wt and AgxtKO mice after starvation. Gyk protein was elevated in kidney of AgxtKO mice independent of the treatment. This was also significant when kept *at libitum*.

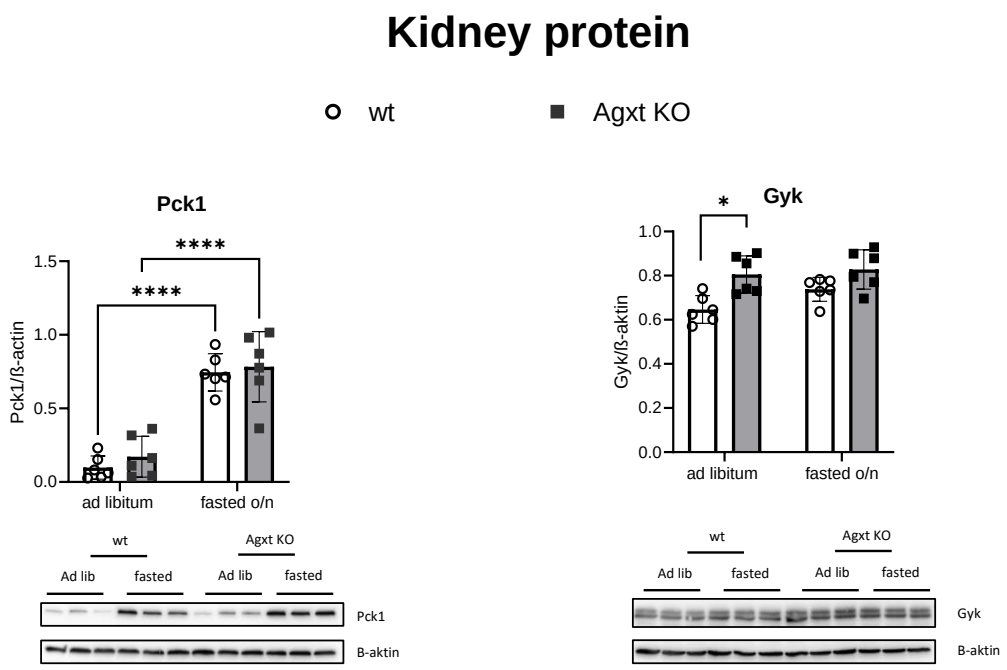

Figure 45: Kidney protein expression of selected glucogenic genes Pck1 and Gyk in wt and AgxtKO mice in *ad libitum* and fasting state (n=6). (All bar diagrams represent the mean ± SD; *p<0.05; Student's t test, unpaired, two sided). Pck1= phosphoenolpyruvate carboxykinase, Gyk= glycerol kinase

The data obtained reveals that the liver mRNA and protein expression of essential glucogenic enzymes is the same between AgxtKO and wt mice – hence – hepatic gluconeogenesis does not seem to be affected in hyperoxaluric mice. However, in the kidney, AgxtKO mice present gene expression changes not only influenced by fasting, but also influenced by the genotype of the mice. Especially the expression changes of *G6pc*, *Gyk* and *Got1* underline that it is the renal gluconeogenesis, which is more affected. Given that previous results show an increased accumulation of oxalate in the kidney rather than in the liver it could be speculated that the observed expression changes are an adaptive response to an inhibitory effect of oxalate on Pc/Pck1-driven gluconeogenesis, leading to upregulation of glycerol-driven gluconeogenesis (via Gyk and G6pc). In addition, upregulation of Got1 could possibly enable more conversion of aspartate to oxaloacetate in the cytosol, which could enter the gluconeogenesis pathway.

3.5.5 Starvation induces NAD^+-signaling pathways

Caloric restriction leads to elevated metabolic/oxidative stress and has a huge impact on common metabolic pathways which are associated with glucose metabolism (glycogenolysis, gluconeogenesis). Redox metabolism - in the form of NAD^+ synthesis and utilization - is also affected in a fasting situation. The most prominent and essential gene that mediates the rate-limiting step of the NAD^+- salvage pathway is the nicotinamide phosphoribosyltransferase (NAMPT). NAMPT catalyzes the reaction from nicotinamide mononucleotide (NMN) to form NAD^+. NAD^+ serves as an electron acceptor in many different pathways including the TCA cycle,which is fundamental in fasting conditions (Yang and Sauve, 2016). To study to which extent Nampt is differently expressed in wt and AgxtKO mice, we analyzed the gene expression of Nampt in the liver and kidney of those mice.

The results showed that the mRNA expression of Nampt in the liver were comparable between the two genotypes. Fasting led to a induction of Nampt in both mice, however this was not significant. An interesting result was observed for the Nampt expression in the kidney. As already mentionied, in AgxtKO mice the kidney displays the organ mostly affected by the accumulation of oxalate. In the *ad libitum* state Nampt mRNA expression was similar. Fasting of AgxtKO mice led to a significant increase of Nampt which suggests that NAD^+ and the NAD^+ synthesis and is more required for metabolic pathways. The upregulation of Nampt in wt mice after fasting was not observed and the levels of Nampt was comparable to the *ad libitum* state (see Fig. 46).

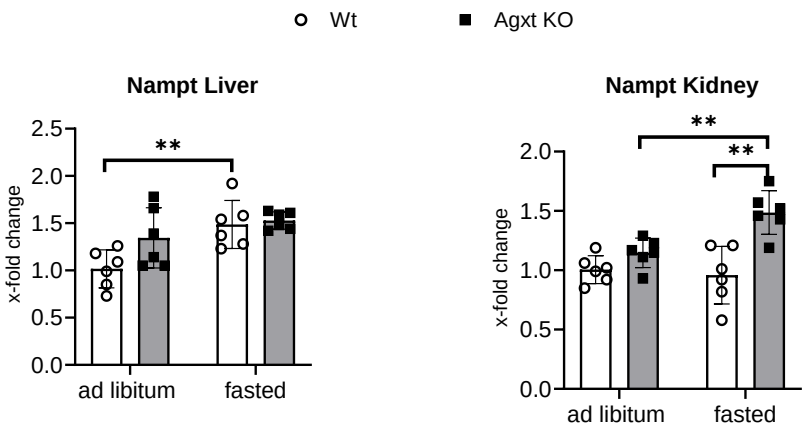

Figure 46: mRNA expression of *Nampt* in the liver and the kidney of wt and AgxtKO mice (n=6). (All bar diagrams represent the mean ± SD; **p<0.01; Student's t test, unpaired, two sided) Nampt= nicotinamide phosphoribosyltransferase

3.6 Expression of Agxt in correlation with its role in gluconeogenesis

The so far obtained results suggest a role for Agxt in supporting gluconeogenesis from pyruvate and amino acids by preventing an accumulation of oxalate that would inhibit the key step of conversion of pyruvate to oxaloacetate. Thus it is conceivable that Agxt becomes upregulated under conditions that enhance the gluconeogenesis flux. A previously reported induction of Agxt by glucagon, the hormone that promotes gluconeogenesis, is in line with a glucogenic supporting function of Agxt (Oda et al., 1993). In addition, the Agxt promotor contains a cAMP response element (CRE), which responds to glucagon signaling (Uchida et al., 1994). Further, it has been shown that in mice deficient in proglucagon peptides, Agxt and other aminotransferases are downregulated under starvation (Watanabe et al., 2012). In a previous study, Gianmoena *et al.* reported a hypermethylation in the promotor region of Agxt in the fatty liver of ob/ob hepatocytes. Interestingly, this hypermethylation affects the CRE binding domain, leading to a reduced transcriptional upregulation of Agxt to the hormone glucagon in the fatty liver (Gianmoena et al., 2021). Glucagon is highly secreted during fasting periods and Agxt has been shown to be inducible via glucagon. In the course of this chapter, the aim of these experiments was to elucidate the pattern of Agxt after glucagon stimulation with a special focus on glucose-associated parameters and the role of a substrate-dependent stimulation of Agxt.

3.6.1 Response of Agxt to glucagon in control mice *in vivo*

To analyze the expression pattern of Agxt under glucogenic conditions, mice at the age of 10 weeks, fed *ad libitum*, were injected intraperitoneally with 1 µg/g body weight glucagon or

solvent (PBS). At the time points of the experiment, the mice were sacrificed and plasma for the analysis of hormones and glucose, as well as liver tissue for immunohistochemical analysis, gene and protein expression analysis were collected. An experimental outline is depicted in the figure below (see Fig. 46).

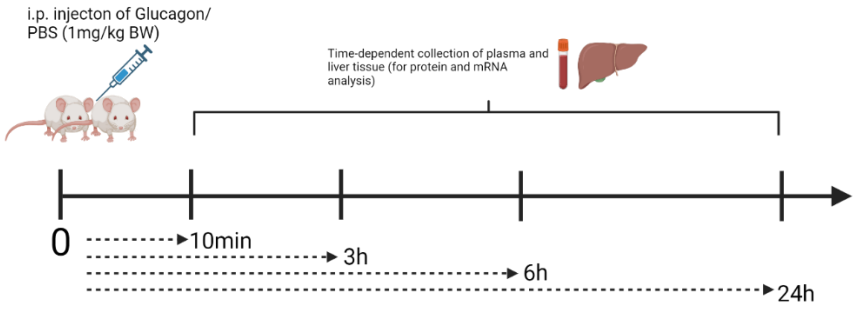

Figure 47: Experimental outline of the glucagon experiment in mice. This figure was created with BioRender.com

3.6.1.1 Glucagon leads to an increase of blood glucose levels

A first read-out of this experiment was the blood glucose levels of the mice. It is expected that the administration of glucagon should result in a rise of blood glucose levels peaking around 15 to 30 minutes after the administration. In this experiment, a similar result was observed. The blood glucose levels peaked 10 minutes after the administration of glucagon and were significantly higher compared to the PBS-treated mice (see Fig. 48).

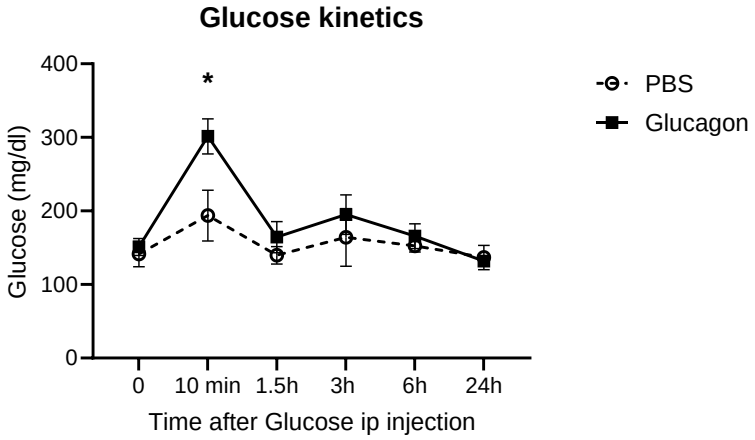

Figure 48: Glucose kinetics after the administration of 1µg/g glucagon *in vivo* (n=3). (All dots represent the mean ± SD; *p<0.05; Student´s t-test, unpaired, two sided). PBS= phosphate-buffered saline

Already 1.5h after the injection of glucagon, the blood glucose levels were already at basal levels indicating a counteractive effect of other hormones like insulin.

3.6.1.2 Glucagon injection results in persistent elevated glucagon and acute rise of insulin levels in plasma

In addition to plasma glucose levels, the plasma concentration of glucagon and insulin, the hormones regulating glucose homeostasis, was quantified by using ELISA. As expected, the plasma glucagon levels increased immediately after glucagon injection and reached levels above the limit of quantification, implying levels higher than >190 pmol/L. The high levels of glucagon were kept constant for up to 24h post-injection. At 24h hours, glucagon levels slowly decreased but were still higher than PBS-treated controls (see Fig. 49). With respect to the plasma insulin levels of the mice, a counteractive effect of insulin in response to the administration of glucagon would be expected. Since glucagon led to a release of glucose from glycogen storages and a rise in blood glucose levels, this should induce secretion of insulin from the β-cells of the pancreas to prevent a further increase of blood glucose.

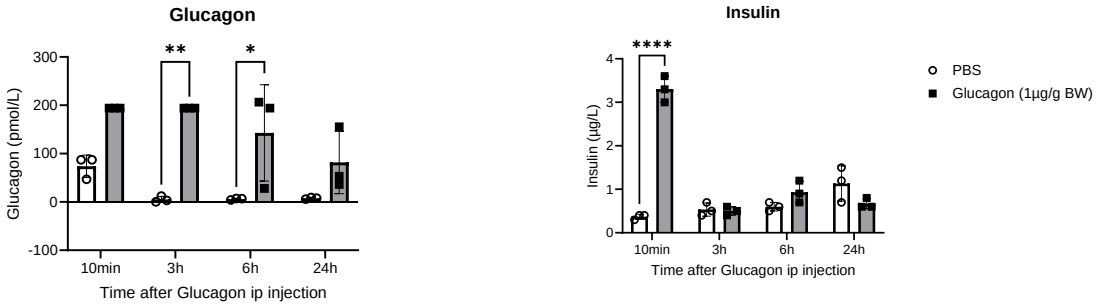

Figure 49: Hormone levels of insuline and glucagon of wt mice after the treatment with glucagon (1µg/g BW) or PBS *in vivo* (n=3). (All bar diagrams represent the mean ± SD; *p<0.05; **p<0.01; ****p<.0001; Student's t test, unpaired, two sided). PBS= phosphate-buffered saline, BW= body weight

The levels of insulin were significantly higher 10 min post glucagon injection compared to PBS-treated controls (see Fig. 49). At the later experimental time points, the insulin levels did not differ between glucagon-treated mice and PBS-treated mice, which goes along with the decrease of glucose 1.5 h post administration of glucagon. The rapid but transient insulin secretion is expected to be provoked by the hyperglycemic peak and consequently induces glucose clearance. These observations confirm that the injection of glucagon exerted the expected biological effects.

3.6.1.3 *Agxt* mRNA is induced by glucagon injection in mice

With having more interest in the role of Agxt in gluconeogenesis, the expression of Agxt on transcriptional and protein levels in the liver was investigated next by qPCR and Western blot respectively. It is known that the Agxt mRNA in the liver is strongly induced 3h after i.p.

administration of glucagon (Satoh et al., 1995). However, the time-resolved expression pattern at both level, mRNA and protein, was not entirely determined. Here, the time course of *Agxt* mRNA expression after the administration of glucagon is shown for the first time. Surprisingly, the transcriptional regulation of Agxt is not an acute effect after the administration of glucagon as it is the case with the rise in blood glucose levels. *Agxt* mRNA upregulation is rather a late event shown 3h post the injection of glucagon compared to PBS-treated mice.

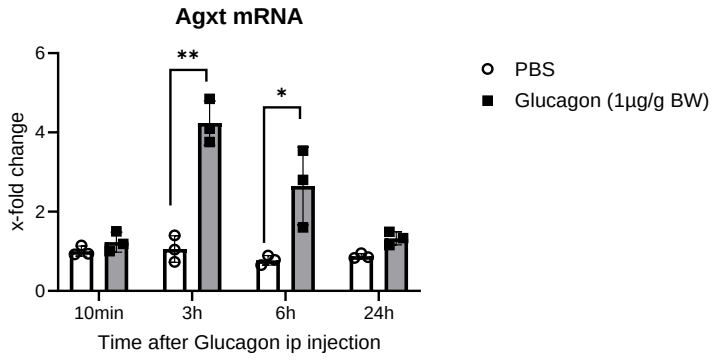

Figure 50: *Agxt* mRNA expression after the treatment with glucagon (1µg/g BW) or PBS *in vivo* (n=3). (All bar diagrams represent the mean ± SD; *p<0.05; **p<0.01; Student's t test, unpaired, two sided). Agxt= Alanine-glyoxylate aminotransferase, PBS= phosphate-buffered saline

The administration of glucagon resulted in a significant increase in *Agxt* mRNA levels compared to the controls after 3h. This higher mRNA expression of *Agxt* was prolonged even after 6h post administration and still significant compared to PBS-treated mice (see Fig. 50). 24h post injection, the mRNA levels of *Agxt* almost declined back to the level of control PBS-injected mice.

3.6.1.4 Protein induction of Agxt via glucagon stimulation is an glucose-independent effect

Related to the findings that *Agxt* mRNA is inducible by glucagon administration, the open question remains whether this is also translated to protein. The Agxt protein expression early after the administration of glucagon did not result in any significant upregulation of the protein, which is in line with findings from the *Agxt* mRNA increasing 3h post administration (see Fig. 50).

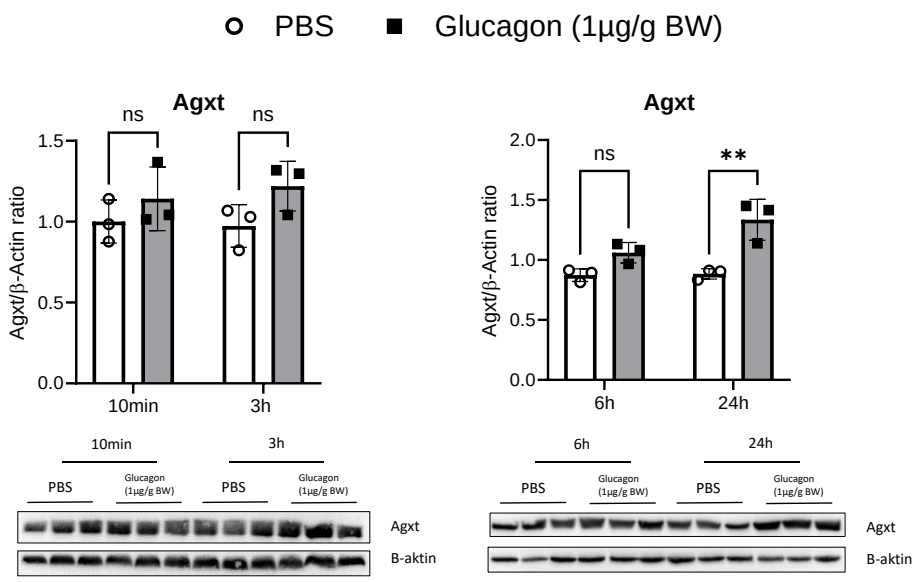

Figure 51: Agxt protein expression after treatment with glucagon (1µg/g BW) or PBS in wt mice *in vivo* (n=3). Western blot displays **(A)** 10min and 3h time point and **(B)** 6h and 24h time point post glucagon administration. (All bar diagrams represent the mean ± SD; **p<0.01; Student's t test, unpaired, two sided). Agxt= alanine-glyoxylate aminotransferase, PBS= phosphate-buffered saline

In contrast to the findings of the strong transcriptional upregulation of *Agxt* at 3h (see Fig. 48), the protein expression of Agxt shifted and increased at the late time points 6h and 24h. This difference was significant compared to PBS-treated controls (see Fig. 51). This is the first evidence, that Agxt protein expression was increased upon prolonged glucagon stimulation.

In addition to studying the influence of glucagon on Agxt expression in the liver, both on transcriptional and translational level, the *in vitro* hepatic glucose production assay was also employed to investigate a possible substrate-dependent stimulation of Agxt expression by using glucogenic substrates. This issue will be addressed next.

3.6.2 Agxt expression is driven by substrate exposure in gluconeogenesis at an early and late time point

For the investigation, whether Agxt is influenced by the exposure to glucogenic substrates, the previously established glucose production assay was used. In the procedure, hepatocytes were cultured for 6h and 24h. Common glucogenic substrates were used (Pyruvate/lactate, glycerol, alanine and glutamine). The cells were harvested and mRNA and protein expression of Agxt was analyzed. The results are shown in the next figures.

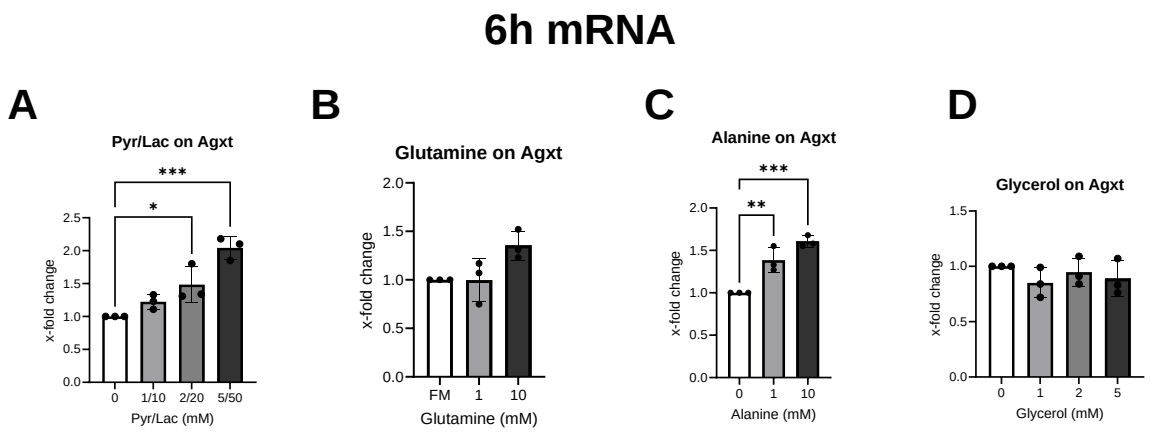

Figure 52: *Agxt* mRNA expression after 6h incubation with glucogenic precursor **(A)** Pyr/Lac, **(B)** Glycerol, **(C)** Glutamine, **(D)** Alanine *in vitro* (n=3). (All bar diagrams represent the mean ± SD; *p<0.05; ***p<0.001; Student's t test, unpaired, two sided).

The mRNA expression of *Agxt* after the 6h incubation with different glucogenic revealed that *Agxt* is significantly induced after the exposure to increasing concentrations of pyruvate/lactate in a concentration-dependent manner (see Fig. 52A). For glutamine, a trend with the highest glutamine concentration was shown; alanine exposure to hepatocytes revealed a concentration-dependent significant induction of *Agxt* at the highest concentration (see Fig. 52B, C). In contrast to this, glycerol did not show any specific pattern of the induction of *Agxt* (see Fig. 52D). The data showed that *Agxt* follows a similar pattern compared to the two other glucogenic enzymes Pck1 and G6pc (see Fig. 12), which were also induced after the incubation with pyruvate/lactate and the amino acids alanine and glutamine.

Regarding the 24h incubation with glucogenic substrates *Agxt* mRNA followed the same pattern observed at 6h incubation.

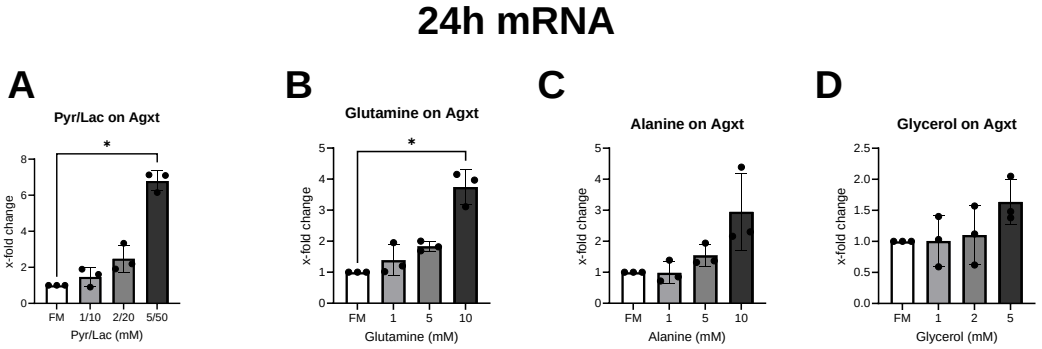

Figure 53: *Agxt* mRNA expression after 24h incubation with glucogenic precursor **(A)** Pyr/Lac, **(B)** Glycerol, **(C)** Glutamine, **(D)** Alanine *in vitro* (n=3). (All bar diagrams represent the mean ± SD; *p<0.05; ***p<0.001; Student's t test, unpaired, two sided).

Agxt mRNA was upregulated in a concentration-dependent manner when exposed to pyruvate/lactate. A significant induction of *Agxt* mRNA was shown at the highest concentration compared to the control (see Fig. 53A). Similarly, the exposure to glutamine also led to a significant induction of Agxt at the highest concentration (see Fig. 53B). Alanine exposure showed a comparable trend for *Agxt* mRNA induction, but this was not significant. Glycerol exposure to hepatocytes did not significantly induce expression of *Agxt*. In a final step, the protein expression of Agxt was analyzed (see Fig. 53D). The analysis revealed that in accordance to the *Agxt* mRNA results, the Agxt protein was significantly elevated after treatment with the highest pyruvate/lactate concentration but remained unaltered by glycerol treatment (see Fig. 54).

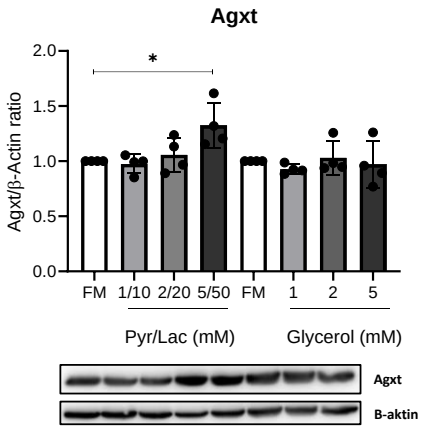

Figure 54: Agxt protein expression after the incubation with increasing concentration of pyruvate/lactate and glycerol (n=4). (All bar diagrams represent the mean ± SD; *p<0.05; Student's t test, unpaired, two sided)

To summarize, the data revealed that *Agxt*, like other glucogenic genes like *Pck1* and *G6pc* (see Fig. 12-13), was also inducible in a very similar pattern, although the extent to which Agxt was induced is less compared to the two other genes. The fact that Agxt becomes upregulated by glucogenic substrates, other than glycerol, that depend on pyruvate carboxylase and Pck1 for glucose production strongly suggest that Agxt plays a supportive role in the production of glucose in this specific pathway. Prevention of excessive oxalate formation, which would exert an inhibitory action on pyruvate carboxylase is one hypothesis that will be discussed in the next chapter.

4 Discussion

An overall goal of this thesis was to investigate a direct or indirect participation of Agxt in different metabolic pathways apart from its role in the detoxification of glyoxylate in the course of hydroxyproline catabolism. Recent studies suggested a possible role of Agxt in the amino-acid driven gluconeogenesis. Further, oxalate, which is the toxic waste product that is produced when Agxt is missing in PH1, is also thought to play a role in gluconeogenesis via its inhibition of Pc and Pck1. To date, no one has studied (1) the role of oxalate in a well-established hyperoxaluric mouse model characterized by elevated systemic oxalate levels focusing on glucose glucose metabolism and (2) the association of Agxt and gluconeogenesis in detail.

In mechanistic studies illustrated in this thesis, it was demonstrated that rescuing Agxt via adeno-associated viral transfection in a hyperoxaluric mouse model using AgxtKO mice and in an NAFLD model using ob/ob mice reinstated the physiological catabolism of hydroxyproline. This was accompanied by a sufficient detoxification of glyoxylate resulting in a urinary excretion of oxalate, which was comparable to healthy control mice.

A first goal of this thesis was to establish a hepatic glucose production assay and to study the inhibitory effect of oxalate *in vitro*. For this purpose, primary mouse hepatocytes were exposed to various common glucogenic substrates and gene and protein expression was analzyed. The results showed that mouse hepatocytes were able to produce glucose from all substrates (pyruvate/lactate, glycerol and amino acids). In line with this, key glucogenic enzymes were also induced after the stimulation by the substrates indicating a successful setup of the assay. Within this working package, the hepatic glucose production assay was used to investigate the inhibitory effect of oxalate. The main finding showed that oxalate inhibits the glucose production from pyruvate/lactate and amino acids, but not from glycerol in primary mouse hepatocytes and primary human hepatocytes.

The second main goal of this thesis was to investigate, whether the previously described findings of the inhibitory effect of oxalate on glucose production is also observed in an in vivo situation. Therefore a hyperoxaluric mouse model was used which was the AgxtKO mice. The results showed that glucose levels did not show a difference between wt and AgxtKO mice independent of the feeding state. Analysis of glucogenic genes in liver was comparable between both genotypes; in the kidney, significant differences were observed for glucogenic

key enzymes G6pc and Gyk which suggest that renal gluconeogenesis seem to be more affected. In vivo analysis of AgxtKO mice revealed reduced body weight loss after starvation overnight compared to wt mice.

The very last goal of this thesis was to study the association of Agxt in the context of gluconeogenesis *in vitro* and *in vivo*. To demonstrate a contribution of Agxt to gluconeogenesis, we used the established hepatic glucose production assay. Here, we could demonstrate that Agxt behaved in a similar manner compared to key glucogenic enzymes G6pc and Pck1 after the exposure to pyruvate/lactate and amino acids. No significant stimulation was observed after treatment with glycerol. To decipher the association of Agxt to gluconeogenesis *in vivo*, mice were treated with glucagon in a time-dependent manner and glucose and hormone levels were monitored. Additionally, gene and protein expression was analyzed. The glucagon stimulation led to a significant rise in blood glucose levels, which declined back to normophysiological levels after 1.5h post administration. Gene expression analysis revealed a significant induction of Agxt, which peaked 3h after glucagon stimulation. Agxt protein was induced from 6h to 24h post initial treatment.

The most important results are discussed in detail in the following chapters.

4.1. Pyruvate/lactate is a physiological substrate for gluconeogenesis

In the first part of this thesis, an *in vitro* hepatic glucose production assay was established to study the capability of primary mouse hepatocytes to synthetize glucose *de novo* from various glucogenic substrates. The aim of this approach was to later investigate the influence of oxalate in the glucose production process. In this *in vitro* system glucose was quantified in the supernatant, and gene as well as protein expression analysis was performed. The results showed that primary mouse hepatocytes were able to produce significant amounts of glucose from all the substrate that the cells were exposed to. For the assay, *in vivo*-relevant substrates (pyruvate/lactate, glycerol, glutamine and alanine) were employed at supraphysiological concentrations. No studies exist where physiological *in vivo* fasting concentrations were applied to an *in vitro* system (Ji et al., 2019; Kalemba et al., 2019; Perry et al., 2020). Moreover, the gene expression analysis showed that the key glucogenic enzyme G6pc, which catalyzes the last step of the gluconeogenesis pathway was upregulated by all substrates. In contrast, Pck1 was upregulated by pyruvate/lactate and the amino acids glutamine and alanine but not by glycerol. This is in agreement with the fact that gluconeogenesis from glycerol does not

require Pck1. While the glucogenic potential of these substrates was expected based on the well documented *in vivo* substrate fueling to the liver during prolonged fasting (e.g. the Cori cycle and the glucose-alanine cycle) these results are in disagreement with a previous study (Kalemba et al., 2019) and need to be discussed. Kalemba *et al.* showed that the glucose production from pyruvate/lactate is not concentration-dependent and that only non-significant, negligible amounts of glucose are produced from it. The comparison to the results of this thesis is shown in the next figure (see Fig. 54). A discrepancy between the results of this thesis and the study of Kalemba *et al.* was also observed when comparing the gene expression analysis. Kalemba *et al.* showed no upregulation of *Pck1* and *G6pc* after the exposure to pyruvate/lactate (Kalemba et al., 2019). This is clearly in contrast to the results presented in this thesis showing a concentration-dependent induction of the two essential glucogenic genes Pck1 and G6pc by pyruvate/lactate, which is consistent with the concomitantly increased production of glucose (see Fig. 55). Different experimental conditions may be a reason for these discrepancies: (1) The duration of the hepatic glucose production assay: In the Kalemba *et al.* paper, the authors incubated the cells with the gluconeogenic substrates for 8h, after which glucose release in the supernatant was quantified, which is different to our setup incubating for 6h. It is however not plausible that this difference can explain the discrepancy. In our study, the hepatocytes continue producing glucose for longer times, as demonstrated by the glucose quantification in the supernatants after 24h.

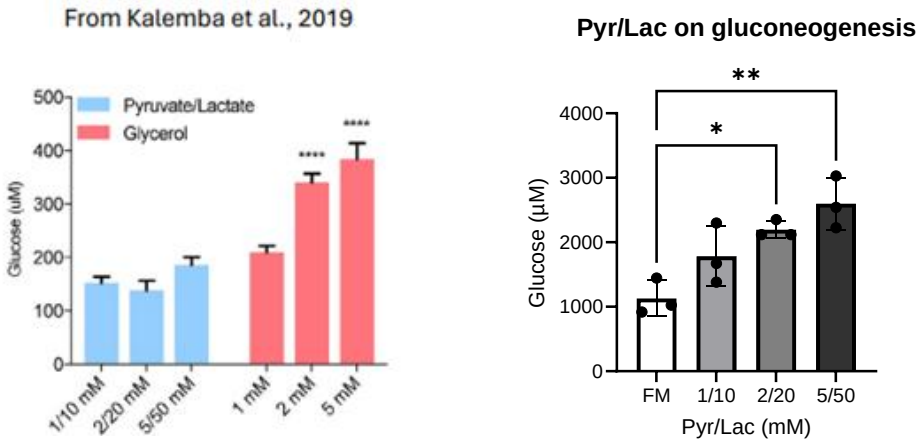

Figure 55: Comparison of the glucose production from pyruvate/lactate from Kalemba *et al.* and the glucose production shown in this thesis.

(2) The pre-treatment of the hepatocytes before starting the glucose production assay: Kalemba *et al.* starved the cells in glucose-containing medium without serum. In contrast to

this, we cultivated the cells in glucose-free and serum-free medium, which guarantees a complete depletion of glycogen stores of the hepatocytes. In this way, our protocol forces substrate-fueled gluconeogenesis, while in the study of Kalema *et al.*, glucose release from glycogenolysis is likely to occur and may even prevent substrate-driven gluconeogenesis. However, according to this scenario, also glycerol-driven gluconeogenesis would not be efficient, and this was not the case. (3) The cultivation time after hepatocyte isolation: Kalemba *et al.* let the hepatocytes rest for 24h after the isolation procedure and performed the hepatic glucose production experiment the next day. Here, the experiment was performed on the same day of isolation of the hepatocytes. This difference bears a potential explanation for the discrepancies in the results between the two studies since it is known that prolonged cultivation of primary mouse hepatocytes – even 24h – leads to significant changes in the gene network activity influencing protein expression. Further, in monolayer cultivation of hepatocytes this loss of gene expression is more pronounced compared to a collagen-sandwich cultivation modality (Godoy et al., 2016). (4) The source of the lactic acid used in the glucose production assay: According to their material and methods article section, Kalemba *et al.* used D-lactic acid, which is not the enantiomer that is naturally occurring in the human body. The human body endogenously produces L-lactic acid from glycolysis via the reduction of pyruvate by lactate dehydrogenase (Kraut and Madias, 2014). Instead, D-lactic acid is produced by some strains of microorganisms and is involved only in rare metabolic pathways (Pohanka, 2020). Since hepatocytes may not be able to utilize non-physiological D-lactic acid to produce glucose, this would explain the discrepancies in the results. If this is the case, it would also explain why the glucogenic genes Pck1 and G6pc are not induced after the exposure to this non-physiological substrate.

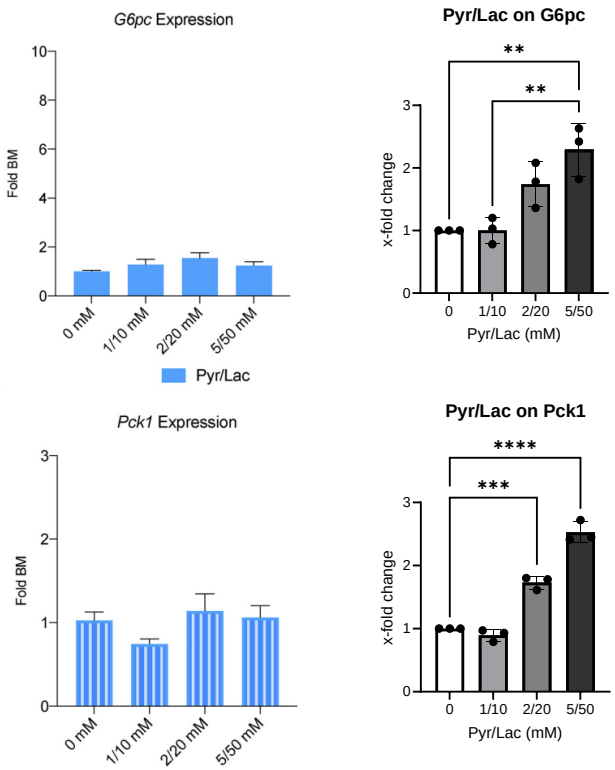

Figure 56: Comparison of the gene expression of *G6pc* and *Pck1* from Kalemba *et al.* and data from this thesis after pyruvate/lactate exposure

Kalemba *et al.* concluded from their results that glycerol and not lactate/pyruvate is the preferred substrate for gluconeogenesis (Kalemba et al., 2019). Published in *vivo* and *in vitro* studies, which investigated substrate utilization under fasting conditions mimicking gluconeogenesis, demonstrate that lactate and glycerol are both main substrates for glucose production (Nishi et al., 2023; Sahoo et al., 2023; Zou et al., 2018). Hence, the observed glucose production from lactate/pyruvate in this thesis is in agreement with such *in vivo* studies.

In conclusion, the hepatic glucose production assay established in this thesis is suitable for assessing different pathways of gluconeogenesis and offers the possibility to study factors that may selectively influence these pathways, for instance small molecule inhibitors, or metabolites such as oxalate, which was explored in this thesis.

4.2 The effect of oxalate on gluconeogenesis in primary mouse hepatocytes

Previous studies have reported that oxalate has an inhibitory effect on gluconeogenesis (Yount and Harris, 1980). This is facilitated by the inhibition of the two key enzymes Pck1 and Pc (Buc et al., 1981). Our goal was to confirm whether oxalate exerts this inhibitory effect on

gluconeogenesis, first in primary mouse hepatocytes *in vitro*, and later investigate whether this results in perturbation of glucose homeostasis at the systemic level.

Applying the newly established *in vitro* hepatic glucose production assay we could confirm that in PMHs and in PHHs, the exposure to oxalate significantly reduced the glucose production from pyruvate/lactate and amino acids compared to oxalate-free exposure. This was the case at concentration of 100 µM of oxalate or higher. In contrast to this, glycerol-derived glucose production was not affected by the exposure of oxalate. This is consistent with the fact that the production of glucose from glycerol does not require the enzyme Pc because glycerol enters the gluconeogenesis pathway at a different step, and thus bypasses the oxalate-blockade. Interestingly, oxalate influences glycolysis by the inhibition of pyruvate kinase in fed rats. Pyruvate kinase facilitates the ultimate step of glycolysis transferring a phosphate group of phospoenolpyruvate to ADP, which leads to the formation of a molecule of ATP and pyruvate.

However, one has to look critically at these result since the concentration of oxalate at which an effect on gluconeogenesis was shown is quite high. The concentration of systemic oxalate in plasma in healthy patients ranges from 1 to 3 µM (Wilson and Liedtke, 1991). Oxalate levels in patients suffering from PH1 and CKD show a much higher variation (ranges from 2 to 133 µmol/L) with supersaturation of oxalate starting from ≥30 µM oxalate (Hillebrand and Hoppe, 2020; Pfau et al., 2021). By now, no one has looked into ofhow much of the oxalate accumulates within the hepatocytes, whether it enters the mitochondria, where pyruvate carboxylase is localized, or how efficiently it is transported out of the cell.

In addition to the the above discussed experiment studying the effect of soluble oxalate on gluconeogenesis, also a more physiological approach was performed by using hydroxyproline as a precursor of oxalate. Hydroxyproline is known to enter the mitochondria of hepatocytes where it is catabolized to glyoxylate. Glyoxylate will be converted to oxalate if the rate of its formation exceeds that of its detoxification. In contrast to exogenous oxalate, the addition of hydroxyproline ensures that oxalate is generated within the hepatocytes, possibly even within the mitochondria where it could target pyruvate carboxylase.

We evaluated the kinetics of hydroxyproline catabolism in a time- and concentration-dependent manner in control hepatocytes by quantifying the appearance of glyoxylate, glycolate and oxalate in the intracellular and extracellular fraction after addition of

hydroxyproline. Glyoxylate accumulates within the cells transiently in the early phase. After its conversion to glycolate and oxalate these two products do not accumulate to high extent; rather they are transported out of the cells very rapidly. However, in AgxtKO hepatocytes the exposure of hydroxyproline resulted in elevated intracellular levels of oxalate and glyoxylate, showing that not only glyoxylate detoxification but also transport of oxalate out of the hepatocytes may be overwhelmed in the absence of Agxt.

When the hepatic production assay was performed in the presence of hydroxyproline, the results showed that the glucose production from the glucogenic substrates lactate/pyruvate and alanine was decreased in control and AgxtKO hepatocytes. However, the effect was significantly higher in the AgxtKO hepatocytes, indicating that the hyperoxaluric model is more affected than control hepatocytes. In contrast, glycerol-driven gluconeogenesis was not affected. These results are consistent with an inhibition of glucose production via Pc and Pck1 caused by hydroxyproline-derived oxalate.

Again, one has to look critically at these result since the concentration of hydroxyproline used was quite high (10 mM). The concentration of hydroxyproline in plasma in healthy patients ranges from 20 to 30 µM (Murguia et al., 1988). In patients with hydroxyprolinemia it can rise 10-fold higher compared to healthy patients. It is reported that in some individuals of hydroxyprolinemia the levels of hydroxyproline in plasma reached up to 500 µM (Staufner et al., 2016) . Thus, further experiments with lower concentrations of hydroxyproline should be conducted. Moreover, experimental evidence for an inhibition of pyruvate carboxylase/ Pck1 by oxalate is missing in our studies, since a Pc activity assay have not been performed.

All in all, the *in vitro* studies have demonstrated that both oxalate and hydroxyproline-derived oxalate compromise gluconeogenesis via Pc and Pck1, even though it remains to be clarified if this happens *in vivo* at physiological concentrations. One consequence derived from such inhibition could be that under conditions of high oxalate burden in glucogenic organs (liver and kidney), gluconeogenesis cannot be fueled from lactate/pyruvate or from amino acids that are converted to pyruvate to enter the gluconeogenic pathway. One possible scenario would be that this results in hypoglycemia; however, since other substrates (glycerol) are also available, compensatory glycerol-fueled gluconeogenesis would be likely to accur. Whether glycerol is the preferred substrate can be validated by C13 metabolic flux analysis, as discussed later.

4.3 Consumption of NAD^+ by glyoxylate detoxification may influence gluconeogenesis

Besides a potential inhibitory effect of oxalate on the two enzymes, another possible explanation for the decrease in glucose production from lactate/pyruvate when AgxtKO hepatocytes are exposed to hydroxyproline (and thus generating glyoxylate, glycolate and oxalate) might be the depletion of redox equivalents that are used for both pathways, the glucogenic pathway as well as the glyoxylate detoxification pathway. It is known that the NAD^+ pool is limited in cells, which makes the usage of NAD^+ a critical measure for the functioning of mitochondria, where key steps of the gluconeogenesis and glyoxylate detoxification take place (Otto et al., 2015; Titov et al., 2016). Glyoxylate oxidation to oxalate by Ldh utilizes NAD^+ as an electron acceptor (Salido et al., 2012).

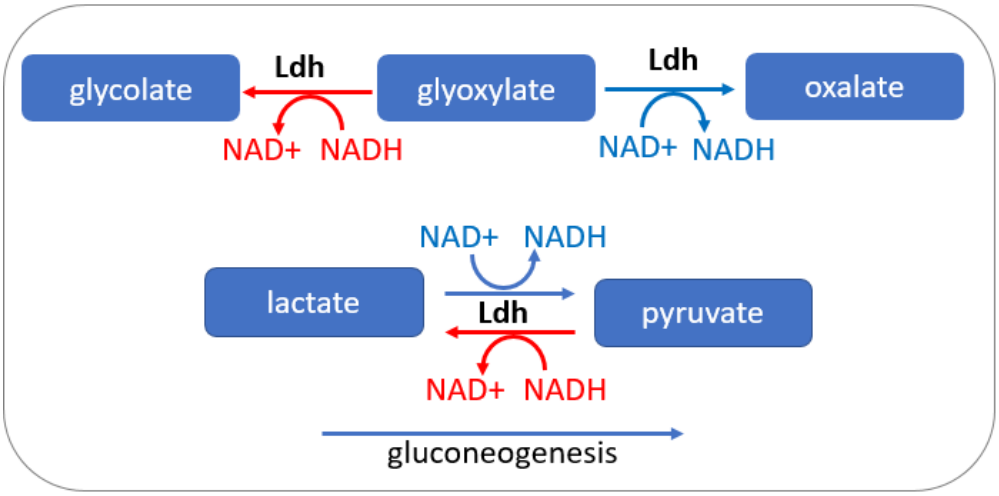

Figure 57: Possible explanation for the reduced glucose production in AgxtKO mice, which describes that the two reactions, catabolism of hydroxyproline and glucose production, require redox equivalents at the expense of NAD^+ resulting in a shortage of NAD^+. Ldh= lactate dehydrogenase, NAD/NADH= Nicotinamide adenine dinucleotide

This mechanism may lead to an accumulation of the reduced redox equivalent NADH. When the levels of NADH reach too high levels, the Ldh-catalyzed reaction associated with gluconeogenesis, which converts lactate to pyruvate, fueling the production of glucose, is unfavorable. Ultimately, this would lead to decreased lactate-derived production of glucose. An increase in NADH does not impair the glyoxylate detoxification since cytosolic Ldh or Grhpr can also reduce glyoxylate to glycolate using NADH. Conclusively, this would mean that both pathways compete for the available NAD^+ pool and this might be critical in the AgxtKO hepatocytes. Of note, Agxt detoxifies glyoxylate to glycine by a transamination reaction that is redox-independent. Thus, AgxtKO hepatocytes lack an important glyoxylate detoxification

pathway that spares NAD+, and accumulate higher levels of glyoxylate, which is ultimately metabolized via Ldh to oxalate, consuming NAD^+.

The enzyme nicotinamide phosphoribosyl transferase (NAMPT) is involved in NAD synthesis and becomes upregulated when required in response to increased cellular demands for NAD^+, e.g. under starvation (Xie et al., 2020; Yang et al., 2007). Hence, NAMPT might be differently regulated in AgxtKO mice compared to wt mice to meet the higher demand of NAD^+ to facilitate both the detoxification of glyoxylate and promotion of gluconeogenesis. From our *in vivo* experiments it was confirmed, that Nampt expression was significantly upregulated in AgxtKO mice after fasting in the kidney. This suggests that NAD^+ biosynthesis might be affected by the exposure of oxalate in the kidney and it is required to induce Nampt to facilitate the de novo generation of NAD^+.

In conclusion, the possibility must be considered that not only the oxalate itself but the detoxification process of the generated glyoxylate, which consumes NAD^+, represents a challenge that influences the performance of gluconeogenesis.

4.4 No influence of oxalate on glucose levels in hyperoxaluric mice *in vivo*

With the results from the *in vitro* experiments, showing that oxalate and the oxalate-precursor hydroxyproline led to an impairment in the lactate/pyruvate-driven glucose production in hepatocytes, we evaluated if this would lead to alterations in glucose homeostasis in an *in vivo* model. Therefore, we used a well-established hyperoxaluric AgxtKO mice model and performed a comprehensive characterization, ranging from plasma analysis to gene and protein expression analysis in fasting conditions.

However, plasma glucose levels were not different between wt and AgxtKO mice independent of *ad libitum* or fasting state. This situation is surprisingly also encountered in mouse models with a liver-specific knockout of Pck1 or Pc. Despite the importance of these enzymes for hepatic gluconeogenesis, Pck1 or Pc -deficient mice do not show significant changes in the fasting blood glucose. In the liver-specific Pck1-KO mice, the organism is able to compensate for the maintenance of glucose homeostasis via a global upregulation of TCA cycle functionality and a maintained glycerol-driven gluconeogenesis (Cappel et al., 2019; She et al., 2003). In the liver-specific Pc-KO, mice maintain normoglycemia in part, by increasing renal gluconeogenesis and elevated ketogenesis to overcome supressed gluconeogenesis and hepatic anaplerosis (Cappel et al., 2019). These two phenomenon might also be applicable for

the AgxtKO mice, in which excess of oxalate presumably inhibits Pc and/or Pck1. The maintenance of euglycemia is so fundamental that several metabolic pathway may compensate for the lack of one to prevent hypoglycemia. This may include glucose production from many different substrates or enhancing gluconeogenesis in other organs than the afftcted one.

Another explanation could be, that oxalate levels generated from endogenous hydroxyproline catabolism are not sufficient to provoke a strong glycemic effect. It should be considered that the normal chow that mice receive does not contain hydroxyproline. Adding 1% hydroxyproline to the diet causes an elevated urinary excretion of oxalate and higher levels of oxalate in the plasma of these mice. This would help to investigate whether oxalate itself promotes changes in gluconeogenesis from an organ' and substrate' perspective, for instance. Specifically, with a higher oxalate burden from the hydroxyproline diet, we would expect a stronger effect of the oxalate inhibition on pyruvate/lactate or amino acids driven gluconeogenesis in the kidney of the mice. As a response, the compensatory upregulation of other pathways like glycerol-driven gluconeogenesis might be induced. This could be either validated using tracer analysis or by gene expression patterns. Though, one should be vigilant about the concentration and duration of hydroxyproline-feeding since this might provoke kidney damage, which makes the study of renal gluconeogenesis difficult. This needs to be addressed in the future. Further, another approach would be to perform metabolic tolerance tests by intraperitoneal injection of glucogenic precursors together with hydroxyproline after fasting leading to high levels oxalate in blood, which hypothetically leads to diminished plasma glucose levels. One would expect no change in blood glucose levels after the administration with glycerol/hydroxyproline and reduced blood glucose levels after treatment with pyruvate/lactate/hydroxyproline.

Plasma amino acids were analyzed in AgxtKO and wt mice and showed significant difference for relevant amino acids that are associated with gluconeogenesis. This can be interpreted in two different ways: either the AgxtKO mice adapts its utilization of amino acids reducing amino-acid driven gluconeogenesis resulting in lower levels of amino acids or it means that the body is excessively using amino acids to produce glucose explaining lower levels of amino acids in the plasma of these mice. Plasma urea levels of AgxtKO mice showed that proteolysis from amino acids is reduced since urea levels were lower suggesting that amino acid-driven gluconeogenesis was affected in hyperoxaluric mice.

Gene expression changes in glyoxylate metabolism genes: It should also be considered that the liver - in addition to Agxt – has a set of other pathways to metabolize glyoxylate and to prevent the formation of oxalate. One possibility is the upregulation of Grhpr, which reduces glyoxylate to glycolate yielding NAD^+ (or $NADP^+$) from NADH (or NADPH). Another possibility is the downregulation of Hao1 to prevent the formation of glyoxylate from glycolate in peroxisomes or the downregulation of Prodh2/Hoga1 in the mitochondria to prevent glyoxylate formation from hydroxyproline catabolism. Possible changes in the expression levels of these genes in liver and kidney tissue of AgxtKO mice have been explored and showed no distinction between AgxtKO and wt mice.

Interestingly, in the kidney of AgxtKO mice, essential glucogenic genes displayed a higher mRNA expression compared to wt mice. This was also translated to the protein expression in those mice. This information provides strong evidence that in AgxtKO mice the renal gluconeogenesis is more affected in comparison to the hepatic gluconeogenesis. Based on the upregulation of Gyk and G6pc it can be concluded that the glycerol-driven gluconeogenesis pathway is more active in the kidneys of AgxtKO mice.

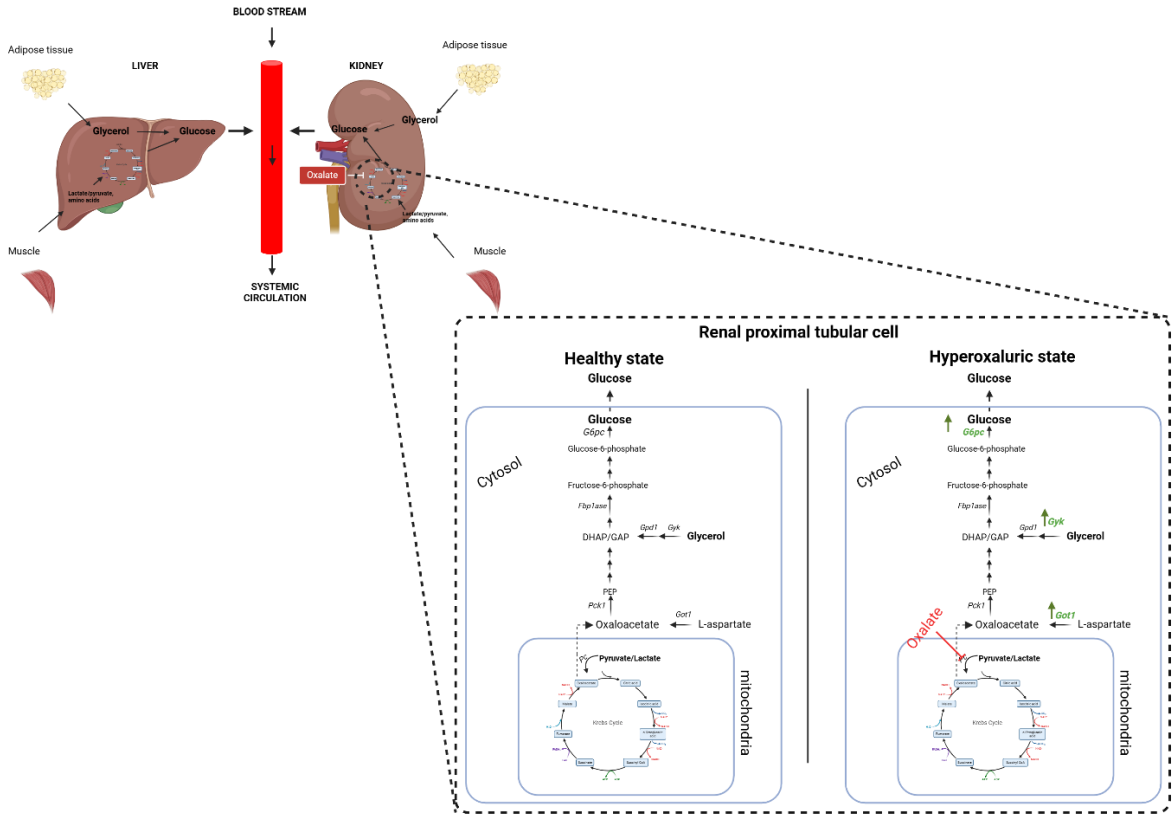

Figure 58: A possible compensatory mechanism in the kidney in the hyperoxaluric mice. Due to inhibition of pyruvate carbobxylase by oxalate, renal tubular cells upregulate Got1 and glycerol-associated genes to maintain renal gluconeogenesis. This figure was created with BioRender.com

This would be in line with the observation that oxalate accumulation was significantly elevated in AgxtKO mice in the kidney tissue. Due to the local accumulation of oxalate in the kidney of AgxtKO mice, it is very likely that the enzyme Pc is functionally impaired. One possible compensatory mechanism besides the enhanced glycerol-driven gluconeogenesis via Gyk and G6pc could also be the upregulation of specific aminotransferases like Got1, which circumvents the Pc-mediated reaction and was also upregulated in the kidneys of AgxtKO mice independent of the feeding state. Got1 catalyzes the transamination of L-aspartate and α-ketoglutarate to form oxaloacetate and L-glutamate that can be immediately used for the synthesis of glucose (Song et al., 2022). The two compensatory mechanism that are described here are shown in figure 58.

4.5 Glucagon-induced Agxt protein expression is independent of glucose kinetics

Many studies have indicated that Agxt expression is upregulated after the treatment with glucagon, which is in line with the observation that the promotor region of Agxt contains a CRE sequence (Oda et al., 1993). Up to date, the pattern of glucagon-induced upregulation of Agxt has only been studied in the context of oxalate formation. Takayama et al. found that oxalate formation from hydroxyproline was markedly reduced when Agxt had been previously induced by glucagon (Takayama et al., 2003). However the pattern of glucagon-induced upregulation of Agxt on gluconeogenesis has never been studied. We investigated the expression of Agxt in correlation with time-dependent effect of glucagon on blood parameters as well as other gene expression changes in the liver *in vivo*. The results obtained showed that glucagon administration induced an immediate rise in blood glucose levels, which was back to normal already 1.5h after injection, as a counter-effect mediated by insulin. The Agxt mRNA peaked 3h after the administration of glucagon, and slowly decreased back to normal after 24h. Thus, Agxt´s mRNA peak occurs posteriorly to the peak of blood glucose levels, and accordingly it cannot be involved in the early glucagon-mediated increase in blood glucose. This was even further underlined by the fact that the protein expression of Agxt increased even later the mRNA, showing a significant increase 24h post administration when the blood glucose levels were back to normal again. An explanation for the discrepancy between the glucose peak after stimulation and the induced protein expression of Agxt after 6h and 24h could be that this event represents a prolonged state of starvation since we observe supraphysiological glucagon levels 24h post stimulation. Regarding the physiological role of the upregulation of Agxt via the stimulation by glucagon it is very likely that it prevents

excessive oxalate formation from amino acid catabolism or from the breakdown of collagen via hydroxyproline to provide the system with carbon sources that can be used for glucose synthesis. Another explanation for this late protein upregulation of Agxt it is possible that Agxt itself provides amino acids to fuel the TCA cycle and maintain the functionality of the cycle.

This would be in line with another finding of this experiment, because not only the aminotransferase Agxt is induced after the stimulation with glucagon. Our glucagon experiment revealed that also Got1, which is an aminotransferase associated with amino acid-driven gluconeogenesis by suppling glucogenic precursors (Goldstein et al., 2013). Under an umbrella of reactions that Got1 faciliates, one particular reactions catalyzes the conversion of α-ketoglutarate and aspartate to form oxaloacetate, which then can be used for the de novo production of glucose via Pck1 (Jiang et al., 2015). In this case, the pattern of *Got1* mRNA expression followed a similar trend to *Agxt* mRNA.

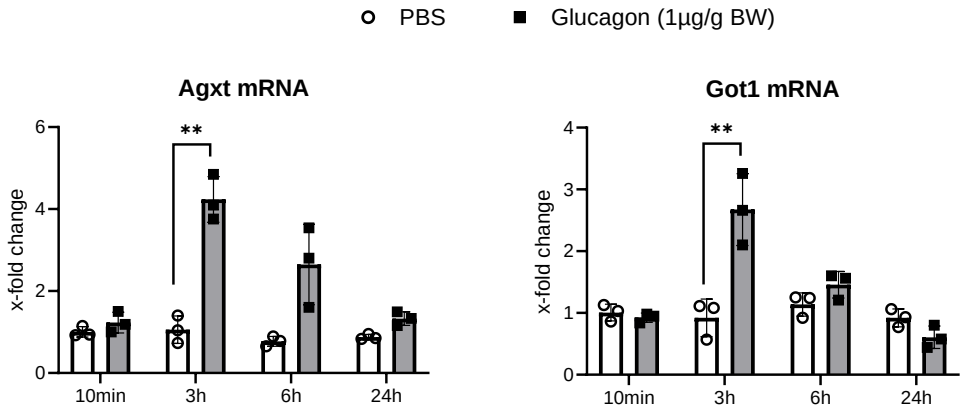

Figure 59: Comparison of the expression pattern of *Agxt* mRNA and aminotransferase *Got1* after stimulation with glucagon (n=3) All bar diagrams represent the mean ± SD; **p<0.01; Student's t test, unpaired, two sided)

A study by Xu et *al.*, which describes the importance of amino acid-driven gluconeogenesis showed that glucagon itself and amino acids – in particular glutamine - are fueling the TCA cycle in a more pronounced way compared to pyruvate/lactate and glycerol *in vitro.* This was underlined by a metabolic flux analysis which showed that glutamine-derived carbon atoms were incorportated in the glucose backbone to a higher percentage compared to common gluconeogenic precursors (Xu et al., 2022).

Because it was observed that glucogenic substrates could induce transcription of gluconeogenesis enzymes in the hepatic glucose production assay, we also investigated the expression of Agxt in this setting. Here, we could see that the *Agxt* mRNA was upregulated

after the exposure to pyruvate/lactate and amino acids but not to glycerol in a concentration-dependent manner after 6h and 24h of incubation. Thus, Agxt follows the same expression pattern as Pck1 and G6pc, which are key glucogenic enzymes, although the magnitude of induction of Agxt is lower compared to the others. Altogether, the induction of Agxt by glucagon and by substrate exposure gives a clear hint towards a association to glucose production. Together with the displayed data in this thesis, it is the first evidence that Agxt is associated with gluconeogenesis, but not directly driving amino-acid driven gluconeogenesis.

4.6 A link between Agxt and muscle proteolysis

One interesting finding, which was discovered in this thesis, was the decreased body weight loss of AgxtKO mice compared to healthy wildtype mice after an overnight starvation. Further analysis of the plasma urea of these mice revealed that AgxtKO mice displayed decreased levels compared to healthy mice. Urea is a marker that characterizes the bound nitrogen from protein turnover/ amino acid-driven gluconeogenesis since unbound nitrogen in the form of ammonia is toxic to the organism. Interestingly, a recent paper by Just *et al.* from 2020 displayed Lkb1 being a suppressor of amino-acid driven gluconeogenesis. Liver-specific deletion of Lkb1 led to changes in whole-body metabolism and ultimately to sarcopenia and cachexia due to diversion of amino acids at the expense of muscle tissue (Just et al., 2020). Specifically, these mice lost way more body weight after an overnight starvation compared to healthy control mice. They found out that among various aminotransferases Agxt was one of the key effectors of the suppression of Lkb1 driving the rigorous body weight loss. They propose Agxt contributes to excessive amino acid-driven gluconeogenesis since it can produce glucose from the catabolism of serine via hydroxypruvate (Just et al., 2020; Rowsell et al., 1969). In this thesis, we observed the exact opposite of body weight loss. A missing Agxt protein protected the mice from loosing more weight compared to healthy mice after an overnight starvation. This suggests that Agxt or indirectly oxalate is eventually associated with muscle-derived proteolysis under fasting conditions. One possible explanation could be that oxalate determines the source of the glucose either from muscle-derived amino acids or from fat-derived glycerol. Hence, In the hyperoxaluric mice the preferred substrate could be glycerol since amino acid-driven glucose production is impaired by the inhibition of Pc. Another explanation could be that oxalate acts a sensor for a feedback-mechanism in the muscle which prevents the proteolysis of the muscle tissue. This needs further investigation to clarify a possible link between Agxt/oxalate and the muscle.

5 Outlook

The presented study and our paper published in 2021 has demonstrated that Agxt plays an important role in the detoxification of glyoxylate preventing the excessive generation of oxalate which leads to a higher susceptibility for the formation of oxalate crystals in the kidney. Apart from this, we could show that oxalate does not only affect glucose homeostasis in the liver, but also the kidney in the context of glucose homeostasis and gluconeogenesis.

A future methological approach would be to perform a metabolic flux analysis (MFA) *in vitro* and *in vivo* to elucidate the fate of glucogenic precursors and how they are incorporated in the generation of glucose when exposed to oxalate. Moreover, this would also highlight the role of TCA intermediates and how oxalate inhibits the functionality of the key enzyme Pc in liver and kidney. It could also be an interesting target to validate the consequences of oxalate accumulation using proximal tubular cells of the kidney, which resemble all genes that are associated with renal gluconeogenesis. In a subsequent approach for the future, the oxalate inhibiting effect on gluconeogenesis could be validated in steatotic mouse models.

As mentioned in the discussion section, the role of redox equivalents should be considered in this context. Since NAD^+/NADH pools are limited in the cells and might be at expense in hydroxyproline detoxification, this could result in a shortage of available NAD^+ which aggravates the conversion of lactate to pyruvate resulting in less glucose production. To address this, the overall turnover and expenses of NAD^+ could be measured *in vitro*. Moreover, the glycolytic activity and functionality of the respiration rate of mitochondria could be investigated, which would help to elucidate differences between AgxtKO hepatocytes and wt hepatocytes in an experimental setting using Seahorse assay.

Another finding in this study was the association of Agxt in the context of gluconeogenesis. Here, we showed that Agxt is both hormonally and substrate-dependently regulated *in vivo* and *in vitro.* In the future, it would be reasonable to figure out if both treatments, glucagon and substrate specificity, enhance Agxt expression levels and if this leads to an increased glucose production compared to the single treatments. From a molecular point, a direct comparison between healthy and Agxt-downregulated or Agxt-deficient mice *in vivo* should help to understand the contribution of Agxt to the production of glucose. Though the overall production might not change, MFA could help to evaluate compensatory mechanism by which the hepatocytes overcome the missing or downregulation of Agxt.

Another interesting research field for the the future could be to investigate the link between Agxt/oxalate and the muscle proteolysis and how they influence each other via e.g. feedback mechanism or by local amino acid availability. This is a topic that has not been in the scope of the research field by now and could be of interest since the body weight loss phenotype in AgxtKO mice was observed. This is especially important considering that disturbed amino-acid metabolism and muscle proteolysis is highly associated with T2DM.

Further, a hepatic glucose production assay was introduced. For the future, we aspire to explore the applicability of this assay by validating drugs that already have pharmaceutical market access targeting gluconeogenesis in the liver and to see whether our assay is a suitable *in vitro* model supporting research and development of new pharmaceutical drugs. If this is successful, a next step would be to validate disease models like ob/ob or diabetic/diabetic (db/db) hepatocytes in this *in vitro* setting and how it matches to published *in vivo* data, e.g. metabolic tolerance tests.

6 Appendix

6.1 Bibliography

Adams, K.J., Pratt, B., Bose, N., Dubois, L.G., St. John-Williams, L., Perrott, K.M., Ky, K., Kapahi, P., Sharma, V., MacCoss, M.J., Moseley, M.A., Colton, C.A., MacLean, B.X., Schilling, B., Thompson, J.W., Alzheimer's Disease Metabolomics Consortium, 2020. Skyline for Small Molecules: A Unifying Software Package for Quantitative Metabolomics. J. Proteome Res. 19, 1447–1458. https://doi.org/10.1021/acs.jproteome.9b00640

Adams, L.A., Anstee, Q.M., Tilg, H., Targher, G., 2017. Non-alcoholic fatty liver disease and its relationship with cardiovascular disease and other extrahepatic diseases. Gut 66, 1138–1153. https://doi.org/10.1136/gutjnl-2017-313884

Akarken, I., Tarhan, H., Ekin, R.G., Çakmak, Ö., Koç, G., İlbey, Y.Ö., Zorlu, F., 2015. Visceral obesity: A new risk factor for stone disease. Can. Urol. Assoc. J. J. Assoc. Urol. Can. 9, E795-799. https://doi.org/10.5489/cuaj.3145

Anyamaneeratch, K., Rojvirat, P., Sukjoi, W., Jitrapakdee, S., 2015. Insights into Transcriptional Regulation of Hepatic Glucose Production. Int. Rev. Cell Mol. Biol. 318, 203–253. https://doi.org/10.1016/bs.ircmb.2015.05.004

Bacchetta, J., Lieske, J.C., 2022. Primary hyperoxaluria type 1: novel therapies at a glance. Clin. Kidney J. 15, i17–i22. https://doi.org/10.1093/ckj/sfab245

Baker, P.R.S., Cramer, S.D., Kennedy, M., Assimos, D.G., Holmes, R.P., 2004. Glycolate and glyoxylate metabolism in HepG2 cells. Am. J. Physiol. Cell Physiol. 287, C1359-1365. https://doi.org/10.1152/ajpcell.00238.2004

Barroso, E., Jurado-Aguilar, J., Wahli, W., Palomer, X., Vázquez-Carrera, M., 2024. Increased hepatic gluconeogenesis and type 2 diabetes mellitus. Trends Endocrinol. Metab. TEM S1043-2760(24)00124–3. https://doi.org/10.1016/j.tem.2024.05.006

Bartlett, S., Espinal, J., Janssens, P., Ross, B.D., 1984. The influence of renal function on lactate and glucose metabolism. Biochem. J. 219, 73–78. https://doi.org/10.1042/bj2190073

Belostotsky, R., Frishberg, Y., 2022. Catabolism of Hydroxyproline in Vertebrates: Physiology, Evolution, Genetic Diseases and New siRNA Approach for Treatment. Int. J. Mol. Sci. 23, 1005. https://doi.org/10.3390/ijms23021005

Belostotsky, R., Seboun, E., Idelson, G.H., Milliner, D.S., Becker-Cohen, R., Rinat, C., Monico, C.G., Feinstein, S., Ben-Shalom, E., Magen, D., Weissman, I., Charon, C., Frishberg, Y., 2010. Mutations in DHDPSL are responsible for primary hyperoxaluria type III. Am. J. Hum. Genet. 87, 392–399. https://doi.org/10.1016/j.ajhg.2010.07.023

Benedict, M., Zhang, X., 2017. Non-alcoholic fatty liver disease: An expanded review. World J. Hepatol. 9, 715–732. https://doi.org/10.4254/wjh.v9.i16.715

Bergman, A., Tan, B., Somayaji, V.R., Calle, R.A., Kazierad, D.J., 2017. A 4-week study assessing the pharmacokinetics, pharmacodynamics, safety, and tolerability of the glucagon receptor antagonist PF-06291874 administered as monotherapy in subjects with type 2 diabetes mellitus. Diabetes Res. Clin. Pract. 126, 95–104. https://doi.org/10.1016/j.diabres.2017.01.019

Bergsland, K.J., Zisman, A.L., Asplin, J.R., Worcester, E.M., Coe, F.L., 2011. Evidence for net renal tubule oxalate secretion in patients with calcium kidney stones. Am. J. Physiol. Renal Physiol. 300, F311-318. https://doi.org/10.1152/ajprenal.00411.2010

Bhasin, B., Ürekli, H.M., Atta, M.G., 2015. Primary and secondary hyperoxaluria: Understanding the enigma. World J. Nephrol. 4, 235–244. https://doi.org/10.5527/wjn.v4.i2.235

Birdsey, G.M., Lewin, J., Cunningham, A.A., Bruford, M.W., Danpure, C.J., 2004. Differential enzyme targeting as an evolutionary adaptation to herbivory in carnivora. Mol. Biol. Evol. 21, 632–646. https://doi.org/10.1093/molbev/msh054

Björkman, O., Felig, P., 1982. Role of the kidney in the metabolism of fructose in 60-hour fasted humans. Diabetes 31, 516–520. https://doi.org/10.2337/diab.31.6.516

Brand, P.H., Cohen, J.J., Bignall, M.C., 1974. Independence of lactate oxidation from net Na+ reabsorption in dog kidney in vivo. Am. J. Physiol. 227, 1255–1262. https://doi.org/10.1152/ajplegacy.1974.227.6.1255

Brar, G., Tsukamoto, H., 2019. Alcoholic and non-alcoholic steatohepatitis: global perspective and emerging science. J. Gastroenterol. 54, 218–225. https://doi.org/10.1007/s00535-018-01542-w

Browning, J.D., Szczepaniak, L.S., Dobbins, R., Nuremberg, P., Horton, J.D., Cohen, J.C., Grundy, S.M., Hobbs, H.H., 2004. Prevalence of hepatic steatosis in an urban population in the United States: impact of ethnicity. Hepatol. Baltim. Md 40, 1387–1395. https://doi.org/10.1002/hep.20466

Brunt, E.M., Wong, V.W.-S., Nobili, V., Day, C.P., Sookoian, S., Maher, J.J., Bugianesi, E., Sirlin, C.B., Neuschwander-Tetri, B.A., Rinella, M.E., 2015. Nonalcoholic fatty liver disease. Nat. Rev. Dis. Primer 1, 15080. https://doi.org/10.1038/nrdp.2015.80

Brzica, H., Breljak, D., Burckhardt, B.C., Burckhardt, G., Sabolić, I., 2013. Oxalate: from the environment to kidney stones. Arh. Hig. Rada Toksikol. 64, 609–630. https://doi.org/10.2478/10004-1254-64-2013-2428

Buc, H.A., Augereau, C., Demaugre, F., Moncion, A., Leroux, J.P., 1983. Influence of oxalate on the rate of the tricarboxylic acid cycle in rat hepatocytes. Biochim. Biophys. Acta 763, 220–223. https://doi.org/10.1016/0167-4889(83)90048-4

Buc, H.A., Demaugre, F., Moncion, A., Leroux, J.P., 1981. Metabolic consequences of pyruvate kinase inhibition by oxalate in intact rat hepatocytes. Biochimie 63, 595–602. https://doi.org/10.1016/s0300-9084(81)80057-0

Bugianesi, E., Moscatiello, S., Ciaravella, M.F., Marchesini, G., 2010. Insulin resistance in nonalcoholic fatty liver disease. Curr. Pharm. Des. 16, 1941–1951. https://doi.org/10.2174/138161210791208875

Burgess, S.C., Hausler, N., Merritt, M., Jeffrey, F.M.H., Storey, C., Milde, A., Koshy, S., Lindner, J., Magnuson, M.A., Malloy, C.R., Sherry, A.D., 2004. Impaired tricarboxylic acid cycle activity in mouse livers lacking cytosolic phosphoenolpyruvate carboxykinase. J. Biol. Chem. 279, 48941–48949. https://doi.org/10.1074/jbc.M407120200

Byrne, C.D., 2013. Ectopic fat, insulin resistance and non-alcoholic fatty liver disease. Proc. Nutr. Soc. 72, 412–419. https://doi.org/10.1017/S0029665113001249

Byrne, C.D., Targher, G., 2015. NAFLD: a multisystem disease. J. Hepatol. 62, S47-64. https://doi.org/10.1016/j.jhep.2014.12.012

Campbell, J.E., Newgard, C.B., 2021. Mechanisms controlling pancreatic islet cell function in insulin secretion. Nat. Rev. Mol. Cell Biol. 22, 142–158. https://doi.org/10.1038/s41580-020-00317-7

Campbell, P.T., Newton, C.C., Patel, A.V., Jacobs, E.J., Gapstur, S.M., 2012. Diabetes and cause-specific mortality in a prospective cohort of one million U.S. adults. Diabetes Care 35, 1835–1844. https://doi.org/10.2337/dc12-0002

Capozzi, M.E., D'Alessio, D.A., Campbell, J.E., 2022. The past, present, and future physiology and pharmacology of glucagon. Cell Metab. 34, 1654–1674. https://doi.org/10.1016/j.cmet.2022.10.001

Cappel, D.A., Deja, S., Duarte, J.A.G., Kucejova, B., Iñigo, M., Fletcher, J.A., Fu, X., Berglund, E.D., Liu, T., Elmquist, J.K., Hammer, S., Mishra, P., Browning, J.D., Burgess, S.C., 2019. Pyruvate-Carboxylase-Mediated Anaplerosis Promotes Antioxidant Capacity by Sustaining TCA Cycle and Redox Metabolism in Liver. Cell Metab. 29, 1291-1305.e8. https://doi.org/10.1016/j.cmet.2019.03.014

Cellini, B., Bertoldi, M., Montioli, R., Paiardini, A., Borri Voltattorni, C., 2007. Human wild-type alanine:glyoxylate aminotransferase and its naturally occurring G82E variant: functional properties and physiological implications. Biochem. J. 408, 39–50. https://doi.org/10.1042/BJ20070637

Cersosimo, E., Garlick, P., Ferretti, J., 2000. Regulation of splanchnic and renal substrate supply by insulin in humans. Metabolism. 49, 676–683. https://doi.org/10.1016/s0026-0495(00)80048-7

Chan, W.-K., Chuah, K.-H., Rajaram, R.B., Lim, L.-L., Ratnasingam, J., Vethakkan, S.R., 2023. Metabolic Dysfunction-Associated Steatotic Liver Disease (MASLD): A State-of-the-Art Review. J. Obes. Metab. Syndr. 32, 197–213. https://doi.org/10.7570/jomes23052

Chandramouli, V., Ekberg, K., Schumann, W.C., Kalhan, S.C., Wahren, J., Landau, B.R., 1997. Quantifying gluconeogenesis during fasting. Am. J. Physiol. 273, E1209-1215. https://doi.org/10.1152/ajpendo.1997.273.6.E1209

Chang, A.Y., Schneider, D.I., 1970. Rate of gluconeogenesis and levels of gluconeogenic enzymes in liver and kidney of diabetic and normal Chinese hamsters. Biochim. Biophys. Acta 222, 587–592. https://doi.org/10.1016/0304-4165(70)90184-4

Chao, A.M., Tronieri, J.S., Amaro, A., Wadden, T.A., 2023. Semaglutide for the treatment of obesity. Trends Cardiovasc. Med. 33, 159–166. https://doi.org/10.1016/j.tcm.2021.12.008

Chen, T.-C., Clark, J., Riddles, M.K., Mohadjer, L.K., Fakhouri, T.H.I., 2020. National Health and Nutrition Examination Survey, 2015-2018: Sample Design and Estimation Procedures. Vital Health Stat. 2. 1–35.

Chomczynski, P., Sacchi, N., 1987. Single-step method of RNA isolation by acid guanidinium thiocyanate-phenol-chloroform extraction. Anal. Biochem. 162, 156–159. https://doi.org/10.1006/abio.1987.9999

Chou, J.Y., Jun, H.S., Mansfield, B.C., 2010. Glycogen storage disease type I and G6Pase-β deficiency: etiology and therapy. Nat. Rev. Endocrinol. 6, 676–688. https://doi.org/10.1038/nrendo.2010.189

Chourpiliadis, C., Mohiuddin, S.S., 2024. Biochemistry, Gluconeogenesis, in: StatPearls. StatPearls Publishing, Treasure Island (FL).

Cloete, L., 2022. Diabetes mellitus: an overview of the types, symptoms, complications and management. Nurs. Stand. R. Coll. Nurs. G. B. 1987 37, 61–66. https://doi.org/10.7748/ns.2021.e11709

Cochat, P., Rumsby, G., 2013. Primary hyperoxaluria. N. Engl. J. Med. 369, 649–658. https://doi.org/10.1056/NEJMra1301564

Curthoys, N.P., Moe, O.W., 2014. Proximal tubule function and response to acidosis. Clin. J. Am. Soc. Nephrol. CJASN 9, 1627–1638. https://doi.org/10.2215/CJN.10391012

Custodio, R.J.P., Hobloss, Z., Myllys, M., Hassan, R., González, D., Reinders, J., Bornhorst, J., Weishaupt, A.-K., Seddek, A., Abbas, T., Friebel, A., Hoehme, S., Getzmann, S., Hengstler, J.G., Van Thriel, C., Ghallab, A., 2023. Cognitive Functions, Neurotransmitter Alterations, and Hippocampal Microstructural Changes in Mice Caused by Feeding on Western Diet. Cells 12, 2331. https://doi.org/10.3390/cells12182331

Danpure, C.J., 1997. Variable peroxisomal and mitochondrial targeting of alanine: glyoxylate aminotransferase in mammalian evolution and disease. BioEssays News Rev. Mol. Cell. Dev. Biol. 19, 317–326. https://doi.org/10.1002/bies.950190409

De Meyts, P., 2004. Insulin and its receptor: structure, function and evolution. BioEssays News Rev. Mol. Cell. Dev. Biol. 26, 1351–1362. https://doi.org/10.1002/bies.20151

Demoulin, N., Aydin, S., Gillion, V., Morelle, J., Jadoul, M., 2022. Pathophysiology and Management of Hyperoxaluria and Oxalate Nephropathy: A Review. Am. J. Kidney Dis. Off. J. Natl. Kidney Found. 79, 717–727. https://doi.org/10.1053/j.ajkd.2021.07.018

Deprince, A., Haas, J.T., Staels, B., 2020. Dysregulated lipid metabolism links NAFLD to cardiovascular disease. Mol. Metab. 42, 101092. https://doi.org/10.1016/j.molmet.2020.101092

Devresse, A., Cochat, P., Godefroid, N., Kanaan, N., 2020. Transplantation for Primary Hyperoxaluria Type 1: Designing New Strategies in the Era of Promising Therapeutic Perspectives. Kidney Int. Rep. 5, 2136–2145. https://doi.org/10.1016/j.ekir.2020.09.022

Dindo, M., Ambrosini, G., Oppici, E., Pey, A.L., O'Toole, P.J., Marrison, J.L., Morrison, I.E.G., Butturini, E., Grottelli, S., Costantini, C., Cellini, B., 2021. Dimerization Drives Proper Folding of Human

Alanine:Glyoxylate Aminotransferase But Is Dispensable for Peroxisomal Targeting. J. Pers. Med. 11, 273. https://doi.org/10.3390/jpm11040273

Ding, Q., Ouyang, J., Fan, B., Cao, C., Fan, Z., Ding, L., Li, F., Tu, W., Jin, X., Wang, J., Shi, Y., 2019. Association between Dyslipidemia and Nephrolithiasis Risk in a Chinese Population. Urol. Int. 103, 156–165. https://doi.org/10.1159/000496208

Donini, S., Ferrari, M., Fedeli, C., Faini, M., Lamberto, I., Marletta, A.S., Mellini, L., Panini, M., Percudani, R., Pollegioni, L., Caldinelli, L., Petrucco, S., Peracchi, A., 2009. Recombinant production of eight human cytosolic aminotransferases and assessment of their potential involvement in glyoxylate metabolism. Biochem. J. 422, 265–272. https://doi.org/10.1042/BJ20090748

Eid, A., Bodin, S., Ferrier, B., Delage, H., Boghossian, M., Martin, M., Baverel, G., Conjard, A., 2006. Intrinsic gluconeogenesis is enhanced in renal proximal tubules of Zucker diabetic fatty rats. J. Am. Soc. Nephrol. JASN 17, 398–405. https://doi.org/10.1681/ASN.2005070742

Einollahi, B., Naghii, M.R., Sepandi, M., 2013. Association of nonalcoholic fatty liver disease (NAFLD) with urolithiasis. Endocr. Regul. 47, 27–32. https://doi.org/10.4149/endo_2013_01_27

Eisner, B., Porten, S., Bechis, S.K., Stoller, M.L., 2010. Diabetic Kidney Stone Formers Excrete More Oxalate and Have Lower Urine pH Than Nondiabetic Stone Formers. J. Urol. 2244–2248.

Elliott, K.A., Greig, M.E., 1937. The metabolism of lactic and pyruvic acids in normal and tumour tissues: The formation of succinate. Biochem. J. 31, 1021–1032. https://doi.org/10.1042/bj0311021

Engelking, L.R., 2015. Gluconeogenesis, in: Textbook of Veterinary Physiological Chemistry. Elsevier, pp. 225–230. https://doi.org/10.1016/B978-0-12-391909-0.50037-2

Ermer, T., Eckardt, K.-U., Aronson, P.S., Knauf, F., 2016. Oxalate, inflammasome, and progression of kidney disease. Curr. Opin. Nephrol. Hypertens. 25, 363–371. https://doi.org/10.1097/MNH.0000000000000229

Eslam, M., Newsome, P.N., Sarin, S.K., Anstee, Q.M., Targher, G., Romero-Gomez, M., Zelber-Sagi, S., Wai-Sun Wong, V., Dufour, J.-F., Schattenberg, J.M., Kawaguchi, T., Arrese, M., Valenti, L., Shiha, G., Tiribelli, C., Yki-Järvinen, H., Fan, J.-G., Grønbæk, H., Yilmaz, Y., Cortez-Pinto, H., Oliveira, C.P., Bedossa, P., Adams, L.A., Zheng, M.-H., Fouad, Y., Chan, W.-K., Mendez-Sanchez, N., Ahn, S.H., Castera, L., Bugianesi, E., Ratziu, V., George, J., 2020. A new definition for metabolic dysfunction-associated fatty liver disease: An international expert consensus statement. J. Hepatol. 73, 202–209. https://doi.org/10.1016/j.jhep.2020.03.039

Evan, A.P., 2010. Physiopathology and etiology of stone formation in the kidney and the urinary tract. Pediatr. Nephrol. Berl. Ger. 25, 831–841. https://doi.org/10.1007/s00467-009-1116-y

Ferrara, C.T., Wang, P., Neto, E.C., Stevens, R.D., Bain, J.R., Wenner, B.R., Ilkayeva, O.R., Keller, M.P., Blasiole, D.A., Kendziorski, C., Yandell, B.S., Newgard, C.B., Attie, A.D., 2008. Genetic networks of liver metabolism revealed by integration of metabolic and transcriptional profiling. PLoS Genet. 4, e1000034. https://doi.org/10.1371/journal.pgen.1000034

Fletcher, B., Gulanick, M., Lamendola, C., 2002. Risk factors for type 2 diabetes mellitus. J. Cardiovasc. Nurs. 16, 17–23. https://doi.org/10.1097/00005082-200201000-00003

Foster, J.D., Pederson, B.A., Nordlie, R.C., 1997. Glucose-6-phosphatase structure, regulation, and function: an update. Proc. Soc. Exp. Biol. Med. Soc. Exp. Biol. Med. N. Y. N 215, 314–332. https://doi.org/10.3181/00379727-215-44142

Francque, S.M., Marchesini, G., Kautz, A., Walmsley, M., Dorner, R., Lazarus, J.V., Zelber-Sagi, S., Hallsworth, K., Busetto, L., Frühbeck, G., Dicker, D., Woodward, E., Korenjak, M., Willemse, J., Koek, G.H., Vinker, S., Ungan, M., Mendive, J.M., Lionis, C., 2021. Non-alcoholic fatty liver disease: A patient guideline. JHEP Rep. Innov. Hepatol. 3, 100322. https://doi.org/10.1016/j.jhepr.2021.100322

Gadiparthi, C., Spatz, M., Greenberg, S., Iqbal, U., Kanna, S., Satapathy, S.K., Broder, A., Ahmed, A., 2020. NAFLD Epidemiology, Emerging Pharmacotherapy, Liver Transplantation Implications and the Trends in the United States. J. Clin. Transl. Hepatol. 8, 215–221. https://doi.org/10.14218/JCTH.2020.00014

Garrelfs, S.F., Frishberg, Y., Hulton, S.A., Koren, M.J., O'Riordan, W.D., Cochat, P., Deschênes, G., Shasha-Lavsky, H., Saland, J.M., Van't Hoff, W.G., Fuster, D.G., Magen, D., Moochhala, S.H., Schalk, G., Simkova, E., Groothoff, J.W., Sas, D.J., Meliambro, K.A., Lu, J., Sweetser, M.T., Garg, P.P., Vaishnaw, A.K., Gansner, J.M., McGregor, T.L., Lieske, J.C., ILLUMINATE-A Collaborators, 2021. Lumasiran, an RNAi Therapeutic for Primary Hyperoxaluria Type 1. N. Engl. J. Med. 384, 1216–1226. https://doi.org/10.1056/NEJMoa2021712

Gastaldelli, A., 2017. Insulin resistance and reduced metabolic flexibility: cause or consequence of NAFLD? Clin. Sci. Lond. Engl. 1979 131, 2701–2704. https://doi.org/10.1042/CS20170987

Gelling, R.W., Du, X.Q., Dichmann, D.S., Romer, J., Huang, H., Cui, L., Obici, S., Tang, B., Holst, J.J., Fledelius, C., Johansen, P.B., Rossetti, L., Jelicks, L.A., Serup, P., Nishimura, E., Charron, M.J., 2003. Lower blood glucose, hyperglucagonemia, and pancreatic alpha cell hyperplasia in glucagon receptor knockout mice. Proc. Natl. Acad. Sci. U. S. A. 100, 1438–1443. https://doi.org/10.1073/pnas.0237106100

Gianmoena, K., 2017. Metabolic alterations in non-alcoholic fatty liver disease (NAFLD): consequences of AGXT downregulation on glyoxylate detoxification. TU Dortmund.

Gianmoena, K., Gasparoni, N., Jashari, A., Gabrys, P., Grgas, K., Ghallab, A., Nordström, K., Gasparoni, G., Reinders, J., Edlund, K., Godoy, P., Schriewer, A., Hayen, H., Hudert, C.A., Damm, G., Seehofer, D., Weiss, T.S., Boor, P., Anders, H.-J., Motrapu, M., Jansen, P., Schiergens, T.S., Falk-Paulsen, M., Rosenstiel, P., Lisowski, C., Salido, E., Marchan, R., Walter, J., Hengstler, J.G., Cadenas, C., 2021. Epigenomic and transcriptional profiling identifies impaired glyoxylate detoxification in NAFLD as a risk factor for hyperoxaluria. Cell Rep. 36, 109526. https://doi.org/10.1016/j.celrep.2021.109526

Giri, B., Dey, S., Das, T., Sarkar, M., Banerjee, J., Dash, S.K., 2018. Chronic hyperglycemia mediated physiological alteration and metabolic distortion leads to organ dysfunction, infection, cancer progression and other pathophysiological consequences: An update on glucose toxicity. Biomed. Pharmacother. 107, 306–328. https://doi.org/10.1016/j.biopha.2018.07.157

Gnesin, F., Thuesen, A.C.B., Kähler, L.K.A., Madsbad, S., Hemmingsen, B., 2020. Metformin monotherapy for adults with type 2 diabetes mellitus. Cochrane Database Syst. Rev. 6, CD012906. https://doi.org/10.1002/14651858.CD012906.pub2

Godoy, P., Widera, A., Schmidt-Heck, W., Campos, G., Meyer, C., Cadenas, C., Reif, R., Stöber, R., Hammad, S., Pütter, L., Gianmoena, K., Marchan, R., Ghallab, A., Edlund, K., Nüssler, A., Thasler, W.E., Damm, G., Seehofer, D., Weiss, T.S., Dirsch, O., Dahmen, U., Gebhardt, R., Chaudhari, U., Meganathan, K., Sachinidis, A., Kelm, J., Hofmann, U., Zahedi, R.P., Guthke, R., Blüthgen, N., Dooley, S., Hengstler, J.G., 2016. Gene network activity in cultivated primary hepatocytes is highly similar to diseased mammalian liver tissue. Arch. Toxicol. 90, 2513–2529. https://doi.org/10.1007/s00204-016-1761-4

Goldstein, I., Yizhak, K., Madar, S., Goldfinger, N., Ruppin, E., Rotter, V., 2013. p53 promotes the expression of gluconeogenesis-related genes and enhances hepatic glucose production. Cancer Metab. 1, 9. https://doi.org/10.1186/2049-3002-1-9

Gray, L.R., Tompkins, S.C., Taylor, E.B., 2014. Regulation of pyruvate metabolism and human disease. Cell. Mol. Life Sci. CMLS 71, 2577–2604. https://doi.org/10.1007/s00018-013-1539-2

Greenblatt, M.B., Tsai, J.N., Wein, M.N., 2017. Bone Turnover Markers in the Diagnosis and Monitoring of Metabolic Bone Disease. Clin. Chem. 63, 464–474. https://doi.org/10.1373/clinchem.2016.259085

Guder, W.G., Ross, B.D., 1984. Enzyme distribution along the nephron. Kidney Int. 26, 101–111. https://doi.org/10.1038/ki.1984.143

Guder, W.G., Schmidt, U., 1974. The localization of gluconeogenesis in rat nephron. Determination of phosphoenolpyruvate carboxykinase in microdissected tubules. Hoppe. Seylers Z. Physiol. Chem. 355, 273–278. https://doi.org/10.1515/bchm2.1974.355.1.273

Guo, W., Tan, H.-Y., Li, S., Wang, N., Feng, Y., 2020. Glutamic-Pyruvic Transaminase 1 Facilitates Alternative Fuels for Hepatocellular Carcinoma Growth-A Small Molecule Inhibitor, Berberine. Cancers 12, 1854. https://doi.org/10.3390/cancers12071854

Hanson, R.W., Owen, O.E., 2013. Gluconeogenesis, in: Encyclopedia of Biological Chemistry. Elsevier, pp. 381–386. https://doi.org/10.1016/B978-0-12-378630-2.00040-2
Hatting, M., Tavares, C.D.J., Sharabi, K., Rines, A.K., Puigserver, P., 2018. Insulin regulation of gluconeogenesis. Ann. N. Y. Acad. Sci. 1411, 21–35. https://doi.org/10.1111/nyas.13435
Higuchi, R., Fockler, C., Dollinger, G., Watson, R., 1993. Kinetic PCR analysis: real-time monitoring of DNA amplification reactions. Biotechnol. Nat. Publ. Co. 11, 1026–1030. https://doi.org/10.1038/nbt0993-1026
Hillebrand, P., Hoppe, B., 2020. Plasma oxalate levels in primary hyperoxaluria type I show significant intra-individual variation and do not correlate with kidney function. Pediatr. Nephrol. 35, 1227–1233. https://doi.org/10.1007/s00467-020-04531-5
Holecek, M., Sispera, L., 2016. Effects of Arginine Supplementation on Amino Acid Profiles in Blood and Tissues in Fed and Overnight-Fasted Rats. Nutrients 8, 206. https://doi.org/10.3390/nu8040206
Holland, P.M., Abramson, R.D., Watson, R., Gelfand, D.H., 1991. Detection of specific polymerase chain reaction product by utilizing the 5'----3' exonuclease activity of Thermus aquaticus DNA polymerase. Proc. Natl. Acad. Sci. 88, 7276–7280. https://doi.org/10.1073/pnas.88.16.7276
Holmes, R.P., Goodman, H.O., Assimos, D.G., 2001. Contribution of dietary oxalate to urinary oxalate excretion. Kidney Int. 59, 270–276. https://doi.org/10.1046/j.1523-1755.2001.00488.x
Holst, J.J., 2019. The incretin system in healthy humans: The role of GIP and GLP-1. Metabolism. 96, 46–55. https://doi.org/10.1016/j.metabol.2019.04.014
Hopp, K., Cogal, A.G., Bergstralh, E.J., Seide, B.M., Olson, J.B., Meek, A.M., Lieske, J.C., Milliner, D.S., Harris, P.C., Rare Kidney Stone Consortium, 2015. Phenotype-Genotype Correlations and Estimated Carrier Frequencies of Primary Hyperoxaluria. J. Am. Soc. Nephrol. JASN 26, 2559–2570. https://doi.org/10.1681/ASN.2014070698
Hoppe, B., 2012. An update on primary hyperoxaluria. Nat. Rev. Nephrol. 8, 467–475. https://doi.org/10.1038/nrneph.2012.113
Houten, S.M., Herrema, H., Te Brinke, H., Denis, S., Ruiter, J.P.N., van Dijk, T.H., Argmann, C.A., Ottenhoff, R., Müller, M., Groen, A.K., Kuipers, F., Reijngoud, D.-J., Wanders, R.J.A., 2013. Impaired amino acid metabolism contributes to fasting-induced hypoglycemia in fatty acid oxidation defects. Hum. Mol. Genet. 22, 5249–5261. https://doi.org/10.1093/hmg/ddt382
Huang, D.Q., El-Serag, H.B., Loomba, R., 2021. Global epidemiology of NAFLD-related HCC: trends, predictions, risk factors and prevention. Nat. Rev. Gastroenterol. Hepatol. 18, 223–238. https://doi.org/10.1038/s41575-020-00381-6
Iynedjian, P.B., Hanson, R.W., 1977. Messenger RNA for renal phosphoenolpyruvate carboxykinase (GTP). Its translation in a heterologous cell-free system and its regulation by glucocorticoids and by changes in acid-base balance. J. Biol. Chem. 252, 8398–8403.
Jaffe, M., 1886. Ueber den Niederschlag, welchen Pikrinsäure in normalem Harn erzeugt und über eine neue Reaction des Kreatinins. bchm 10, 391–400. https://doi.org/10.1515/bchm1.1886.10.5.391
Janah, L., Kjeldsen, S., Galsgaard, K.D., Winther-Sørensen, M., Stojanovska, E., Pedersen, J., Knop, F.K., Holst, J.J., Wewer Albrechtsen, N.J., 2019. Glucagon Receptor Signaling and Glucagon Resistance. Int. J. Mol. Sci. 20, 3314. https://doi.org/10.3390/ijms20133314
Jensen, T.L., Kiersgaard, M.K., Sørensen, D.B., Mikkelsen, L.F., 2013. Fasting of mice: a review. Lab. Anim. 47, 225–240. https://doi.org/10.1177/0023677213501659
Ji, X., Zhou, F., Zhang, Y., Deng, R., Xu, W., Bai, M., Liu, Y., Shao, L., Wang, X., Zhou, L., 2019. Butyrate stimulates hepatic gluconeogenesis in mouse primary hepatocytes. Exp. Ther. Med. 17, 1677–1687. https://doi.org/10.3892/etm.2018.7136
Jiang, X., Chang, H., Zhou, Y., 2015. Expression, purification and preliminary crystallographic studies of human glutamate oxaloacetate transaminase 1 (GOT1). Protein Expr. Purif. 113, 102–106. https://doi.org/10.1016/j.pep.2015.05.010
Jitrapakdee, S., Wallace, J.C., 1999. Structure, function and regulation of pyruvate carboxylase. Biochem. J. 340 (Pt 1), 1–16. https://doi.org/10.1042/bj3400001

Just, P.-A., Charawi, S., Denis, R.G.P., Savall, M., Traore, M., Foretz, M., Bastu, S., Magassa, S., Senni, N., Sohier, P., Wursmer, M., Vasseur-Cognet, M., Schmitt, A., Le Gall, M., Leduc, M., Guillonneau, F., De Bandt, J.-P., Mayeux, P., Romagnolo, B., Luquet, S., Bossard, P., Perret, C., 2020. Lkb1 suppresses amino acid-driven gluconeogenesis in the liver. Nat. Commun. 11, 6127. https://doi.org/10.1038/s41467-020-19490-6

Kalemba, K.M., Wang, Y., Xu, H., Chiles, E., McMillin, S.M., Kwon, H., Su, X., Wondisford, F.E., 2019. Glycerol induces G6pc in primary mouse hepatocytes and is the preferred substrate for gluconeogenesis both in vitro and in vivo. J. Biol. Chem. 294, 18017–18028. https://doi.org/10.1074/jbc.RA119.011033

Kasper, P., Martin, A., Lang, S., Kütting, F., Goeser, T., Demir, M., Steffen, H.-M., 2021. NAFLD and cardiovascular diseases: a clinical review. Clin. Res. Cardiol. Off. J. Ger. Card. Soc. 110, 921–937. https://doi.org/10.1007/s00392-020-01709-7

Kebede, M., Favaloro, J., Gunton, J.E., Laybutt, D.R., Shaw, M., Wong, N., Fam, B.C., Aston-Mourney, K., Rantzau, C., Zulli, A., Proietto, J., Andrikopoulos, S., 2008. Fructose-1,6-bisphosphatase overexpression in pancreatic beta-cells results in reduced insulin secretion: a new mechanism for fat-induced impairment of beta-cell function. Diabetes 57, 1887–1895. https://doi.org/10.2337/db07-1326

Kemper, M.J., Conrad, S., Müller-Wiefel, D.E., 1997. Primary hyperoxaluria type 2. Eur. J. Pediatr. 156, 509–512. https://doi.org/10.1007/s004310050649

Klein, K.L., Wang, M.S., Torikai, S., Davidson, W.D., Kurokawa, K., 1981. Substrate oxidation by isolated single nephron segments of the rat. Kidney Int. 20, 29–35. https://doi.org/10.1038/ki.1981.100

Knight, J., Jiang, J., Assimos, D.G., Holmes, R.P., 2006. Hydroxyproline ingestion and urinary oxalate and glycolate excretion. Kidney Int. 70, 1929–1934. https://doi.org/10.1038/sj.ki.5001906

Kohjimoto, Y., Sasaki, Y., Iguchi, M., Matsumura, N., Inagaki, T., Hara, I., 2013. Association of Metabolic Syndrome Traits and Severity of Kidney Stones: Results From a Nationwide Survey on Urolithiasis in Japan. Am. J. Kidney Dis. Off. J. Natl. Kidney Found. 61, 923–929.

Kraut, J.A., Madias, N.E., 2014. Lactic acidosis. N. Engl. J. Med. 371, 2309–2319. https://doi.org/10.1056/NEJMra1309483

Lamia, K.A., Papp, S.J., Yu, R.T., Barish, G.D., Uhlenhaut, N.H., Jonker, J.W., Downes, M., Evans, R.M., 2011. Cryptochromes mediate rhythmic repression of the glucocorticoid receptor. Nature 480, 552–556. https://doi.org/10.1038/nature10700

LaMoia, T.E., Shulman, G.I., 2021. Cellular and Molecular Mechanisms of Metformin Action. Endocr. Rev. 42, 77–96. https://doi.org/10.1210/endrev/bnaa023

Lee, S.M.L., Schelcher, C., Demmel, M., Hauner, M., Thasler, W.E., 2013. Isolation of human hepatocytes by a two-step collagenase perfusion procedure. J. Vis. Exp. JoVE. https://doi.org/10.3791/50615

Lee, Y., Wang, M.-Y., Du, X.Q., Charron, M.J., Unger, R.H., 2011. Glucagon receptor knockout prevents insulin-deficient type 1 diabetes in mice. Diabetes 60, 391–397. https://doi.org/10.2337/db10-0426

Legouis, D., Faivre, A., Cippà, P.E., de Seigneux, S., 2022. Renal gluconeogenesis: an underestimated role of the kidney in systemic glucose metabolism. Nephrol. Dial. Transplant. Off. Publ. Eur. Dial. Transpl. Assoc. - Eur. Ren. Assoc. 37, 1417–1425. https://doi.org/10.1093/ndt/gfaa302

Legouis, D., Ricksten, S.-E., Faivre, A., Verissimo, T., Gariani, K., Verney, C., Galichon, P., Berchtold, L., Feraille, E., Fernandez, M., Placier, S., Koppitch, K., Hertig, A., Martin, P.-Y., Naesens, M., Pugin, J., McMahon, A.P., Cippà, P.E., de Seigneux, S., 2020. Altered proximal tubular cell glucose metabolism during acute kidney injury is associated with mortality. Nat. Metab. 2, 732–743. https://doi.org/10.1038/s42255-020-0238-1

Li, X.M., Salido, E.C., Shapiro, L.J., 1999. The mouse alanine:glyoxylate aminotransferase gene (Agxt1): cloning, expression, and mapping to chromosome 1. Somat. Cell Mol. Genet. 25, 67–77. https://doi.org/10.1023/b:scam.0000007142.36524.58

Lieske, J.C., de la Vega, L.S.P., Gettman, M.T., Slezak, J.M., Bergstralh, E.J., Melton, L.J., Leibson, C.L., 2006. Diabetes mellitus and the risk of urinary tract stones: a population-based case-control

study. Am. J. Kidney Dis. Off. J. Natl. Kidney Found. 48, 897–904. https://doi.org/10.1053/j.ajkd.2006.09.002
Liu, Y., Zhao, Ying, Shukha, Y., Lu, H., Wang, L., Liu, Z., Liu, C., Zhao, Yang, Wang, H., Zhao, G., Liang, W., Fan, Y., Chang, L., Yurdagul, A., Pattillo, C.B., Orr, A.W., Aviram, M., Wen, B., Garcia-Barrio, M.T., Zhang, J., Liu, W., Sun, D., Hayek, T., Chen, Y.E., Rom, O., 2021. Dysregulated oxalate metabolism is a driver and therapeutic target in atherosclerosis. Cell Rep. 36, 109420. https://doi.org/10.1016/j.celrep.2021.109420
Livak, K.J., Schmittgen, T.D., 2001. Analysis of Relative Gene Expression Data Using Real-Time Quantitative PCR and the 2−ΔΔCT Method. Methods 25, 402–408. https://doi.org/10.1006/meth.2001.1262
Loomba, R., Sanyal, A.J., 2013. The global NAFLD epidemic. Nat. Rev. Gastroenterol. Hepatol. 10, 686–690. https://doi.org/10.1038/nrgastro.2013.171
Looyens, C., Giraud, R., Neto Silva, I., Bendjelid, K., 2021. Burkitt lymphoma and lactic acidosis: A case report and review of the literature. Physiol. Rep. 9. https://doi.org/10.14814/phy2.14737
Lubinus Badillo, F.G., Cala, O.L.O., Vera Campos, S.N., Villarreal Ibañez, E.D., 2020. Relationship Between Urolithiasis and Fatty Liver Disease: Findings in Computed Tomography. Tomogr. Ann Arbor Mich 6, 1–4. https://doi.org/10.18383/j.tom.2020.00020
MacDonald, P.E., Rorsman, P., 2023. Metabolic Messengers: glucagon. Nat. Metab. 5, 186–192. https://doi.org/10.1038/s42255-022-00725-3
Madiraju, A.K., Erion, D.M., Rahimi, Y., Zhang, X.-M., Braddock, D.T., Albright, R.A., Prigaro, B.J., Wood, J.L., Bhanot, S., MacDonald, M.J., Jurczak, M.J., Camporez, J.-P., Lee, H.-Y., Cline, G.W., Samuel, V.T., Kibbey, R.G., Shulman, G.I., 2014. Metformin suppresses gluconeogenesis by inhibiting mitochondrial glycerophosphate dehydrogenase. Nature 510, 542–546. https://doi.org/10.1038/nature13270
Mahfood Haddad, T., Hamdeh, S., Kanmanthareddy, A., Alla, V.M., 2017. Nonalcoholic fatty liver disease and the risk of clinical cardiovascular events: A systematic review and meta-analysis. Diabetes Metab. Syndr. 11 Suppl 1, S209–S216. https://doi.org/10.1016/j.dsx.2016.12.033
Manns, J.M., 2011. SDS-Polyacrylamide Gel Electrophoresis (SDS-PAGE) of Proteins. Curr. Protoc. Microbiol. 22, A.3M.1-A.3M.13. https://doi.org/10.1002/9780471729259.mca03ms22
Mantovani, A., Petracca, G., Beatrice, G., Csermely, A., Lonardo, A., Schattenberg, J.M., Tilg, H., Byrne, C.D., Targher, G., 2022. Non-alcoholic fatty liver disease and risk of incident chronic kidney disease: an updated meta-analysis. Gut 71, 156–162. https://doi.org/10.1136/gutjnl-2020-323082
Masuoka, H.C., Chalasani, N., 2013. Nonalcoholic fatty liver disease: an emerging threat to obese and diabetic individuals. Ann. N. Y. Acad. Sci. 1281, 106–122. https://doi.org/10.1111/nyas.12016
McCullough, K., Sharma, P., Ali, T., Khan, I., Smith, W.C.S., MacLeod, A., Black, C., 2012. Measuring the population burden of chronic kidney disease: a systematic literature review of the estimated prevalence of impaired kidney function. Nephrol. Dial. Transplant. Off. Publ. Eur. Dial. Transpl. Assoc. - Eur. Ren. Assoc. 27, 1812–1821. https://doi.org/10.1093/ndt/gfr547
McGuinness, O.P., Fugiwara, T., Murrell, S., Bracy, D., Neal, D., O'Connor, D., Cherrington, A.D., 1993. Impact of chronic stress hormone infusion on hepatic carbohydrate metabolism in the conscious dog. Am. J. Physiol. 265, E314-322. https://doi.org/10.1152/ajpendo.1993.265.2.E314
Medina-Santillán, R., López-Velázquez, J.A., Chávez-Tapia, N., Torres-Villalobos, G., Uribe, M., Méndez-Sánchez, N., 2013. Hepatic manifestations of metabolic syndrome. Diabetes Metab. Res. Rev. https://doi.org/10.1002/dmrr.2410
Meisner, H., Loose, D.S., Hanson, R.W., 1985. Effect of hormones on transcription of the gene for cytosolic phosphoenolpyruvate carboxykinase (GTP) in rat kidney. Biochemistry 24, 421–425. https://doi.org/10.1021/bi00323a027
Méndez-Lucas, A., Duarte, J.A.G., Sunny, N.E., Satapati, S., He, T., Fu, X., Bermúdez, J., Burgess, S.C., Perales, J.C., 2013. PEPCK-M expression in mouse liver potentiates, not replaces, PEPCK-C mediated gluconeogenesis. J. Hepatol. 59, 105–113. https://doi.org/10.1016/j.jhep.2013.02.020

Meng, J., Zhang, C., Wang, D., Zhu, L., Wang, L., 2022. Mitochondrial GCN5L1 regulates cytosolic redox state and hepatic gluconeogenesis via glycerol phosphate shuttle GPD2. Biochem. Biophys. Res. Commun. 621, 1–7. https://doi.org/10.1016/j.bbrc.2022.06.092
Mergenthaler, P., Lindauer, U., Dienel, G.A., Meisel, A., 2013. Sugar for the brain: the role of glucose in physiological and pathological brain function. Trends Neurosci. 36, 587–597. https://doi.org/10.1016/j.tins.2013.07.001
Merz, K.E., Thurmond, D.C., 2020. Role of Skeletal Muscle in Insulin Resistance and Glucose Uptake. Compr. Physiol. 10, 785–809. https://doi.org/10.1002/cphy.c190029
Meydan, N., Barutca, S., Caliskan, S., Camsari, T., 2003. Urinary stone disease in diabetes mellitus. Scand. J. Urol. Nephrol. 37, 64–70. https://doi.org/10.1080/00365590310008730
Meyer, C., Stumvoll, M., Dostou, J., Welle, S., Haymond, M., Gerich, J., 2002. Renal substrate exchange and gluconeogenesis in normal postabsorptive humans. Am. J. Physiol. Endocrinol. Metab. 282, E428-434. https://doi.org/10.1152/ajpendo.00116.2001
Meyer, C., Stumvoll, M., Nadkarni, V., Dostou, J., Mitrakou, A., Gerich, J., 1998. Abnormal renal and hepatic glucose metabolism in type 2 diabetes mellitus. J. Clin. Invest. 102, 619–624. https://doi.org/10.1172/JCI2415
Miyajima, H., Oda, T., Ichiyama, A., 1989. Induction of mitochondrial serine:pyruvate aminotransferase of rat liver by glucagon and insulin through different mechanisms. J. Biochem. (Tokyo) 105, 500–504. https://doi.org/10.1093/oxfordjournals.jbchem.a122695
Moey, L.H., Abdul Azize, N.A., Yakob, Y., Leong, H.Y., Keng, W.T., Chen, B.C., Ngu, L.H., 2018. Fructose-1,6-bisphosphatase deficiency as a cause of recurrent hypoglycemia and metabolic acidosis: Clinical and molecular findings in Malaysian patients. Pediatr. Neonatol. 59, 397–403. https://doi.org/10.1016/j.pedneo.2017.11.006
Mueller, K.M., Themanns, M., Friedbichler, K., Kornfeld, J.-W., Esterbauer, H., Tuckermann, J.P., Moriggl, R., 2012. Hepatic growth hormone and glucocorticoid receptor signaling in body growth, steatosis and metabolic liver cancer development. Mol. Cell. Endocrinol. 361, 1–11. https://doi.org/10.1016/j.mce.2012.03.026
Müller, T.D., Finan, B., Clemmensen, C., DiMarchi, R.D., Tschöp, M.H., 2017a. The New Biology and Pharmacology of Glucagon. Physiol. Rev. 97, 721–766. https://doi.org/10.1152/physrev.00025.2016
Müller, T.D., Finan, B., Clemmensen, C., DiMarchi, R.D., Tschöp, M.H., 2017b. The New Biology and Pharmacology of Glucagon. Physiol. Rev. 97, 721–766. https://doi.org/10.1152/physrev.00025.2016
Murguia, M.J., Vailas, A., Mandelbaum, B., Norton, J., Hodgdon, J., Goforth, H., Riedy, M., 1988. Elevated plasma hydroxyproline: A possible risk factor associated with connective tissue injuries during overuse. Am. J. Sports Med. 16, 660–664. https://doi.org/10.1177/036354658801600619
Musso, G., Gambino, R., Tabibian, J.H., Ekstedt, M., Kechagias, S., Hamaguchi, M., Hultcrantz, R., Hagström, H., Yoon, S.K., Charatcharoenwitthaya, P., George, J., Barrera, F., Hafliðadóttir, S., Björnsson, E.S., Armstrong, M.J., Hopkins, L.J., Gao, X., Francque, S., Verrijken, A., Yilmaz, Y., Lindor, K.D., Charlton, M., Haring, R., Lerch, M.M., Rettig, R., Völzke, H., Ryu, S., Li, G., Wong, L.L., Machado, M., Cortez-Pinto, H., Yasui, K., Cassader, M., 2014. Association of non-alcoholic fatty liver disease with chronic kidney disease: a systematic review and meta-analysis. PLoS Med. 11, e1001680. https://doi.org/10.1371/journal.pmed.1001680
Nauck, M.A., Quast, D.R., Wefers, J., Meier, J.J., 2021. GLP-1 receptor agonists in the treatment of type 2 diabetes - state-of-the-art. Mol. Metab. 46, 101102. https://doi.org/10.1016/j.molmet.2020.101102
Nishi, K., Yoshii, A., Abell, L., Zhou, B., Frausto, R., Ritterhoff, J., McMillen, T.S., Sweet, I., Wang, Y., Gao, C., Tian, R., 2023. Branched-chain keto acids inhibit mitochondrial pyruvate carrier and suppress gluconeogenesis in hepatocytes. Cell Rep. 42, 112641. https://doi.org/10.1016/j.celrep.2023.112641

Nizet, A., Cavalier, E., Stenvinkel, P., Haarhaus, M., Magnusson, P., 2020. Bone alkaline phosphatase: An important biomarker in chronic kidney disease – mineral and bone disorder. Clin. Chim. Acta 501, 198–206. https://doi.org/10.1016/j.cca.2019.11.012
Noguchi, T., Takada, Y., 1978. Peroxisomal localization of serine:pyruvate aminotransferase in human liver. J. Biol. Chem. 253, 7598–7600.
Nordlie, R.C., Foster, J.D., Lange, A.J., 1999. Regulation of glucose production by the liver. Annu. Rev. Nutr. 19, 379–406. https://doi.org/10.1146/annurev.nutr.19.1.379
Oda, T., Funai, T., Ichiyama, A., 1990. Generation from a single gene of two mRNAs that encode the mitochondrial and peroxisomal serine:pyruvate aminotransferase of rat liver. J. Biol. Chem. 265, 7513–7519.
Oda, T., Nishiyama, K., Ichiyama, A., 1993. Characterization and sequence analysis of rat serine:pyruvate/alanine:glyoxylate aminotransferase gene. Genomics 17, 59–65. https://doi.org/10.1006/geno.1993.1283
Oh, K.-J., Han, H.-S., Kim, M.-J., Koo, S.-H., 2013. Transcriptional regulators of hepatic gluconeogenesis. Arch. Pharm. Res. 36, 189–200. https://doi.org/10.1007/s12272-013-0018-5
Okun, J.G., Rusu, P.M., Chan, A.Y., Wu, Y., Yap, Y.W., Sharkie, T., Schumacher, J., Schmidt, K.V., Roberts-Thomson, K.M., Russell, R.D., Zota, A., Hille, S., Jungmann, A., Maggi, L., Lee, Y., Blüher, M., Herzig, S., Keske, M.A., Heikenwalder, M., Müller, O.J., Rose, A.J., 2021. Liver alanine catabolism promotes skeletal muscle atrophy and hyperglycaemia in type 2 diabetes. Nat. Metab. 3, 394–409. https://doi.org/10.1038/s42255-021-00369-9
Otto, A.M., Hintermair, J., Janzon, C., 2015. NADH-linked metabolic plasticity of MCF-7 breast cancer cells surviving in a nutrient-deprived microenvironment. J. Cell. Biochem. 116, 822–835. https://doi.org/10.1002/jcb.25038
Owen, O.E., Felig, P., Morgan, A.P., Wahren, J., Cahill, G.F., 1969. Liver and kidney metabolism during prolonged starvation. J. Clin. Invest. 48, 574–583. https://doi.org/10.1172/JCI106016
Pearson, M.J., Unger, R.H., Holland, W.L., 2016. Clinical Trials, Triumphs, and Tribulations of Glucagon Receptor Antagonists. Diabetes Care 39, 1075–1077. https://doi.org/10.2337/dci15-0033
Perry, R.J., Zhang, D., Guerra, M.T., Brill, A.L., Goedeke, L., Nasiri, A.R., Rabin-Court, A., Wang, Y., Peng, L., Dufour, S., Zhang, Y., Zhang, X.-M., Butrico, G.M., Toussaint, K., Nozaki, Y., Cline, G.W., Petersen, K.F., Nathanson, M.H., Ehrlich, B.E., Shulman, G.I., 2020. Glucagon stimulates gluconeogenesis by INSP3R1-mediated hepatic lipolysis. Nature 579, 279–283. https://doi.org/10.1038/s41586-020-2074-6
Petersen, K.F., Price, T., Cline, G.W., Rothman, D.L., Shulman, G.I., 1996. Contribution of net hepatic glycogenolysis to glucose production during the early postprandial period. Am. J. Physiol. 270, E186-191. https://doi.org/10.1152/ajpendo.1996.270.1.E186
Petersen, M.C., Vatner, D.F., Shulman, G.I., 2017. Regulation of hepatic glucose metabolism in health and disease. Nat. Rev. Endocrinol. 13, 572–587. https://doi.org/10.1038/nrendo.2017.80
Pfau, A., Ermer, T., Coca, S.G., Tio, M.C., Genser, B., Reichel, M., Finkelstein, F.O., März, W., Wanner, C., Waikar, S.S., Eckardt, K.-U., Aronson, P.S., Drechsler, C., Knauf, F., 2021. High Oxalate Concentrations Correlate with Increased Risk for Sudden Cardiac Death in Dialysis Patients. J. Am. Soc. Nephrol. JASN 32, 2375–2385. https://doi.org/10.1681/ASN.2020121793
Pfau, A., Wytopil, M., Chauhan, K., Reichel, M., Coca, S.G., Aronson, P.S., Eckardt, K.-U., Knauf, F., 2020. Assessment of Plasma Oxalate Concentration in Patients With CKD. Kidney Int. Rep. 5, 2013–2020. https://doi.org/10.1016/j.ekir.2020.08.029
Phang, J.M., 2022. The regulatory mechanisms of proline and hydroxyproline metabolism: Recent advances in perspective. Front. Oncol. 12, 1118675. https://doi.org/10.3389/fonc.2022.1118675
Pilkis, S.J., Claus, T.H., 1991. Hepatic gluconeogenesis/glycolysis: regulation and structure/function relationships of substrate cycle enzymes. Annu. Rev. Nutr. 11, 465–515. https://doi.org/10.1146/annurev.nu.11.070191.002341
Pohanka, M., 2020. D-Lactic Acid as a Metabolite: Toxicology, Diagnosis, and Detection. BioMed Res. Int. 2020, 3419034. https://doi.org/10.1155/2020/3419034

Pouwels, S., Sakran, N., Graham, Y., Leal, A., Pintar, T., Yang, W., Kassir, R., Singhal, R., Mahawar, K., Ramnarain, D., 2022. Non-alcoholic fatty liver disease (NAFLD): a review of pathophysiology, clinical management and effects of weight loss. BMC Endocr. Disord. 22, 63. https://doi.org/10.1186/s12902-022-00980-1

Prochownik, E.V., Wang, H., 2021. The Metabolic Fates of Pyruvate in Normal and Neoplastic Cells. Cells 10, 762. https://doi.org/10.3390/cells10040762

Purdue, P.E., Takada, Y., Danpure, C.J., 1990. Identification of mutations associated with peroxisome-to-mitochondrion mistargeting of alanine/glyoxylate aminotransferase in primary hyperoxaluria type 1. J. Cell Biol. 111, 2341–2351. https://doi.org/10.1083/jcb.111.6.2341

Qin, S., Wang, S., Wang, X., Wang, J., 2018. Non-alcoholic fatty liver disease and the risk of urolithiasis: A systematic review and meta-analysis. Medicine (Baltimore) 97, e12092. https://doi.org/10.1097/MD.0000000000012092

Rena, G., Hardie, D.G., Pearson, E.R., 2017. The mechanisms of action of metformin. Diabetologia 60, 1577–1585. https://doi.org/10.1007/s00125-017-4342-z

Rokka, A., Antonenkov, V.D., Soininen, R., Immonen, H.L., Pirilä, P.L., Bergmann, U., Sormunen, R.T., Weckström, M., Benz, R., Hiltunen, J.K., 2009. Pxmp2 is a channel-forming protein in Mammalian peroxisomal membrane. PloS One 4, e5090. https://doi.org/10.1371/journal.pone.0005090

Romeo, S., Kozlitina, J., Xing, C., Pertsemlidis, A., Cox, D., Pennacchio, L.A., Boerwinkle, E., Cohen, J.C., Hobbs, H.H., 2008. Genetic variation in PNPLA3 confers susceptibility to nonalcoholic fatty liver disease. Nat. Genet. 40, 1461–1465. https://doi.org/10.1038/ng.257

Rowsell, E.V., Snell, K., Carnie, J.A., Al-Tai, A.H., 1969. Liver-L-alanine-glyoxylate and L-serine-pyruvate aminotransferase activities: an apparent association with gluconeogenesis. Biochem. J. 115, 1071–1073. https://doi.org/10.1042/bj1151071

Rui, L., 2014. Energy metabolism in the liver. Compr. Physiol. 4, 177–197. https://doi.org/10.1002/cphy.c130024

Ryoo, J.-H., Suh, Y.J., Shin, H.C., Cho, Y.K., Choi, J.-M., Park, S.K., 2014. Clinical association between non-alcoholic fatty liver disease and the development of hypertension. J. Gastroenterol. Hepatol. 29, 1926–1931. https://doi.org/10.1111/jgh.12643

Sahoo, B., Srivastava, M., Katiyar, A., Ecelbarger, C., Tiwari, S., 2023. Liver or kidney: Who has the oar in the gluconeogenesis boat and when? World J. Diabetes 14, 1049–1056. https://doi.org/10.4239/wjd.v14.i7.1049

Salido, E., Pey, A.L., Rodriguez, R., Lorenzo, V., 2012. Primary hyperoxalurias: disorders of glyoxylate detoxification. Biochim. Biophys. Acta 1822, 1453–1464. https://doi.org/10.1016/j.bbadis.2012.03.004

Samuel, V.T., Liu, Z.-X., Qu, X., Elder, B.D., Bilz, S., Befroy, D., Romanelli, A.J., Shulman, G.I., 2004. Mechanism of hepatic insulin resistance in non-alcoholic fatty liver disease. J. Biol. Chem. 279, 32345–32353. https://doi.org/10.1074/jbc.M313478200

Sasaki, M., Sasako, T., Kubota, N., Sakurai, Y., Takamoto, I., Kubota, T., Inagi, R., Seki, G., Goto, M., Ueki, K., Nangaku, M., Jomori, T., Kadowaki, T., 2017. Dual Regulation of Gluconeogenesis by Insulin and Glucose in the Proximal Tubules of the Kidney. Diabetes 66, 2339–2350. https://doi.org/10.2337/db16-1602

Satoh, S., Yamamoto, A., Iwata, K., Oda, T., Okuda, K., Higashi, S., Setoguchi, T., Tashiro, Y., 1995. Quantitative cryoimmunogold electron microscopic studies on induction of serine: pyruvate aminotransferase in rat liver mitochondria by administration of glucagon. Cell Struct. Funct. 20, 89–96. https://doi.org/10.1247/csf.20.89

Schriewer, A., Brink, M., Gianmoena, K., Cadenas, C., Hayen, H., 2017. Oxalic acid quantification in mouse urine and primary mouse hepatocyte cell culture samples by ion exclusion chromatography-mass spectrometry. J. Chromatogr. B Analyt. Technol. Biomed. Life. Sci. 1068–1069, 239–244. https://doi.org/10.1016/j.jchromb.2017.10.032

Seglen, P.O., 1976. Chapter 4 Preparation of Isolated Rat Liver Cells, in: Prescott, D.M. (Ed.), Methods in Cell Biology. Academic Press, pp. 29–83. https://doi.org/10.1016/S0091-679X(08)61797-5

Sharma, R., Tiwari, S., 2021. Renal gluconeogenesis in insulin resistance: A culprit for hyperglycemia in diabetes. World J. Diabetes 12, 556–568. https://doi.org/10.4239/wjd.v12.i5.556
Shavit, L., Ferraro, P.M., Johri, N., Robertson, W., Walsh, S.B., Moochhala, S., Unwin, R., 2015. Effect of being overweight on urinary metabolic risk factors for kidney stone formation. Nephrol. Dial. Transplant. Off. Publ. Eur. Dial. Transpl. Assoc. - Eur. Ren. Assoc. 30, 607–613. https://doi.org/10.1093/ndt/gfu350
She, P., Burgess, S.C., Shiota, M., Flakoll, P., Donahue, E.P., Malloy, C.R., Sherry, A.D., Magnuson, M.A., 2003. Mechanisms by which liver-specific PEPCK knockout mice preserve euglycemia during starvation. Diabetes 52, 1649–1654. https://doi.org/10.2337/diabetes.52.7.1649
She, P., Shiota, M., Shelton, K.D., Chalkley, R., Postic, C., Magnuson, M.A., 2000. Phosphoenolpyruvate carboxykinase is necessary for the integration of hepatic energy metabolism. Mol. Cell. Biol. 20, 6508–6517. https://doi.org/10.1128/MCB.20.17.6508-6517.2000
Singh, G., Krauthamer, M., Bjalme-Evans, M., 2022. Wegovy (semaglutide): a new weight loss drug for chronic weight management. J. Investig. Med. Off. Publ. Am. Fed. Clin. Res. 70, 5–13. https://doi.org/10.1136/jim-2021-001952
Soleimani, M., Rastegar, A., 2016. Pathophysiology of Renal Tubular Acidosis: Core Curriculum 2016. Am. J. Kidney Dis. 68, 488–498. https://doi.org/10.1053/j.ajkd.2016.03.422
Song, Z., Yang, Y., Wu, Y., Zheng, M., Sun, D., Li, H., Chen, L., 2022. Glutamic oxaloacetic transaminase 1 as a potential target in human cancer. Eur. J. Pharmacol. 917, 174754. https://doi.org/10.1016/j.ejphar.2022.174754
Staufner, C., Haack, T.B., Feyh, P., Gramer, G., Raga, D.E., Terrile, C., Sauer, S., Okun, J.G., Fang-Hoffmann, J., Mayatepek, E., Prokisch, H., Hoffmann, G.F., Kölker, S., 2016. Genetic cause and prevalence of hydroxyprolinemia. J. Inherit. Metab. Dis. 39, 625–632. https://doi.org/10.1007/s10545-016-9940-2
Steinberg, G.R., Hardie, D.G., 2023. New insights into activation and function of the AMPK. Nat. Rev. Mol. Cell Biol. 24, 255–272. https://doi.org/10.1038/s41580-022-00547-x
Tanase, D.M., Gosav, E.M., Costea, C.F., Ciocoiu, M., Lacatusu, C.M., Maranduca, M.A., Ouatu, A., Floria, M., 2020. The Intricate Relationship between Type 2 Diabetes Mellitus (T2DM), Insulin Resistance (IR), and Nonalcoholic Fatty Liver Disease (NAFLD). J. Diabetes Res. 2020, 3920196. https://doi.org/10.1155/2020/3920196
Targher, G., Byrne, C.D., Lonardo, A., Zoppini, G., Barbui, C., 2016. Non-alcoholic fatty liver disease and risk of incident cardiovascular disease: A meta-analysis. J. Hepatol. 65, 589–600. https://doi.org/10.1016/j.jhep.2016.05.013
Targher, G., Chonchol, M.B., Byrne, C.D., 2014. CKD and nonalcoholic fatty liver disease. Am. J. Kidney Dis. Off. J. Natl. Kidney Found. 64, 638–652. https://doi.org/10.1053/j.ajkd.2014.05.019
Targher, G., Corey, K.E., Byrne, C.D., 2021a. NAFLD, and cardiovascular and cardiac diseases: Factors influencing risk, prediction and treatment. Diabetes Metab. 47, 101215. https://doi.org/10.1016/j.diabet.2020.101215
Targher, G., Tilg, H., Byrne, C.D., 2021b. Non-alcoholic fatty liver disease: a multisystem disease requiring a multidisciplinary and holistic approach. Lancet Gastroenterol. Hepatol. 6, 578–588. https://doi.org/10.1016/S2468-1253(21)00020-0
Thiel, G., Al Sarraj, J., Stefano, L., 2005. cAMP response element binding protein (CREB) activates transcription via two distinct genetic elements of the human glucose-6-phosphatase gene. BMC Mol. Biol. 6, 2. https://doi.org/10.1186/1471-2199-6-2
Thonpho, A., Sereeruk, C., Rojvirat, P., Jitrapakdee, S., 2010. Identification of the cyclic AMP responsive element (CRE) that mediates transcriptional regulation of the pyruvate carboxylase gene in HepG2 cells. Biochem. Biophys. Res. Commun. 393, 714–719. https://doi.org/10.1016/j.bbrc.2010.02.067
Titov, D.V., Cracan, V., Goodman, R.P., Peng, J., Grabarek, Z., Mootha, V.K., 2016. Complementation of mitochondrial electron transport chain by manipulation of the NAD+/NADH ratio. Science 352, 231–235. https://doi.org/10.1126/science.aad4017

Tonon, F.A., Kemmelmeier, F.S., Bracht, A., Ishii-Iwamoto, E.L., Nascimento, E.A., 1998. Metabolic effects of oxalate in the perfused rat liver. Comp. Biochem. Physiol. B Biochem. Mol. Biol. 121, 91–97. https://doi.org/10.1016/s0305-0491(98)10131-1

Towle, H.C., Kaytor, E.N., Shih, H.M., 1997. Regulation of the expression of lipogenic enzyme genes by carbohydrate. Annu. Rev. Nutr. 17, 405–433. https://doi.org/10.1146/annurev.nutr.17.1.405

Uchida, C., Funai, T., Oda, T., Ohbayashi, K., Ichiyama, A., 1994. Regulation by glucagon of serine: pyruvate/alanine: glyoxylate aminotransferase gene expression in cultured rat hepatocytes. J. Biol. Chem. 269, 8849–8856.

Unger, R.H., Orci, L., 1975. The essential role of glucagon in the pathogenesis of diabetes mellitus. Lancet Lond. Engl. 1, 14–16. https://doi.org/10.1016/s0140-6736(75)92375-2

Valle, M., 2017. Pyruvate Carboxylase, Structure and Function. Subcell. Biochem. 83, 291–322. https://doi.org/10.1007/978-3-319-46503-6_11

Vandewalle, A., Wirthensohn, G., Heidrich, H.G., Guder, W.G., 1981. Distribution of hexokinase and phosphoenolpyruvate carboxykinase along the rabbit nephron. Am. J. Physiol. 240, F492-500. https://doi.org/10.1152/ajprenal.1981.240.6.F492

Waikar, S.S., Srivastava, A., Palsson, R., Shafi, T., Hsu, C.-Y., Sharma, K., Lash, J.P., Chen, J., He, J., Lieske, J., Xie, D., Zhang, X., Feldman, H.I., Curhan, G.C., Chronic Renal Insufficiency Cohort study investigators, 2019. Association of Urinary Oxalate Excretion With the Risk of Chronic Kidney Disease Progression. JAMA Intern. Med. 179, 542–551. https://doi.org/10.1001/jamainternmed.2018.7980

Walker, J.M., 2009. The Bicinchoninic Acid (BCA) Assay for Protein Quantitation, in: Walker, J.M. (Ed.), The Protein Protocols Handbook, Springer Protocols Handbooks. Humana Press, Totowa, NJ, pp. 11–15. https://doi.org/10.1007/978-1-59745-198-7_3

Watanabe, C., Seino, Y., Miyahira, H., Yamamoto, M., Fukami, A., Ozaki, N., Takagishi, Y., Sato, J., Fukuwatari, T., Shibata, K., Oiso, Y., Murata, Y., Hayashi, Y., 2012. Remodeling of hepatic metabolism and hyperaminoacidemia in mice deficient in proglucagon-derived peptides. Diabetes 61, 74–84. https://doi.org/10.2337/db11-0739

Whittamore, J.M., Hatch, M., 2017. The role of intestinal oxalate transport in hyperoxaluria and the formation of kidney stones in animals and man. Urolithiasis 45, 89–108. https://doi.org/10.1007/s00240-016-0952-z

Wilson, D.M., Liedtke, R.R., 1991. Modified enzyme-based colorimetric assay of urinary and plasma oxalate with improved sensitivity and no ascorbate interference: reference values and sample handling procedures. Clin. Chem. 37, 1229–1235.

Wu, S., Wu, F., Ding, Y., Hou, J., Bi, J., Zhang, Z., 2016. Association of non-alcoholic fatty liver disease with major adverse cardiovascular events: A systematic review and meta-analysis. Sci. Rep. 6, 33386. https://doi.org/10.1038/srep33386

Xie, N., Zhang, L., Gao, W., Huang, C., Huber, P.E., Zhou, X., Li, C., Shen, G., Zou, B., 2020. NAD+ metabolism: pathophysiologic mechanisms and therapeutic potential. Signal Transduct. Target. Ther. 5, 227. https://doi.org/10.1038/s41392-020-00311-7

Xing, L., Quinn, P.G., 1993. Involvement of 3',5'-cyclic adenosine monophosphate regulatory element binding protein (CREB) in both basal and hormone-mediated expression of the phosphoenolpyruvate carboxykinase (PEPCK) gene. Mol. Endocrinol. Baltim. Md 7, 1484–1494. https://doi.org/10.1210/mend.7.11.8114762

Xu, H., Wang, Y., Kwon, H., Shah, A., Kalemba, K., Su, X., He, L., Wondisford, F.E., 2022. Glucagon changes substrate preference in gluconeogenesis. J. Biol. Chem. 298, 102708. https://doi.org/10.1016/j.jbc.2022.102708

Xu, J., Wei, Y., Huang, Y., Wei, X., 2023. Regulatory Effects and Molecular Mechanisms of Tea and Its Active Compounds on Nonalcoholic Fatty Liver Disease. J. Agric. Food Chem. https://doi.org/10.1021/acs.jafc.2c07702

Xue, H.H., Fujie, M., Sakaguchi, T., Oda, T., Ogawa, H., Kneer, N.M., Lardy, H.A., Ichiyama, A., 1999. Flux of the L-serine metabolism in rat liver. The predominant contribution of serine dehydratase. J. Biol. Chem. 274, 16020–16027. https://doi.org/10.1074/jbc.274.23.16020

Yang, H., Yang, T., Baur, J.A., Perez, E., Matsui, T., Carmona, J.J., Lamming, D.W., Souza-Pinto, N.C., Bohr, V.A., Rosenzweig, A., de Cabo, R., Sauve, A.A., Sinclair, D.A., 2007. Nutrient-sensitive mitochondrial NAD+ levels dictate cell survival. Cell 130, 1095–1107. https://doi.org/10.1016/j.cell.2007.07.035

Yang, Y., Sauve, A.A., 2016. NAD(+) metabolism: Bioenergetics, signaling and manipulation for therapy. Biochim. Biophys. Acta 1864, 1787–1800. https://doi.org/10.1016/j.bbapap.2016.06.014

Yki-Järvinen, H., 2014. Non-alcoholic fatty liver disease as a cause and a consequence of metabolic syndrome. Lancet Diabetes Endocrinol. 2, 901–910. https://doi.org/10.1016/S2213-8587(14)70032-4

Youngson, A., Cowey, C.B., Walton, M.J., 1982. Some properties of serine pyruvate aminotransferase purified from liver of rainbow trout Salmo gairdneri. Comp. Biochem. Physiol. Part B Comp. Biochem. 73, 393–398. https://doi.org/10.1016/0305-0491(82)90303-0

Younossi, Z., Anstee, Q.M., Marietti, M., Hardy, T., Henry, L., Eslam, M., George, J., Bugianesi, E., 2018. Global burden of NAFLD and NASH: trends, predictions, risk factors and prevention. Nat. Rev. Gastroenterol. Hepatol. 15, 11–20. https://doi.org/10.1038/nrgastro.2017.109

Yount, E.A., Harris, R.A., 1980. Studies on the inhibition of gluconeogenesis by oxalate. Biochim. Biophys. Acta 633, 122–133. https://doi.org/10.1016/0304-4165(80)90044-6

Zhang, C.-H., Zhou, B.-G., Sheng, J.-Q., Chen, Y., Cao, Y.-Q., Chen, C., 2020. Molecular mechanisms of hepatic insulin resistance in nonalcoholic fatty liver disease and potential treatment strategies. Pharmacol. Res. 159, 104984. https://doi.org/10.1016/j.phrs.2020.104984

Zimmer, D.B., Magnuson, M.A., 1990. Immunohistochemical localization of phosphoenolpyruvate carboxykinase in adult and developing mouse tissues. J. Histochem. Cytochem. Off. J. Histochem. Soc. 38, 171–178. https://doi.org/10.1177/38.2.1688895

Zou, H., Liu, Q., Meng, L., Zhou, J., Da, C., Wu, X., Jiang, L., Shou, J., Hua, H., 2018. Chemical genetic-based phenotypic screen reveals novel regulators of gluconeogenesis in human primary hepatocytes. Npj Genomic Med. 3, 20. https://doi.org/10.1038/s41525-018-0062-7

6.2 List of tables

Table 1: Equipment 41
Table 2: Consumables 43
Table 3: Chemicals and dyes 44
Table 4: Commercial buffer and reagents 46
Table 5: Prepared buffered and reagents 46
Table 6: Buffers for histological stainings 48
Table 7: Perfusion buffers 48
Table 8: Commercial assay and kits 49
Table 9: Medium and supplements 50
Table 10: Additional supplements for cell culture 50
Table 11: Mice 51
Table 12: Mice feeding 51
Table 13: Primary antibodies for Western blotting and Immunhistochemistry 51
Table 14: Secondary antibodies for Western Blotting 51
Table 15: Taqman gene expression assay for qRT-PCR (Life technologies) 52
Table 16: Adeno-associated viral vectors used for gene transfer in mice 52
Table 17: Fixation protocol for histological stainings 54
Table 18: Overview of different plating systems for in vitro experiments 58
Table 19: Program for reverse transcription of RNA to cDNA 60
Table 20: Program for PCR amplification 61
Table 21: Composition of separation buffer for Western blots 63
Table 22: Constitution of stacking buffer for Western blots 64
Table 23: Antibodies used for Western blots 65

6.3 List of figures

Figure 1: Metabolic pathways in the generation of glucose under fasting (glycogenolysis, gluconeogenesis) and *ad libitum* conditions (glycogenesis, glycolysis) (adapted from Müller et al., 2017b). 18
Figure 2: Schematic illustration of the de novo production of glucose in the kidney. Glucogenic enzymes are restricted to the cortical space of the kidney, whereas glycolytic enzymes are exclusively expressed in the medullar space of the kidney (adapted from Sharma and Tiwari, 2021) 22
Figure 3: Illustration of the possible origins contributing to the progression and manifestation of NAFLD (adapted from Xu et al., 2023)..... 25
Figure 4: Dietary uptake of oxalate or precursors of oxalate can result in less intestinal oxalate degradation by microbiota. Additionally, higher intestinal malabsorption of oxalate results in less-efficient oxalate secretion resulting in elevated plasma oxalate levels. In primary hyperoxaluria, the liver produces more endogenous oxalate due to malfunctioning of respective enzymes leading to chronic kidney disease (adapted from Demoulin et al., 2022). 30
Figure 5: Schematic illustration of the glyoxylate metabolism in the hepatocytes and its genetic deficiencies in PH. PH1 and PH2 indicated by a downregulation of AGXT (blue) and GRHPR (light green),which results in accumulation of glyoxylate, which is further metabolized by LDH to oxalate. PH3 is the consequence of malfunctioning of HOGA (blue)(adapted from Demoulin et al., 2022). 34
Figure 6: Illustration of the detoxifying reaction mediated by Agxt. L-alanine is deaminated and glyoxylate represents the amino group acceptor producing glycine. As a result of the deamination of L-Alanine, pyruvate is produced (adapted from Donini et al., 2009)..... 35
Figure 7: A possible involvement of Agxt in gluconeogenesis (adapted from Xue et al., 1999)..... 37
Figure 8: The current hypothesis claims that due to elevated levels of oxalate in the liver inhibition of key enzyme in TCA cycle takes place, which leads to a compromisation of glucose production under fasting conditions in hyperoxaluric mice. This figure was created with BioRender.com 40
Figure 9: Brief description of the hepatic glucose production (HGP) assay..... 59
Figure 10: 6h exposure of glucogenic precursors in primary mouse hepatocytes; **(A)** glucose production from increasing concentration of pyruvate/lactate (n=3); **(B)** glucose production from increasing concentrations of glycerol (n=3); **(C)** glucose production from increasing concentrations of alanine (n=1/3); **(D)** glucose production from increasing concentrations of glutamine (n=1/3). (All bar diagrams represent the mean ± SD. *p < 0.05; **p < 0.01; Student's t test, unpaired, two sided). 72
Figure 11: 24h exposure of glucogenic precursors in primary mouse hepatocytes; **(A)** glucose production from increasing concentration of pyruvate/lactate (n=3); **(B)** glucose production from increasing concentrations of glycerol (n=3); **(C)** glucose production from increasing concentrations of alanine (n=3); **(D)** glucose production from increasing concentrations of glutamine (n=3). (All bar diagrams represent the mean ± SD. *p < 0.05; **p < 0.01; ***p<0.001;****p<0.0001; Student's t test, unpaired, two sided) 74
Figure 12: 6h mRNA expression analysis of **(A)** Pck1 and G6pc after incubation with pyruvate/lactate (n=3); **(B)** Pck1 and G6pc after incubation with glycerol (n=3); **(C)** Pck1 and G6pc after incubation with glutamine (n=3); (**D)** Pck1 and G6pc after incubation with alanine (n=3). (All bar diagrams represent the mean ± SD. *p < 0.05; **p < 0.01; ***p<0.001; ****p<0.0001, Student's t test, unpaired, two sided). Pck1= phosphoenolpyruvate carboxykinase, G6pc= glucose-6-phosphatase..... 75
Figure 13: 24h mRNA expression analysis of **(A)** Pck1 and G6pc after incubation with pyruvate/lactate (n=3); **(B)** Pck1 and G6pc after incubation with glycerol (n=3); **(C)** Pck1 and G6pc after incubation with glutamine (n=4); (**D)** Pck1 and G6pc after incubation with alanine (n=4). (All bar diagrams represent the mean ± SD. *p < 0.05; **p < 0.01, Student's t test, unpaired, two sided). Pck1= phosphoenolpyruvate carboxykinase, G6pc= glucose-6-phosphatase..... 76

Figure 14: Western blot of **(A)** Pck1 after the exposure to pyruvate/lactate and glycerol (n=4); **(B**) G6pc after the incubation with pyruvate/lactate and glycerol (n=3). (All bar diagrams represent the mean ± SD. ***p < 0.001; ****p < 0.0001, Student's t test, unpaired, two sided). Pck1= phosphoenolpyruvate carboxykinase, G6pc= glucose-6-phosphatase 77
Figure 15: Western blot of **(A)** Pck1 after the exposure to alanine and glutamine (n=3); **(B**) G6pc after the incubation with alanine and glutamine (n=3). (All bar diagrams represent the mean ± SD. *p<0.05; ***p < 0.001, Student's t test, unpaired, two sided). Pck1= phosphoenolpyruvate carboxykinase, G6pc= glucose-6-phosphatase 78
Figure 16: Concentration response curve of oxalate in primary mouse hepatocytes (grey dots represent the results of at least three biological replicates, black dots denote the concentration-wise mean. The vertical blue line indicate the EC20 (n=3)). 79
Figure 17: Quantification of intracellular oxalate in a time- and concentration-dependent manner (n=2/3). (All bar diagrams represent the mean ± SD.*p<0.05; **p<0.01; ***p < 0.001 compared to 0 µM oxalate; Student's t test, unpaired, two sided). Ala = alanine, Ox = oxalate 80
Figure 18: Glucose production in primary mouse hepatocytes from **(A)** pyruvate/lactate (2/20 mM) co-exposed with increasing concentrations of oxalate (n=4) **(B)** alanine (10 mM) co-exposed with increasing concentrations of oxalate (n=4) (All bar diagrams represent the mean ± SD.*p<0.05; **p<0.01; ***p < 0.001; Student's t test, unpaired, two sided). Ala = alanine, Ox = oxalate 81
Figure 19: Glucose production in primary mouse hepatocytes from glycerol (5 mM) co-exposed with increasing concentrations of oxalate (n=4). 82
Figure 20: Concentration response curve of oxalate in human hepatocytes (grey dots represent the results of at least three biological replicates, black dots denote the concentration-wise mean. The vertical blue line indicate the EC20. The vertical dotted grey line indicate the confidence intervals (n=3)). 82
Figure 21: Glucose production in primary human hepatocytes from **(A)** pyruvate/lactate (2/20 mM) co-exposed with increasing concentrations of oxalate (n=4); **(B)** alanine (10 mM) co-exposed with increasing concentrations of oxalate (n=4). (All bar diagrams represent the mean ± SD.*p<0.05; **p<0.01; ***p < 0.001; Student's t test, unpaired, two sided). Ala = alanine, Ox = oxalate 84
Figure 22: Glucose production in primary human hepatocytes from glycerol (5 mM) co-exposed with increasing concentrations of oxalate (n=4). Ox = oxalate 85
Figure 23: Concentration response curve of hydroxyproline in primary mouse hepatocytes (grey dots represent the results of at least three biological replicates, black dots denote the concentration-wise mean. The vertical blue line indicate the EC20 (n=3)). 86
Figure 24: Supernatant and intracellular levels of glyoxylate from wt hepatocytes after exposure to increasing concentration of hydroxyproline (n=3). (All bar diagrams represent the mean ± SD.*p<0.05; **p<0.01; ***p < 0.01 compared to 0 mM Hyp; Student's t test, unpaired, two sided). 87
Figure 25: Supernatant and intracellular levels of glycolate from wt hepatocytes after exposure to increasing concentration of hydroxyproline (n=3). (All bar diagrams represent the mean ± SD.*p<0.05; **p<0.01 compared to 0 mM Hyp; Student's t test, unpaired, two sided). 87
Figure 26: Supernatant and intracellular levels of oxalate from wt hepatocytes after exposure to increasing concentration of hydroxyproline (n=3). (All bar diagrams represent the mean ± SD.*p<0.05; **p<0.01; ****p < 0.001 compared to 0 mM Hyp; Student's t test, unpaired, two sided). 88
Figure 27: Intracellular and extracellular levels of **(A)** oxalate, **(B)** glyoxylate and **(C)** glycolate after the exposure to 10 mM Hydroxyproline in wt and AgxtKO hepatocytes (n=1). wt= wt, Hyp= hydroxyproline 90
Figure 28: Experimental setup for the hepatic glucose production assay incubated with glucogenic precursor and hydroxyproline 91

Figure 29: **(A)** Glucose production in primary mouse hepatocytes from pyruvate/lactate, alanine and glycerol when co-exposed with 10mM hydroxyproline (n=3/4); **(B)** Oxalate quantification in the supernatant of the same experiment from part (A) of this figure (n=1/2). (All bar diagrams represent the mean ± SD.*p<0.05; **p<0.01; ****p < 0.0001; Student's t test, unpaired, two sided). wt= wt .. 92
Figure 30: (A) Western Blot analysis of wt and AgxtKO mice; **(B)** Plasma and urine oxalate levels in wt and AgxtKO mice (n=4); **(C)** HE and PAS stainings of liver and kidney of wt and AgxtKO mice ; **(D)** Oxalate accumulation in kidney and liver tissue of wt and AgxtKO mice (n=4). (All bar diagrams represent the mean ± SD.*p<0.05; ****p < 0.0001; Student's t test, unpaired, two sided).HE= Haematoxylin/Eosin, PAS= Periodic acid Schiff, wt= wildtype 93
Figure 31: (A) Experimental outline of the AAV-experiment including urine collections on day 11 and 21 post AAV administration; **(B)** Immunohistochemical staining of Agxt in AgxtKO + AAV-Agxt, AgxtKO and wt mice; **(C)** Western Blot of AAV-transduced AgxtKO mice, AgxtKO mice and wt mice; **(D)** Plasma and urine oxalate levels of AgxtKO + AAV-Agxt, AgxtKO and wt mice (n=4). (All bar diagrams represent the mean ± SD.*p<0.05; ***p<0.001; ****p < 0.0001; Student's t test, unpaired, two sided).Figure (A) was created with BioRender.com. AAV= adeno-associated virus 94
Figure 32: (A) mRNA expression analysis of various genes participating in the catabolism of hydroxyproline in ob/+ and ob/ob mice (n=5); **(B)** Quantification of Agxt protein expression and Western Blot of ob/+ and ob/ob mice (n=6). (All bar diagrams represent the mean ± SD.*p<0.05; **p<0.01; ***p<0.001; Student's t test, unpaired, two sided). Agxt= alanine-glyoxylate aminotransferase, Grhpr= glyoxylate and hydroxypyruvate reductase, Hao1= hydroxyacid oxidase1, Hoga1= 4-hydroxy-2-oxoglutarate aldolase1, Prodh2= proline dehydrogenase 2 95
Figure 33: (A) Experimental outline of the AAV-experiment in ob/ob and control ob/+ mice; **(B)** Plasma and urine oxalate levels of AAV-Agxt-ob/ob mice, AAV-EGFP-obob mice and control ob/+ mice (n=5); **(C)** Immunohistochemical staining of AAV-Agxt-ob/ob mice, AAV-EGFP-ob/ob mice and control ob/+ mice); **(D)** Western blot of AAV-Agxt-ob/ob mice, AAV-EGFP-ob/ob mice and control ob/+ mice . (All bar diagrams represent the mean ± SD.*p<0.05; **p<0.01; ***p<0.001; Student's t test, unpaired, two sided). Figure (A) was created with BioRender.com. AAV= adeno-associated virus, Agxt= alanine-glyoxylate aminotransferase, EGFP= enhanced green fluorescent protein, Hyp= hydroxyproline, NCD= normal chow diet 96
Figure 34: Blood glucose levels of wt and AgxtKO mice in the ad libitum and fasting state (n=6). (All bar diagrams represent the mean ± SD; ***p<0.001; ****p < 0.0001; Student's t test, unpaired, two sided) 97
Figure 35: body weight loss of wt and AgxtKO mice after an overnight starvation (n=6). (All bar diagrams represent the mean ± SD; **p<0.01; Student's t test, unpaired, two sided). bw= body weight 98
Figure 36: Clinical plasma parameters from wt and AgxtKO mice in the ad libitum and fasting state (n=6) (All bar diagrams represent the mean ± SD; *p<0.05; **p< 0.01; Student's t test, unpaired, two sided). BUN= blood urea nitrogen, ALP= alkaline phosphatase, ALB= albumin, TP= total protein, ALT= alanine aminotransferase, AST= aspartate aminotransferase 99
Figure 37: Plasma amino acid levels in wt and AgxtKO mice in the **(A)** ad libitum and **(B)** fasting state (n=6). (All bar diagrams represent the mean ± SD; *p<0.05; **p<0.01; #p>0.1; Student's t test, unpaired, two sided) 101
Figure 38: Liver tissue amino acid levels of wt and AgxtKO mice in the **(A)** ad libitum and **(B)** fasting state (n=6) (All bar diagrams represent the mean ± SD)..... 102
Figure 39: Kidney tissue amino acid levels in wt and AgxtKO mice in the **(A)** ad libitum and **(B)** fasting state (n=6) (All bar diagrams represent the mean ± SD; *p<0.05; Student's t test, unpaired, two sided) 103
Figure 40: (A) mRNA expression of essential hydroxyproline catabolism gene of wt and AgxtKO mice in the liver after either ad libitum or starvation (n=6). **(B)** Illustration of hydroxyproline catabolism

and its essential enzymes (All bar diagrams represent the mean ± SD; *p<0.05; *p<0.01; ***p<0.001, ****p<0.0001; Student's t test, unpaired, two sided). This figure was created with BioRender.com. Grhpr= glyoxylate and hydroxypyruvate reductase, Hao1= Hydroxyacid oxidase1, Hoga1= Hydroxy-oxoglutarate aldolase, Ldha= Lactate dehydrogenase, Prodh2= Proline dehydrogenase 104
Figure 41: mRNA expression of essential hydroxyproline catabolism gene of wt and AgxtKO mice in the kidney after either ad libitum or starvation (n=6; for Grhpr: n=3).(All bar diagrams represent the mean ± SD;**p<0.01; Student's t test, unpaired, two sided). Grhpr= glyoxylate and hydroxypyruvate reductase, Hao1= Hydroxyacid oxidase1, Hoga1= Hydroxy-oxoglutarate aldolase, Ldha= Lactate dehydrogenase, Prodh2= Proline dehydrogenase 105
Figure 42: Liver mRNA expression of various glucose-associated genes of wt and AgxtKO mice in ad libitum and fasting state (n=6). (All bar diagrams represent the mean ± SD; *p<0.05; **p< 0.01; ***p<0.001; Student's t test, unpaired, two sided). G6pc= glucose-6-phosphatase, Pck1= phosphoenolpyruvate carboxykinase, Fbp1= fructose-1, 6-bisphosphatase, Gyk= glycerol kinase, Gpd1= glycerol-3-phosphate dehydrogenase, Gpt1= Glutamic pyruvic transaminase 1, Got1= glutamic-oxaloacetic transaminase 1 107
Figure 43: Liver protein expression of common glucogenic genes Pck1 and Gyk in wt and AgxtKO mice in ad libitum and fasting state (n=6). (All bar diagrams represent the mean ± SD; *p<0.05; Student's t test, unpaired, two sided). Pck1= phosphoenolpyruvate carboxykinase, Gyk= glycerol kinase..... 108
Figure 44: Kidney mRNA expression of various glucose-associated genes of wt and AgxtKO mice in ad libitum and fasting state (n=6). (All bar diagrams represent the mean ± SD; *p<0.05; ***p<0.001; Student's t test, unpaired, two sided). G6pc= glucose-6-phosphatase, Pck1= phosphoenolpyruvate carboxykinase, Fbp= fructose-1,6-bisphosphatase, Gyk= glycerol kinase, Gpd1= glycerol-3-phosphate dehydrogenase, Gpt1= Glutamic pyruvic aminotransfase 1, Got1= glutamic-oxaloacetic transaminase 1 109
Figure 45: Kidney protein expression of selected glucogenic genes Pck1 and Gyk in wt and AgxtKO mice in ad libitum and fasting state (n=6). (All bar diagrams represent the mean ± SD; *p<0.05; Student's t test, unpaired, two sided). Pck1= phosphoenolpyruvate carboxykinase, Gyk= glycerol kinase..... 110
Figure 46: mRNA expression of Nampt in the liver and the kidney of wt and AgxtKO mice (n=6). (All bar diagrams represent the mean ± SD; **p<0.01; Student's t test, unpaired, two sided) Nampt= nicotinamide phosphoribosyltransferase..... 112
Figure 47: Experimental outline of the glucagon experiment in mice. This figure was created with BioRender.com 113
Figure 48: Glucose kinetics after the administration of 1µg/g glucagon in vivo (n=3). (All dots represent the mean ± SD; *p<0.05; Student´s t-test, unpaired, two sided). PBS= phosphate-buffered saline 113
Figure 49: Hormone levels of insuline and glucagon of wt mice after the treatment with glucagon (1µg/g BW) or PBS in vivo (n=3). (All bar diagrams represent the mean ± SD; *p<0.05; **p<0.01; ****p<.0001; Student's t test, unpaired, two sided). PBS= phosphate-buffered saline, BW= body weight 114
Figure 50: Agxt mRNA expression after the treatment with glucagon (1µg/g BW) or PBS in vivo (n=3). (All bar diagrams represent the mean ± SD; *p<0.05; **p<0.01; Student's t test, unpaired, two sided). Agxt= Alanine-glyoxylate aminotransferase, PBS= phosphate-buffered saline 115
Figure 51: Agxt protein expression after treatment with glucagon (1µg/g BW) or PBS in wt mice in vivo (n=3). Western blot displays **(A)** 10min and 3h time point and **(B)** 6h and 24h time point post glucagon administration. (All bar diagrams represent the mean ± SD; **p<0.01; Student's t test, unpaired, two sided). Agxt= alanine-glyoxylate aminotransferase, PBS= phosphate-buffered saline116

Figure 52: Agxt mRNA expression after 6h incubation with glucogenic precursor **(A)** Pyr/Lac, **(B)** Glycerol, **(C)** Glutamine, **(D)** Alanine in vitro (n=3). (All bar diagrams represent the mean ± SD; *p<0.05; ***p<0.001; Student's t test, unpaired, two sided). 117
Figure 53: Agxt mRNA expression after 24h incubation with glucogenic precursor **(A)** Pyr/Lac, **(B)** Glycerol, **(C)** Glutamine, **(D)** Alanine in vitro (n=3). (All bar diagrams represent the mean ± SD; *p<0.05; ***p<0.001; Student's t test, unpaired, two sided). 117
Figure 54: Agxt protein expression after the incubation with increasing concentration of pyruvate/lactate and glycerol (n=4). (All bar diagrams represent the mean ± SD; *p<0.05; Student's t test, unpaired, two sided) 118
Figure 55: Comparison of the glucose production from pyruvate/lactate from Kalemba et al. and the glucose production shown in this thesis. 121
Figure 56: Comparison of the gene expression of G6pc and Pck1 from Kalemba et al. and data from this thesis after pyruvate/lactate exposure 123
Figure 57: Possible explanation for the reduced glucose production in AgxtKO mice, which describes that the two reactions, catabolism of hydroxyproline and glucose production, require redox equivalents at the expense of NAD^+ resulting in a shortage of NAD^+. Ldh= lactate dehydrogenase, NAD/NADH= Nicotinamide adenine dinucleotide..... 126
Figure 58: A possible compensatory mechanism in the kidney in the hyperoxaluric mice. Due to inhibition of pyruvate carbobxylase by oxalate, renal tubular cells upregulate Got1 and glycerol-associated genes to maintain renal gluconeogenesis. This figure was created with BioRender.com 129
Figure 59: Comparison of the expression pattern of Agxt mRNA and aminotransferase Got1 after stimulation with glucagon (n=3) All bar diagrams represent the mean ± SD; **p<0.01; Student's t test, unpaired, two sided) 131

6.4 Publications

Gianmoena, K., Gasparoni, N., Jashari, A., Gabrys, P., Grgas, K., Ghallab, A., Nordström, K., Gasparoni, G., Reinders, J., Edlund, K., Godoy, P., Schriewer, A., Hayen, H., Hudert, C.A., Damm, G., Seehofer, D., Weiss, T.S., Boor, P., Anders, H.-J., Motrapu, M., Jansen, P., Schiergens, T.S., Falk-Paulsen, M., Rosenstiel, P., Lisowski, C., Salido, E., Marchan, R., Walter, J., Hengstler, J.G., Cadenas, C., 2021. Epigenomic and transcriptional profiling identifies impaired glyoxylate detoxification in NAFLD as a risk factor for hyperoxaluria. Cell Rep. 36, 109526. https://doi.org/10.1016/j.celrep.2021.109526

6.5 Eidesstaatliche Erklärung (Affidavit)

Eidesstattliche Versicherung (Affidavit)

Name, Vorname
(Surname, first name)

Matrikel-Nr.
(Enrolment number)

Belehrung:

Wer vorsätzlich gegen eine die Täuschung über Prüfungsleistungen betreffende Regelung einer Hochschulprüfungsordnung verstößt, handelt ordnungswidrig. Die Ordnungswidrigkeit kann mit einer Geldbuße von bis zu 50.000,00 € geahndet werden. Zuständige Verwaltungsbehörde für die Verfolgung und Ahndung von Ordnungswidrigkeiten ist der Kanzler/die Kanzlerin der Technischen Universität Dortmund. Im Falle eines mehrfachen oder sonstigen schwerwiegenden Täuschungsversuches kann der Prüfling zudem exmatrikuliert werden, § 63 Abs. 5 Hochschulgesetz NRW.

Die Abgabe einer falschen Versicherung an Eides statt ist strafbar.

Wer vorsätzlich eine falsche Versicherung an Eides statt abgibt, kann mit einer Freiheitsstrafe bis zu drei Jahren oder mit Geldstrafe bestraft werden, § 156 StGB. Die fahrlässige Abgabe einer falschen Versicherung an Eides statt kann mit einer Freiheitsstrafe bis zu einem Jahr oder Geldstrafe bestraft werden, § 161 StGB.

Die oben stehende Belehrung habe ich zur Kenntnis genommen:

Official notification:

Any person who intentionally breaches any regulation of university examination regulations relating to deception in examination performance is acting improperly. This offence can be punished with a fine of up to EUR 50,000.00. The competent administrative authority for the pursuit and prosecution of offences of this type is the chancellor of the TU Dortmund University. In the case of multiple or other serious attempts at deception, the candidate can also be unenrolled, Section 63, paragraph 5 of the Universities Act of North Rhine-Westphalia.

The submission of a false affidavit is punishable.

Any person who intentionally submits a false affidavit can be punished with a prison sentence of up to three years or a fine, Section 156 of the Criminal Code. The negligent submission of a false affidavit can be punished with a prison sentence of up to one year or a fine, Section 161 of the Criminal Code.

I have taken note of the above official notification.

Ort, Datum
(Place, date)

Unterschrift
(Signature)

Titel der Dissertation:
(Title of the thesis):

Ich versichere hiermit an Eides statt, dass ich die vorliegende Dissertation mit dem Titel selbstständig und ohne unzulässige fremde Hilfe angefertigt habe. Ich habe keine anderen als die angegebenen Quellen und Hilfsmittel benutzt sowie wörtliche und sinngemäße Zitate kenntlich gemacht.
Die Arbeit hat in gegenwärtiger oder in einer anderen Fassung weder der TU Dortmund noch einer anderen Hochschule im Zusammenhang mit einer staatlichen oder akademischen Prüfung vorgelegen.

I hereby swear that I have completed the present dissertation independently and without inadmissible external support. I have not used any sources or tools other than those indicated and have identified literal and analogous quotations.

The thesis in its current version or another version has not been presented to the TU Dortmund University or another university in connection with a state or academic examination.*

*Please be aware that solely the German version of the affidavit ("Eidesstattliche Versicherung") for the PhD thesis is the official and legally binding version.

Ort, Datum
(Place, date)

Unterschrift
(Signature)

technische universität
dortmund

Fakultät für Chemie
und Chemische Biologie

Datum: _____

An die/den Vorsitzende/n des Promotionsausschusses
der Fakultät für Chemie und Chemische Biologie der TU Dortmund

Eigenständigkeitserklärung für Dissertationen

nach der Ergänzung zur Promotionsordnung vom 29.10.2010
(Promotionsstudiengang) am 20.11.2023

Ich versichere hiermit an Eides statt, dass ich die vorliegende Dissertation mit dem folgenden Titel

_____

_____

_____

selbstständig und ohne unzulässige fremde Hilfe verfasst habe. Ich habe keine anderen als die angegebenen Quellen und Hilfsmittel benutzt sowie wörtliche und sinngemäße Zitate kenntlich gemacht. Ich erkläre zudem, dass ich beim Einsatz von Schreib- und Bildwerkzeugen, die durch Künstliche Intelligenz (KI) unterstützt werden, diese in der Übersicht verwendeter Hilfsmittel mit ihrem Produktnamen, meiner Bezugsquelle sowie der spezifischen Methodik vollständig aufgeführt habe und, bei Übernahme von durch generative Schreibwerkzeuge erstellten Texten, die betreffenden Textstellen in der Arbeit als mit KI-generierter Unterstützung verfasst gekennzeichnet habe. Die Arbeit hat in gleicher oder ähnlicher Form noch keiner Prüfungsbehörde vorgelegen. Ich habe sichergestellt, dass durch die Verwendung generativer Modelle kein fremdes geistiges Eigentum verletzt wurde und ich kein wissenschaftliches Fehlverhalten etwa in Form von Plagiaten begangen habe.

Name: _____, Vorname _____

Matrikelnummer: _____

Datum, Unterschrift _____

Stand 29.01.2024

6.6 Acknowledgements

First and foremost, I would like to thank **Dr. Cristina Cadenas** for her inspirational scientific support during my entire PhD period at IfaDo. I have never experienced and met a comparable person, who has this enormous drive and passion for doing research. Thank you for the countless discussion and your input for the establishment of this thesis! Apart from this, I would also thank you for the personal advice that went beyond work stuff.

Furthermore, I would like to thank **Prof. Dr. Jan G. Hengstler** for giving me the opportunity to prepare this thesis in the department of toxicology, for the fruitful scientific discussions in our regular meetings and for having you as first reviewer.

Also thanks to **Prof. Dr. Christoph van Thriel** for taking the position as the second reviewer of this thesis.

Moreover, I would like to thank my entire group Interorgan Toxicology – former and present members. Starting from **Adelina Jashari** and **Katharina Grgas**, who I worked with for the most time of my PhD. Especially Adelina, whom I have learned a lot from in the beginning and introduced me to all techniques we have been using. This holds true also for Katharina, who has a remarkable technical understanding of in vitro and in vivo techniques – not just helping me with many mice perfusions. Further, I would like to thank **Rami Hayajneh, Zhwan Mahmoud, Sara Bauer** and **Gideon Alimba Chibuisi** for being so nice group members and for their outstanding work attitude.

Not to forget, I would also thank the numerous co-workers at **IfADo**, especially the **toxicology department**, for the great working environment and for the support whenever I needed it the most. Thank you, **Rosemarie Marchan** (being my office neighbor and only Bayern supporter), **Ahmed Ghallab, Monika Turajski, Wolfram Föllmann, Georgia Günter, Simon Schäfers, Wiebke Albrecht, Tim Brecklinghaus, Gregor Leonhardt, Annika Glotzbach**, **Anastasia Oprisko, Maiju Myllys, Daniela Gonzales, Antonia Thomitzek** and **Andreas Scholtz-Illigens**.

Besides, a special thanks to people of the StemNet group. A big thanks to **David Feuerborn** and **Patrick Nell**, who have become way more than just work colleagues. Our extensive discussions during lunch break (which I am grateful to be invited to) covering topics like politics or even everyday life problems always helped me to escape from the work/research bubble. Especially the dining nights were so much fun with you and will always put a huge smile on my face!

Further, I would like to thank my **entire family** and **friends** who have always been there for me in the last few years and have support me throughout my entire academic career. A special thank goes to my parents, **Claudia** and **Stephan,** being the best parents one could dream of and my brother **Julian**.

At last, I would thank another IfaDo colleague - who has become way more than just a colleague – **Karolina Zajac** being there for me all the time and whenever I needed it the most. Without you, your patience, motivation and support, I definitely would not have made it this far! Thank you!